PHOTOELECTRON DIFFRACTION CALCULATIONS FOR ADSORBATE SYSTEMS

by

Malcolm Steven Woolfson, B.Sc.

A thesis submitted for the degree of

Doctor of Philosophy, University of Warwick,

Department of Physics

October 1981

ABSTRACT

The aim of this work is to assess the potential usefulness of photoelectron diffraction in the determination of surface structure. A review is first made of the theory of photoelectron diffraction from crystalline surfaces. Then, calculations of the variation of intensity with azimuthal angle are performed for various model systems, in order to investigate the sensitivity of the diffraction patterns to structural and non-structural parameters. It is found that for detector angles lying approximately half-way between the surface and surface normal, and for some photon energies, the diffraction patterns are sensitive to structure. For some energies, the patterns are found to be sensitive to non-structural parameters, making it necessary to know these parameters to a high precision. Then, an analysis is made of data taken in the azimuthal mode for 4d emission from c(2 x 2) and p(2 x 2)Te adsorbed on Ni(001) and for 4d emission from $(\sqrt{3} \times \sqrt{3})R30^{\circ}$I adsorbed on Ag(111). By transfering parameters from the relevant LEED calculation quite good agreement between theory and experiment is obtained for I on Ag(111) but the agreement is poor for both coverages of Te on Ni(001). Subsequently the case of normal emission from the 4d levels of c(2 x 2)Te on Ni(001) is looked at, the aim being to resolve the discrepancy that has been found to exist between theory and experiment. This discrepancy is resolved by using the energy dependent Hara potential rather than Slater exchange in the construction of the Te potential. The use of this new potential for Te also leads to improved agreement with the experimental data taken with the azimuthal mode. Then, an investigation is made as to whether the Lee and Beni potential, which takes into account screened exchange and correlation effects is an improvement over the Hara potential in the description of electron scattering. To this end calculations are performed of the total and differential cross-

sections for atomic Xe, Kr and Ar using the Slater, Hara and Lee and Beni potentials, and a comparison is made with experiment gas phase data. Hara exchange is found to be superior to the Lee and Beni potential especially at low energies. It is suggested that the inadequacy of the Lee and Beni potential is due to a breakdown of the Local Density Approximation and the success of the Hara potential is due to a cancellation of errors. Angle-resolved photoemission from adsorbed molecules is then looked at in order to assess the importance of multiple scattering. It is found that near to a resonance it is essential to incorporate multiple scattering. It is found that the Mattheis prescription of superposing atomic charge densities is inadequate in describing the emission and scattering properties of molecules, and it is preferable to use the Scattered-Wave Xα method which more realistically describes the distribution of charge within the molecule.

It is concluded that if core-state photoelectron diffraction is going to be used as a surface structural technique then it is essential that energy dependent potentials be used in the description of the emission and scattering properties of the surface atoms. For valence emission from adsorbed molecules it is suggested that the Mattheis prescription should be dispensed with in constructing the molecular potential.

CONTENTS

PAGE

PAGE

LIST OF FIGURES

ACKNOWLEDGEMENTS

I am grateful to my supervisor Dr. B. W. Holland for his encouragement and help during the course of this work and for patiently checking my thesis prior to typing.

I would like to thank Professors A. J. Forty and P. N. Butcher for providing me with facilities to carry out research within the Department of Physics.

Thanks are also due to:-

Drs. D. P. Woodruff and P. D. Johnson - for valuable discussions, for carrying out some of the calculations that are presented in this thesis and for providing me with data prior to publication.

Drs. A. D. Cox and J. McInnes - for their help in computer graphics.

Dr. H. Farrell - for providing me with data prior to publication.

Sandra Callanan - for her quick and efficient typing of this thesis and for decyphering my scrawl.

I have also benefitted from discussions with Drs. R. F. Pettifer and G. J. R. Jones.

I gratefully acknowledge the Science Research Council for supporting me financially during the course of this work.

I would finally like to thank my parents for their support and encouragement during the course of this work and for raising my spirits whenever the going got tough.

DECLARATION

All the work in this thesis is my own except where stated otherwise, and was carried out in the Department of Physics at the University of Warwick from October 1978 to September 1981.

Parts of this work have already been published as papers with the following references.

Phys. Rev. B21, 3119 (1980).

Solid State Comm., 35, 225 (1980)

Solid State Comm., 38, 961 (1981)

Other parts of this work will be published as papers in Vacuum and Surface Science.

To my parents

CHAPTER 1

INTRODUCTION

A fundamental quantity of interest in solid state physics is the structure of a crystal. Knowing the structure one can then proceed to calculate the electronic, magnetic and vibrational properties of the crystal. For over half a century the structures of many complicated crystals of industrial and medical importance have been determined by the technique of X-ray diffraction. However, due to the penetrating power of the X-rays this technique can only give information about the structure of the bulk of the crystal and it can give no information about the arrangement of the surface atoms.

Many important processes, such as catalysis and corrosion, occur at the surface of a solid. To study such phenomena in detail there is a need to know about the nature of the bonding between the surface atoms and the adsorbed atom or molecule. This requires a knowledge of the position of the adsorbate with respect to the substrate atoms. Another problem of interest is the reconstruction of the atoms at the surface of a metal or semiconductor to form a structure differing from that in the bulk. This problem is clearly of importance in the electronics industry.

It has been known since Davisson and Germer's classic experiment, (Davisson and Germer (1927)), that information about surface structure may be obtained by sending in a beam of low energy electrons and observing the diffraction pattern of those electrons that are elastically scattered out of the crystal. That this may be done is due to the fact that in the energy range 50 eV - 300 eV, the electronic mean free path in many crystals is typically of the order of $\sim$ 10 Å. By looking at the diffraction patterns it is possible to determine the size and shape of the unit cell. However,

in order to determine the bonding site and vertical spacing ($d_\perp$) of an adsorbed atom or molecule one has to study the variation of the intensity of the elastically scattered electrons with energy or angle. A detailed analysis of such data is difficult, because it is now known that one needs to consider multiple scattering of the incident electrons by the surface atoms, (see e.g. Beeby (1968)). This technique is known as Low Energy Electron Diffraction (LEED). In LEED, because of the importance of multiple scattering effects, one has to postulate the structure first and then see whether the calculated intensity (I) versus energy (V) curves agree with experiment. Thus one may have to postulate a considerable number of structures before one can obtain agreement between theory and experiment. Consequently, it is only possible to study simple surface systems such as clean surfaces and surfaces with adsorbed atoms or small molecules. The effort in calculating LEED curves is considerable but a lot of work has been carried out into formulating perturbative methods (see e.g. Pendry (1974), Van Hove and Tong (1979)), and with the ever increasing power of computers it has become fairly straightforward to perform such calculations.

Although LEED has been successful in solving over a hundred structures, it has still come up against difficulties when investigating systems such as H on Ni where the scattering power of the adsorbate (H) is far weaker than that of the substrate (Ni). In this case the positions and relative intensities of the peaks in the I:V curves can be very insensitive to the position of the adsorbate atom and an accurate determination of $d_\perp$ and the bonding site is difficult.

In recent years it has been suggested (Liebsch (1974, 1976a), Woodruff (1975)) that one should be able to obtain a more sensitive probe to surface structure if one looks at the angle-resolved intensity of elastically

scattered electrons that have been emitted from an adsorbate. This new method is very similar to LEED except that now the "source" of the electrons is the adsorbate whose position we are trying to find. Hence, in theory, the resulting diffraction curves should be more sensitive than LEED to the position of the adsorbate with respect to the substrate atoms. Theories of electron emission from crystalline surfaces that use a LEED-type of formalism to incorporate multiple scattering effects have been formulated in several different ways, (Pendry (1975, 1976), Holland (1975), Liebsch (1976), Li et al (1977)), and it is clear that one may perform such calculations by only making small modifications to existing LEED computer programs. Electrons may be emitted from adsorbates by either Auger or photoemission processes. The latter method is preferred for surface structure analysis because in Auger emission, several initial states can contribute to a particular final state thus making such a calculation very involved. One requires the energy of the emitted electron to be in the energy range 30 eV to 200 eV in order to minimise the electron mean free path and so maximise the surface sensitivity of the diffraction patterns. It is thus desirable to use a synchrotron in these studies so that one may vary the photoelectron kinetic energy in this energy range. This new surface technique has come to be known as photoelectron diffraction.

Various modes of data collection have been used in photoelectron diffraction experiments. In one mode, one focuses on a particular initial state, (usually a core state), the light source and the detector are kept fixed with respect to each other and the intensity of the electrons is measured as a function of the angle of rotation of the crystal about the surface normal. For core-state emission the anisotropy in the angular resolved intensity will be entirely due to scattering effects and contributions

from the details of the initial state will then be minimised. This method should then maximise the sensitivity of the diffraction pattern to structure. Also if data is taken for the full 360° rotation of the crystal then the symmetry in the data should be the same as the symmetry of the surface Bravais net. This then provides a check on the reliability of the data. We shall refer to this mode of data collection as the azimuthal mode.

A second method that has been employed is to look at the emission from a particular initial state, (again usually a core state), keep the detector and light source fixed with respect to each other and then vary the photon energy ($\hbar\omega$) and the retarding voltage in the detector so that one measures the intensity (I) of electrons emitted from this state as a function of $\hbar\omega$. Usually electrons emitted normal to the surface are monitored. The I:$\hbar\omega$ curves so produced are similar in nature to LEED I:V curves. The disadvantage of using this mode of data collection is that for emission from initial states specified by quantum numbers n and ℓ where $n \neq \ell + 1$, the photoelectron diffraction curve is dominated by effects that are purely atomic in nature (Cooper (1962)) and the effects of scattering result in minor perturbations on the experimental curve, (Li and Tong (1979)), thus reducing the sensitivity to structure. However, for initial states where $n = \ell + 1$ the atomic photoionization cross-section is a smooth function of energy, (Cooper (1962)), and the photoelectron diffraction curves are then dominated by multiple scattering effects. This mode of data collection is referred to as the Constant Initial State (CIS) mode.

A third mode of data collection that has been used is to focus on a particular initial state and to vary the polar angle of either the detector or light source with respect to the surface normal. For emission from core states the angular resolved intensity depends on both initial state and multiple scattering effects. For emission from valence levels,

the data is known to be mainly dominated by the symmetry of the initial state with respect to the surface and this has been used to determine the orientation of small molecules adsorbed on various metal surfaces, (see e.g. Williams (1980)).

Photoelectron diffraction experiments using both the azimuthal and CIS modes have been performed on various atomic adsorbate systems that have already been "solved" by LEED. The main aim has been to see whether by using the same structural and non-structural parameters as LEED in the photoelectron diffraction calculation one can obtain agreement between theory and experiment. This has successfully been done using the CIS mode for the surface systems Ni(001) - c(2 x 2)Se and Ni(001) - p(2 x 2)Se (Kevan et al (1978, 1979), Li and Tong (1979), Kevan et al (1981)), Ni(001) - c(2 x 2)Na (Williams et al (1979), Li and Tong (1979)), and Ni(001) - c(2 x 2)CO (Allyn et al (1977), Li and Tong (1978)) and, using the azimuthal mode, for Ni(001) - c(2 x 2)Na (Woodruff et al (1978)), Cu(001) and Cu(001) - c(2 x 2)O (Kono et al (1978a, 1978b), Ni(001) - c(2 x 2)CO, (Petersson et al (1979)), and TaS_2 (Liebsch (1976b)).

Experiments using the third mode of data collection have been mainly carried out on molecular adsorbate systems where the aim has been to determine the symmetry of the valence levels of the molecule with respect to the surface and so deduce the orientation of the molecule. The substrate is assumed to merely orient the molecule and the wavefunctions for the various molecular orbitals are approximated by those for the free molecule and the effects of scattering are usually neglected. Selection rules are applied to the various molecular orbitals to determine their symmetry with respect to the surface (Allyn et al (1977), Lloyd et al (1977), Bandy et al (1979)). More quantitative calculations have been performed for adsorbed CO (Davenport (1976)) and W(110) - N_2 (Umbach et al (1980)) where multiple scattering in the final state has been included.

For CO the effects of substrate scattering and scattering between molecules have not been included in the calculations.

The aim of this work is to further assess the capability of photoelectron diffraction to determine surface structure. We shall look at data taken from atomic and molecular adsorbate systems. In Chapter 2 of this thesis we will outline the formulation of Holland (1975, 1977) of the theory of diffraction effects for photoemission from crystalline surfaces. We shall also describe the method that is adopted in the construction of the atomic potentials that are used in the description of the emission and scattering processes. Chapters 3 and 4 will be concerned with work on core-state emission from adsorbate atoms where the azimuthal mode has been used to collect the data. In Chapter 3 we will first present model calculations for various adsorbate systems, the aim being to decide on the experimental configuration that will result in us obtaining optimum sensitivity to structure. Then, we will proceed to look at the sensitivity of the diffraction patterns to small changes in the detector angle, and the energy and angle of incidence of the radiation. If the diffraction patterns are sensitive to these non-structural parameters then this means that these parameters need to be known very accurately. Sensitivity to these parameters could also degrade the structural sensitivity of the diffraction patterns. Chapter 4 will deal with comparisons between theory and experiment for the adsorbate systems Ni(001) - c(2 x 2)Te, Ni(001) - p(2 x 2)Te and Ag(111) - $(\sqrt{3} \times \sqrt{3})R30^{\circ}$ which have already been studied by LEED, and, for $(\sqrt{3} \times \sqrt{3})R30^{\circ}$ on Ag(111), also by Surface Extended X-ray Absorption Fine Structure (SEXAFS). We shall be interested in seeing whether we can transfer structural and non-structural parameters directly from the LEED calculation. In Chapter 5 we will look at the case of CIS normal emission from the 4d levels of c(2 x 2)Te adsorbed on Ni(001) where controversy has arisen over the mismatch that has been obtained between theory (Li and Tong (1979))

and experiment (McGovern et al (1979)). This will lead us to discuss the construction of more sophisticated potentials for use in photoelectron diffraction calculations. In Chapter 6 we will look at angle-resolved photoemission data for various molecular adsorbate systems. We will analyse the data in a more quantitative way than has been done before. In particular we shall take into account the effects of interference between electrons emitted from different atomic centres as well as the influence of the atomic potentials on the emitted electron. This will enable us to assess the accuracy of the various qualitative analyses that have previously been used. Then we will look at the effects of molecule-molecule and molecule-substrate scattering for the particular case of CO on Ni to determine the importance of these processes. Finally, in Chapter 7, the results of the previous chapters will be discussed and suggestions for further work will be made.

REFERENCES FOR CHAPTER 1

Allyn, C. L., Gustafsson, T. and Plummer, E. W.,
Chem. Phys. Lett. 47, 127 (1977).

Bandy, B. J., Lloyd, D. R., and Richardson, N. V.,
Surf. Sci. 89, 344 (1979).

Beeby, J. L., J. Phys. C1, 82 (1968).

Cooper, J. W., Phys. Rev. 128, 682 (1962).

Davenport, J. W., Phys. Rev. Lett. 36, 945 (1976).

Davisson, C. J. and Germer, L. H., Phys. Rev. 30, 705, (1927).

Holland, B. W., J. Phys. C8, 2679 (1975).

Holland, B. W., Surf. Sci. 68, 490 (1977).

Kevan, S. D., Rosenblatt, D. H., Denley, D., Lu B-C., and Shirley, D. A.,
Phys. Rev. Lett. 41, 1565 (1978).

Kevan, S. D., Rosenblatt, D. H., Denley, D., Lu, B-C., and Shirley, D. A.,
Phys. Rev. B20, 4133 (1979).

Kevan, S. D., Tobin, J. G., Rosenblatt, D. H., Davis, R., and Shirley, D. A.,
Phys. Rev. B23, 493 (1981).

Kono, S., Fadley, C. S., Hall, N. F. T. and Hussain, Z.,
Phys. Rev. Lett. 41, 117 (1978a).

Kono, S., Goldberg, S. M., Hall, N. F. T., and Fadley, C. S.,
Phys. Rev. Lett. 41, 1831, (1978b).

Li, C. H., Lubinsky, A. R. and Tong, S. Y.,
Phys. Rev. B17, 3128 (1977).

Li, C. H. and Tong, S. Y., Phys. Rev. Lett, 40, 46 (1978).

Li, C. H. and Tong, S. Y., Phys. Rev. Lett. 42, 901 (1979a).

Li, C. H. and Tong, S. Y., Phys. Rev. B19, 1769 (1979b).

Li, C. H. and Tong, S. Y., Phys. Rev. Lett, 43, 526 (1979c).

Liebsch, A., Phys. Rev. Lett. 32, 1203 (1974).

Liebsch, A., Phys. Rev. B13, 544 (1976a)

Liebsch, A., Solid Stat Comm., 19, 1193 (1976b).

Lloyd, D. R., Quinn, C. M. and Richardson, N. V., Surf. Sci. 68, 547 (1977).

McGovern, I. T., Eberhardt, W. and Plummer, E. W., Solid State Comm. 32, 963 (1979).

Pendry, J. B., Low Energy Electron Diffraction, (Academic Press, London 1974).

Pendry, J. B., J. Phys. C8, 2413 (1975).

Pendry, J. B., Surf. Sci. 57, 679 (1976).;

Petersson, L-G., Kono, S., Hall, N. F. T., Fadley, C. S., and Pendry, J. B., Phys. Rev. Lett. 42, 1545 (1979).

Umbach, E., Schuhl, A. and Menzel, D., Solid State Comm. 36, 93 (1980).

Van Hove, M. A., and Tong, S. Y., Surface Crystallography by LEED, (Springer -Verlag, Berlin, 1979).

Williams, R. H., Rep. Prog. Phys. 43, 1357 (1980).

Williams, G. P., Cerrina, F., McGovern, I. T. and Lapeyre, G. J., Solid Stat Comm. 31, 15 (1979).

Woodruff, D. P., Surf. Sci. 53, 538 (1975).

Woodruff, D. P., Norman, D., Holland, B. W., Smith, N. V., Farrell, H. H. and Traum, M. M., Phys. Rev. Lett. 41, 1130 (1978).

Fig. 2.1: Cross-section and profile of the muffin-tin potential, (photocopied from Pendry (1974)).

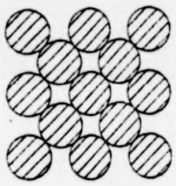

Cross-section of a crystal divided into muffin tins.

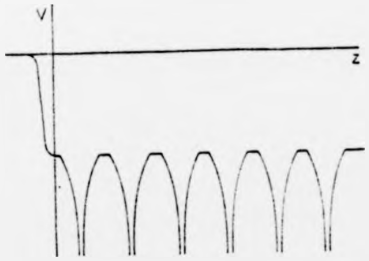

A cross-section of the potential in a crystal. Note the regions of constant potential between the ion cores, and the barrier at the surface.

CHAPTER 2

THEORY OF ANGLE-RESOLVED PHOTOEMISSION FROM THE CORE STATES OF ADSORBATES

2.1. The Model Surface

The calculation of the angle-resolved intensity of electrons emitted from the core-state of an adsorbate may be separated into two parts: (i) the calculation of the wave-function of the electron emitted from the atomic orbital and (ii) the calculation of the perturbation of this wavefunction due to multiple scattering of the electron by atoms in the adlayer and substrate. The ion-core potentials within the crystal are modelled by the muffin-tin approximation,(Loucks (1967)). In this approximation, the potential about each atom is assumed to be spherically symmetric up to a distance R_{MT} from the centre of the atom. Outside this limit the potential is averaged out to a constant, V_r (Fig. 2.1). The potentials of neighbouring atoms are assumed not to overlap. This approximation is known to be a good one from LEED work on metals and insulators, (see e.g. Pendry (1974)). The constant inner potential V_r is assumed to suddenly become zero at the surface (Fig. 2.1). It is assumed that this barrier refracts but does not scatter the outgoing electron; this approximation should be alright as realistically the surface barrier is a smooth function of position and so would reflect very weakly. The ion-cores are embedded in a valence electron gas. It is known from work on LEED, (Pendry, (1974)), that inelastic collisions of the emitted electron with the electron gas may be simulated by adding a constant imaginary part to the crystal potential thus making the electron wavevector complex. Thus the wavefunction for the elastically scattered electron will be damped. It is assumed that the vibrations of the atoms due to thermal

effects are isotropic and uncorrelated. It may then be shown, (Duke and Laramore (1970), Laramore and Duke (1970), Holland (1971)), that such effects may be taken into account by making the atomic phase shifts complex. The polarization vector $\underline{A}$ will vary in a complicated way with distance into the substrate, (Kliewer (1978), Feibelman (1978), Mukhopadyay and Lundquist (1978)). However, for core state emission where, experimentally, photon energies well above the plasmon energy are used, it should be a good approximation to take $\underline{A}$ as having no spatial dependence. Many-body effects such as plasmon excitation and creation of electron-hole pairs are normally assumed to have a negligible effect on the angle resolved photoelectron intensity.

The derivation of the wavefunction for the emitted electron from an atomic orbital that we will describe below is due to Holland (1977). Alternative derivations exist, (see Feuerbacher and Willis (1976) for further references).

2.2. Theory of Photoemission from an Atomic Orbital

The Hamiltonian for the atom and electromagnetic field is given by (see e.g. Dirac (1967)):

$$H = \frac{1}{2m}\left(\hat{\underline{p}} - \frac{e}{c}\hat{\underline{A}}\right)^2 + V(r) + H_{rad} \qquad (2.1)$$

where $V(r)$ is the atomic potential, $\hat{\underline{A}}$ is the vector potential operator and H_{rad} is the Hamiltonian for the radiation. If it is assumed that $\hat{\underline{A}}$ is independent of position so that $[\hat{\underline{p}}, \hat{\underline{A}}] = 0$, and that terms of order $(\hat{\underline{A}})^2$ may be ignored then we may write:

$$H = H_o + H_1 + H_{rad} \quad , \qquad (2.2)$$

where $H_o = \frac{\hat{\underline{p}}^2}{2m} + V(r)$ is the atomic Hamiltonian and

$$H_1 = -\frac{e}{mc}\hat{\underset{\sim}{A}}.\hat{\underset{\sim}{p}} \tag{2.3}$$

is the term representing the electron-photon interaction. We are only concerned with the effect of the perturbation H_1 on the unperturbed system so from now on we ignore H_{rad}. Using the method of second quantization, H_1 may be re-written as:

$$H_1 = -\frac{e}{mc}\hat{\underset{\sim}{p}}.\sum_{\underset{\sim}{q}\alpha}\left[\frac{hc^2}{\omega\Omega}\right]^{\frac{1}{2}} e^{i\underset{\sim}{q}.\underset{\sim}{r}}\underset{\sim}{\varepsilon}_{\underset{\sim}{q}\alpha}(a_{\underset{\sim}{q}\alpha} + a^{+}_{-\underset{\sim}{q}\alpha}) \quad , \tag{2.4}$$

where ω is the photon frequency, α is a polarization index, Ω is a normalization volume, $\underset{\sim}{q}$ is a photon wavevector, $\underset{\sim}{\varepsilon}_{\underset{\sim}{q}\alpha}$ is the polarization vector of the electromagnetic field and $a_{\underset{\sim}{q}\alpha}$ and $a^{\dagger}_{\underset{\sim}{q}\alpha}$ are respectively the annihilation and creation operators for the photons with wavevector $\underset{\sim}{q}$.

Let the unperturbed wavefunction for the system be $|i\rangle$. Then we may write:

$$|i\rangle = |p\rangle|n\ell m\rangle$$

where $|n\ell m\rangle$ is the initial state of the electron and $|p\rangle$ is the wavefunction for the electromagnetic field. Let the perturbed wavefunction be $|i^{+}\rangle$. Then $|i^{+}\rangle$ may be related to $|i\rangle$ by the Lippmann-Schwinger equation (see e.g. Roman (1965)):

$$|i^{+}\rangle = |i\rangle + \lim_{\eta\to 0^{+}} \frac{1}{E-H_o+i\eta} H_1|i^{+}\rangle \tag{2.5}$$

where $H|i^{+}\rangle = E|i^{+}\rangle$, $H_o|i\rangle = E_i|i\rangle$ and η is a positive real number that prevents the Green operator $(E-H_o+i\eta)^{-1}$ becoming singular. In writing down equation (2.5) it is assumed that both H and H_o have a continuum of states so that for each state $|i\rangle$ in the continuous part of the H_o-spectrum which has an energy E_i, there corresponds a state $|i^{+}\rangle$ in the continuous part of the H-spectrum with the same energy. The boundary condition on $|i^{+}\rangle$ is that as $t\to-\infty$ it coincides with $|i\rangle$, and the

perturbation is slowly added on as t increases. A zeroth order solution to equation (2.5) is to put $|i^+\rangle = |i\rangle$. Inserting this on the right hand side equation (2.5) and inserting the identity operator $\sum|r\rangle\langle r|$ into the second term on the right-hand side $|i^+\rangle$ may be written to first order in the perturbation as:

$$|i^+\rangle = |i\rangle + \lim_{\eta\to 0^+} \sum_r \frac{\langle r|H_1|i\rangle}{E-E_r+i\eta}\,|r\rangle \qquad (2.6)$$

One now takes the scalar product of equation (2.6) with the null photon, (or electromagnetic vacuum state), $|0\rangle$. On the right-hand side only those terms of the form $|r\rangle = |0\rangle|\varepsilon\ell'm'\rangle$ survive where $|\varepsilon\ell'm'\rangle$ is an eigenfunction of the atomic Hamiltonian. For radiation in the ultra-violet part of the electromagnetic spectrum, one may approximate $|\underset{\sim}{q}.\underset{\sim}{r}|<<1$ in equation (2.4) so that $\exp(i\underset{\sim}{q}.\underset{\sim}{r}) = 1$. Also it is assumed that initially there is one photon with wavevector $\underset{\sim}{q}$. Making all these assumptions the wavefunction for the emitted electron $|n\ell m+\rangle$ may be written as:

$$|n\ell m+\rangle = \gamma \sum_{\ell',m'} \int \frac{d\varepsilon\rho_{\ell'm'}(\varepsilon)\langle\varepsilon\ell'm'|\underset{\sim}{\varepsilon}.\underset{\sim}{p}|n\ell m\rangle}{\varepsilon_n + \hbar\omega - \varepsilon + i\eta}\,|\varepsilon\ell'm'\rangle\,, \qquad (2.7)$$

where $\gamma = -\frac{e}{mc}\left(\frac{\hbar c^2}{\omega\Omega}\right)^{\frac{1}{2}}$, and $\rho_{\ell'm'}(\varepsilon)$ is the density of states for the emitted electron. Outside the muffin-tin, $|\varepsilon\ell'm'\rangle$ may be written in the co-ordinate representation as

$$|\varepsilon\ell'm'\rangle = Y_{\ell'm'}(\underset{\sim}{r})[e^{i\delta_{\ell'}}h^+_{\ell'}(kr) + e^{-i\delta_{\ell'}}h^-_{\ell'}(kr)]\,,$$

where $k = \left(\frac{2m\varepsilon}{\hbar^2}\right)^{\frac{1}{2}}$ and $h^+_\ell(kr)$ and $h^-_\ell(kr)$ are respectively Hankel functions of the first and second kind as defined by Messiah (1964). The quantity $\delta_{\ell'}$ is the $\ell'^{\text{-th}}$ phase shift of the atom and it depends on the electron kinetic energy and the details of the atomic potential. The method that is used to calculate this quantity will be described later. $|n\ell m^+\rangle$ may

be written in the co-ordinate representation as:

$$\langle \underset{\sim}{r}|n\ell m^{+}\rangle \equiv \psi^{o}_{e}(\underset{\sim}{r}) = \gamma \int \sum_{\ell' m'} d\varepsilon \rho_{\ell' m'}(\varepsilon) \frac{\langle \varepsilon \ell' m' | \underset{\sim}{\varepsilon}.\underset{\sim}{p} | n\ell m\rangle}{\varepsilon_n + \hbar\omega - \varepsilon + i\eta}$$

$$\times Y_{\ell' m'}(\underset{\sim}{r}) \left[e^{i\delta_{\ell'}} h^{+}_{\ell'}(kr) + e^{-i\delta_{\ell'}} h^{-}_{\ell'}(kr) \right] \qquad (2.8)$$

Integrating over ε:

$$\psi^{o}_{e}(\underset{\sim}{r}) = i\pi\gamma \sum_{\ell' m'} e^{i\delta_{\ell'}} \rho_{\ell' m'}(\varepsilon_n + \hbar\omega) \langle \varepsilon_n + \hbar\omega, \ell' m' | \underset{\sim}{\varepsilon}.\underset{\sim}{p} | n\ell m\rangle$$

$$\times Y_{\ell' m'}(\underset{\sim}{r}) h^{+}_{\ell'}(kr) \qquad (2.9)$$

where $\frac{\hbar^2 k^2}{2m} = \varepsilon_n + \hbar\omega$ is the kinetic energy of the outgoing electron. This term represents a superposition of outgoing spherical waves centred on the emitting atom.

Converting to the co-ordinate representation let us write:

$$\langle r|n\ell m\rangle = U_{n\ell}(r) Y_{\ell m}(\theta,\phi)$$

and

$$\langle r|\varepsilon_n + \hbar\omega, \ell' m'\rangle = R_{\ell'}(r)\, Y_{\ell' m'}(\theta,\phi) \ ,$$

where θ and ϕ are respectively the polar and azimuthal angles of the emitted electron with respect to the inward surface normal.

Performing the angular integrations, it may be shown that:

$$\psi^{o}_{e}(\underset{\sim}{r}) = \frac{\gamma\pi\hbar\rho\sigma_{n\ell,\ell+1} e^{i\delta_{\ell+1}} h^{+}_{\ell+1}(kr)}{[(2\ell+1)(2\ell+3)]^{\frac{1}{2}}} \Big\{ -\tfrac{1}{2}[(\ell+1+m)(\ell+2+m)]^{\frac{1}{2}} e^{-i\phi'}$$

$$\times \sin\theta' \, Y_{\ell+1,m+1}(\theta,\phi)$$

$$+ \tfrac{1}{2}[(\ell+1-m)(\ell+2-m)]^{\frac{1}{2}} e^{i\phi'}$$

$$\times \sin\theta' \, Y_{\ell+1,m-1}(\theta,\phi)$$

$$+ [(\ell+1)^2 - m^2]^{\frac{1}{2}} \cos\theta' Y_{\ell+1,m}(\theta,\phi) \Big\}$$

$$+\frac{\gamma\pi\hbar\rho\sigma_{n\ell,\ell-1}e^{i\delta_{\ell-1}}h^{+}_{\ell-1}(Kr)}{[(2\ell+1)(2\ell-1)]^{\frac{1}{2}}}\Bigg\{\tfrac{1}{2}[(\ell-1-m)(\ell-m)]^{\frac{1}{2}}e^{-i\phi'}\times\sin\theta' Y_{\ell-1,m+1}(\theta,\phi)$$

$$-\tfrac{1}{2}[(\ell+m-1)(\ell+m)]^{\frac{1}{2}}e^{i\phi'}\times\sin\theta' Y_{\ell-1,m-1}(\theta,\phi)$$

$$+(\ell^2-m^2)^{\frac{1}{2}}\cos\theta' Y_{\ell-1,m}(\theta,\phi)\Bigg\} \qquad (2.10)$$

where (θ',ϕ') are the angular coordinates of the A-vector. The quantity $\sigma_{n\ell,\ell'}$ is known as the photoionization amplitude for the orbital $|n\ell m\rangle$ and it gives the probability that the emitted electron will have orbital quantum number ℓ'. Equation (2.10) shows that the quantum numbers (ℓ', m') for the emitted electron are given by the well-known selection rules:

$$\ell' = \ell\pm1 \; ; \quad m' = m, m\pm1 \quad ,$$

It may be shown (Appendix 1) that $\sigma_{n\ell,\ell'}$ may be written as:

$$\sigma_{n\ell,\ell'} = \int_0^\infty U_{n\ell}(r)\, r\left[\frac{d}{dr} \pm \frac{(2\ell+1\pm1)}{2r}\right] R_{\ell'}(r)\, r dr: \quad \ell' = \ell\pm1 \qquad (2.11)$$

Alternatively using the relation

$$\underset{\sim}{P} = m\dot{\underset{\sim}{r}} = \frac{m}{ih}[\underset{\sim}{r},H]$$

$\sigma_{n\ell,\ell'}$ may be written as:

$$\sigma_{n\ell,\ell'} = -\frac{m\omega}{\hbar}\int_0^\infty r^3 R_{\ell'}(r)\, U_{n\ell}(r)\, dr \qquad (2.12)$$

Finally using the relation:

$$(\varepsilon_n-\varepsilon)\langle\varepsilon\ell'm'|\underset{\sim}{P}|n\ell m\rangle$$

$$= \langle\varepsilon\ell'm'|[\underset{\sim}{P},H]|n\ell m\rangle$$

$$= \langle\varepsilon\ell'm'|[\underset{\sim}{P},\underset{\sim}{V}]|n\ell m\rangle$$

$$= -i\hbar\langle\varepsilon\ell'm'|\underset{\sim}{\nabla}V|n\ell m\rangle \quad ,$$

on obtains the "acceleration form" for $\sigma_{n\ell,\ell'}$:

$$\sigma_{n\ell,\ell'} = \frac{1}{\hbar\omega}\int_0^\infty R_{\ell'}(r)\left[\frac{dV(r)}{dr}\right]U_{n\ell}(r)r^2dr \qquad (2.13)$$

For the muffin-tin approximation equation (2.13) will be most convenient to use, for then dV(r)/dr is zero outside R_{MT}, so that we only need to integrate out to R_{MT}. Further details of the calculation of this qunatity will be presented in section (2.4).

If we consider emission from an atomic core-state $|n\ell m>$, we would have to take account of the $(2\ell+1)$-fold degeneracy of the corresponding energy level by incoherently summing the intensities from the orbitals $|n\ell\ell>$, $|n\ell,\ell-1>$,..., $|n\ell, -(\ell-1)>$, $|n\ell,-\ell>$ to find the total intensity of the emitted electron. For emission from valence states, e.g. a bond between two atoms, one would first have to calculate the initial state as a linear combination of atomic orbitals (LCAO), (see e.g. Coulson (1965)), in order to use the above formalism to calculate the emitted electron intensity. In the case of a bond between an adatom and the substrate such a calculation is difficult, (Grimley (1976)).

2.3. Emission from a Crystal Surface

We now need to consider the perturbation of $\psi_e^o(\underset{\sim}{r})$ due to multiple scattering of the emitted electron off the ion cores in the surface region. It has been shown that multiple scattering can significantly effect the photoelectron diffraction pattern, (McDonnell et al (1975), Woodruff (1975), Tong and Van Hove (1976), Liebsch (1976)). This problem has been extensively studied in the context of LEED, where the emphasis has been on the development of perturbation schemes that are both accurate and efficient to run on a computer, (see Van Hove and Tong (1979) for a review of perturbation methods in LEED).

The multiple scattering series for electron emission has been formulated in different ways (Pendry 1975,1976), Holland (1975), Liebsch

(1976), Li et al (1977)). We will outline below the formulation of the multiple scattering series due to Holland (1975).

2.3.1. The General Multiple Scattering Series

The emitting atom is placed at position vector $\underline{e}$. The Hamiltonian for the emitted electron may be written as:

$$H = H_o' + V$$

where:

$$H_o' = -\frac{\hbar^2}{2m}\nabla^2 + V_o \quad ,$$

V_o is the constant complex potential mentioned earlier and V is the potential due to the ion cores which are modelled by the muffin tin approximation.

In LEED work, the real part of the complex potential is usually calculated by aligning theoretical peak positions with experiment in the I:V spectra. The imaginary part of V_o, (related to the mean free path), is varied until the peak widths are reproduced by the theory. In general, the I:V curves are insensitive to $\mathrm{Im}(V_o)$. Of course this procedure assumes that the complex potential is energy independant, but this is known to be a good approximation over the energy range of interest, (see e.g. Pendry (1974)). It is assumed that the complex potential that is used in the LEED calculation for a particular system may be transferred to the photoelectron diffraction calculation for this system. The electron wavevector in the crystal, K, will be complex and is given by:

$$K^2 = \frac{2m}{\hbar^2}(E - V_o) \qquad (2.14)$$

where the convention has been used that $\mathrm{Re}(V_o)<0$ and $\mathrm{Im}(V_o)<0$.

Let ψ be the wavefunction of the electron at the detector. Then, from the Lippmann-Schwinger equation, (Roman (1965)):

$$\psi = (\underline{1} + \underline{\underline{G}}\underline{\underline{T}})\psi^{\circ} \tag{2.15}$$

where $\psi^{\circ} \equiv |n\ell m\rangle$ is the initial state, T is the T-matrix representing multiple scattering by the ion cores and $G = (E-H_{\circ})^{-1}$. T may be expanded in a multiple scattering series, (see e.g. Beeby (1968), Holland (1977)), and ψ then becomes:

$$\psi = (\underline{1} + \underline{\underline{G}} \sum_{\underline{s}\neq\underline{e}} \hat{\underline{\underline{t}}}_{\underline{s}} + \underline{\underline{G}} \sum_{\substack{\underline{s},\underline{s}' \\ (\underline{s}\neq\underline{s}'\neq\underline{e})}} \hat{\underline{\underline{t}}}_{\underline{s}} \underline{\underline{G}} \hat{\underline{\underline{t}}}_{\underline{s}'} + \ldots\ldots)\psi^{\circ}_{\underline{e}} \tag{2.16}$$

where $\hat{\underline{\underline{t}}}_{\underline{s}}$ is the T-matrix for the ion core at $\underline{s}$. $\psi^{\circ}_{\underline{e}}$ is given in the co-ordinate representation outside the muffin-tin radius by equation (2.10) and $\psi^{\circ}_{\underline{e}}$ is related to ψ° by:

$$\psi^{\circ}_{\underline{e}} = (\underline{1} + \underline{\underline{G}}\,\hat{\underline{\underline{t}}}_{\underline{e}})\psi^{\circ}$$

We rewrite equation (2.10) as:

$$\psi^{\circ}_{\underline{e}}(\underline{r}-\underline{e}) = \sum_{\ell,m} b_{\ell m} h^{+}_{\ell}(K|\underline{r}-\underline{e}|) Y_{\ell m}(\underline{r}-\underline{e}) \quad . \tag{2.17}$$

In the co-ordinate representation (2.16) may be rewritten as:

$$\psi(\underline{r},\underline{e}) = \psi^{\circ}_{\underline{e}}(\underline{r}-\underline{e}) + \iint \underline{\underline{G}}(\underline{r}-\underline{r}') \sum_{\underline{s}(\neq\underline{e})} \hat{\underline{\underline{t}}}_{\underline{s}}(\underline{r}',\underline{r}'')\psi^{\circ}_{\underline{e}}(\underline{r}''-\underline{e}) \quad d^3\underline{r}'d^3\underline{r}''$$

$$+ \iiiiint \underline{\underline{G}}(\underline{r}-\underline{r}') \sum_{\substack{\underline{s},\underline{s}' \\ (\underline{s}\neq\underline{s}',\underline{s}'\neq\underline{e})}} \hat{\underline{\underline{t}}}_{\underline{s}}(\underline{r}',\underline{u})\underline{\underline{G}}(\underline{u}-\underline{u}')\hat{\underline{\underline{t}}}_{\underline{s}'}(\underline{u}',\underline{r}'')\psi^{\circ}_{\underline{e}}(\underline{r}''-\underline{e})$$

$$\times\, d^3\underline{r}'d^3\underline{u}d^3\underline{u}'d^3\underline{r}''$$

$$+ \ldots\ldots \tag{2.18}$$

where

$$G(\underline{r}) = \frac{2m}{\hbar^2}\left(\frac{1}{2\pi}\right)^3 \int \frac{\exp(i\underline{k}.\underline{r})}{K^2-k^2}\, d^3\underline{k} \tag{2.19}$$

and

$$\hat{t}_{\underset{\sim}{s}}(\underset{\sim}{r},\underset{\sim}{r}') = V_{\underset{\sim}{s}}(\underset{\sim}{r})\delta(\underset{\sim}{r}-\underset{\sim}{r}') + \int V_{\underset{\sim}{s}}(\underset{\sim}{r})G(\underset{\sim}{r}-\underset{\sim}{r}'')\hat{t}_{\underset{\sim}{s}}(\underset{\sim}{r}'',\underset{\sim}{r}') \quad d^3\underset{\sim}{r}''$$

where $V_{\underset{\sim}{s}}(\underset{\sim}{r})$ is the potential of the ion core at $\underset{\sim}{s}$. The position dependence of the $\hat{t}_{\underset{\sim}{s}}$ terms are removed by putting $\underset{\sim}{r}'-\underset{\sim}{s} = \underset{\sim}{x}$ etc. and

$$\hat{t}_{\underset{\sim}{s}}(\underset{\sim}{x},\underset{\sim}{x}') = \hat{t}_{\underset{\sim}{s}}(\underset{\sim}{x}+\underset{\sim}{s},\underset{\sim}{x}'+\underset{\sim}{s}) \quad .$$

2.3.2. The Unscattered Term

The combination of spherical waves, (equation 2.17), is now expanded in plane waves by using the relation, (Appendix 2):

$$h_\ell^+(K|\underset{\sim}{r}-\underset{\sim}{e}|)Y_{\ell m}(\underset{\sim}{r}-\underset{\sim}{e}) = \frac{-i^{-\ell}}{2\pi^2 K}\int d^3\underset{\sim}{k}\,\frac{\exp[i\underset{\sim}{k}.(\underset{\sim}{r}-\underset{\sim}{e})]j_\ell(kx)Y_{\ell m}(\underset{\sim}{k})}{(K^2-k^2)j_\ell(Kx)} \qquad (2.20)$$

$\underset{\sim}{k}$ is resolved into components parallel ($\underset{\sim}{k}_{11}$) and perpendicular ($k_\perp$) to the surface. Integration of equation (2.20) over $k_\perp$ gives the required expansion

$$h_\ell^+(K|\underset{\sim}{r}-\underset{\sim}{e}|)Y_{\ell m}(\underset{\sim}{r}-\underset{\sim}{e}) = \frac{i}{2\pi K}\int d^2\underset{\sim}{k}_{11}\frac{i^{-\ell}}{k_\perp}Y_{\ell m}(\underset{\sim}{k})\exp[i\underset{\sim}{k}.(\underset{\sim}{r}-\underset{\sim}{e})] \qquad (2.21)$$

The assumption is now made that the superposition of plane waves (2.21) is refracted but not scattered by the surface. Hence, from equations (2.21) and (2.17), the contribution to the amplitude of the plane wave with wave-vector $\underset{\sim}{k}$ at the detector may be written as:

$$\alpha^o(\underset{\sim}{k},\underset{\sim}{e}) = \exp(-i\underset{\sim}{k}.\underset{\sim}{e})\underset{\sim}{D}(\underset{\sim}{k})\underset{\sim}{A} \qquad (2.22)$$

where $\underset{\sim}{A}$ is a vector with elements $A_{\ell m} = \frac{2\pi i}{K}b_{\ell m}$ and $\underset{\sim}{D}(\underset{\sim}{k})$ is a vector with elements $D_{\ell m} = \frac{i^{-\ell}}{k_\perp}Y_{\ell m}(\underset{\sim}{k})$.

2.3.3. Single-Scattering Terms

The single-scattering terms are of the form:

$$\alpha'(\underset{\sim}{r},\underset{\sim}{s},\underset{\sim}{e}) = \iint G(\underset{\sim}{r}-\underset{\sim}{s}-\underset{\sim}{x})\hat{t}_{\underset{\sim}{s}}(\underset{\sim}{x},\underset{\sim}{x}')\psi^{o}_{\underset{\sim}{e}}(\underset{\sim}{x}'+\underset{\sim}{s}-\underset{\sim}{e})\,d^3\underset{\sim}{x}d^3\underset{\sim}{x}' \qquad (2.23)$$

By expanding the factors $\psi^{o}_{\underset{\sim}{e}}(\underset{\sim}{x}'+\underset{\sim}{s}-\underset{\sim}{e})$, $G(\underset{\sim}{r}-\underset{\sim}{s}-\underset{\sim}{x})$ and $\exp(-i\underset{\sim}{k}.\underset{\sim}{x})$ in spherical harmonics and integrating over $\underset{\sim}{x}$ and $\underset{\sim}{x}'$ it may be shown (Holland (1975)) that the contribution to the plane wave of the detector with wavevector $\underset{\sim}{k}$ from single scattering terms may be written as:

$$\alpha'(\underset{\sim}{k},\underset{\sim}{e}) = \underset{\sim}{D}(\underset{\sim}{k}) \sum_{\underset{\sim}{s}(\neq\underset{\sim}{e})} \exp(-i\underset{\sim}{k}.\underset{\sim}{s})\hat{t}_{\underset{\sim}{s}}\ \underset{\sim}{G}(\underset{\sim}{s}-\underset{\sim}{e})\underset{\sim}{A} \qquad (2.24)$$

where $t_{\underset{\sim}{s}}$ is a diagonal matrix with elements $t_{s}^{\ell\ell}$ given by (Beeby (1968)).

$$t_{s}^{\ell\ell} = -\frac{1}{2ik}\left[\exp(2i\delta_{\ell}^{s})-1\right] \qquad (2.25)$$

δ_{ℓ}^{s} being the ℓ^{th} phase shift of the atom at $\underset{\sim}{s}$.

2.3.4. The Multiple Scattering Series for a Crystal

The analysis in section (2.3.3) may be extended to double and higher order scatterings and the full multiple scattering series may then be written as:

$$\alpha(\underset{\sim}{k},\underset{\sim}{e}) = \underset{\sim}{D}(\underset{\sim}{k})\Big[\exp(-i\underset{\sim}{k}.\underset{\sim}{e})\underset{\sim}{1} + \sum_{\underset{\sim}{s}(\neq\underset{\sim}{e})} \exp(i\underset{\sim}{k}.\underset{\sim}{s})t_{\underset{\sim}{s}}\ \underset{\sim}{G}(\underset{\sim}{s}-\underset{\sim}{e})$$

$$+ \sum_{\substack{\underset{\sim}{s},\underset{\sim}{s}' \\ (\underset{\sim}{s}\neq\underset{\sim}{s}';\,\underset{\sim}{s}'\neq\underset{\sim}{e})}} \exp(-i\underset{\sim}{k}.\underset{\sim}{s})t_{\underset{\sim}{s}}\ \underset{\sim}{G}(\underset{\sim}{s}-\underset{\sim}{s}')t_{\underset{\sim}{s}'}\ \underset{\sim}{G}(\underset{\sim}{s}'-\underset{\sim}{e}) + \ldots\Big]\underset{\sim}{A} \qquad (2.26)$$

The above series applies to any system of atoms. It is now assumed that the crystal surface has the translational symmetry of a Bravais net. Each layer is divided into subplanes with each subplane having one atom per primitive unit cell, (see Beeby (1968)). The position of each atom may be written as:

$$\underset{\sim}{s}_i = \underset{\sim}{P}_i + \underset{\sim}{d}_{\nu_i} \tag{2.27}$$

where $\underset{\sim}{d}_{\nu_i}$ is the position of the origin of sub-plane ν_i containing $\underset{\sim}{s}_i$ and $\underset{\sim}{P}_i$ is a Bravais net vector.

The multiple-scattering series may now be written as:

$$\alpha(\underset{\sim}{k},\underset{\sim}{e}) = \exp(-i\underset{\sim}{k}.\underset{\sim}{e})\underset{\sim}{D}(\underset{\sim}{k})[\underset{\sim}{1} + \sum_{\nu\neq\nu_e} \underset{\sim}{\tau}_\nu \underset{\sim}{G}^{\nu\nu_e}(\underset{\sim}{k})$$

$$+ \sum_{\substack{\nu(\neq\nu') \\ \nu'(\neq\nu_e)}} \underset{\sim}{\tau}_\nu \underset{\sim}{G}^{\nu\nu'} \underset{\sim}{\tau}_{\nu'} \underset{\sim}{G}^{\nu'\nu_e}(\underset{\sim}{k}) + \ldots.]\underset{\sim}{\tau}_{\nu_e} \underset{\sim}{t}^{-1}_{\nu_e} \underset{\sim}{A} \quad , \tag{2.28}$$

where

$$\underset{\sim}{\tau}_{\nu_e} = [\underset{\sim}{1} - \underset{\sim}{t}_{\nu_e} \underset{\sim}{G}^{SP}(\underset{\sim}{k})]^{-1} \underset{\sim}{t}_{\nu_e}$$

is the T-matrix for scattering within the emitter subplane only,

$$\underset{\sim}{\tau}_\nu = [\underset{\sim}{1} - \underset{\sim}{t}_\nu \underset{\sim}{G}^{SP}(\underset{\sim}{k})]^{-1} \underset{\sim}{t}_\nu \qquad \nu\neq\nu_e$$

is the T-matrix for scattering within subplane $\nu\neq\nu_e$, and the terms $\underset{\sim}{G}^{\nu\nu'}(\underset{\sim}{k})$ and $\underset{\sim}{G}^{\nu\nu}(\underset{\sim}{k}) \equiv \underset{\sim}{G}^{SP}(\underset{\sim}{k})$ are structure factors which depend on the geometry of the surface atoms and the electron energy in the crystal. These structure factors are given by:

$$\underset{\sim}{G}^{\nu\nu'}(\underset{\sim}{k}) = \exp(-i\underset{\sim}{k}.\underset{\sim}{d}_{\nu\nu'}) \sum_{\underset{\sim}{P}} \exp(-i\underset{\sim}{k}.\underset{\sim}{P})\underset{\sim}{G}(\underset{\sim}{P}+\underset{\sim}{d}_{\nu\nu'}), \quad (\nu\neq\nu') \tag{2.29a}$$

where $\underset{\sim}{d}_{\nu\nu'} = \underset{\sim}{d}_\nu - d_{\nu'} \neq 0$, and

$$\underset{\sim}{G}^{SP}(\underset{\sim}{k}) = \sum_{\underset{\sim}{P}(\neq O)} \exp(-i\underset{\sim}{k}.\underset{\sim}{P})\underset{\sim}{G}(\underset{\sim}{P}) \tag{2.29b}$$

The terms $\underset{\sim}{\tau}_\nu$, $\underset{\sim}{G}^{\nu\nu'}(\underset{\sim}{k})$ and $\underset{\sim}{G}^{SP}(\underset{\sim}{k})$ occur in LEED theory, (Beeby (1968)), but the term $\underset{\sim}{\tau}_{\nu_e} \underset{\sim}{t}^{-1}_{\nu_e}$ representing emission and multiple scattering within the emitter subplane is peculiar to electron emission.

The physical interpretation of the multiple scattering series is straightforward. The first term represents electrons reaching the detector having scattered in all possible ways within the emitter subplane only.

The next term represents an electron emitted from an atom in subplane ν_e, scattering in all possible ways within this subplane, then propagating through the $\underline{G}^{\nu\nu_e}(\underline{k})$ term to subplane ν, scattering in all possible ways within this subplane through the $\underline{\tau}_\nu$ term and then propagating through the $\underline{D}(\underline{k})$ term to the detector. The other terms in the series may be similarly interpreted. Finally the intensity $I(\underline{k},\underline{e})$ at the detector will be given by:

$$I(\underline{k},\underline{e}) = |\alpha(\underline{k},\underline{e})|^2 \tag{2.30}$$

2.3.5. Computation of the Multiple-Scattering Series

The multiple scattering series, equation (2.28), may be evaluated by writing it as:

$$\alpha(\underline{k},\underline{e}) = \exp(-i\underline{k}.\underline{e})\underline{D}(\underline{k})(\sum_\nu \underline{T}_\nu)\underline{A} \tag{2.31}$$

where

$$\underline{T}_\nu = \underline{\tau}_\nu \underline{t}_\nu^{-1}\delta_{\nu\nu_e} + \underline{\tau}_\nu \sum_{\nu' \neq \nu} \underline{G}^{\nu\nu'}(\underline{k})\underline{T}_{\nu'} \tag{2.32}$$

(Beeby (1968), Tong and Van Hove (1977)). It is then straightforward to solve for $\{\underline{T}_\nu\}$ from equation (2.32) by inversion of a matrix. However, in practice, the matrix to be inverted is large, and requires considerable core-storage on a computer. Sometimes, because of core-storage restrictions it is impossible to perform such a calculation. Therefore, as mentioned before, the emphasis in LEED theory is to formulate quick and efficient perturbative methods to evaluate equation (2.28). In this section we will describe the Reverse Scattering Perturbation Theory formulated by Zimmer and Holland (1975).

The multiple scattering series is first written as:

$$\alpha(\underline{k},\underline{e}) = \exp(-i\underline{k}.\underline{e})\underline{D}(\underline{k})\sum_\nu \underline{B}_\nu \tag{2.33}$$

The next term represents an electron emitted from an atom in subplane ν_e, scattering in all possible ways within this subplane, then propagating through the $\underline{G}^{\nu\nu_e}(\underline{k})$ term to subplane ν, scattering in all possible ways within this subplane through the $\underline{\tau}_\nu$ term and then propagating through the $\underline{D}(\underline{k})$ term to the detector. The other terms in the series may be similarly interpreted. Finally the intensity $I(\underline{k},\underline{e})$ at the detector will be given by:

$$I(\underline{k},\underline{e}) = |\alpha(\underline{k},\underline{e})|^2 \tag{2.30}$$

2.3.5. Computation of the Multiple-Scattering Series

The multiple scattering series, equation (2.28), may be evaluated by writing it as:

$$\alpha(\underline{k},\underline{e}) = \exp(-i\underline{k}.\underline{e})\underline{D}(\underline{k})(\sum_\nu \underline{T}_\nu)\underline{A} \tag{2.31}$$

where

$$\underline{T}_\nu = \underline{\tau}_\nu \underline{t}_\nu^{-1}\delta_{\nu\nu_e} + \underline{\tau}_\nu \sum_{\nu'\neq\nu} \underline{G}^{\nu\nu'}(\underline{k})\underline{T}_{\nu'} \tag{2.32}$$

(Beeby (1968), Tong and Van Hove (1977)). It is then straightforward to solve for $\{\underline{T}_\nu\}$ from equation (2.32) by inversion of a matrix. However, in practice, the matrix to be inverted is large, and requires considerable core-storage on a computer. Sometimes, because of core-storage restrictions it is impossible to perform such a calculation. Therefore, as mentioned before, the emphasis in LEED theory is to formulate quick and efficient perturbative methods to evaluate equation (2.28). In this section we will describe the Reverse Scattering Perturbation Theory formulated by Zimmer and Holland (1975).

The multiple scattering series is first written as:

$$\alpha(\underline{k},\underline{e}) = \exp(-i\underline{k}.\underline{e})\underline{D}(\underline{k})\sum_\nu \underline{B}_\nu \tag{2.33}$$

where $\underline{B}_\nu$ is the sum of all terms in equation (2.28) that represent an electron having a final scattering event in subplane ν. The subplanes are now numbered from ν=1 to V=N starting in the top layer, and then having numbered all the subplanes in this layer we then go to the next layer down and so on.

Let $\underline{B}_\nu = \underline{B}_\nu^+ + \underline{B}_\nu^-$

where:

$$\underline{B}_\nu^+ = \sum_{\nu'>\nu} \underline{\tau}_\nu \underline{G}^{\nu\nu'}(\underline{k}) \underline{B}_{\nu'} \tag{2.34}$$

and

$$\underline{B}_\nu^- = \sum_{\nu'<\nu} \underline{\tau}_\nu \underline{G}^{\nu\nu'}(\underline{k}) \underline{B}_{\nu'} \tag{2.35}$$

Now let $\underline{B}_\nu^{-(n)}$ ($\underline{B}_\nu^{+(n)}$) represent the contribution to $\underline{B}_\nu^-$ ($\underline{B}_\nu^+$) from all scattering paths where the electron has reversed direction n times with respect to the ordering of the subplanes.

Therefore

$$\underline{B}_\nu^{-(n)} = \underline{\tau}_\nu \sum_{\nu'<\nu} \underline{G}^{\nu\nu'}(\underline{k}) [\underline{B}_{\nu'}^{-(n)} + \underline{B}_{\nu'}^{+(n-1)}] \tag{2.36a}$$

and

$$\underline{B}_\nu^{+(n)} = \underline{\tau}_\nu \sum_{\nu'>\nu} \underline{G}^{\nu\nu'}(\underline{k}) [\underline{B}_{\nu'}^{+(n)} + \underline{B}_{\nu'}^{-(n-1)}] \tag{2.36b}$$

with the boundary conditions:

$$\text{(i)} \quad \underline{B}_\nu^{-(0)} = 0: \quad \nu < \nu_e \tag{2.37a}$$

$$\text{(ii)} \quad \underline{B}_\nu^{+(0)} = 0: \quad \nu > \nu_e \tag{2.37b}$$

$$\text{(iii)} \quad \underline{B}_{\nu_e}^{-(0)} = \underline{B}_{\nu_e}^{+(0)} = \underline{\tau}_{\nu_e} \underline{t}_{\nu_e}^{-1} \underline{A} \tag{2.37c}$$

Hence from equations (2.36) and (2.37) to zeroth order in reverse scattering it is found that

$$\sum_\nu \underline{B}_\nu^{(0)} = \sum_\nu [\underline{B}_\nu^{-(0)} + \underline{B}_\nu^{+(0)}] - \underline{\tau}_{\nu_e} \underline{t}_{\nu_e}^{-1} \underline{A} \tag{2.38}$$

The $-\underline{\tau}_{\nu e}\underline{t}_{\nu e}^{-1}\underline{A}$ term is necessary, because without it we would be counting twice scattering within the emitter subplane only. $\underline{B}_{\nu}^{+(1)}$ and $\underline{B}_{\nu}^{-(1)}$ ($\nu=1,2....N$) may then be found by substituting for $\underline{B}_{\nu}^{+(0)}$ and $\underline{B}_{\nu}^{-(0)}$ in equations (2.36a) and (2.36b). Finally to M^{th} order in reverse scattering the amplitude of the electron at the detector is given by:

$$\alpha(\underline{k},\underline{e}) = \exp(-i\underline{k}.\underline{e})\underline{D}(\underline{k}) \sum_{\nu=1}^{N}\sum_{n=0}^{M}[\underline{B}_{\nu}^{-(n)} + \underline{B}_{\nu}^{+(n)}]$$

$$- \underline{\tau}_{\nu e}\underline{t}_{\nu e}^{-1}\underline{A} \qquad (2.38)$$

Being an iterative procedure, the convergence of the above series may be easily checked.

2.4. Calculation of the Atomic Potential

In the derivation of the angle-resolved intensity from an atomic orbital, two quantities were mentioned:

(i) the set of phase shifts δ_{ℓ} ($\ell=0,1,2...$) for each atomic type, and

(ii) the photoionization amplitudes for the orbital, given by:

$$\sigma_{n\ell,\ell\pm1} = \frac{1}{\hbar\omega}\int_{0}^{R_{MT}} R_{\ell\pm1}(r)\,\frac{dV(r)}{dr}\,U_{n\ell}(r)\,r^{2}dr \qquad (2.39)$$

In the muffin-tin approximation it may be shown, (Roman (1965), that the ℓ^{th} phase shift for an atom is given by:

$$e^{2i\delta_{\ell}} = \frac{L_{\ell}h_{\ell}^{-}(kR_{MT}) - (h_{\ell}^{-}(kR_{MT}))'}{L_{\ell}h_{\ell}^{+}(kR_{MT}) - (h_{\ell}^{+}(kR_{MT}))'} \qquad (2.40)$$

where k is the electron wavevector in the crystal and

$$L_{\ell} = \left[\frac{1}{R_{\ell}(r)}\,\frac{dR_{\ell}(r)}{dr}\right]_{r=R_{MT}} \qquad (2.41)$$

which is the logarithmic derivative of $R_\ell(r)$, the radial part of the wavefunction of the emitted electron, evaluated at $r=R_{MT}$. $R_\ell(r)$ may be found by numerically integrating the radial Schrödinger equation:

$$\frac{d^2}{dr^2}[rR_\ell(r)] + (k^2 - V(r) - \frac{\ell(\ell+1)}{r^2})(rR_\ell(r)) = 0 \qquad (2.42)$$

where $V(r)$ is the atomic potential.

Therefore, to calculate the phase shifts and $\sigma_{n\ell,\ell\pm1}$ we need to be able to calculate $U_{n\ell}(r)$ and $V(r)$. Herman and Skilman (1963) and Clementi and Raetti (1974) have calculated $U_{n\ell}(r)$ for various atoms in the ground state by using the self-consistent Hartree-Fock method. The problem of constructing $V(r)$ for a crystal has been extensively studied in the field of band structure theory. We will use a formulation which is based on a scheme which is described in Loucks, with extensions by Pendry (1974). The atomic potential is split up as:

$$V(r) = V_c(r) + V_x(r) + V_i(r) \qquad (2.43)$$

where $V_c(r)$ is the total Coulombic potential, $V_x(r)$ is the total exchange potential and $V_i(r)$ is the ionic contribution to the potential. It should be emphasised that each of these terms include contributions from neighbouring atoms. We shall now describe how each of the terms on the right-hand side of equation (2.43) are calculated.

2.4.1. Calculation of the Coulombic Potential, $V_c(r)$

The Coulombic potential of an isolated atom, $V_c^a(r)$, may be split up as:

$$V_c^a(r) = V_{ce}^a(r) + V_{cn}^a(r) \qquad (2.44)$$

where $V_{ce}^a(r)$ is the contribution to $V_c^a(r)$ arising from the electrons bound to the atom and $V_{cn}^a(r)$ is the contribution from the nuclear charge. In Hartree atomic units

$$V^a_{cn}(r) = \frac{z}{r} \tag{2.45}$$

where z is the nuclear charge, and $V^a_{ce}(r)$ may be found from Poisson's equation

$$\nabla^2 V^a_{ce}(r) = -4\pi\rho^a(r) \tag{2.46}$$

where $\rho^a(r)$ is the spherically averaged charge density of the electrons bound to the atom. $\rho^a(r)$ is given by:

$$\rho^a(r) = \sum_n \sum_\ell 2(2\ell+1) f_{n\ell} |U_{n\ell}(r)|^2 \tag{2.47}$$

where $f_{n\ell}$ is the fractional occupation of the atomic state specified by quantum numbers n and ℓ, and the summations run over occupied states.

The method employed for solving equation (2.46) may be found in Loucks (1967). The spherically symmetric contributions to $V^a_c(r)$ from neighbouring atoms is added in by use of the Löwdin alpha expansion method,(Löwdin (1956)). The final result is that the spherically symmetric contribution at the point $\underline{r}_2$ measured with respect to the origin of atom 2, due to the spherically symmetric Coulombic potential $V^a_c(r_1)$ at the point $\underline{r}_1$, measured with respect to the origin of atom 1 is given by:

$$V^a_c(a,r_2) = \frac{1}{2ar_2} \int_{|a-r_2|}^{a+r_2} r_1 V^a_c(r_1) dr_1 \tag{2.48}$$

where a is the distance between the two origins. Thus the contributions to the Coulombic potential from neighbouring atoms are added in as:

$$V_c(r) = V^a_c(r) + \sum_i V^a_c(a_i,r) \quad . \tag{2.49}$$

2.4.2. Calculation of the Exchange Potential, $V_x(r)$.

The calculation of $V_x(r)$, the atomic exchange potential, by the Hartree-Fock method is extremely complicated. Dirac (1930) calculated the exchange interaction V^i_x between an electron with wave-vector k_i and

a free electron gas as:

$$V_x^i = -\frac{2}{\pi} k_F F(\eta) \tag{2.50}$$

(where Hartree atomic units are used), where $k_F = (3\pi^2\rho)^{1/3}$, ρ is the charge density of the electron gas, $\eta = k_i/k_F$ and

$$F(\eta) = \frac{1}{2} + \frac{(1-\eta^2)}{4\eta} \ln\left|\frac{1+\eta}{1-\eta}\right| \tag{2.51}$$

In the Local Density Approximation (LDA), each small volume element of the electron cloud bound to the nucleus is assumed to behave like an infinite free electron gas with the charge density of that element. Thus within the LDA, the exchange interaction between an electron with wave-vector k_i and the electrons bound to the nucleus is given by:

$$V_x^i(r) = -\frac{2}{\pi} k_F(r)\ F(\eta(r)) \tag{2.51a}$$

where now $\rho = \rho(r)$.

Slater (1951) averaged $V_x^i(r)$ over all electron energies below the Fermi level, and found for the average value of $F(\eta)$:

$$[F(\eta)]_{AV} = \frac{\int_0^1 F(\eta)\eta^2 d\eta}{\int_0^1 \eta^2 d\eta} = \frac{3}{4} \tag{2.52}$$

Thus the averaged potential, (for all the electrons bound to the atom), is given by:

$$V_x(r) = -3\alpha \left\{\frac{3\rho(r)}{8\pi}\right\}^{1/3} \tag{2.53}$$

with $\alpha = 1$. $V_x(r)$ is now easy to compute. Kohn and Sham (1965) later showed by a more elaborate calculation that $V_x(r)$ should be given by equation (2.53), but with $\alpha = 2/3$. In practice, equation (2.53) has been used to calculate the exchange potential with α being allowed to vary between 0 and 1; this procedure is known as the Slater Xα approximation.

Schwartz (1972) has calibrated α for various atoms by computing the potential energy, V, and kinetic energy, T, using the Hartree-Fock equations and Xα orbitals and varying α until the Virial Theorem, $V = -2T$ is satisfied. In this way, it has been found that α varies from about 0.77 for light atoms such as He down to 0.70 for heavier atoms such as Nb. The Xα approximation has been successful in atomic and molecular orbital calculations, and in band structure calculations (see e.g. Slater (1979)).

For a crystal, following the prescription described in Loucks, $\rho(r)$ is found by the superposition of atomic charge densities from neighbouring atoms onto the atomic charge density $\rho^a(r)$, in the same way as was done for the Coulomb potential, i.e.:

$$\rho(r) = \rho^a(r) + \sum_i \rho^a(a_i, r) \qquad (2.54)$$

It should be noted that this procedure neglects the effects of bonding between neighbouring atoms. Having found $\rho(r)$ from equation (2.54), $V_x(r)$ may then be found from equation (2.53).

The Xα approximation has been used to calculate atomic potentials in LEED and it has been found on the whole adequate to put $\alpha = 1$ in equation (2.53) to calculate the exchange contribution to the atomic potential. The success of using this approximation in LEED is surprising, because the Xα method was originally only intended to be used to calculate ground state properties of atoms, molecules and solids. This is a very different situation from the LEED problem where the scattering electrons have kinetic energies many times larger than the Fermi energy.

2.4.3. Calculation of the Ionic Contribution, $V_i(r)$.

To include ionic effects in the calculation, point charges are placed at the centres of each atom j at $\underline{r}_j$, and the ionic contribution $V_i(r)$ is found from:

$$V_i(r) = \sum_j \frac{Z_j}{|\underline{r}-\underline{r}_j|}$$

where Z_j is the ionicity of atom j. In all our calculations of the atomic phase shifts and photoionization amplitudes we will not have cause to add on this contribution and we shall set $V_i(r) = 0$.

2.4.4. Calculation of the Constant Potential Between Muffin-Tins.

In the programs that we use, random points within the crystal lattice are chosen by a Monte-Carlo procedure. From those points outside the muffin-tin radius, the total potential is found and this is then divided by the number of points outside the muffin tins to obtain an estimate for the average potential between muffin tins. This constant potential should in theory be used as the real part of the inner potential in our photoelectron diffraction calculations. In practice, however, as mentioned before, it has been found in the case of LEED that this quantity is best determined empirically by aligning theoretical with experimental peaks in the I:V curves.

2.4.5. Practical Considerations

The calculation of the phase shifts and photoionization amplitudes described above are carried out by the "MUFFPOT" computer programs, (available from Daresbury Laboratory). This program is based on programs published in Loucks (1967) and Pendry (1974), with modifications.

A question now arises as to the crystal structure that we should use to calculate the atomic potential. It has generally been found that adequate phase shifts may be computed, for use in LEED calculations, by putting the atom of interest onto the bulk crystal lattice. The muffin tin radius is chosen to be equal to half the distance between nearest neighbours. This approximation has been found inadequate in LEED

calculations for CO on Ni (001) where it has been found (Tong et al (1980)) that it is better to perform Xα calculations for a NiCO molecule in order to obtain adequate phase shifts for C and O. Initially we put $\alpha = 1$ in equation (2.53) to calculate the exchange contribution to the potential.

A problem now arises in the fact that the phase shifts $\{\delta_\ell\}$ occur in two parts of the calculation; (i) in the description of the wavefunction of the unscattered emitted electron, (equation (2.10)), and (ii) in describing the scattering of the electron by the surface atoms through the factor $t_{\underline{s}}^{\ell\ell}$ in equation (2.25). The question now should be asked whether we should be using the same set of phase shifts for the emitter in the two parts of the calculation, given that the electron will be experiencing a different potential in each case. In (i), for example, one could take into account the effect of the hole potential on the outgoing electron by calculating phase shifts using the wavefunctions for the neutral atom, but decreasing by one the number of electrons in the shell from which the electron has been emitted and increasing by one the charge on the nucleus. This approximation assumes that the other electrons of the atom do not have time to respond to the creation of this hole during the emission process. However, in process (ii), the electron will be scattering off both neutral atoms and unrelaxed atoms, and so it is not clear which phase shifts we should be using, in this part of the calculation for the atoms in the emitter subplane. In any case we cannot use different phase shifts for parts (i) and (ii) of the calculation, because it has been assumed in the derivation of $I(\underline{k},\underline{e})$ that the surface potential is periodic in the surface plane, and so we must use the same phase shifts for both parts.

We shall in fact use phase shifts for the neutral atom in our calculation, because these have been found adequate to describe the experimental data in LEED and photoelectron diffraction.

REFERENCES FOR CHAPTER 2

Beeby, J. L., J. Phys. C1, 82 (1968).

Clementi, E., and Roetti, C., At. Data. Nucl. Data Tables, 14, 177 (1974).

Coulson, C. A., Valence, Second Edition, (Oxford University Press, 1965).

Dirac, P. A. M., Proc. Camb. Phil. Soc., 26, 376 (1930).

Dirac, P. A. M., The Principles of Quantum Mechanics, (Oxford University Press, 1967).

Duke, C. B., and Laramore, G. E., Phys. Rev. 2, B4765 (1970).

Feibelman, P. J., Phys. Rev. B14, 762 (1976).

Feuerbacher, B. and Willis, R. F., J. Phys. C9, 169 (1976).

Grimley, T. B., in: NATO Advanced Study Institute. Electronic Structure and Reactivity of Metal Surfaces, eds. E. G. Derouane and A. A. Lucas, (Plenum, New York, 1976).

Herman, F. and Skillman, S., Atomic Structure Calculations, (Prentice-Hall, 1963).

Holland, B. W., Surf. Sci. 28, 258 (1971).

Holland, B. W., J. Phys. C8, 2679 (1975).

Holland, B. W., Surf. Sci. 68, 490 (1977).

Kliewer, K. L. in 'Photoemission and the Electronic Properties of Surfaces', eds. B. Feuerbacher, B. Fitton, and R. F. Willis, (Wiley, New York, 1978).

Kohn, W. and Sham, L. J., Phys. Rev. 140, A1133 (1965).

Landau, D. and Lifschitz, E. M., Quantum Mechanics - Non Relativistic Theory, (Pergamon, London, 1959).

Laramore, G. E. and Duke, C. B., Phys. Rev. B2 , 4783 (1970).

Li, C. H., Lubinsky, A. R. and Tong. S. Y., Phys. Rev. B17, 3128 (1977).

Liebsch, A., Phys. Rev. B13, 544 (1976).

Loucks, T., Augmented Plane Wave Method,(Benjamin, New York 1967).

Löwdin, P. O., Adv. Phys. 5, 1 (1956).

McDonnell, L., Woodruff, D. P. and Holland, B. W., Surf. Sci. 51, 249 (1975).

Messiah, A., Quantum Mechanics, (Amsterdam, North Holland, 1964).

Mukhopadyay, G. and Lundqvist, S., Physica Scripta, 17, 69 (1978).

Pendry, J. B., Low Energy Electron Diffraction, (Academic Press, London, 1974).

Pendry, J. B., J. Phys. C8, 2413 (1975).

Pendry, J. B., Surf. Sci. 57, 679 (1976).

Roman, P., Advanced Quantum Theory, (Addison-Wesley, Reading, 1965).

Schwartz, K., Phys. Rev. B5, 2466 (1972).

Slater, J. C., Phys. Rev. 81, 385 (1951).

Slater, J. C., The Calculation of Molecular Orbitals, (Wiley, New York, 1979).

Tong, S. Y., Maldano, A., Li, C. H., and Van Hove, M. A., Surf. Sci. 94, 73 (1980).

Tong, S. Y. and Van Hove, M. A., Solid State Comm. 19, 543 (1976).

Tong, S. Y., and Van Hove,M. A., Phys. Rev. B16, 1459 (1977).

Van Hove, M. A. and Tong, S. Y., Surface Crystallography by LEED, (Springer-Verlag, Berlin, 1979).

Woodruff, D. P., Surface Science, 53, 538 (1975).

Zimmer, R. S. and Holland, B. W., J. Phys. C8, 2395 (1975).

CHAPTER 3

THE SENSITIVITY OF AZIMUTHAL PHOTOELECTRON DIFFRACTION PATTERNS TO STRUCTURAL AND NON-STRUCTURAL PARAMETERS

3.1. Introduction

Before we make detailed comparisons with experiment, we will first turn to the question of how sensitive azimuthal photoelectron diffraction is to changes in structural and non-structural parameters as compared with other surface techniques. Also we will try to see whether we can decide on the experimental configuration that will give us optimum sensitivity to structure, (i.e. $d_\perp$ and bonding site). We shall then determine how sensitive azimuthal photoelectron diffraction is to changes in non-structural parameters such as the detector angle, the angle of incidence of the radiation and the photon energy. If the diffraction patterns are sensitive to these parameters then this means that it is necessary to perform the experiments with great precision.

3.2. Sensitivity of the Diffraction Patterns to Structural Parameters

We shall first turn our attention to the system Ni(001) - c(2 x 2)Na which has already been studied by LEED, (Andersson and Pendry (1975), Demuth et al (1975)), and CIS normal emission, (Williams et al (1979), Li and Tong (1979a)). From LEED it has been concluded that in the c(2 x 2) configuration the Na atoms distribute themselves in the hollows on the Ni(001) surface with a $d_\perp$-spacing of 2.23 Å. Li and Tong's CIS calculations agree with the experimental data using the LEED structure. Azimuthal photoelectron diffraction experiments have been performed on this system where emission from the Na2p level was studied (Woodruff et al (1978)).

The detector was set at 30° to the surface normal. The radiation which came from the Tantalus storage ring was p-polarised and incident on the surface at 45° to the outward normal in the same plane as the detector, with the $\underset{\sim}{A}$-vector and detector on the same side of the surface normal. Photon energies of 80 eV, 90 eV and 100 eV were used corresponding to electron kinetic energies in vacuo of approximately 46 eV, 56 eV and 66 eV respectively. In all the theoretical and experimental plots that we will show, azimuth ϕ = 0° corresponds to the Ni[100] direction.

In the calculations, the Ni inner potential (11 eV) and the electron mean free path (8 Å) are taken from the LEED calculation, (Demuth et al (1975)), as are all the structural parameters. The phase shifts for Ni are taken from a Wakoh band structure calculation (Wakoh (1965)), and the Na phase shifts are calculated by the procedure described in section (2.4), where Clementi wavefunctions, (Clementi and Roetti (1974)) are used to calculate the electron density. The other parameters that we need that do not occur in a LEED calculation are the photoionization amplitudes $\sigma_{n\ell,\ell+1}$ and $\sigma_{n\ell,\ell-1}$, (equation (2.13)), for the Na2p state. At the time that these calculations were carried out the 'MUFPOT' programs had not been adapted to calculate these quantities. However, by looking at McGuire's (McGuire (1970)) photoionization cross-section calculations for Na2p, we can estimate the magnitude of the ratio $\sigma_{n\ell,\ell+1}/\sigma_{n\ell,\ell-1}$ as being ≈ 5 in the energy range of interest. Ambiguities enter into the sign of this ratio but in any case we have found from our calculations that the photoelectron diffraction patterns for this system are relatively insensitive to the magnitude and sign of this ratio. It should be noted that this insensitivity to the ratio may not hold for other systems. The scattering electron is described by six partial waves and the multiple scattering series is evaluated to sixth order in reverse scattering. Calculations are performed for one layer of Na and six layers of Ni, (making thirteen subplanes in all).

Fig. 3.1: Comparison between theory and experiment for the azimuthal dependence of photoemission from the Na 2p levels for Ni(001) - c(2 x 2)Na at kinetic energies 46 eV and 56 eV. The full curves include full adsorbate-substrate scattering and the dashed curves adsorbate intra-layer scattering only.

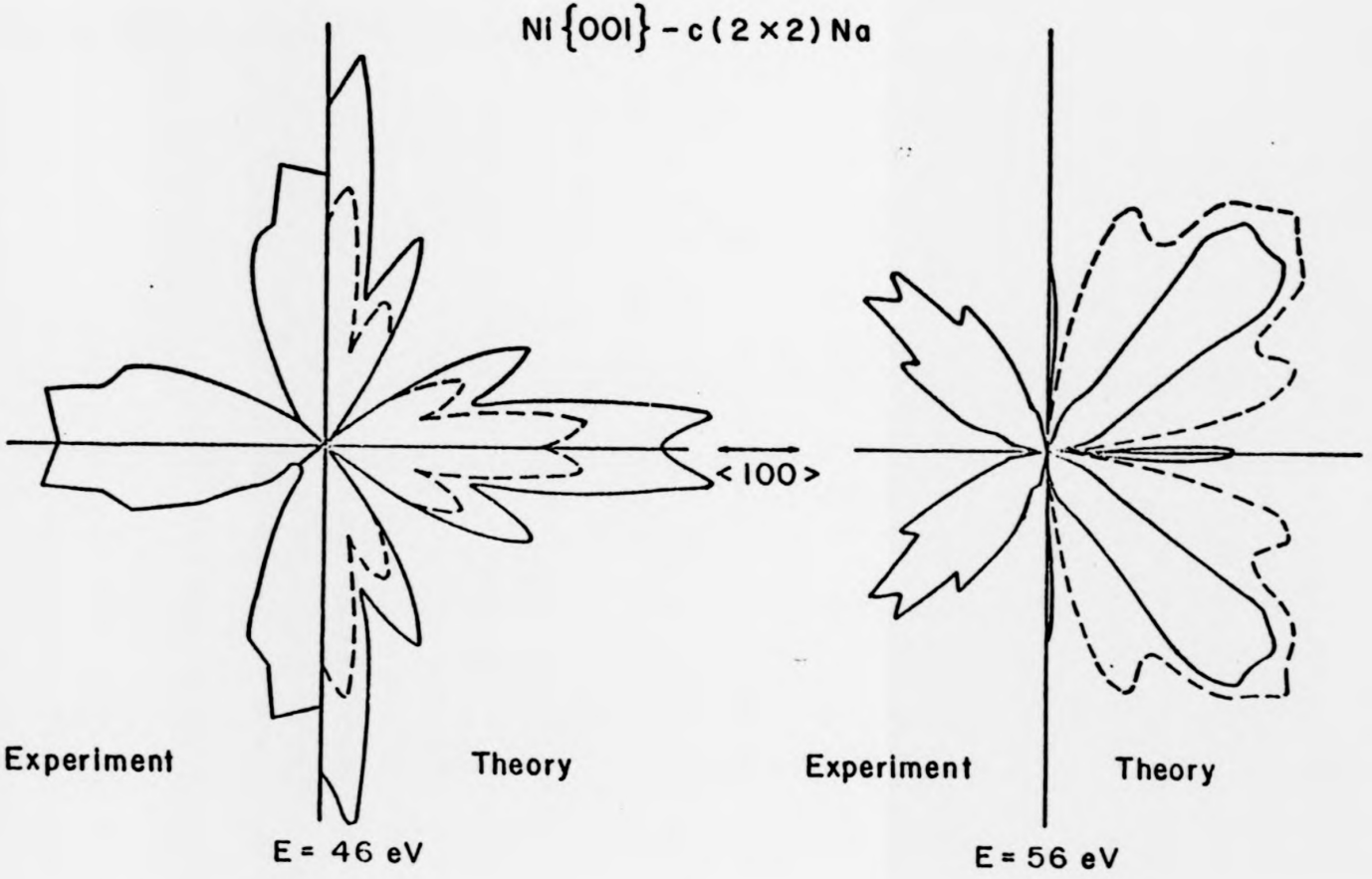
Ni {001} - c(2×2) Na
<100>
Experiment
Theory
E = 46 eV
Experiment
Theory
E = 56 eV

The calculation for $\hbar\omega$ = 100 eV unfortunately does not converge. We present in Fig.(3.1) the calculations and experimental data, (Woodruff et al (1978)), for photon energies $\hbar\omega$ = 80 eV and 90 eV, (these calculations were performed by Dr. D. Norman). For the purposes of clarity the curves have been plotted with the minimum intensity subtracted out. It is seen that there is very good agreement between theory and experiment for both curves with all the minor features of the data being reproduced by the theory. We should now ask how sensitive the curves are to changes in $d_\perp$ and bonding site. Extensive calculations varying these parameters have been performed for $\hbar\omega$ = 80 eV. It has been found that the curves are insensitive to whether one puts the Na atom in a bridge site, one-fold site or four-fold site. Also, varying the $d_\perp$-spacing over a range of 0.4 Å does not significantly alter the overall shape of the curve. This suggests that the majority of the scattering is taking place within the Na overlayer only. This is discouraging from the point of view of structural determination because it is scattering between the adlayer and substrate that is going to give us information on the position of the Na atom. Li and Tong (Li and Tong (1979b)) have come to similar conclusions with their work on Se 3d emission from Ni(001) - c(2 x 2)Se, where it has been found that the azimuthal diffraction pattern for three different photon energies are insensitive to changes in structure. It has been suggested that this may be a general phenomenum for azimuthal photoelectron diffraction.

To test whether this is the case with Na on Ni we perform calculations for $\hbar\omega$ = 80 eV and 90 eV where we just consider scattering within the Na overlayer. Our results are shown in Fig. (3.1) where we compare the overlayer calculations with full thirteen subplane calculations. As expected, the overlayer calculation for $\hbar\omega$ = 80 eV is almost identical in overall shape to the full calculation. However, the overlayer calculation for

Fig. 3.2: Calculations for the azimuthal variation of photoelectron intensity for Na 2p emission from Ni(001) - c(2 x 2)Na at 30° to outward surface normal for photon energy 90 eV for the following configurations:

(a) four-fold, $d_{\perp}$ = 2.13 Å

(b) four-fold, $d_{\perp}$ = 2.33 Å

(c) bridge

(d) one-fold structure.

R is the ratio of the maximum to the minimum intensity.

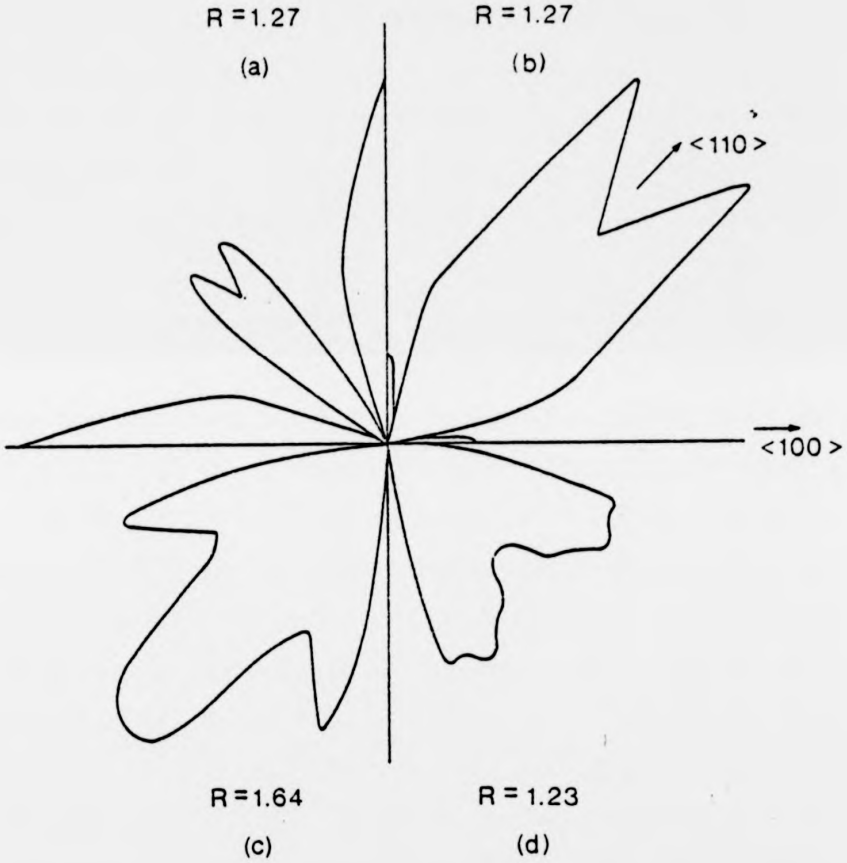
R = 1.27
(a)
R = 1.27
(b)
<110>
<100>
R = 1.64
(c)
R = 1.23
(d)

$\hbar\omega$ = 90 eV is markedly different from the full calculation suggesting that scattering between the overlayer and substrate is significant and therefore at this energy there should be sensitivity of the diffraction pattern to structure. To test whether this is the case, we have performed full, thirteen subplane calculations for $\hbar\omega$ = 90 eV for different bonding sites and $d_\perp$-spacings. Our results are shown in Fig. (3.2). In particular we see that in going from $d_\perp$ = 2.13 Å to 2.33 Å in the four-fold site, the main lobe in the diffraction pattern changes from being in the [100] direction to the [110] direction. Our findings thus show that at some photon energies, azimuthal photoelectron diffraction will be sensitive to structure, whilst at other energies it will not. This stresses the importance of using a synchrotron in these studies so that a large range of photon energies may be used.

We now turn to the question of how one should set up the experiment to optimise the sensitivity of the diffraction pattern to changes in $d_\perp$ and to changes in the bonding site. To optimise the sensitivity of the diffraction pattern to changes in $d_\perp$ we need to set the detector to an angle that will maximise the change in path difference due to a change in $d_\perp$ between electrons emanating from the adlayer and those emanating from the substrate, i.e. one should set the detector to monitor electrons emanating from the crystal at normal exit angle. Thus CIS normal emission should be sensitive to changes in $d_\perp$ and indeed theoretical work (Li and Tong (1979ab)) has shown this to be the case. For azimuthal work, one has to monitor electrons off-normal in order to obtain appreciable anisotropy in the diffraction pattern. Our calculations for $\hbar\omega$ = 90 eV, where the detector is set near to normal ($\theta = 30^\circ$) show that in azimuthal work we can also obtain sensitivity to $d_\perp$. To optimise the sensitivity of the patterns to changes in the bonding site we require there to be sensitivity to lateral displacements. By the above argument this means that maximum

Fig. 3.3: As for fig. 3.2 except that the detector angle is now set at 80° to the outward normal and (d) is the overlayer calculation.

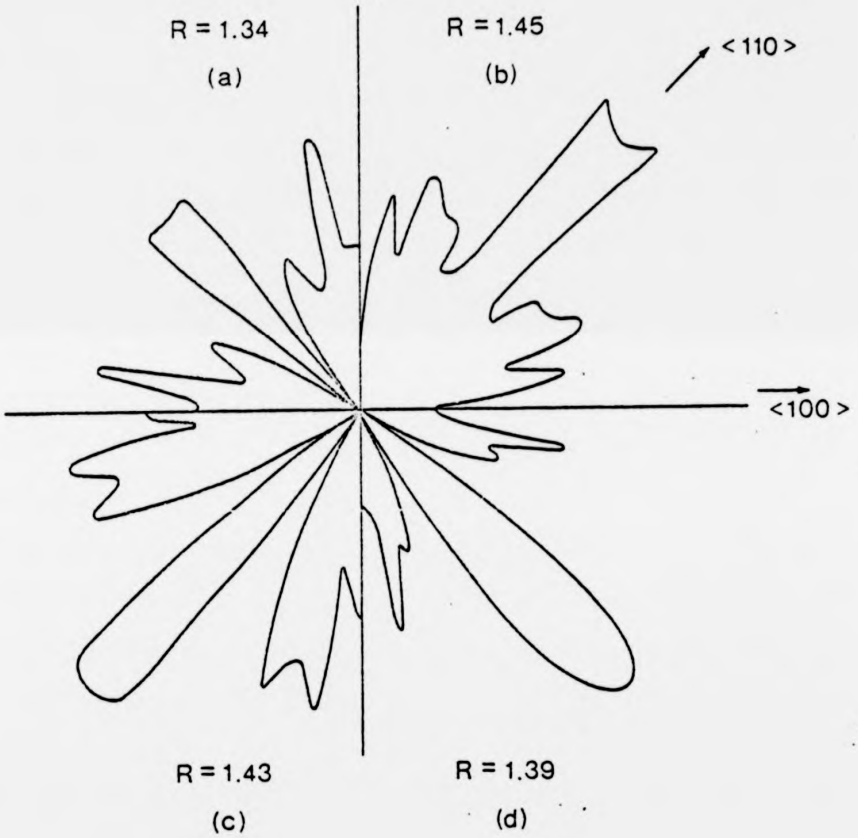
R = 1.34
(a)
R = 1.45
(b)
< 110 >
< 100 >
R = 1.43
(c)
R = 1.39
(d)

sensitivity to the bonding site should be obtained by monitoring electrons emanating from the crystal surface at grazing exit. To see whether this argument holds we carry out azimuthal photoelectron diffraction calculations for $\hbar\omega$ = 90 eV but now the detector is set at an angle of 10° to the surface. In fig. (3.3) we present calculations for Na bonded at a bridge site ($d_{\perp}$ = 2.52 Å), and at the four fold site ($d_{\perp}$ = 2.13 Å and 2.33 Å). We see that the diffraction patterns are very similar to each other. It appears that the diffraction patterns are insensitive to the bonding site in contradiction to the arguments outlined above. This would suggest that at grazing exit, scattering within the Na overlayer is the dominant contribution to the diffraction pattern. This is confirmed if we calculate the diffraction pattern considering scattering within the Na overlayer only, (fig. (3.3d)). This is similar to the thirteen subplane calculations for the bridge and four-fold sites. This contradiction may be explained by the fact that we have missed out an important factor in our argument, that is, the damping of the electron wave by inelastic collisions with the electron gas in the surface region. The substrate wave will be damped by a factor $\exp\{-\ell/d_{\perp}\cos\theta\}$ with respect to the adlayer wave, where ℓ is the mean free path and θ is the angle that the outgoing electron makes with the surface normal before refraction by the surface barrier. This factor will be very small for large θ, and so for grazing exit adlayer contributions will in general dominate. Thus data taken at grazing exit would be useless for structural studies.

Finally in this section on structural sensitivity, we will consider how many subplanes one needs in order to perform an adequate calculation. It is well known in LEED that in order to perform an adequate calculation one has to include a number of layers down to a depth corresponding to approximately four times the mean free path, (see e.g. Pendry (1974)).

Fig. 3.4: Calculations for the azimuthal variation of photoelectron intensity for Na 2p emission from Ni(001) - c(2 x 2)Na, (electron kinetic energy 55 eV) and Se3d emission from Ni(001) - c(2 x 2)Se, (electron kinetic energy 29 eV), varying the number of layers. Upper panel: scattering within the overlayer only, middle panel: scattering between the top three layers. Lower panel: scattering between the top seven layers.

In each case the detector angle is set at 30° to the outward surface normal, and the radiation is p-polarised and incident on the surface at 45° to the surface normal with the detector and light source in the same plane but on opposite sides of the surface normal.

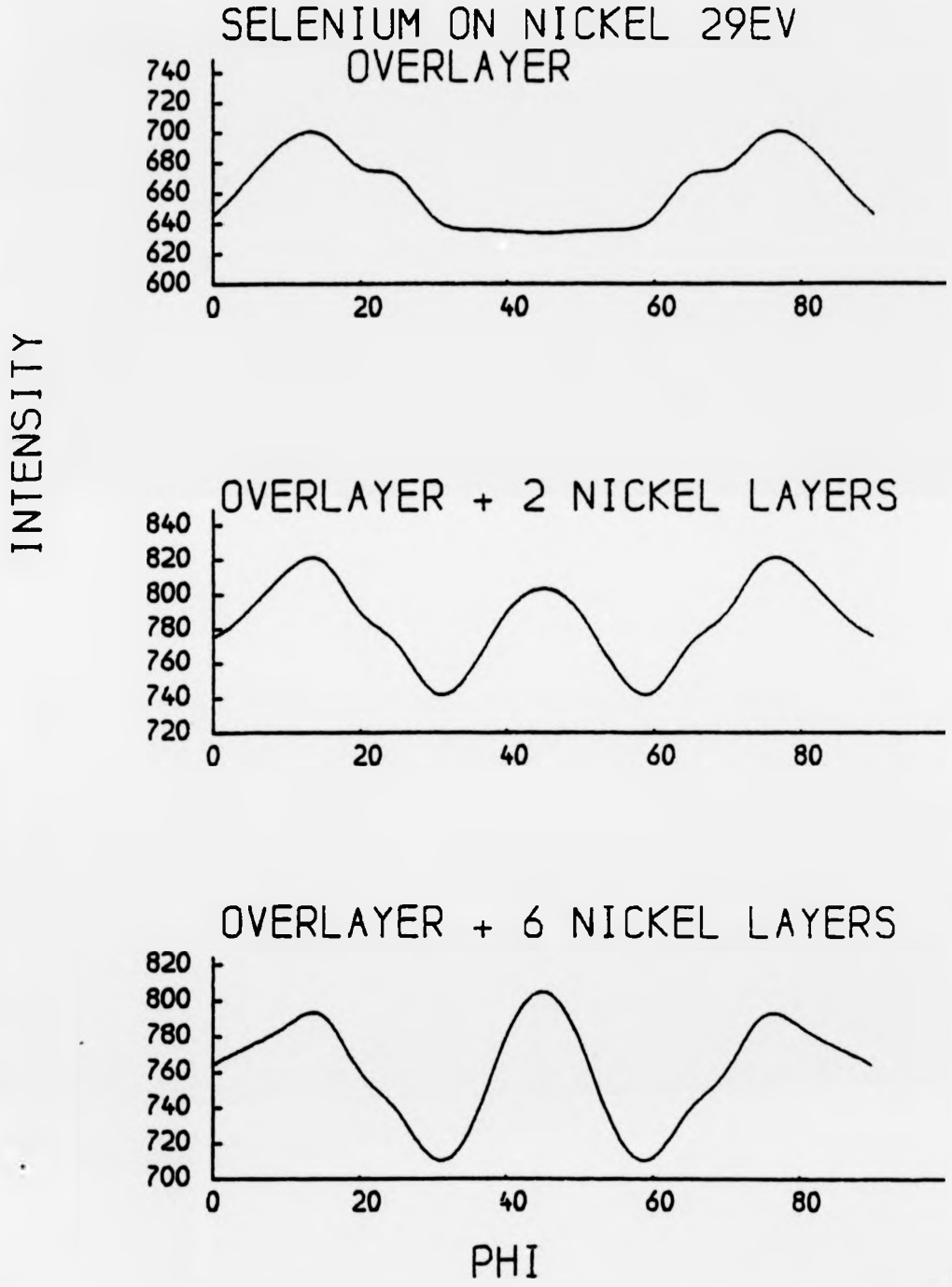
SELENIUM ON NICKEL 29EV
OVERLAYER
740
720
700
680
660
640
620
600
0
20
40
60
80
INTENSITY
OVERLAYER + 2 NICKEL LAYERS
840
820
800
780
760
740
720
0
20
40
60
80
OVERLAYER + 6 NICKEL LAYERS
820
800
780
760
740
720
700
0
20
40
60
80
PHI

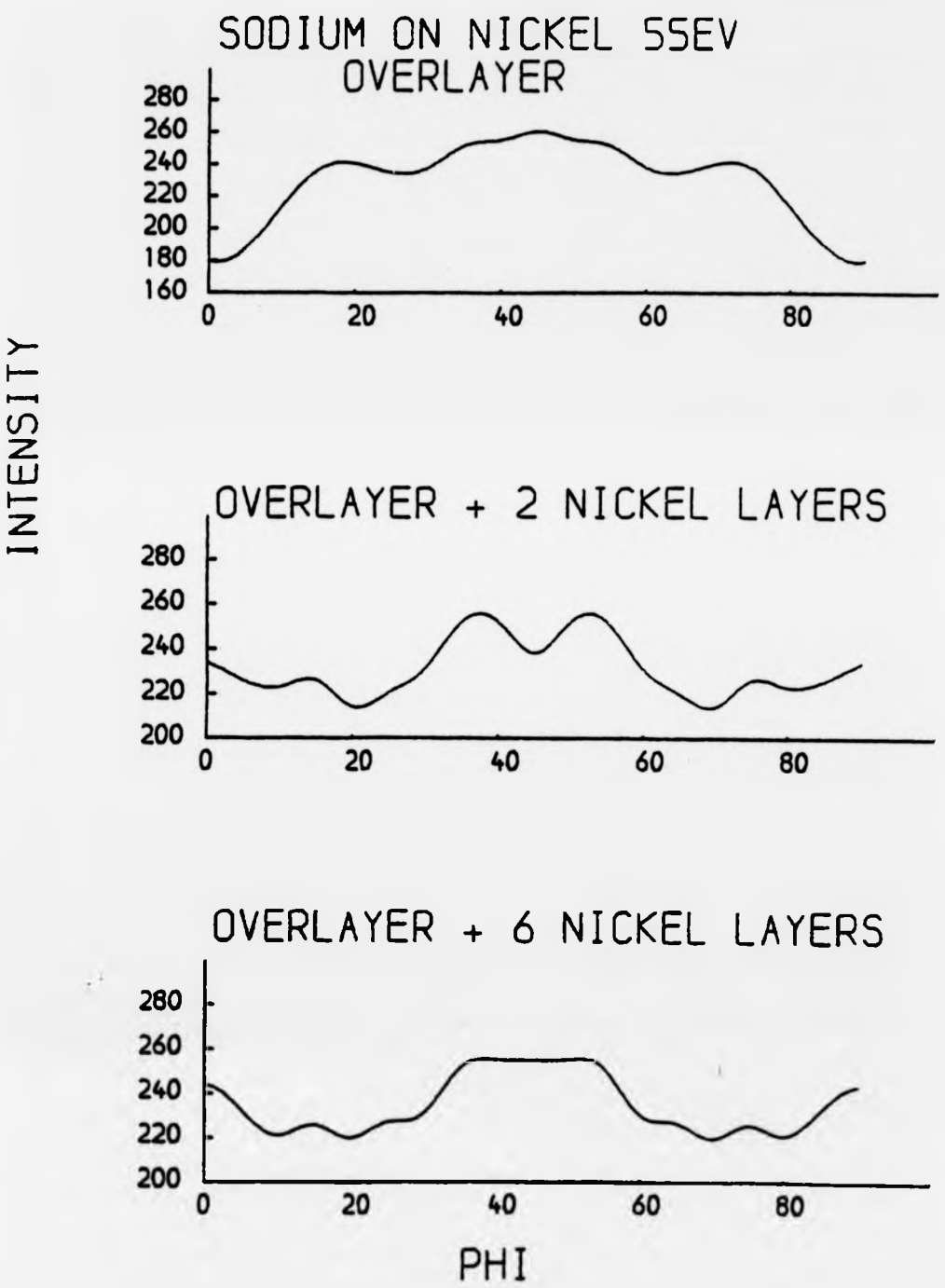
SODIUM ON NICKEL 55EV
OVERLAYER
280
260
240
220
200
180
160
0
20
40
60
80
INTENSITY
OVERLAYER + 2 NICKEL LAYERS
280
260
240
220
200
0
20
40
60
80
OVERLAYER + 6 NICKEL LAYERS
280
260
240
220
200
0
20
40
60
80
PHI

This can be very costly in computer time and it would be of interest to see whether we need to go that deep in azimuthal photoelectron diffraction calculations. In Fig. (3.4) we present calculations at various electron energies for Na 2p emission from Ni(001) - c(2 x 2)Na and Se 3d emission from Ni(001) - c(2 x 2)Se where we have considered scattering taking place in (i) the adsorbate overlayer only (ii) the adsorbate layer plus two substrate layers and (iii) the adsorbate layer plus six substrate layers. We see that for both cases whilst there are significant differences between calculations (i) and (ii), there are only minor differences between calculations (ii) and (iii). Calculations at several other energies for these systems show a similar behaviour, namely that the most important scattering processes take place in the top few layers only, and that scattering of the electron off deeper layers may be ignored. The reason why we do not have to go as deep as LEED in photoelectron diffraction calculations is that whilst in LEED one has a plane wave incident on the surface, in photoelectron diffraction, the wavefunction of the emitted electron already has a $^{1}/_{r}$ dependence as well as being damped by inelastic processes. Thus, in photoelectron diffraction, the most important scattering processes will take place nearer to the crystal surface than in LEED. Thus as a first approximation in the analysis of the experimental data, we should perform calculations that include scattering in the top three or four layers only. If we then find a structure that gives us reasonable agreement with experiment, we should then include more layers in order to refine the calculation. Of course there may be situations where scattering off deeper substrate layers will be important, although our calculations suggest that this should be a rare occurence.

Fig. 3.6: Calculations for the azimuthal variation of photoelectron intensity for Te 4d emission from Ni(001) - c(2 x 2)Te for (a) angle of incidence = 47° (broken curve) and (b) angle of incidence = 45° (full curve). In each case the detector angle is set at 32° to the surface normal.

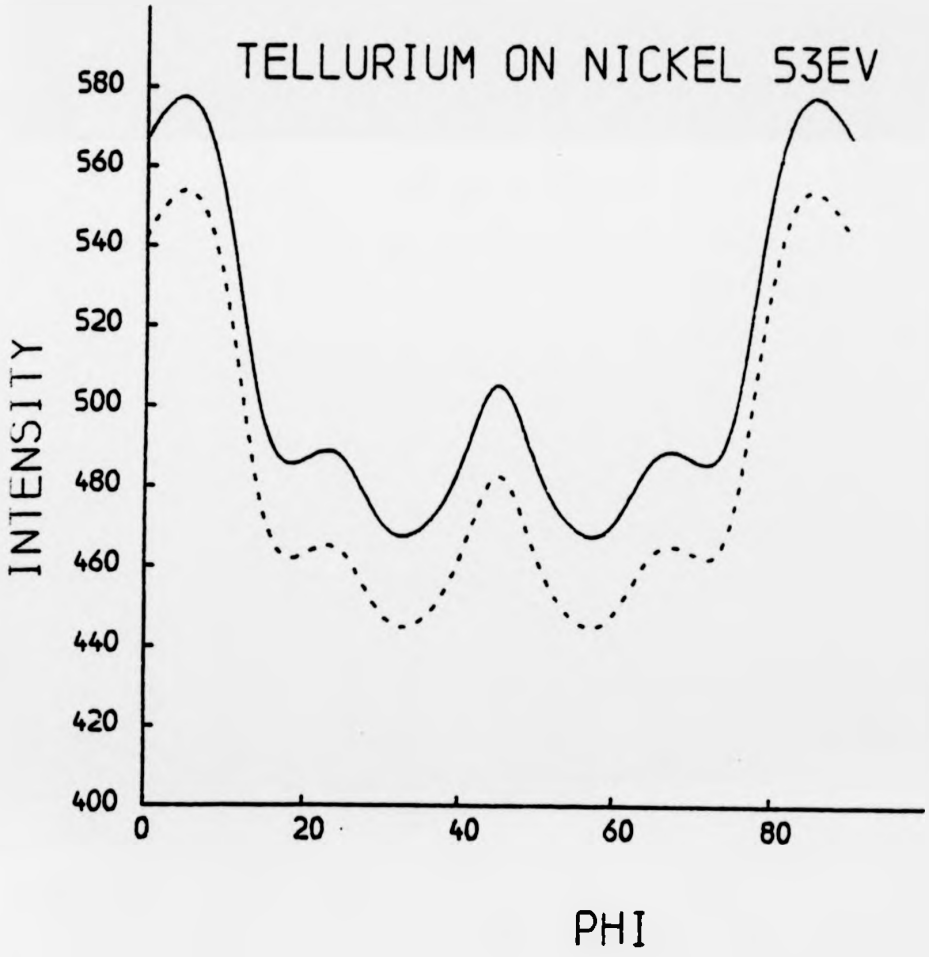
TELLURIUM ON NICKEL 53EV
INIENSITY
580
560
540
520
500
480
460
440
420
400
0
20
40
60
80
PHI

Fig. 3.5: Calculations for the azimuthal variation of photoelectron intensity for Te 4d emission from Ni(001) - c(2 x 2)Te for detector angles 32° (broken curves) and 30° (full curves) for electron kinetic energies 43 eV and 53 eV in the vacuum.

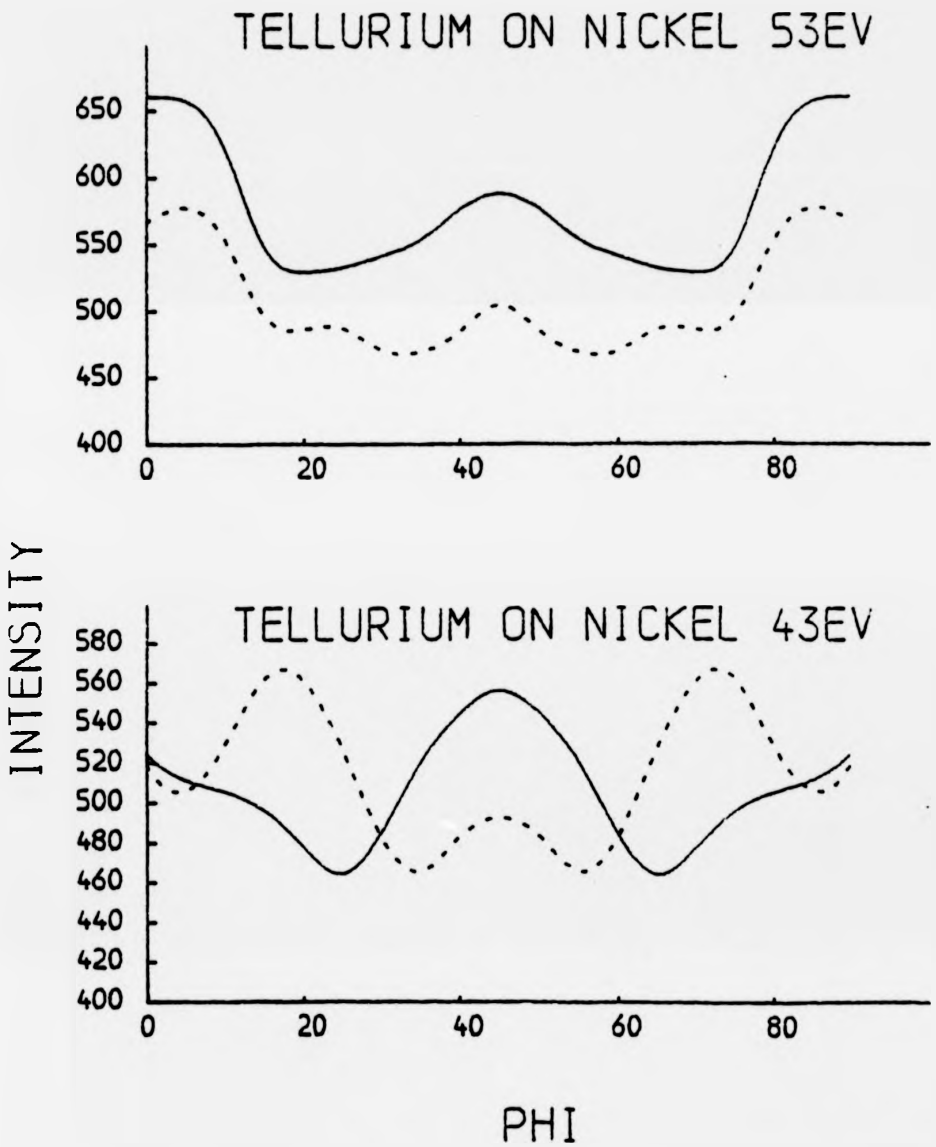
TELLURIUM ON NICKEL 53EV
650
600
550
500
450
400
0
20
40
60
80
TELLURIUM ON NICKEL 43EV
580
560
540
520
500
480
460
440
420
400
0
20
40
60
80
INTENSITY
PHI

3.3. Sensitivity of Diffraction Patterns to Non-Structural Parameters.

We must now consider how sensitive the diffraction patterns are to small changes in non-structural parameters such as the detector angle (θ), the angle of incidence of the electromagnetic wave (ψ) and the photon energy ($\hbar\omega$). These parameters are only known to a certain accuracy, and it is important to know whether the diffraction patterns vary significantly over the range of uncertainty of these parameters. We shall look at the case of Te 4d emission from Ni(001) - c(2 x 2)Te, with the structural and non-structural parameters taken from the LEED calculation, (Demuth et al (1973ab, 1974)). The method of calculating the phase shifts is the same as that for Na.

We first look at the sensitivity of the diffraction pattern to changes in θ. In fig. (3.5) we show calculations for two electron energies where the polar angle has been changed by 2^{o} from its nominal value of 30^{o}. At 43 eV electron kinetic energy this results in a dramatic change in the diffraction pattern whilst at 53 eV the change is quite small. Thus at some photon energies there will be considerable sensitivity of the diffraction pattern to small changes in θ. Thus θ should be known to a high accuracy in order to ensure the reliability of the data.

We next consider the sensitivity of the diffraction pattern to changes in ψ, the angle of incidence of the radiation. In fig. (3.6) we show the effect of changing ψ by 2^{o} from its nominal value of 45^{o} for electron energy 53 eV in the vacuum. The overall shape of the diffraction pattern has hardly changed at all indicating that there is very little sensitivity at these photon energies to small changes in ψ. We have generally found this to be the case at these energies. In connection with this it may be asked how refraction of the electromagnetic wave at the crystal surface alters the diffraction pattern. By using Whittaker's (Whittaker (1978)), formulae for the Fresnel equations and data for the dielectric constant

Fig. 3.7: Calculations for the azimuthal variation of photoelectron intensity for Te4d emission from Ni(001) - c(2 x 2)Te.

Upper panel: kinetic energy = 48 eV

Middle panel: kinetic energy = 51 eV

Lower panel: kinetic energy = 53 eV.

In each case the detector is set at 30° to the surface normal.

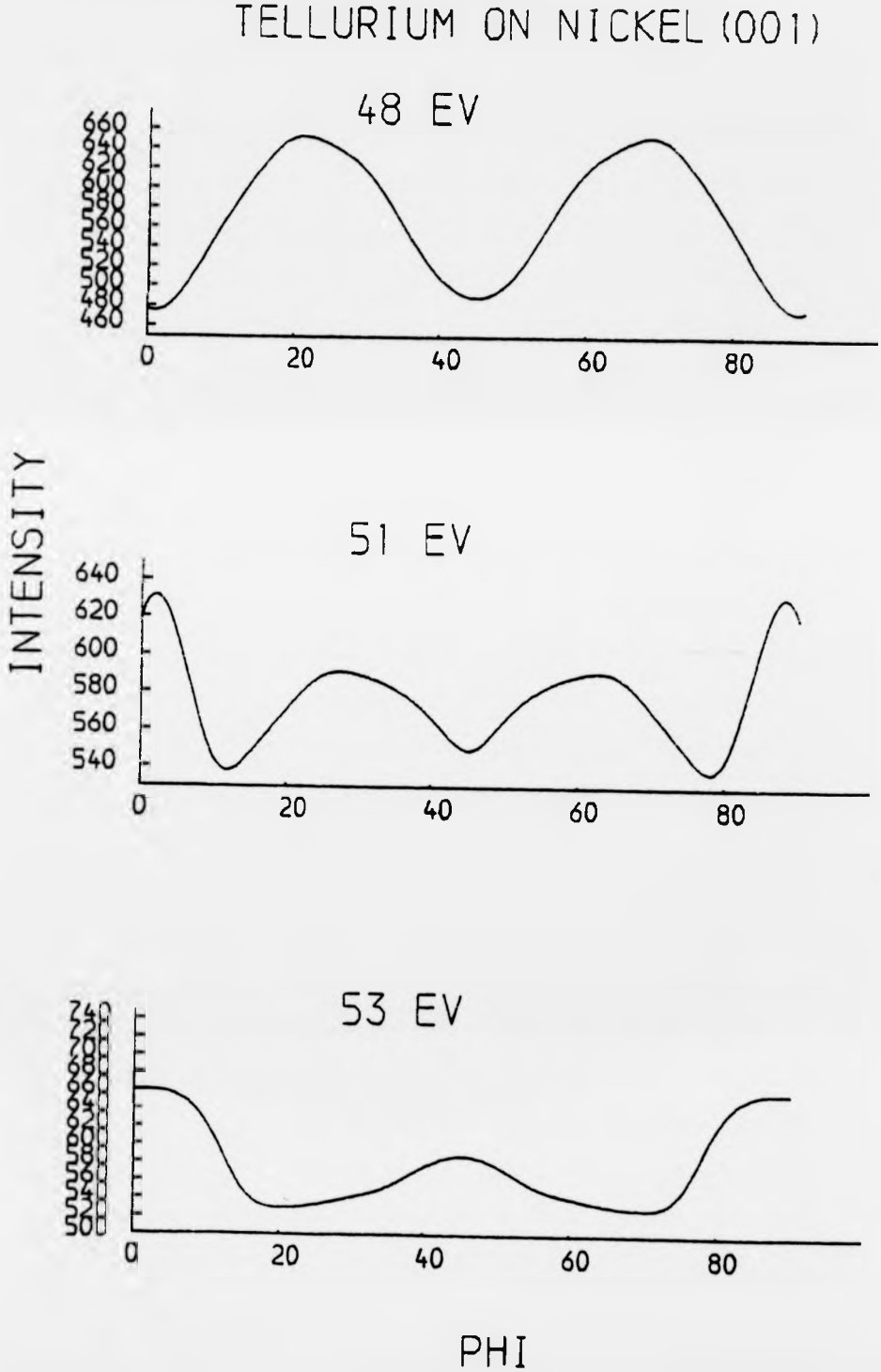
TELLURIUM ON NICKEL (001)
48 EV
660
640
620
600
580
560
540
520
500
480
460
0
20
40
60
80
INTENSITY
51 EV
640
620
600
580
560
540
0
20
40
60
80
53 EV
74
72
70
68
66
64
62
60
58
56
54
52
50
0
20
40
60
80
PHI

of Ni from Wehenkel and Gauthe (1974), we calculate that at $\hbar\omega$ = 80 eV the electromagnetic wave will be refracted by $\simeq 0.2^{\circ}$. Our calculations for the sensitivity to ψ would then suggest that refraction of the electromagnetic wave will have a negligible effect on the diffraction pattern at these energies. Later, in our studies on the emission from oriented molecules where HeI ($\hbar\omega$ = 21.2 eV) and HeII ($\hbar\omega$ = 40.8 eV) radiation is used we shall see that we will then have to include refraction of the electromagnetic wave into our calculations.

We finally turn to the question of the sensitivity of the diffraction pattern to changes in the photon energy. In fig. (3.7) we show plots for the case of Te 4d emission from Ni(001) - c(2 x 2)Te for electron kinetic energies 48 eV, 51 eV and 53 eV in the vacuum. There is little change in the shape of the curve between 51 eV and 53 eV but between 48 eV and 51 eV there is a dramatic change. We have found it to be the general case that in some energy ranges the diffraction patterns are insensitive to small changes in the photon energy whilst in other energy ranges the diffraction patterns are very sensitive to such changes. This is important for emission from shallow core states of heavy atoms where spin-orbit splitting makes it necessary to downgrade the energy resolution of the analyser to $\sim$ 2 eV. Therefore when analysing experimental data we should perform calculations for closely spaced intervals of energy to take into account this uncertainty in the electron energy.

3.4. Summary

Our model calculations for Na, Te and Se adsorbed on Ni(001) demonstrate the advantages and disadvantages of azimuthal photoelectron diffraction as a technique for surface structure determination. On the positive side we have found that at some photon energies we can achieve considerable sensitivity to changes in the structural parameters. The fact that at some energies there is little sensitivity is not a serious

drawback because with synchrotron radiation one has access to a wide range of photon energies. Our calculations also suggest that optimum sensitivity to structure is obtained for polar emission angles lying approximately midway between the surface and surface normal. Also on the plus side we have found that we can perform an adequate calculation by only including the top three or four layers of atoms. This is a saving on computational time as compared with LEED. Our calculations indicate that at the photon energies that are used in the experiments, one can ignore refraction of the electromagnetic wave at the surface.

On the negative side we have found that we can also obtain unwanted sensitivity to small changes in the polar angle and photon energy. Thus, experiments should be performed for closely spaced intervals of energy and polar angle to make it easier to fit trends in the data by the theory.

REFERENCES FOR CHAPTER 3

Andersson, S. and Pendry, J. B., Solid State Comm. 16, 563 (1975).

Clementi, E. and Roetti, C., At. Data Nucl. Data Tables, 14, 177 (1974).

Demuth, J. E., Jepsen D. W. and Marcus, P. M., Phys. Rev. Lett. 31, 540 (1973a).

Demuth, J. E., Jepsen, D. W. and Marcus, P. M., J. Phys. C6, L307 (1973b).

Demuth, J. E., Marcus, P. M., Jepsen, D. W., Phys. Rev. Lett. 32, 1182 (1974).

Demuth, J. E., Jepsen, D. W. and Marcus, P. M., J. Phys. C8, L25 (1975).

Li. C. H., and Tong, S. Y., Phys. Rev. B19, 1769 (1979a).

Li. C. H. and Tong, S. Y., Phys. Rev. Lett., 42, 901 (1979b).

McGuire, E. J., Res. Rep. Sandia Laboratories, Albuquerque, New Mexico(USA), SC-RR-721 (1970).

Pendry, J. B., Low Energy Electron Diffraction (Academic Press, London, 1974).

Wakoh, S., J. Phys. Soc. Japan, 20, 1984 (1965).

Wehenkel, C. and Gauthe, B., Phys. Stat. Sol. (b), 64, 515 (1974).

Whittaker, M. A. B., J. Phys. C11, L151 (1978).

Williams, G. P., Cerrina, F., McGovern, I. T. and Lapeyre, G. J., Solid St. Comm. 31, 15 (1979).

Woodruff, D. P., Norman, D., Holland, B. W., Smith, N. V., Farrell, H. H. and Traum, M. M., Phys. Rev. Lett. 41, 1130 (1978).

CHAPTER 4

CORE STATE EMISSION: COMPARISON BETWEEN THEORY AND EXPERIMENT

4.1. Introduction

The last chapter dealt with the sensitivity of azimuthal photoelectron diffraction patterns to changes in structural and non-structural parameters. We have seen that in some cases photoelectron diffraction has the potential to determine surface structure to a greater accuracy than LEED. However, to determine just how accurate this technique is we must first compare theory with data taken for surface systems that have already been analysed by LEED. If we come to the same conclusions as LEED for the structures for these known systems this will then give us confidence to tackle unknown structures.

In section (4.2) we review the photoelectron diffraction work that has already been carried out for various adsorbate systems. In section (4.3) we then analyse data that has been taken for the surface systems Ni(001) - c(2 x 2)Te, Ni(001) - p(2 x 2)Te and Ag(111) - $(\sqrt{3} \times \sqrt{3})R30^{\circ}$I. We are particularly interested in seeing whether parameters such as the inner potential and atomic phase shifts are directly transferable from the LEED calculations. Finally in section (4.4) the results that are obtained will be discussed.

4.2. Review of Past Work

Photoelectron diffraction experiments using the CIS mode have been performed on the atomic adsorbate systems Ni(001) - c(2 x 2)Na (Williams et al (1979)), Ni(001) - c(2 x 2)Se and Ni(001) - p(2 x 2)Se (Kevan et al (1978, 1979, 1981)), and Ni(001) - c(2 x 2)Te (McGovern et al (1979)). The structures for these systems have already been determined by LEED. For Ni(001) - c(2 x 2)Na, where electrons emitted from the Na2p levels were monitored, good agreement has been obtained between theory (Li and Tong (1979)) and experiment for the positions of the diffraction peaks by using

the structure determined by LEED, (Andersson and Pendry (1975), Demuth et al (1975)). The agreement has not been so good for the relative intensities of the various peaks and this has been attributed to uncertainties in the calculation of the Na2p photoionization amplitudes. For Ni(001) - p(2 x 2)Se and Ni(001) - c(2 x 2)Se where emission from the Se3d levels were studied, excellent agreement has been obtained between theory (Li and Tong (1979)) and experiment for both the relative heights and positions of the various diffraction peaks, again by using the LEED structure (Demuth et al (1973), Van Hove and Tong (1975)). Model calculations have shown that the positions of the peaks in the CIS curve are very sensitive to changes in $d_\perp$ and the bonding site; (e.g. a change of + 0.4 Å in $d_\perp$ produces a - 18 eV shift for one of the diffraction peaks). The photoelectron diffraction curve for c(2 x 2)Se has been found to be fairly insensitive to the models chosen for the Se and Ni potentials which is a very desirable result. Kevan el al (1981) have proceeded to look at the temperature dependence of the CIS normal emission curves for the c(2 x 2) structure, and have found that the temperature dependence of the peak intensities is similar to that found in EXAFS. This has led Kevan et al to postulate that a simpler theory than that used in LEED may be found for the calculation of CIS normal emission curves.

The optimistic findings for these two systems have been overshadowed by the work on Te4d normal emission from Ni(001) - c(2 x 2)Te. McGovern et al (1979) have found there to be poor agreement between their experimental data and the calculations of Li and Tong (1979). The positions and relative intensities of the various peaks in the data are poorly described by the theory. It has been concluded from this that all comparisons between theory and experiment for photoelectron diffraction must be considered suspect until this discrepancy is resolved. We will investigate further this particular problem in the next chapter.

The first calculation of the azimuthal distribution of photoelectron intensity for emission from a surface system, where full multiple scattering has been taken into account and where a comparison has been made with experiment is Liebsch's work on the layer compound TaS_2 (Liebsch (1976)). Excellent agreement has been obtained between theory and experiment (Smith et al (1974)) and this calculation has convincingly shown that one has to put multiple scattering into a photoelectron diffraction calculation in order to properly describe the experimental data. The first such comparison for an adsorbate system is for Na2p emission from Ni(001) - c(2 x 2)Na (Woodruff et al (1978)). We have already noted in Chapter 3 that there is excellent agreement between theory and experiment. We have also seen that for the data taken at photon energy $\hbar\omega$ = 90 eV there is considerable sensitivity of the diffraction pattern to changes in structure.

Similar work has been performed on the system Cu(001) - c(2 x 2)O (Kono et al (1978a,b) where the azimuthal distribution of photoelectron intensity has been measured for emission from the O1s levels. The binding energy for this state is 536 eV below the vacuum level so for this particular case it is necessary to use X-radiation. It has been found that adequate agreement with experiment may be obtained by just using single-scattering theory. Optimum agreement with experiment has been obtained by assuming that the O atom bonds at the hollow sites and is coplanar with the top layer of Cu atoms, a finding that is at odds with the original LEED analysis, (McDonnell et al (1974)). X-ray photoelectron diffraction experiments have also been performed on the well studied surface system Ni(001) - c(2 x 2)CO, (Petersson et al (1979)). Here, emission from the C1s and O1s levels have been separatly studied, and the intensity has been measured as a function of the polar angle of the detector. When O1s is studied there is found to be little variation

of the intensity with polar angle. However, the polar angle variation of the intensity of electrons emitted from the C1s level show a large peak at normal exit angle. Single-scattering calculations show that this may be explained by the strong forward scattering by the O atom of the C1s electrons, if one assumes that CO bonds perpendicular to the Ni(001) surface with the C atom nearest to the substrate, (Andersson and Pendry (1979), Passier et al (1979)). Because backscattering processes are weak at these energies (∿ 1000 eV) this model explains why not much variation of the intensity is observed when O1s electrons are looked at.

It should be emphasised that with the obvious exception of the photoionization amplitudes all the parameters that have been used in the above calculations have been directly transferred from the appropriate LEED calculation.

4.3. Analysis of Data for I on Ag(111) and Te on Ni(001)

In this section we concentrate on the analysis of photoelectron data taken for the surface systems Ni(001) - c(2 x 2)Te and Ni(001) - p(2 x 2)Te (Woodruff (1980)) and Ag(111) - $(\sqrt{3} \times \sqrt{3})R30^{\circ}$I (Farrell et al (1981 a,b). These systems have already been analysed by LEED and Ag(111) - $(\sqrt{3} \times \sqrt{3})R30^{\circ}$I has also been analysed by Surface Extended X-ray Absorption Fine Structure (SEXAFS (Citrin et al (1978)). It is of interest to see whether we can come to the same conclusions as these other techniques as regards the structures for these adsorbate systems.

4.3.1. Ag(111) - $(\sqrt{3} \times \sqrt{3})R30^{\circ}$I

Recently, photoelectron diffraction experiments using synchrotron radiation have been performed for emission from the 4d levels of I adsorbed on the (111) surface of Ag (Farrell et al (1981a)). It is observed from LEED patterns that there are at least four ways that the

I atoms can distributed themselves on the surface depending on the amount of I present. One of these phases, the $(\sqrt{3} \times \sqrt{3})R30^{\circ}$ structure has already been analysed by LEED (Forstmann et al (1973)) and SEXAFS (Citrin et al (1978)). It has been concluded from LEED that the I atoms distribute themselves in the hollows on the Ag surface that are directly the atoms in the third Ag layer down with a $d_{\perp}$ -spacing of 2.25 Å. It should be noted that there is another type of hollow site on the Ag(111) surface that is directly above an atom in the second Ag layer down. SEXAFS predicts an Ag-I bond length of 2.87 ± 0.03 Å (corresponding to a $d_{\perp}$-spacing of 2.33 ± 0.02 Å), but cannot as yet distinguish between the two different hollow sites.

Photoelectron diffraction experiments using the azimuthal mode have been performed on the $(\sqrt{3} \times \sqrt{3})R30^{\circ}$ and (1x1) phases using two different experimental geometries. The radiation is p-polarised and incident on the surface at 45° to the surface normal. In one set of experiments, the detector is set in the same plane as the incident radiation and on the same side of the surface normal as the A-vector. The data should then be three-fold symmetric with mirror planes along the $\langle 11\bar{2} \rangle$ directions. In the second configuration the detector is set to be perpendicular to the plane containing the A-vector and in a clockwise direction looking down onto the crystal surface. The data for this new configuration should still be three-fold symmetric but there will no longer be mirror symmetries present.

4.3.1.1. Analysis of the Data for the In-plane Configuration

We firstly look at the data taken for the experimental configuration where the detector and incident light are coplanar. The experimental data for the $(\sqrt{3} \times \sqrt{3})R30^{\circ}$ phase is shown in fig. (4.1). The detector is set at angles varying between 25° and 40° to the surface normal. $\phi = 0^{\circ}$ corresponds to the $[\bar{1}12]$ azimuth. It should be noted that the data are

Fig. 4.1: Experimental data (dashed line) for the ($\sqrt{3}$ x $\sqrt{3}$) R30° phase, (Farrell et al (1980)), of I adsorbed on Ag(111). The detector angle is set at 25° to the surface normal. The radiation is p-polarised and is incident on the surface at 45° to the surface normal with the detector and light source in the same plane but on opposite sides of the surface normal. The full curves are the calculations of Kang et al (1980).
(Photocopied from Kang et al (1980)).

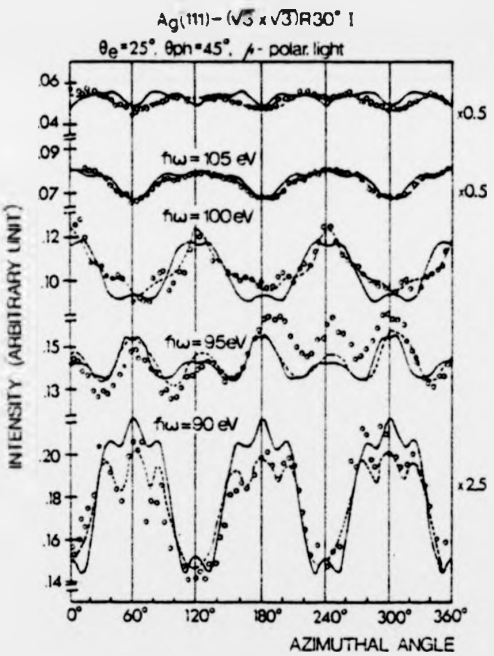

Comparison between theory (solid lines) and experiment (broken lines) for Ag(111)-$(\sqrt{3} \times \sqrt{3})$R30° I at 3-fold site and $\lambda_{\perp} = 2.339$ Å. The data are normalized with theory at 95 eV and scaled: 1.0 at 100 eV, 2.5 at 90 eV, 0.5 at 105 eV and 110 eV respectively.

markedly three-fold symmetric indicating that scattering between the I overlayer and Ag substrate is an important contribution to the diffraction patterns. If scattering were mainly to take place within the I overlayer then the data would tend to six-foldedness. Thus it should be possible to extract structural information from these curves.

In our calculations, the electron mean free path (7.6 Å) and the inner potential (11 eV) are taken from the original LEED calculation (Forstmann et al (1973)). The surface is modelled by a slab consisting of one I and three Ag layers. The scattering electron is described by six partial waves. The multiple scattering series is evaluated to fourteenth order in reverse scattering. The phase shifts for I and Ag and the photo-ionization amplitudes for I 4d are calculated by the method described in section (2.4), with the Ag atom put into the environment that it would occupy in the bulk (i.e. in an fcc lattice) whilst the I atom is put onto a simple cubic lattice with the lattice parameter put equal to twice the covalent radius. It should be noted that there are no significant changes in the I and Ag phase shifts when these atoms are put onto a Ag I lattice. Initially we put $\alpha=1$ into the calculation of the exchange potential in equation (2.53). We set $d_{\perp} = 2.33$ Å, the value determined by SEXAFS, (Citrin et al (1978)), and the bonding site is chosen to be the same as that predicted by LEED. During the course of our calculations Kang et al (1980) published calculations for some of the data presented in fig. (4.1), and they obtained better agreement with experiment than we did. Kang et al had calculated the I and Ag potentials using a different method to the one we have employed. The Ag phase shifts had been calculated from a bulk band structure potential, (Stoner et al (1978)) and the I potential had been calculated by the Scattered Wave Xα (SW-Xα) method for a $(AgI)_3I$ cluster and we later learnt that α had been set equal to 0.75, (Tong (1980)), in the calculation of

Fig. 4.4: Effect of varying the bonding site for electron kinetic energies 35 eV, 45 eV and 55 eV and $\theta = 25^{\circ}$. Full curves: I atom over Ag atom in third Ag layer down. Dashed curves: I atom over Ag atom in second Ag layer down.

IODINE ON SILVER

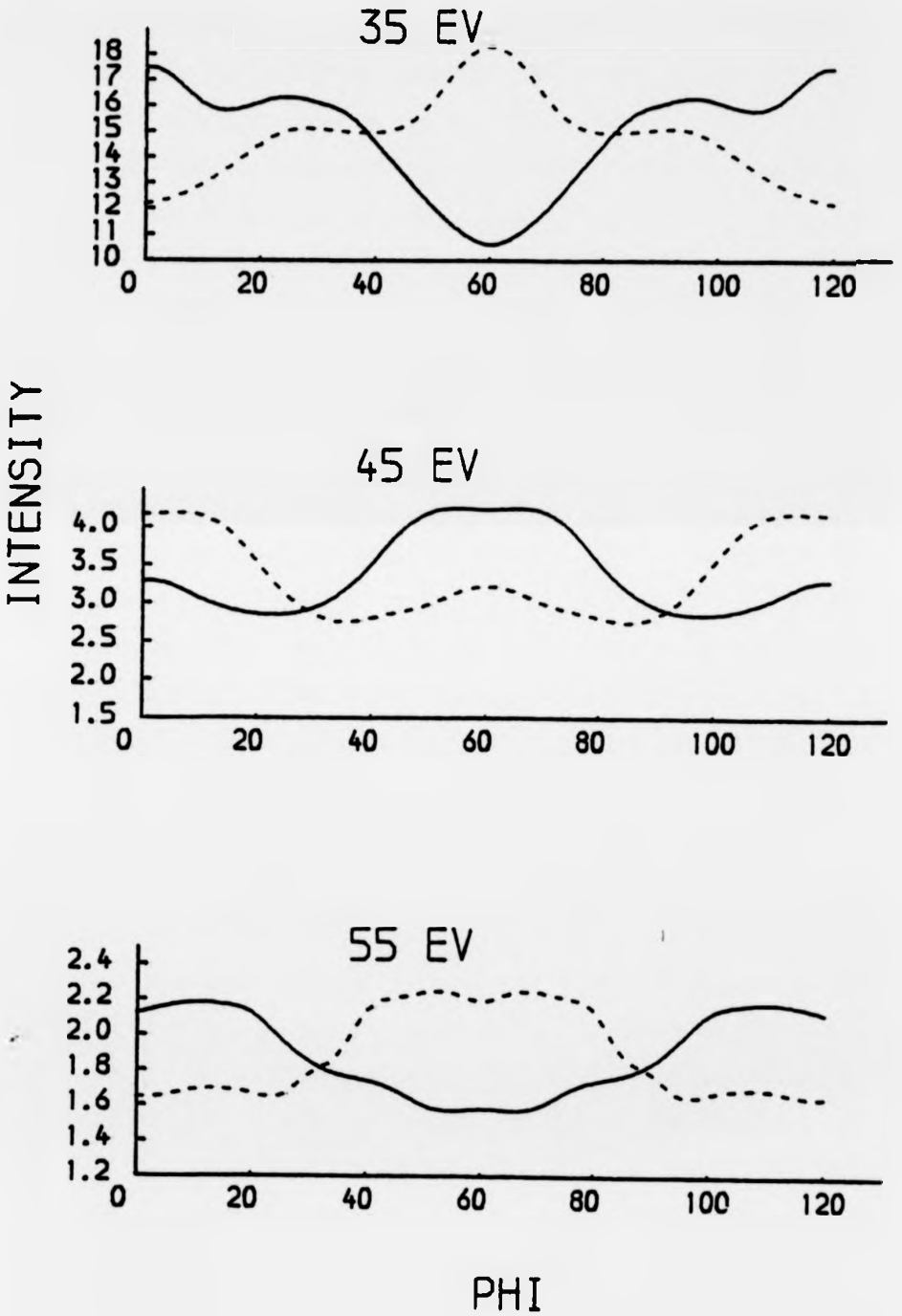

Fig. 4.3: Comparison between theory (full lines) and experiment (dashed lines) for I 4d emission from Ag(111) - $(\sqrt{3} \times \sqrt{3})R30^{\circ}$I:

(a) detector angle (θ) = 25°, electron kinetic energies 35 eV, 45 eV and 55 eV,

(b) detector angle (θ) = 40°, electron kinetic energies 40 eV, 45 eV and 50 eV.

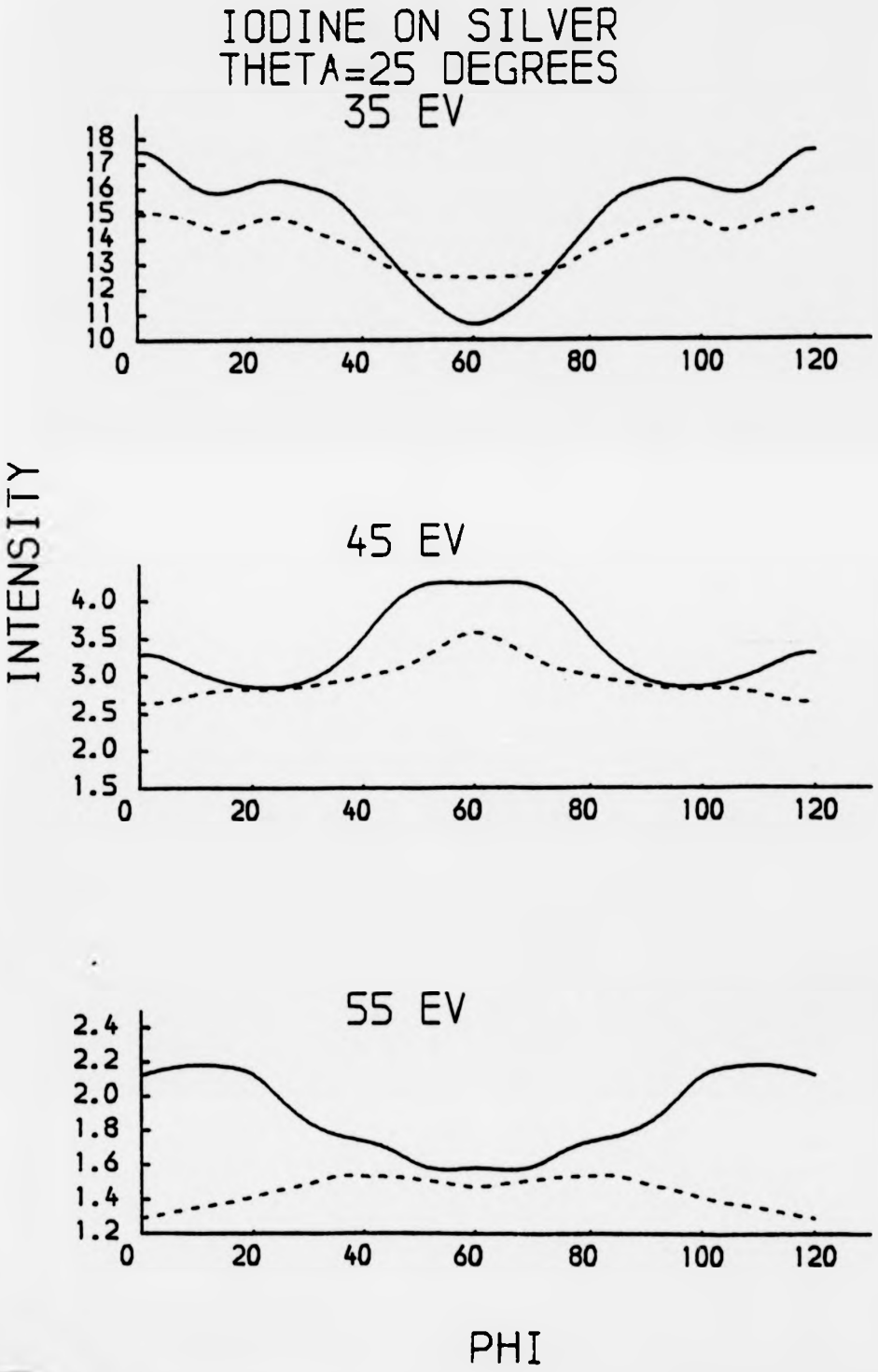
IODINE ON SILVER
THETA=25 DEGREES
35 EV
18
17
16
15
14
13
12
11
10
0
20
40
60
80
100
120
INTENSITY
45 EV
4.0
3.5
3.0
2.5
2.0
1.5
0
20
40
60
80
100
120
55 EV
2.4
2.2
2.0
1.8
1.6
1.4
1.2
0
20
40
60
80
100
120
PHI

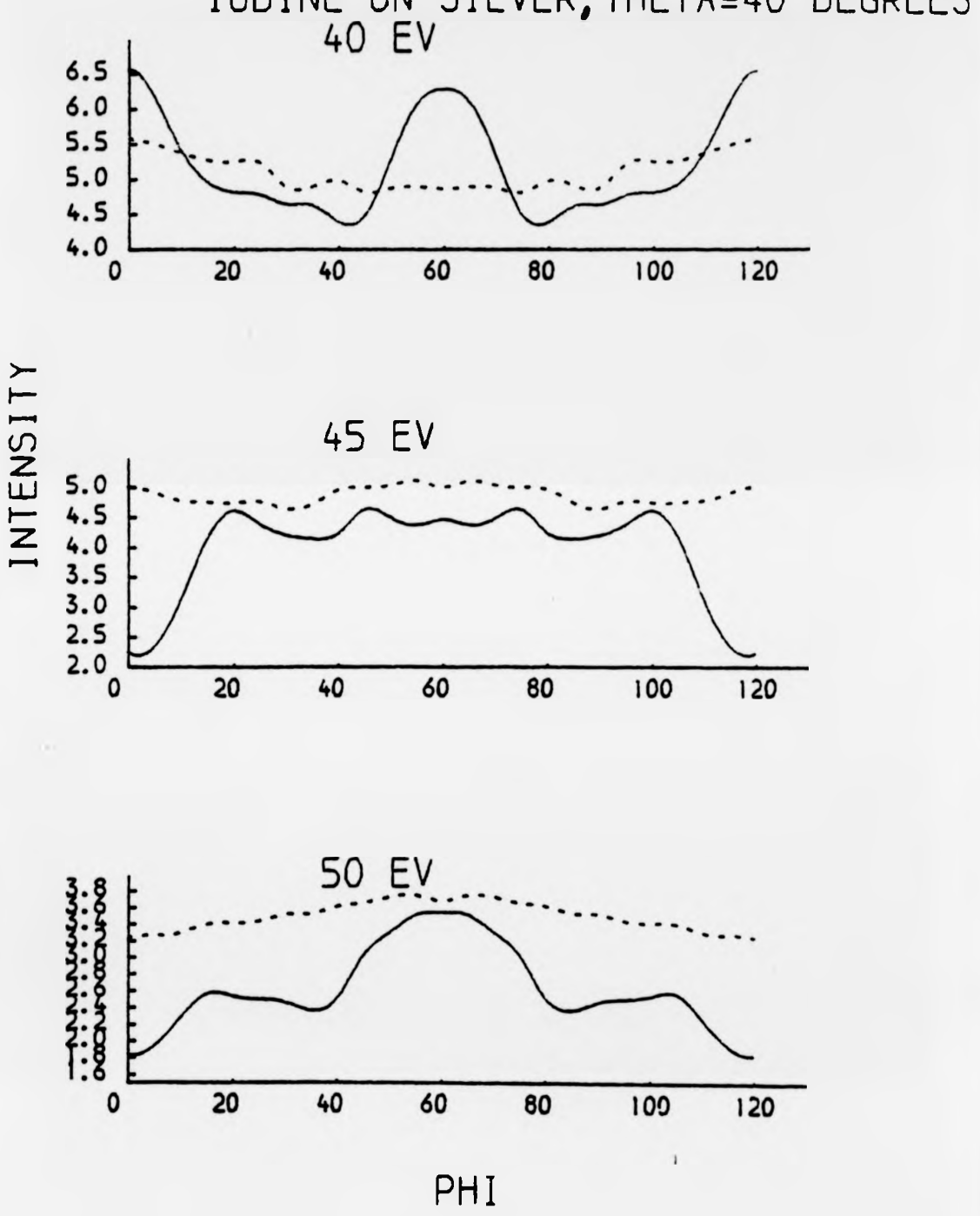
IODINE ON SILVER, THETA=40 DEGREES
40 EV
6.5
6.0
5.5
5.0
4.5
4.0
0
20
40
60
80
100
120
INTENSITY
45 EV
5.0
4.5
4.0
3.5
3.0
2.5
2.0
0
20
40
60
80
100
120
50 EV
0
20
40
60
80
100
120
PHI

Fig. 4.1: Experimental data (dashed line) for the ($\sqrt{3}$ x $\sqrt{3}$) R30° phase, (Farrell et al (1980)), of I adsorbed on Ag(111). The detector angle is set at 25° to the surface normal. The radiation is p-polarised and is incident on the surface at 45° to the surface normal with the detector and light source in the same plane but on opposite sides of the surface normal. The full curves are the calculations of Kang et al (1980).
(Photocopied from Kang et al (1980)).

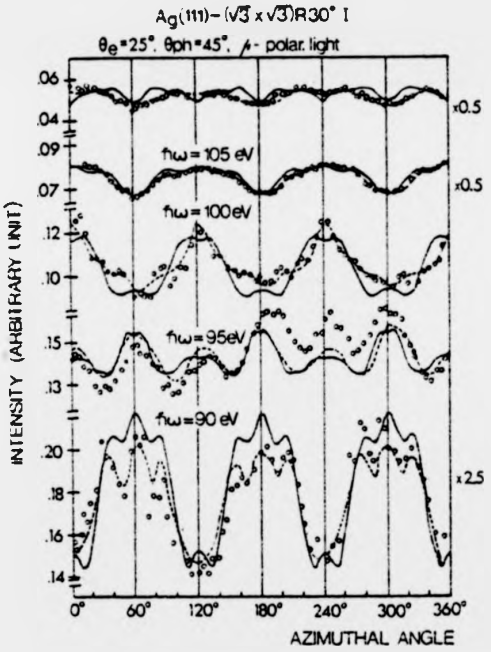

Comparison between theory (solid lines) and experiment (broken lines) for Ag(111)-(√3 x √3)R30° I at 3-fold site and $d_{\perp}$ = 2.339 Å. The data are normalized with theory at 95 eV and scaled: 1.0 at 100 eV, 2.5 at 90 eV, 0.5 at 105 eV and 110 eV respectively.

markedly three-fold symmetric indicating that scattering between the I overlayer and Ag substrate is an important contribution to the diffraction patterns. If scattering were mainly to take place within the I overlayer then the data would tend to six-foldedness. Thus it should be possible to extract structural information from these curves.

In our calculations, the electron mean free path (7.6 Å) and the inner potential (11 eV) are taken from the original LEED calculation (Forstmann et al (1973)). The surface is modelled by a slab consisting of one I and three Ag layers. The scattering electron is described by six partial waves. The multiple scattering series is evaluated to fourteenth order in reverse scattering. The phase shifts for I and Ag and the photo-ionization amplitudes for I 4d are calculated by the method described in section (2.4), with the Ag atom put into the environment that it would occupy in the bulk (i.e. in an fcc lattice) whilst the I atom is put onto a simple cubic lattice with the lattice parameter put equal to twice the covalent radius. It should be noted that there are no significant changes in the I and Ag phase shifts when these atoms are put onto a Ag I lattice. Initially we put α=1 into the calculation of the exchange potential in equation (2.53). We set $d_\perp$ = 2.33 Å, the value determined by SEXAFS, (Citrin et al (1978)), and the bonding site is chosen to be the same as that predicted by LEED. During the course of our calculations Kang et al (1980) published calculations for some of the data presented in fig. (4.1), and they obtained better agreement with experiment than we did. Kang et al had calculated the I and Ag potentials using a different method to the one we have employed. The Ag phase shifts had been calculated from a bulk band structure potential, (Stoner et al (1978)) and the I potential had been calculated by the Scattered Wave Xα (SW-Xα) method for a $(AgI)_3I$ cluster and we later learnt that α had been set equal to 0.75, (Tong (1980)), in the calculation of

Fig. 4.2: Effect of varying α on the calculated photoelectron diffraction curves for I 4d emission from Ag(111) - $(\sqrt{3} \times \sqrt{3})R30^{\circ}I$, for electron kinetic energy 45 eV.

Upper full curve: $\alpha = 0.75$

Lower full curve: $\alpha = 1$

Dashed curve: experimental data, (Farrell et al (1980)).

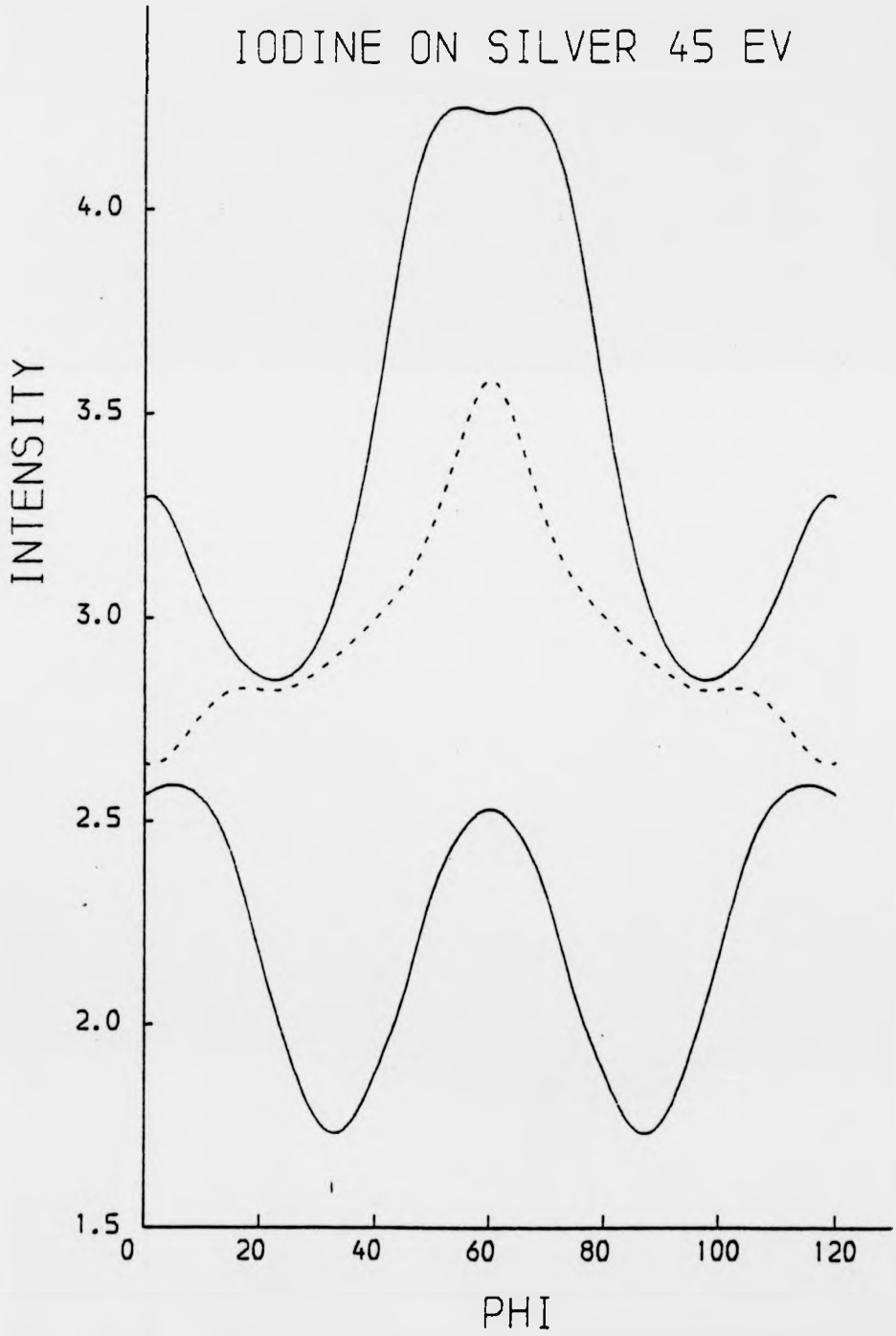
IODINE ON SILVER 45 EV
INTENSITY
4.0
3.5
3.0
2.5
2.0
1.5
0
20
40
60
80
100
120
PHI

Fig. 4.3: Comparison between theory (full lines) and experiment (dashed lines) for I 4d emission from Ag(111) - $(\sqrt{3} \times \sqrt{3})R30^{\circ}I$:
(a) detector angle (θ) = 25°, electron kinetic energies 35 eV, 45 eV and 55 eV,
(b) detector angle (θ) = 40°, electron kinetic energies 40 eV, 45 eV and 50 eV.

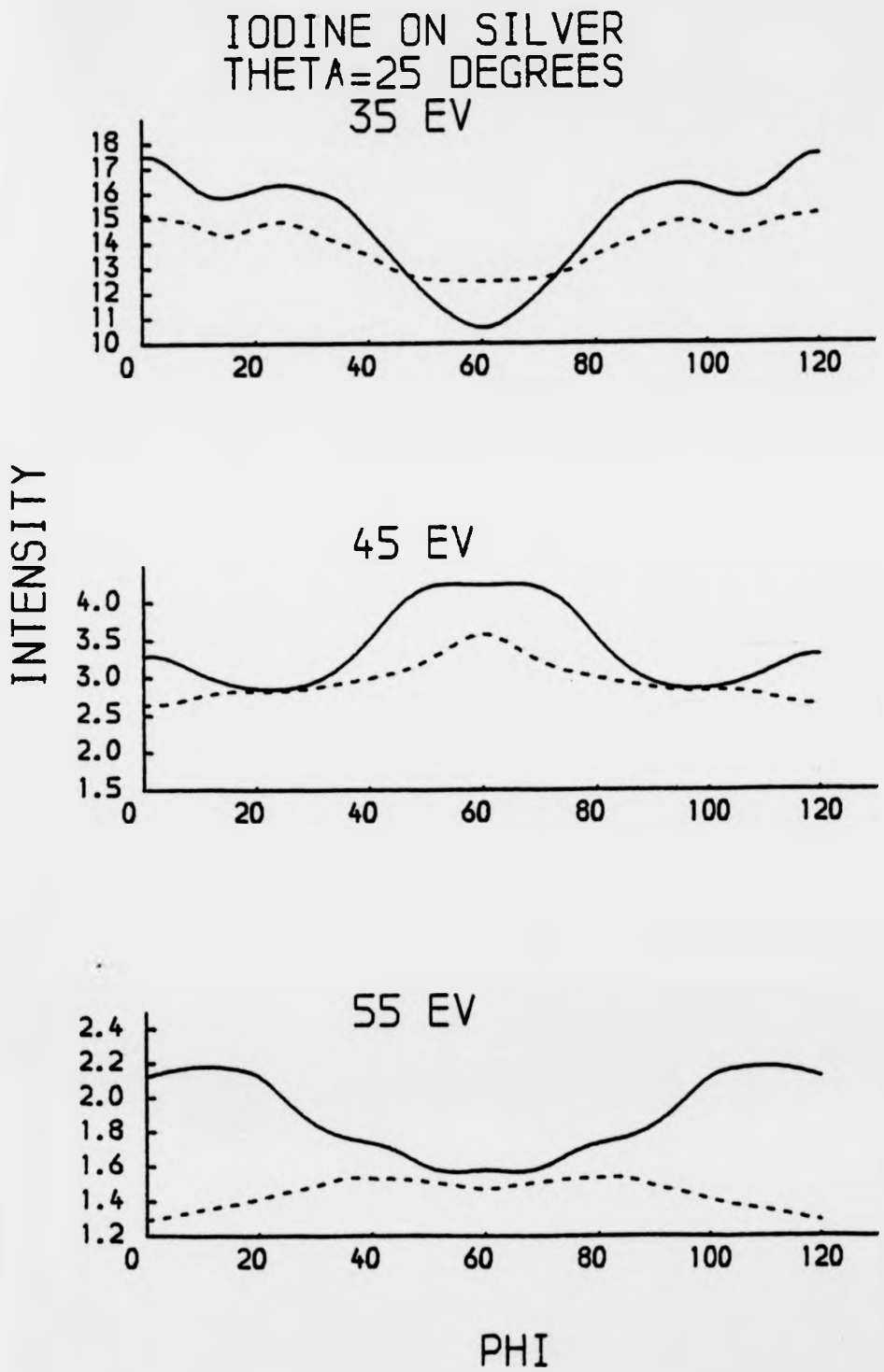
IODINE ON SILVER
THETA=25 DEGREES
35 EV
18
17
16
15
14
13
12
11
10
0
20
40
60
80
100
120
INTENSITY
45 EV
4.0
3.5
3.0
2.5
2.0
1.5
0
20
40
60
80
100
120
55 EV
2.4
2.2
2.0
1.8
1.6
1.4
1.2
0
20
40
60
80
100
120
PHI

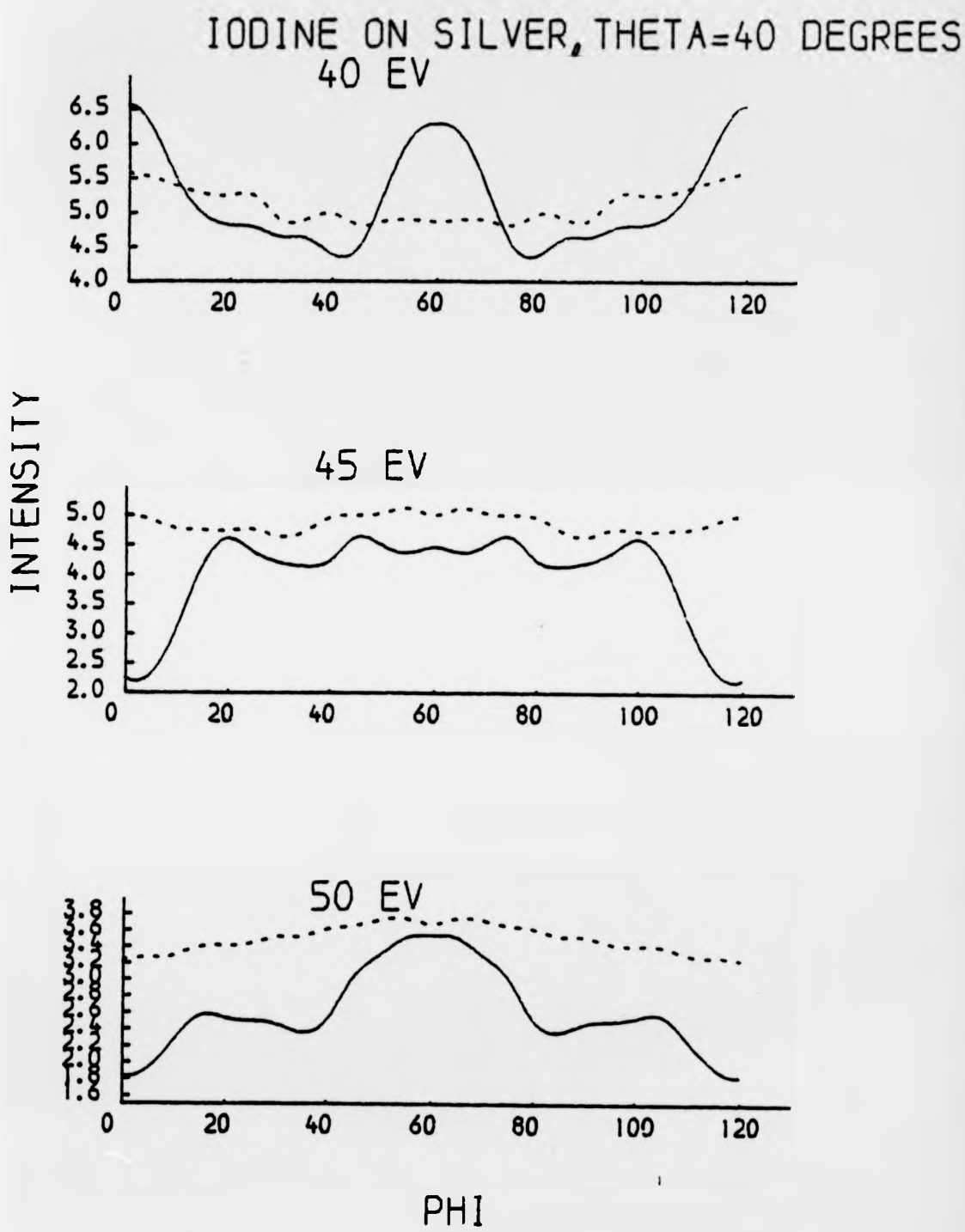
IODINE ON SILVER, THETA=40 DEGREES
40 EV
6.5
6.0
5.5
5.0
4.5
4.0
0
20
40
60
80
100
120
INTENSITY
45 EV
5.0
4.5
4.0
3.5
3.0
2.5
2.0
0
20
40
60
80
100
120
50 EV
0
20
40
60
80
100
120
PHI

Fig. 4.4: Effect of varying the bonding site for electron kinetic energies 35 eV, 45 eV and 55 eV and $\theta = 25^{\circ}$. Full curves: I atom over Ag atom in third Ag layer down. Dashed curves: I atom over Ag atom in second Ag layer down.

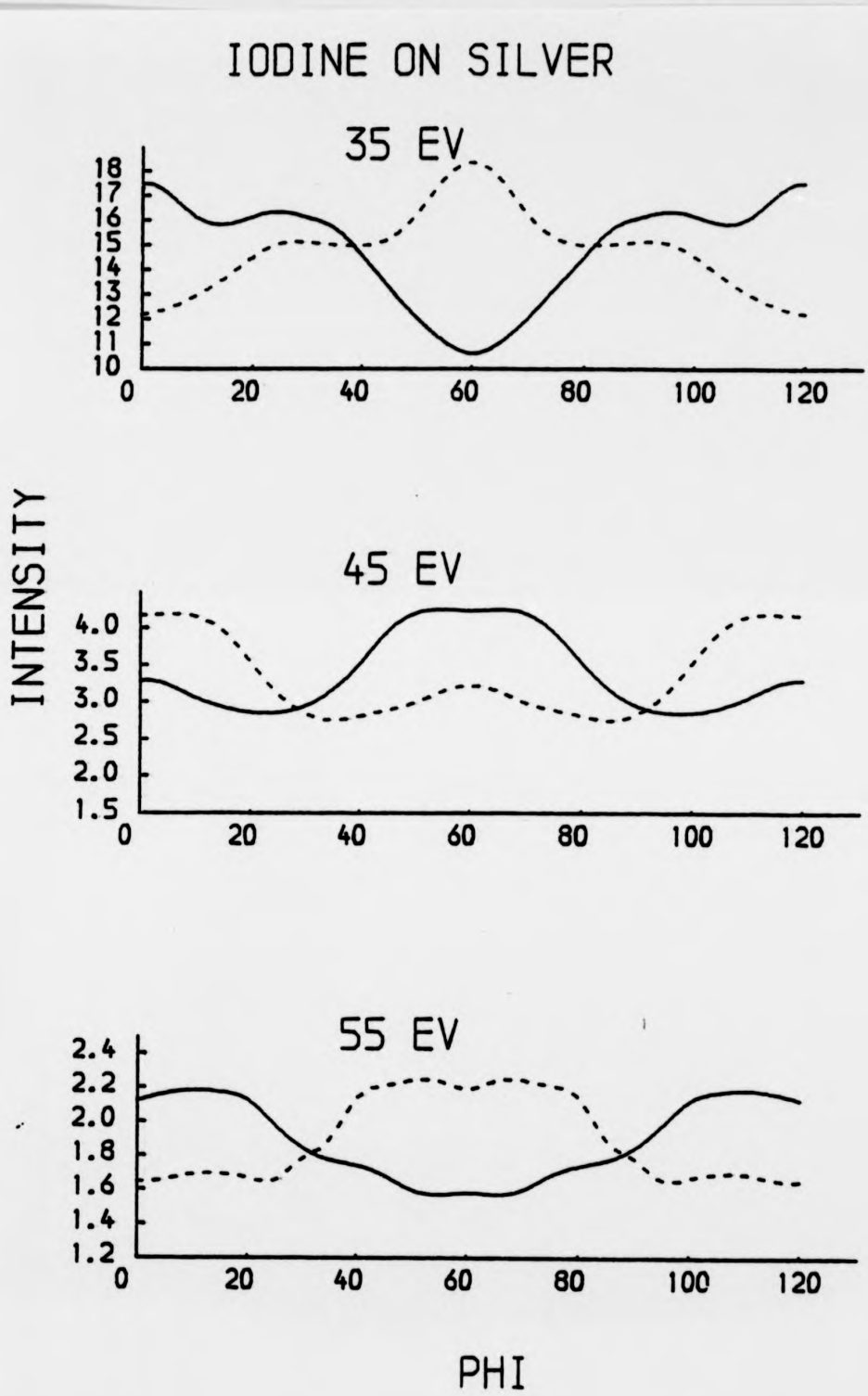
IODINE ON SILVER
35 EV
18
17
16
15
14
13
12
11
10
0
20
40
60
80
100
120
INTENSITY
45 EV
4.0
3.5
3.0
2.5
2.0
1.5
0
20
40
60
80
100
120
55 EV
2.4
2.2
2.0
1.8
1.6
1.4
1.2
0
20
40
60
80
100
120
PHI

exchange potentials for I and Ag. The MUFPOT programs that we have been using cannot simulate a molecular cluster, but we have recalculated the I and Ag potentials putting $\alpha = 0.75$. This value for α is close to the Schwartz value for these atoms, (Schwartz (1972)). We have found that by using these new phase shifts and I 4d photoionisation amplitudes we are able to obtain better agreement between theory and experiment for some energies. An example of such an improvement for electron kinetic energy (E) equal to 45 eV is shown in fig. (4.2).

A comparison between our calculations and the experimental data is shown in fig. (4.3). The calculation for E = 45 eV, $\theta = 30^{\circ}$ and 35°, E = 40 eV, $\theta = 25^{\circ}$ and E = 50 eV, $\theta = 25^{\circ}$ do not converge adequately and so we do not present them here. We should first note that our calculations for $\theta = 25^{\circ}$ correspond very closely to Kang et al's calculations, (Fig. (4.1). The agreement between theory and experiment is fair for E = 35 eV, $\theta = 25^{\circ}$, E = 45 eV, $\theta = 25^{\circ}$ and E = 50 eV, $\theta = 40^{\circ}$. For E = 45 eV and 50 eV, $\theta = 40^{\circ}$, additional structure appears in the calculations that is not observed experimentally. However, the overall features of the data are reproduced by the theory. For E = 55 eV, $\theta = 25^{\circ}$ the agreement between theory and experiment is non-existent. However, the data at this energy are unreliable; this may be clearly seen by looking at the raw data points for this energy in fig. (4.1).

It is of interest to see whether the calculated diffraction curves are very sensitive to changing the bonding site to the other type of hollow on the Ag(111) surface. In fig. (4.4) we show the effects of such a change for electron kinetic energies 35 eV, 45 eV and 55 eV and $\theta = 25^{\circ}$. We see that the curves are indeed very sensitive to changing the bonding site. It is interesting to note that for each energy the curve for the second bonding site is very similar in shape to the curve

Fig. 4.5: Effect of varying $d_\perp$ for electron kinetic energies 35 eV, 45 eV, and 55 eV and $\theta = 25^\circ$. Full curves: $d_\perp = 2.23$ Å. Dashed curves: $d_\perp = 2.43$ Å.

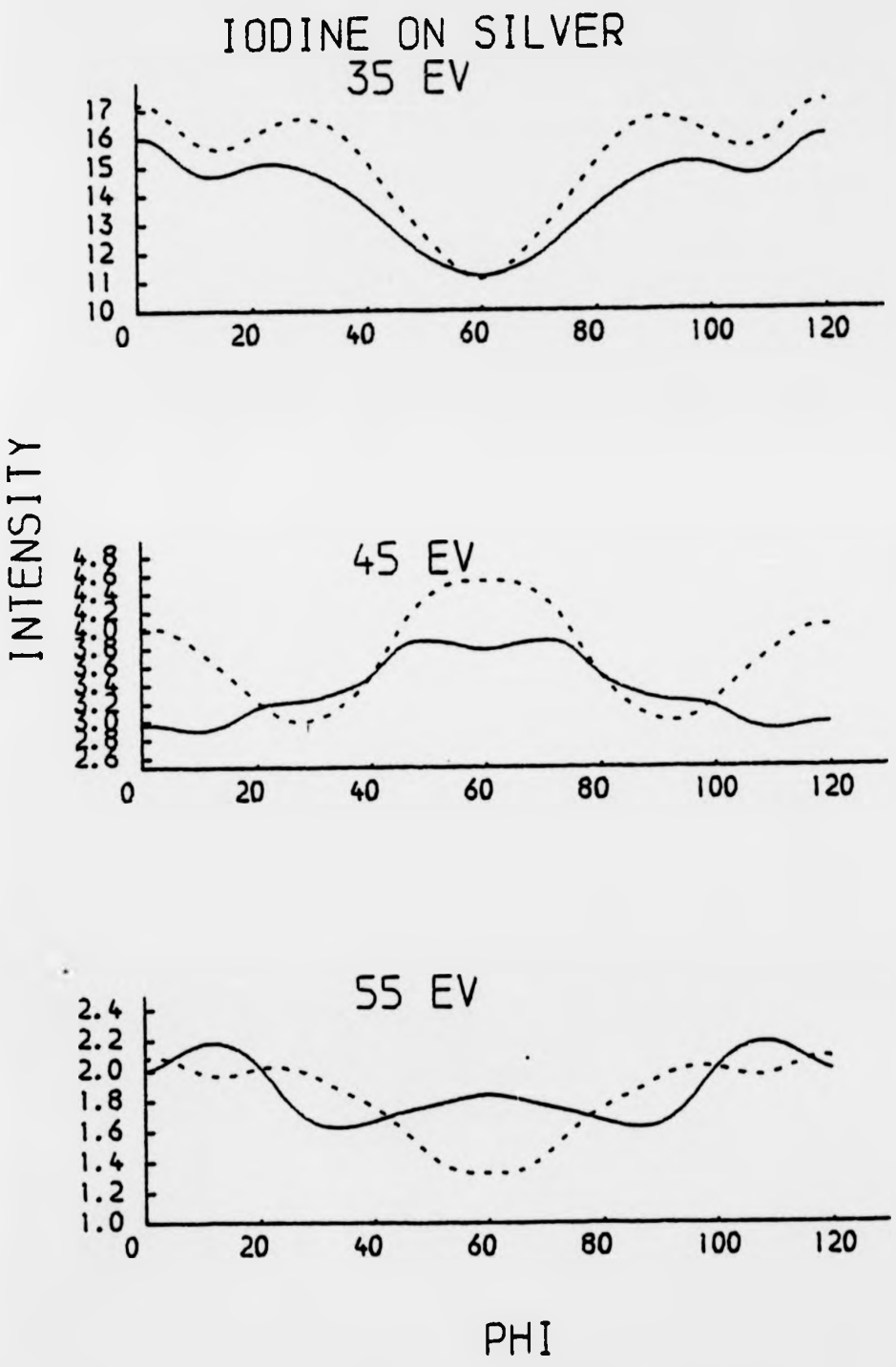
IODINE ON SILVER
35 EV
45 EV
55 EV
INTENSITY
PHI
17
16
15
14
13
12
11
10
2.4
2.2
2.0
1.8
1.6
1.4
1.2
1.0
0
20
40
60
80
100
120

Figure 4.6: Experimental data (dashed lines) for the ($\sqrt{3}\times\sqrt{3}$) phase, (Farrell et al (1980a)), of I adsorbed on Ag(111). The detector angle is set at 25° to the surface normal. The radiation is p-polarised and incident on the surface at 45° to the surface normal with the detector and light source in the same plane but on opposite sides of the surface normal. The full curves are the calculations of Kang et al (1980).
(Photocopied from Kang et al (1980)).

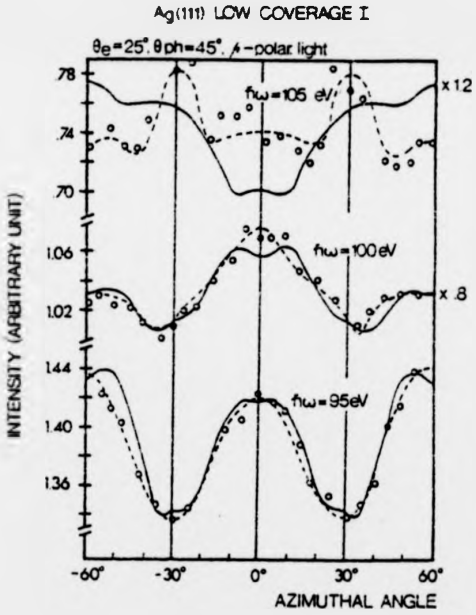

Comparison between theory averaged over the two 3-fold sites (solid lines) and experiment at low coverage: $\theta_2 \sim 0.14$ (broken lines). Small circles indicate actual experimental da data. The data are normalized with theory at 95 eV and scales: 0.8 at 100 eV and 1.2 at 105 eV respectively.

for the first bonding site except that the second curve appears to be rotated by 60° from the first curve. By inspection of the geometry of the Ag(111) surface, this would suggest that for this particular experimental configuration, the diffraction patterns are dominated by scattering between the I and nearest neighbour Ag atoms. Scattering within the I overlayer or off deeper Ag layers give only small contributions to the diffraction patterns. However, this observation does not necessarily hold for other experimental configurations or for other adsorbate systems. We have found there to be much less sensitivity of the diffraction patterns to changes in $d_\perp$. In fig. (4.5) we present calculations for E = 35 eV, 45 eV and 55 eV where $d_\perp$ has been varied by ± 0.1 Å from the value determined by SEXAFS (Citrin et al (1978)). For E = 35 eV the diffraction curve is very insensitive to a 0.2 Å change in $d_\perp$. For E = 55 eV the diffraction pattern is quite sensitive to such a change in $d_\perp$. For E = 45 eV the diffraction curve for $d_\perp$ = 2.23 Å is very similar to that for $d_\perp$ = 2.33 Å, but a marked change is observed when $d_\perp$ is increased to 2.43 Å. Thus for this particular adsorbate system the diffraction patterns are in general less sensitive to changes in $d_\perp$ than to changes in the bonding site. Kang et al (1980), who have performed calculations for a wider range of values of $d_\perp$ than we have done, have come to similar conclusions as regards the structural sensitivity of the photoelectron diffraction patterns. In particular, our calculations suggest that $d_\perp$ is not going to be determined to any greater accuracy than LEED.

Farrell et al (1981a) have also taken data for the so-called (1x1) phase which occurs for coverages below about 0.25 monolayers when no long range order is detected by LEED. The experimental data for this coverage are shown in fig. (4.6). For each energy the diffraction patterns look like six-fold versions of their $(\sqrt{3} \times \sqrt{3})R30^\circ$ counterparts. Because of this, Farrell et al suggest that in this phase the I atoms distribute

Figure 4.7: Comparison between theory (full curves) and experiment (dashed curves) for the data taken with the detector and light source in perpendicular planes (Farrell). The detector angle is set at 40° to the surface normal.

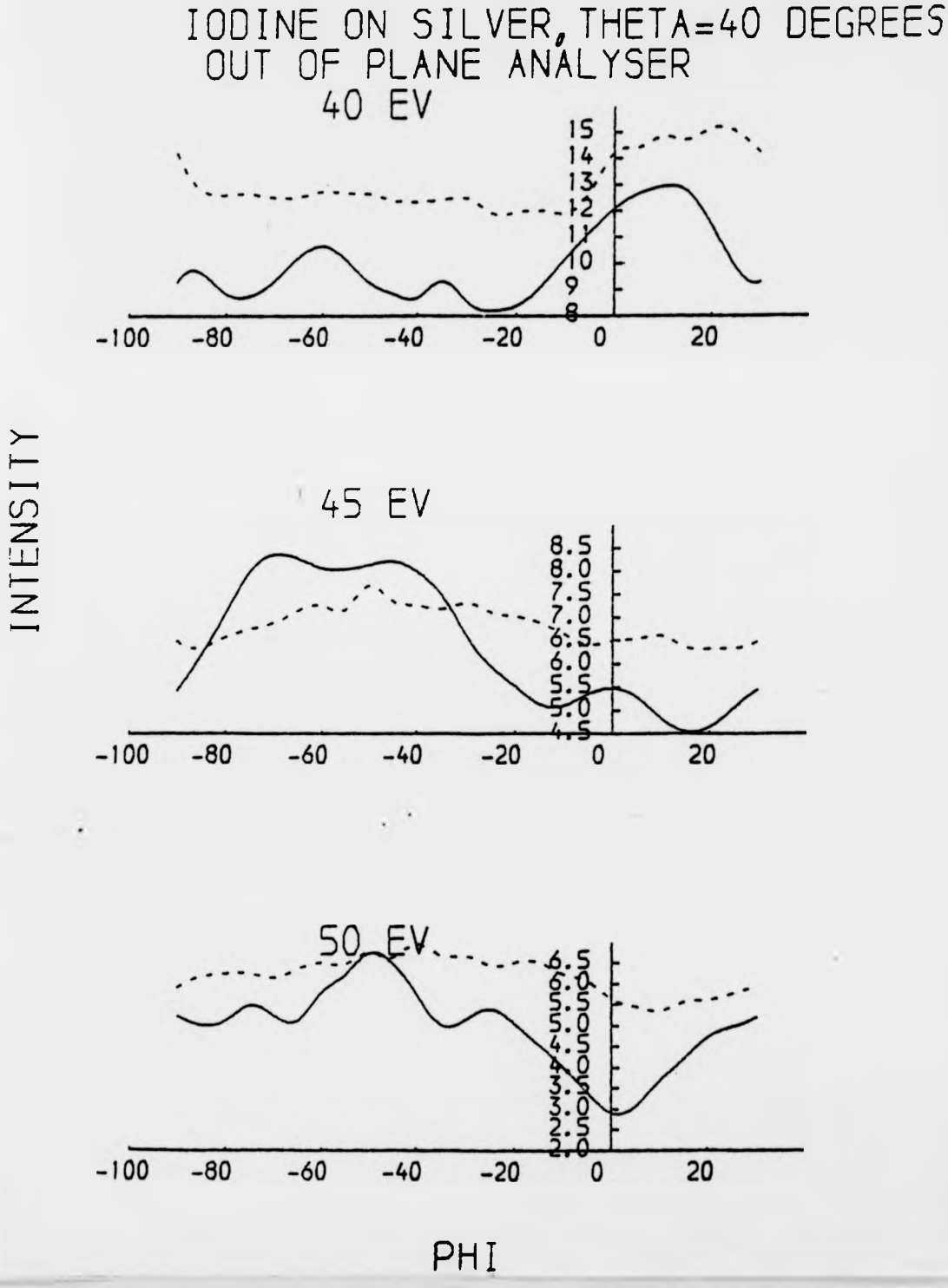
IODINE ON SILVER, THETA=40 DEGREES
OUT OF PLANE ANALYSER
40 EV
45 EV
50 EV
INTENSITY
PHI
-100
-80
-60
-40
-20
0
20

themselves on the Ag surface in a random manner in both types of hollow site. Kang et al have analysed the data for this phase by calculating the azimuthal anisotropy from (a) a $(\sqrt{3} \times \sqrt{3})R30^{\circ}$ coverage of I for an I atom sitting in a hollow site directly over an atom in the third Ag layer and (b) a $(\sqrt{3} \times \sqrt{3})R30^{\circ}$ coverage of I for an I atom sitting in the other type of hollow site. An average is taken of the intensities from (a) and (b). This analysis assumes that (i) scattering between the I and Ag atoms is more important than scattering within the I overlayer (which has already been shown to be the case), (ii) the I atom is the same distance above the Ag surface for both types of hollow site and (iii) the I atoms occupy both type of hollow site in equal proportions. Kang et al's calculations for this phase are shown in fig. (4.6). The calculations for E = 40 eV and 45 eV are in excellent agreement with experiment, whilst for E = 50 eV the agreement is only fair. Thus, the originally proposed structure for this phase (Farrell et al (1981a)), is probably not far wrong.

4.3.1.2. Analysis of the Data Taken with the Out-of-Phase Configuration

We now turn to the analysis of the data that is taken with the detector positioned in a plane perpendicular to that of the light source. The experimental curves which are shown as dotted curves in fig. (4.7) have only been taken for the $(\sqrt{3} \times \sqrt{3})R30^{\circ}$ phase. Photon energies between 95 eV and 110 eV are used and the detector is set at polar angles varying between 25° and 40° with respect to the surface normal. As expected, there are no longer mirror symmetries along the $\langle 11\bar{2} \rangle$ directions. The setting of the radiation source is the same as before. We do not analyse the data taken at E = 55 eV, because they are thought to be unreliable at this energy. The calculations for E = 45 eV and $\theta = 30^{\circ}$, 35° and 40° do not adequately converge. The theoretical curves are shown as full curves

in fig. (4.7). The first point to note is that there is far more anisotropy in the theoretical calculations than there is in the experimental data. There is good agreement between theory and experiment for E = 40 eV, but the agreement is poor for the other two energies.

4.3.1.3. Discussion

We have fitted most of the data for Ag(111) - $(\sqrt{3} \times \sqrt{3})R30^{\circ}$I for both experimental configurations using the structure determined by SEXAFS and LEED, although some discrepancies between theory and experiment have been found to occur. Whilst we have confirmed the LEED finding on the bonding site, we cannot determine $d_{\perp}$ to any greater accuracy than LEED because the photoelectron diffraction curves are found to be not very sensitive to small changes in this parameter.

We should point out that, recently, various groups have performed further LEED experiments on Ag(111) - $(\sqrt{3} \times \sqrt{3})R30^{\circ}$I. Considerable difficulty has been encountered in reproducing the original experimental data of Forstmann et al (1973); the data for some beams cannot be reproduced at all, (Jona (1980)]. This raises the question as to whether the old and new LEED experiments were performed on the same structure. Also, since this phase appears to be difficult to reproduce experimentally, can we be sure that the photoelectron diffraction and SEXAFS experiments were performed for the same structure as the original LEED experiment? To make matters worse it has only been found possible to reproduce the original calculations of Forstmann et al if one assumes a muffin tin radius of $\sim$ 2.5 Å in the calculation of the I phase shifts, (which is approximately half the distance between the I atoms in the $(\sqrt{3} \times \sqrt{3})R30^{\circ}$ structure). Such a value is large, considering that the covalent radius of I is only $\sim$ 1.3 Å. Therefore, until this controversy is resolved, the structure for the $(\sqrt{3} \times \sqrt{3})R30^{\circ}$ phase must remain an open question. If

we were to assume that the photoelectron diffraction experiments were performed on the same structure as the original LEED experiment, then our analysis, along with the analysis of Kang et al (1980) would suggest that the originally determined bonding site is correct, but we can only say that $d_\perp$ lies somewhere in the region of the values determined by LEED and SEXAFS.

4.3.2. Ni(001) - c(2 x 2)Te and Ni(001) - p(2 x 2)Te

It is known from the examination of LEED patterns that there are at least four different ordered structures that Te atoms can adopt when adsorbed on Ni(001), (Becker and Hagstrum (1975)). At about ½ a monolayer coverage the Te atoms adopt a c(2 x 2) configuration, whilst for coverages less than ∿ ½, the atoms form a p(2 x 2) configuration. The structures for both of these phases have already been analysed by LEED. For the c(2 x 2) configuration it has been concluded that the Te atoms sit in the four-fold hollows on the Ni(001) surface with a $d_\perp$-spacing of 1.9 ± 0.1 Å (Demuth et al (1973ab, 1974)). For the p(2 x 2) coverage, the LEED analysis determines the bonding site to be the same as for the c(2 x 2) coverage, and the $d_\perp$-spacing has been determined to be in the region of 1.8 - 1.9 ± 0.1 Å (Van Hove and Tong (1975)).

Recently, photoelectron diffraction experiments using the azimuthal mode have been performed on the surface systems Ni(001) - c(2 x 2)Te and Ni(001) - p(2 x 2)Te, (Woodruff (1980)). Emission from the Te4d levels is studied. Photon energies in the range 80 eV and 105 eV have been used corresponding to electron kinetic energies 33 eV and 58 eV in the vacuum. The detector is set at polar angles varying between 30° and 45° with respect to the surface normal. The radiation is p-polarised and is incident on the surface at 45° to the surface normal in the same place as the detector, with the light source and detector being on opposite sides of the surface normal.

Figure 4.8: Photoelectron diffraction calculations (full curves) for the Te4d emission from Ni(001) - c(2 x 2)Te and from Ni(001) - p(2 x 2)Te for various electron kinetic energies. The experimental data are shown as dashed curves. The detector angle (θ) = 30° for the p(2 x 2) data, and for the c(2 x 2)data, θ is set at both 30° and 45° with respect to the surface normal.

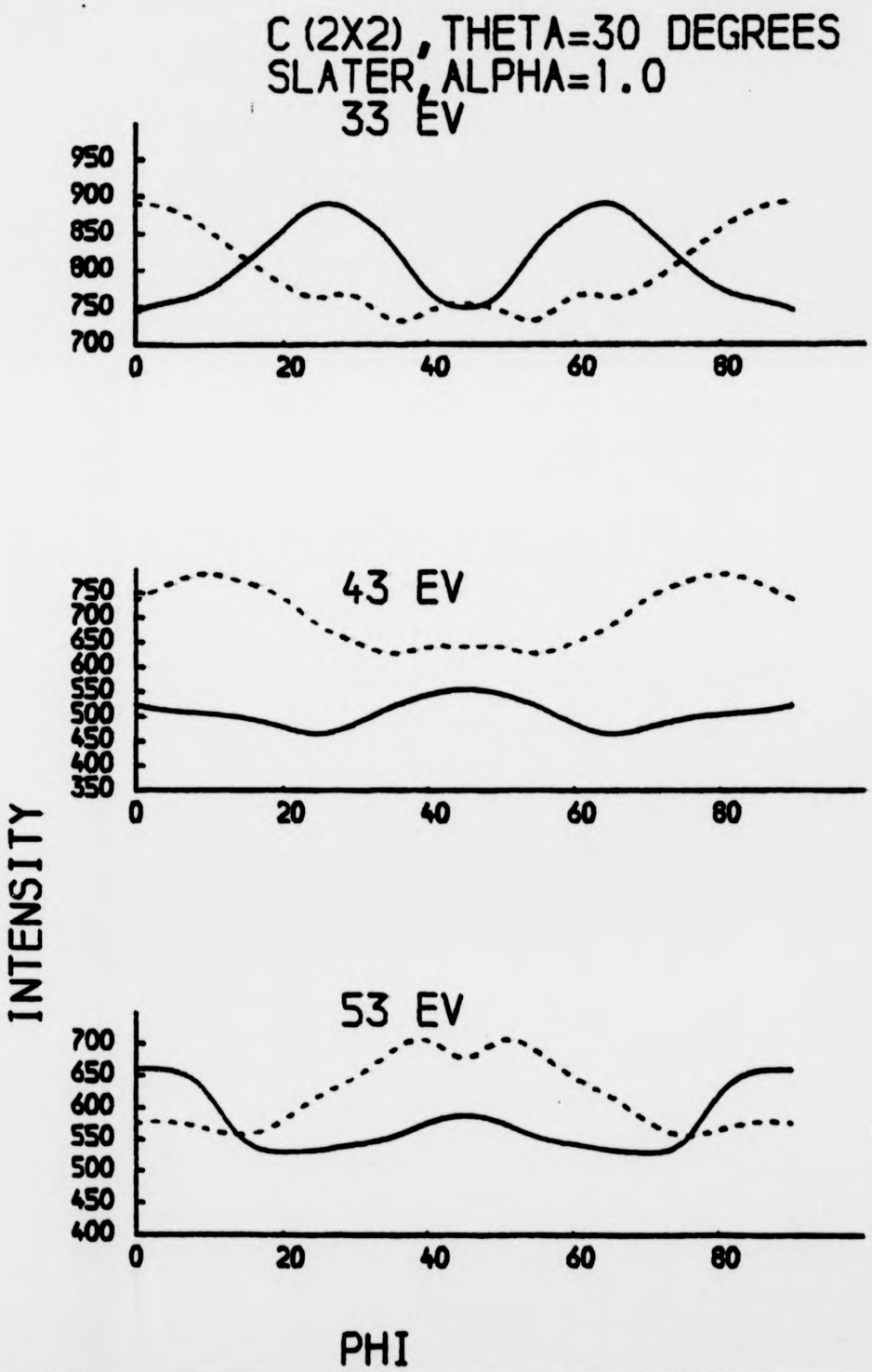
C (2X2), THETA=30 DEGREES
SLATER, ALPHA=1.0
33 EV
950
900
850
800
750
700
0
20
40
60
80
43 EV
750
700
650
600
550
500
450
400
350
0
20
40
60
80
INTENSITY
53 EV
700
650
600
550
500
450
400
0
20
40
60
80
PHI

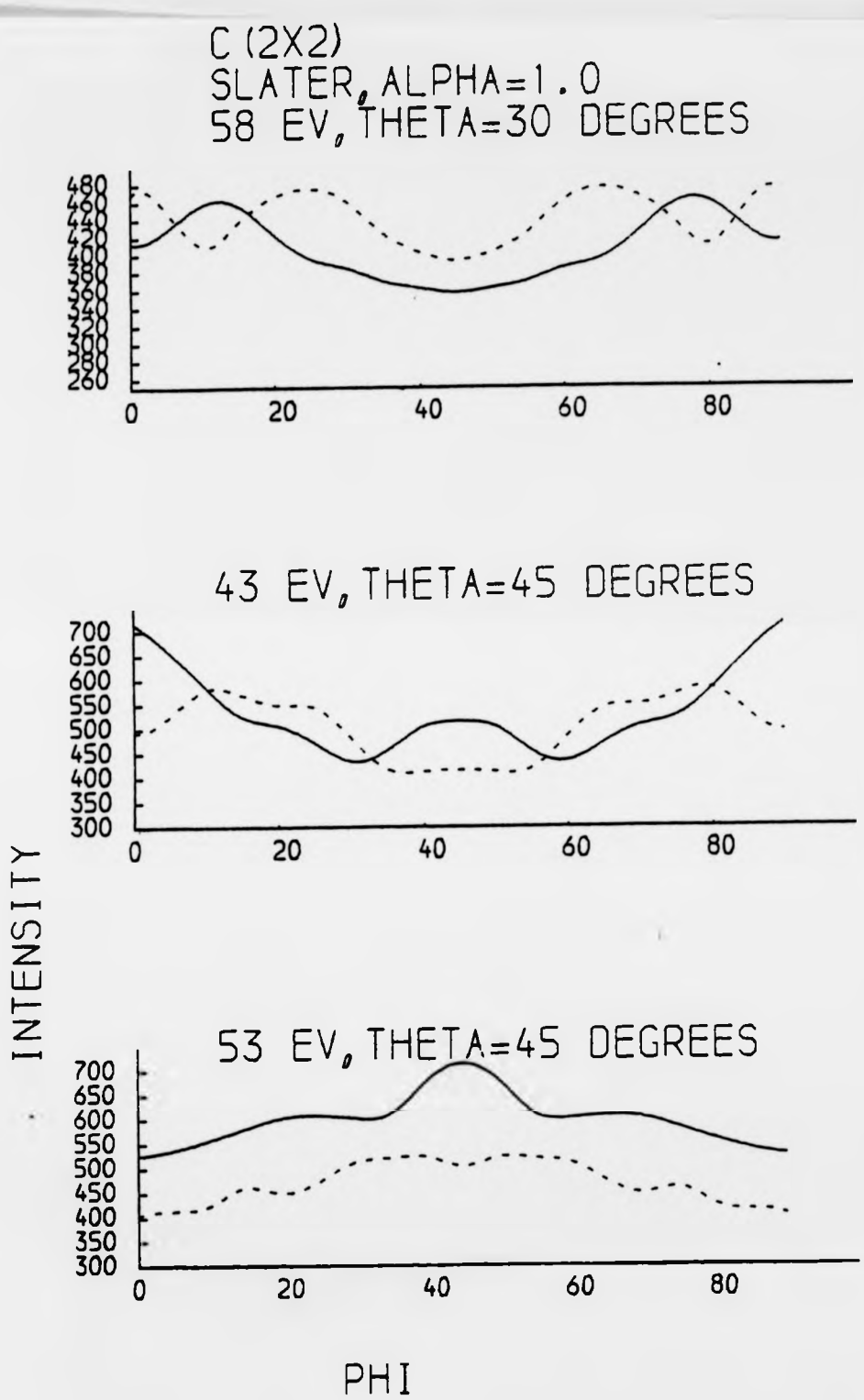
C (2X2)
SLATER, ALPHA=1.0
58 EV, THETA=30 DEGREES
480
460
440
420
400
380
360
340
320
300
280
260
0
20
40
60
80
43 EV, THETA=45 DEGREES
700
650
600
550
500
450
400
350
300
0
20
40
60
80
53 EV, THETA=45 DEGREES
700
650
600
550
500
450
400
350
300
0
20
40
60
80
INTENSITY
PHI

P (2X2)
SLATER, ALPHA=1.0
38 EV

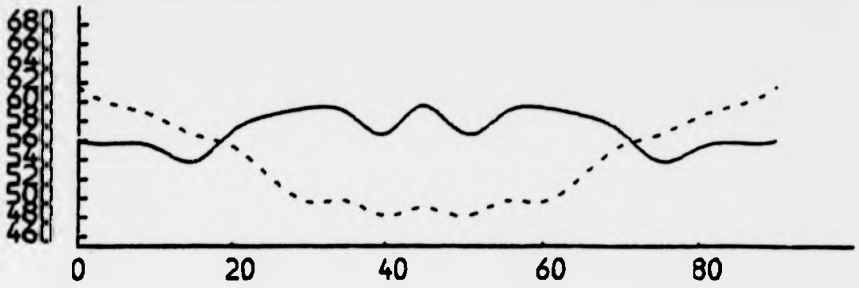

43 EV

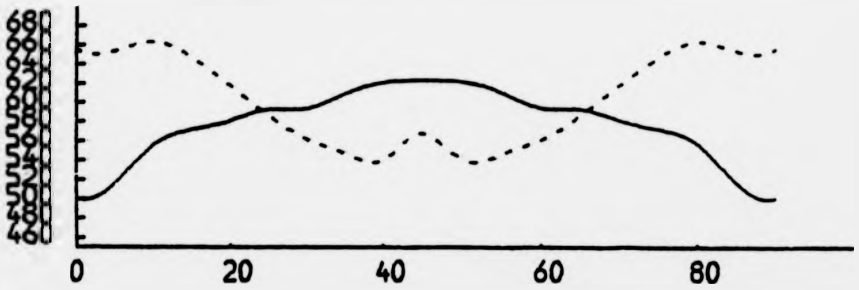

48 EV

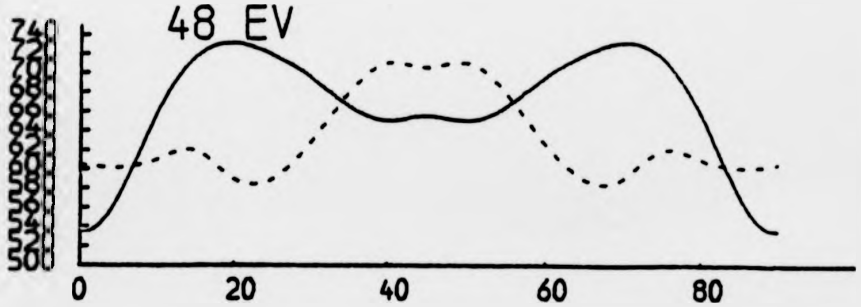

INTENSITY

PHI

Figure 4.9: Photoelectron diffraction calculations for Te 4d emission from Ni(001) - c(2 x 2)Te, where the $d_\perp$-spacing is varied by ± 0.1 Å from the LEED value, (Demuth et al (1973ab, 1974).

$\theta = 30^\circ$ for all energies

Full curves: $d_\perp = 2.0$ Å

Broken curves: $d_\perp$ a 1.8 Å

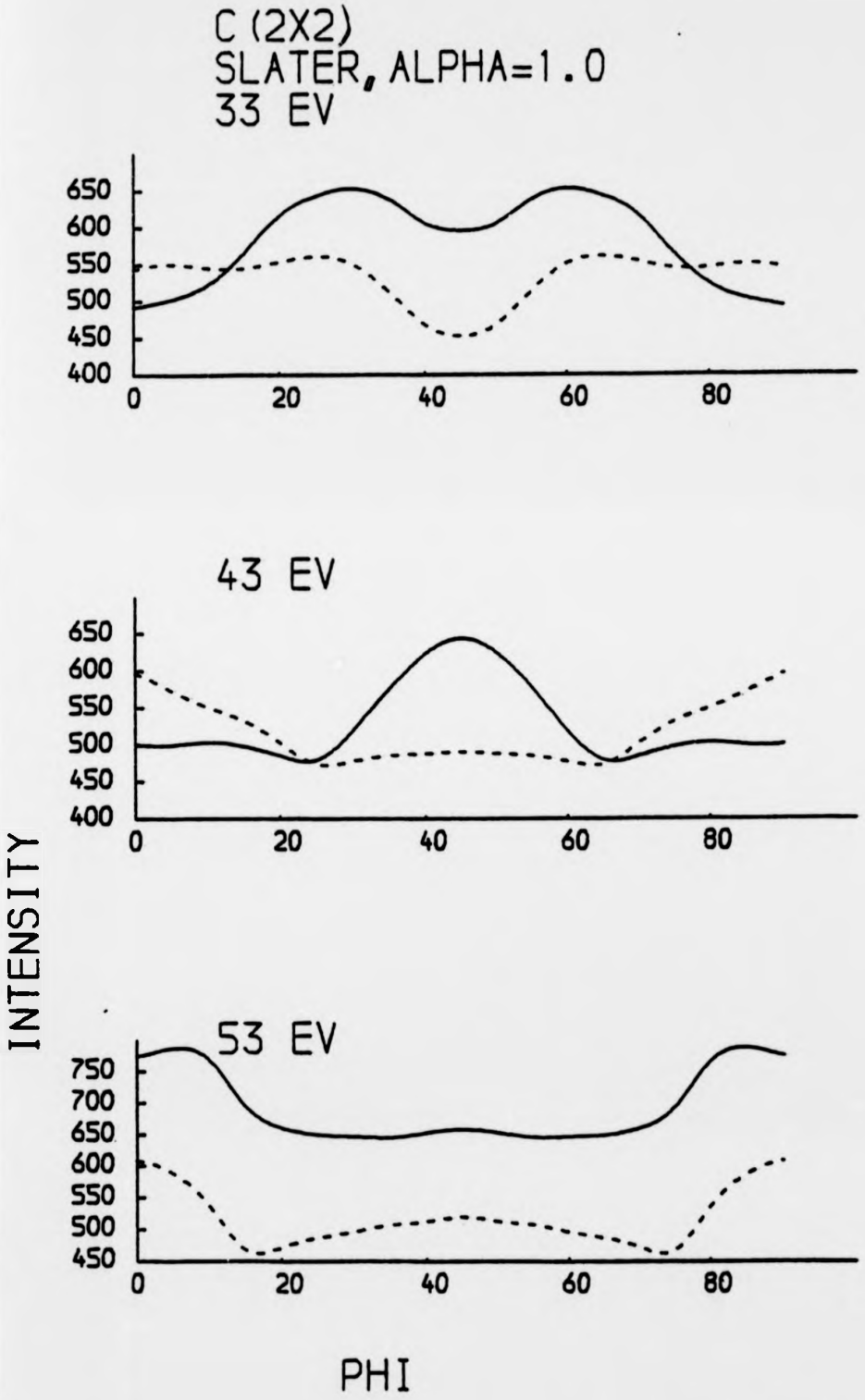
C (2X2)
SLATER, ALPHA=1.0
33 EV
650
600
550
500
450
400
0
20
40
60
80
43 EV
650
600
550
500
450
400
0
20
40
60
80
53 EV
750
700
650
600
550
500
450
0
20
40
60
80
INTENSITY
PHI

In the calculations, the phase shifts for Te are computed by the method described in section (2.4) with the Te atoms being put onto a simple cubic lattice and putting $\alpha = 1$ into the calculation of the exchange potential, (equation(2.53)). At the time that these calculations were being performed, the MUFFPOT program had not been adapted to calculate the Te4d photoionisation amplitudes. However, it is clear that in the energy range of interest the Te4d → f cross-section dominates, (McGuire (1970)), and so in this case the sign and magnitude of the ratio $\sigma(4d \rightarrow f)$: $\sigma(4d \rightarrow p)$ is not critical in the determination of the angle-resolved intensity. The Ni phase shifts are calculated from the Wakoh potential, (Wakoh (1965)). The inner potential (11eV) and the electron mean free path (8 Å) are taken from the LEED calculation for this system, (Demuth et al (1973ab, 1974)). The $d_\perp$-spacing is put equal to 1.9 Å for both the c(2 x 2) and p(2 x 2) coverages. The surface is modelled by a slab consisting of one Te layer and two Ni layers. We saw in Chapter 3 that the lower Ni layers have a very small effect on the diffraction patterns. The scattering electron is described by six partial waves and the multiple scattering series is evaluated to sixth order in reverse scattering.

The calculations for some of the data for both coverages of Te are shown in fig. (4.8). There is very little agreement between theory and experiment for most energies. The change in shape of the calculated diffraction curves with increasing energy is different to the corresponding trend in the experimental data. From our findings in Chapter 3 on the structural sensitivity of the diffraction patterns for this system, an obvious thing to do is to alter the $d_\perp$-spacing as this quantity is only known to an accuracy of ± 0.1 Å from the LEED analysis. Calculations for $d_\perp$ = 1.8 Å and 2.0 Å are shown in fig. (4.9) for electron kinetic energies 33 eV, 43 eV and 53 eV. There is clearly no better agreement with experiment for either $d_\perp$-spacing. From our findings on the sensitivity at some energies of the diffraction patterns to small changes in non-structural

Figure 4.10: Effects of changing the detector angle θ by $\pm 2^{\circ}$ from its nominal value of 30° with respect to the surface normal.

Full curves: $\theta = 28^{\circ}$

Broken curves: $\theta = 32^{\circ}$

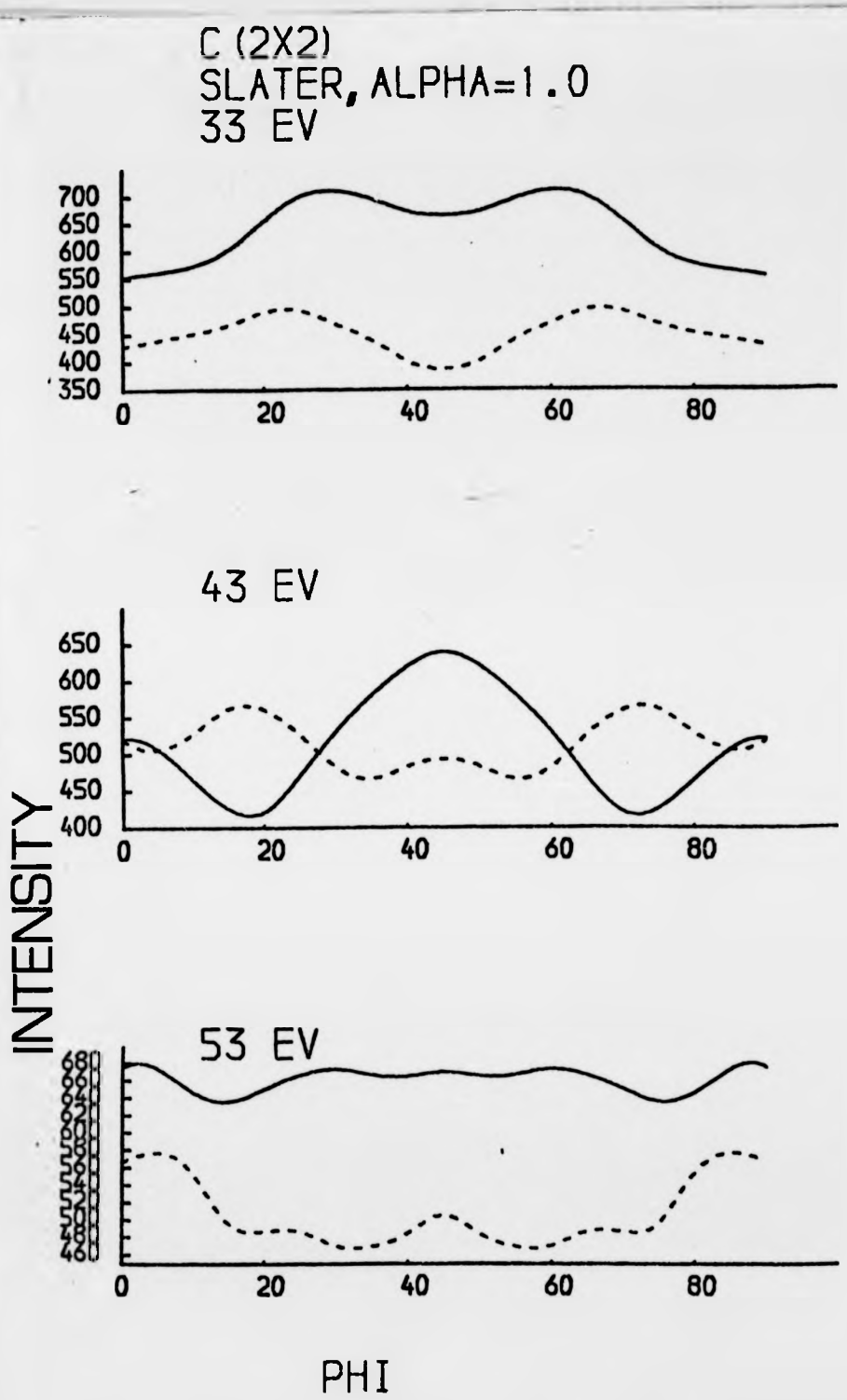
C (2X2)
SLATER, ALPHA=1.0
33 EV
700
650
600
550
500
450
400
350
0
20
40
60
80
43 EV
650
600
550
500
450
400
0
20
40
60
80
INTENSITY
53 EV
0
20
40
60
80
PHI

Figure 4.11: Effects of changing the bonding site on the photoelectron diffraction curves.

Full curves: Te atom adsorbed at the bridge site.

Broken curves: Te atom adsorbed at the one-fold site.

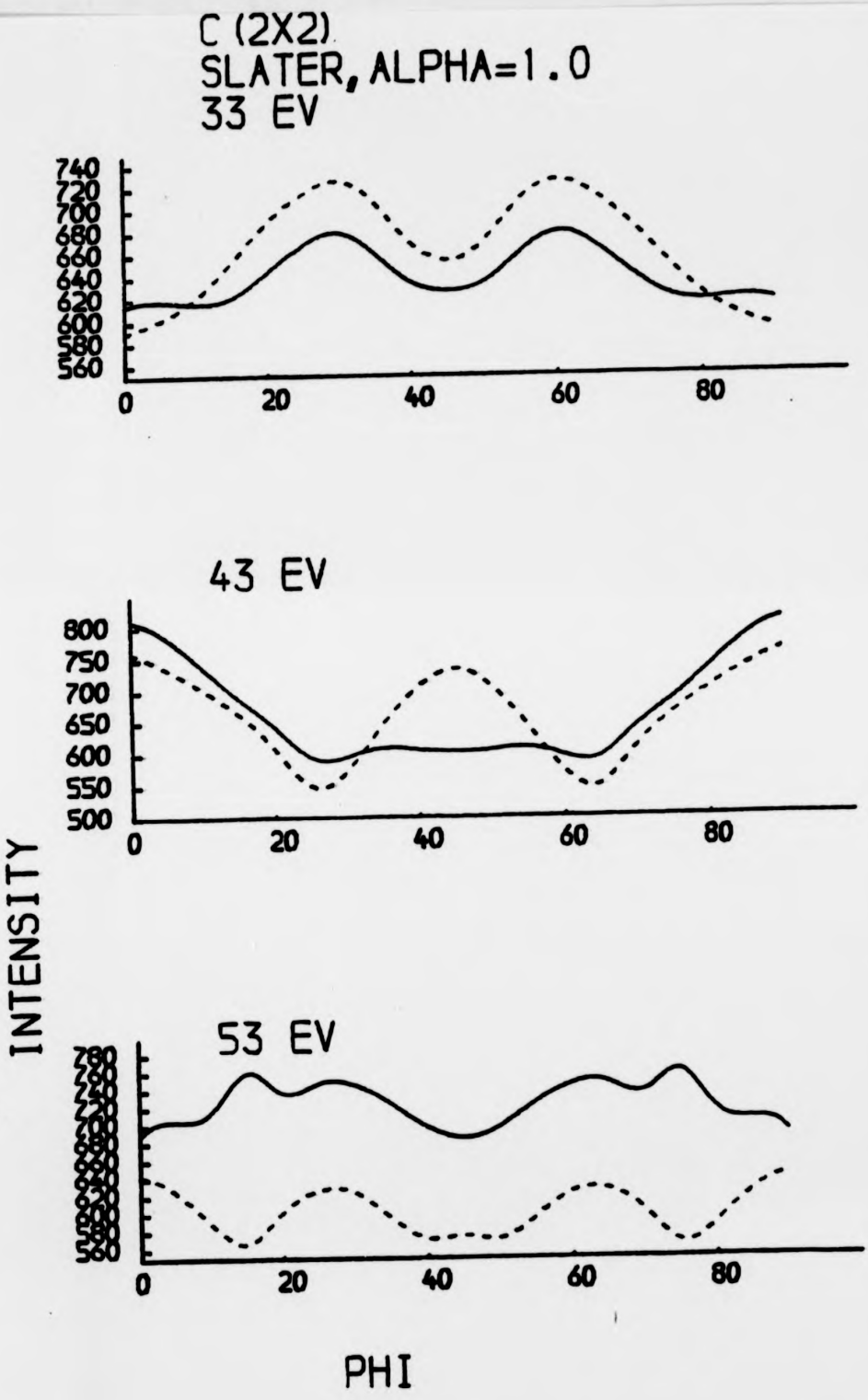
C (2X2)
SLATER, ALPHA=1.0
33 EV
740
720
700
680
660
640
620
600
580
560
0
20
40
60
80
43 EV
800
750
700
650
600
550
500
0
20
40
60
80
INTENSITY
53 EV
0
20
40
60
80
PHI

parameters, it is of interest to see whether we can improve matters by changing the detector angle by $\pm 2^{\circ}$, (although in actual fact the uncertainty in this parameter is less than this). In fig. (4.10) whislt we see that some of the diffraction patterns are different from those for $\theta = 30^{\circ}$, we can still get no nearer to matching the experimental data. We must now consider changing the bonding site of the Te atom, a rather drastic measure, because this would then contradict the findings of the original LEED analysis. The effects of changing the bonding site from the four-fold to the one-fold and bridge sites for electron kinetic energies 33 eV, 43 eV and 53 eV are shown in fig. (4.11) and again it is apparent that we can get no nearer to matching the data.

Finally in this section, we should mention that there is a possibility that our difficulties in matching the data may be caused by the presence of disordered domains of Te on the Ni surface, (Becker and Hagstrum (1975)). In LEED this problem is not too serious because the ordered domains show up as sharp spots in the LEED pattern, whilst the disordered domains show up as a continuous background. By concentrating on these spots one is homing in on the contributions from the ordered domains of Te on the surface. Inevitably one will also be picking up scattering from disordered domains, but it is possible to estimate how serious a problem this is by comparing the intensities of the spots with the intensity of the background. In angle-resolved photoemission, where discrete beams of electrons are not produced, one is not able to select the contributions from the ordered domains, and hence one is detecting emission from both the ordered and disordered parts of the Te overlayer. There is no satisfactory way that this may be taken into account in the calculations. However this is only speculation and the cause of our difficulties in matching the data may lie elsewhere.

4.4. Summary

We have obtained fairly good agreement between theory and experiment (Farrell et al (1981ab)) for the system Ag(111) - $(\sqrt{3} \times \sqrt{3})R30^{\circ}I$ using the bonding site determined by LEED (Forstmann et al (1973)) and the $d_{\perp}$-spacing determined by SEXAFS, (Citrin et al (1978)). Our calculations are found to be no more sensitive to $d_{\perp}$ than LEED, but there is considerable sensitivity to changes in the bonding site due to the dominance of scattering between the I atoms and nearest neighbour Ag atoms.

For both Ni(001) - c(2 x 2)Te and Ni(001) - p(2 x 2)Te we obtain poor agreement between theory and experiment, (Woodruff (1980)). Small variations in the structural and non-structural parameters in the calculation do not improve matters. We have also noted that the presence of disordered domains of the Te atoms may be causing the problems that we encounter in matching the data; this problem would not be serious when doing a LEED analysis on this system.

REFERENCES FOR CHAPTER 4

Andersson, S. and Pendry, J. B., Solid State Comm., 16, 569 (1975).

Andersson, S. and Pendry, J. B., Phys. Rev. Lett. 43, 363 (1979).

Becker, G. E. and Hagstrum, H. D., J. Vac. Sci. Technol., 12, 234 (1975).

Citrin, P. H., Eisenberger, P. E. and Hewitt, R. C., Phys. Rev. Lett, 41, 309 (1978).

Demuth, J. E., Jepsen, D. W. and Marcus, P. M., Phys. Rev. Lett. 31, 540, (1973a).

Demuth, J. E., Jepsen, D. W. and Marcus, P. M., J. Phys. C6, L307 (1973b).

Demuth, J. E., Marcus, P. M. and Jepsen, D. W., Phys. Rev. Lett. 32, 1182 (1974).

Demuth, J. E., Jepsen, D. W. and Marcus, P. M., J. Phys. C8, L25 (1975).

Farrell, H. H., Traum, M. M., Smith, N. V., Royer, W. A., Woodruff, D. P. and Johnson, P. D. Surf. Sci.

Farrell, H. H., Lasser, R., Smith, N. V. and Traum, M. M. to be published (1981b).

Forstmann, F., Berndt, W. and Büttner, P., Phys. Rev. Lett. 30, 17 (1973).

Jona, F., Private Communication

Kevan, S. D., Rosenblatt, D. H., Denley, D. Lu, B-C, and Shirley, D. A., Phys. Rev. Lett. 41, 1565 (1978).

Kevan, S. D., Rosenblatt, D. H., Denley, D., Lu, B-C, and Shirley, D. A., Phys. Rev. B20, 4133 (1979).

Kevan, S. D., Tobin, J. G., Rosenblatt, D. H., Davis, R. F. and Shirley, D. A., Phys. Rev. B23, 493 (1981).

Kang, W. M., Li, C. H. and Tong, S. Y., Solid State Comm. 36, 149 (1980).

Kono, S., Fadley, C. S., Hall, N. F. T. and Hussain, Z., Phys. Rev. Lett. 41, 117 (1978a).

Kono, S., Goldberg, S. M., Hall, N. F. T. and Fadley, C. S., Phys. Revl. Lett. 41, 1831 (1978b).

Li, C. H. and Tong, S. Y., Phys. Rev. Lett. 42, 901 (1979a).

Li, C. H. and Tong, S. Y., Phys. Rev. B19, 1769 (1979b).

Liebsch, A., Solid State Comm. 19, 1193 (1976).

McDonnell, L., Woodruff, D. P., Mitchell, K. A. R., Surf. Sci. 45, 1 (1974).

McGovern, I. T., Eberhardt, W. and Plummer, E. W., Solid State Comm. 32, 963 (1979).

McGuire, E. J., Res. Rep. Scandia Laboratories, Albuquerque, New Mexico (USA), SC-RR-721 (1970).

Passier, M., Ignatiev, A., Jona, F., Jepsen, D. W. and Marcus, P. M., Phys. Rev. Lett. 43, 360 (1979).

Petersson, L-G, Kono, S., Hall, N. F. T., Fadley, C. S., and Pendry, J. B., Phys. Rev. Lett. 42, 1545 (1979).

Schwartz, K., Phys. Rev. B5, 2466 (1972).

Smith, N. V., Traum, M. M. and Di Salvo, F. J., Solid State Comm. 15, 211 (1974).

Stoner, N., Van Hove, M. A., Tong, S. Y. and Webb, M. B., Phys. Rev. Lett. 40, 243 (1978).

Tong, S. Y., (1980), private communication.

Van Hove, M. A. and Tong, S. Y., J. Vac. Sci. Technol. 12, 230 (1975).

Wakoh, S., J. Phys. Soc. Japan, 20, 1984 (1965).

Williams, G. P., Cerrina, F., McGovern, I. T. and Lapeyre, G. J., Solid State Comm. 31, 15 (1979).

Woodruff, D. P., Norman, D., Holland, B. W., Smith, N. V., Farrell, H. H. and Traum, M. M., Phys. Rev. Lett. 41, 1130 (1978).

Woodruff, D. P., (1980), private communication.

CHAPTER 5

CHOICE OF MODEL POTENTIAL FOR PHOTOELECTRON DIFFRACTION

5.1. Introduction

We have already mentioned that problems have been encountered in work on the energy dependence of the normal emission intensity from the 4d levels of c(2 x 2)Te adsorbed on Ni(001). McGovern et al (1979) have found it impossible to match their experimental data for this system with the calculations of Li and Tong (1979b). The aim of this chapter is to explain why such a discrepancy has arisen and how it may be resolved. This will then lead us to discuss further the calculation of the atomic potential that is used in photoelectron diffraction and related calculations.

5.2. The Calculation of the Atomic Potential

The atomic photoionization cross-section for emission from an initial state specified by quantum numbers n and ℓ is given by (Cooper (1962))

$$S_{n\ell}(E) = \frac{4\pi\alpha a_o^2}{3}(E+E_c)\{(\ell+1)|\sigma_{n\ell,\ell+1}|^2+\ell|\sigma_{n\ell,\ell-1}|^2\} \qquad (5.1)$$

where $\alpha = (1/137)$ is the fine structure constant, a_o is the Bohr radius, E is the kinetic energy of the electron with respect to the muffin-tin zero, E_c is the binding energy of the electron with respect to the muffin-tin zero and $\sigma_{n\ell,\ell+1}$ and $\sigma_{n\ell,\ell-1}$ are the photoionization amplitudes as defined in equation (2.12). In the calculation of the photoionization cross-sections for various atomic levels, it is known that one can classify the initial state into one of two categories depending on the behaviour of the cross-section with energy, (Cooper (1962)). For intial states with $n=\ell+1$, the photoionization cross-section is a smooth function

CHAPTER 5

CHOICE OF MODEL POTENTIAL FOR PHOTOELECTRON DIFFRACTION

5.1. Introduction

We have already mentioned that problems have been encountered in work on the energy dependence of the normal emission intensity from the 4d levels of c(2 x 2)Te adsorbed on Ni(001). McGovern et al (1979) have found it impossible to match their experimental data for this system with the calculations of Li and Tong (1979b). The aim of this chapter is to explain why such a discrepancy has arisen and how it may be resolved. This will then lead us to discuss further the calculation of the atomic potential that is used in photoelectron diffraction and related calculations.

5.2. The Calculation of the Atomic Potential

The atomic photoionization cross-section for emission from an initial state specified by quantum numbers n and ℓ is given by (Cooper (1962))

$$S_{n\ell}(E) = \frac{4\pi\alpha a_o^2}{3}(E+E_c)\{(\ell+1)|\sigma_{n\ell,\ell+1}|^2+\ell|\sigma_{n\ell,\ell-1}|^2\} \qquad (5.1)$$

where $\alpha = (1/137)$ is the fine structure constant, a_o is the Bohr radius, E is the kinetic energy of the electron with respect to the muffin-tin zero, E_c is the binding energy of the electron with respect to the muffin-tin zero and $\sigma_{n\ell,\ell+1}$ and $\sigma_{n\ell,\ell-1}$ are the photoionization amplitudes as defined in equation (2.12). In the calculation of the photoionization cross-sections for various atomic levels, it is known that one can classify the initial state into one of two categories depending on the behaviour of the cross-section with energy, (Cooper (1962)). For intial states with $n=\ell+1$, the photoionization cross-section is a smooth function

Figure 5.1: Photoionisation cross-sections for Cu3d and Ag4d, (photocopied from Cooper (1962)).

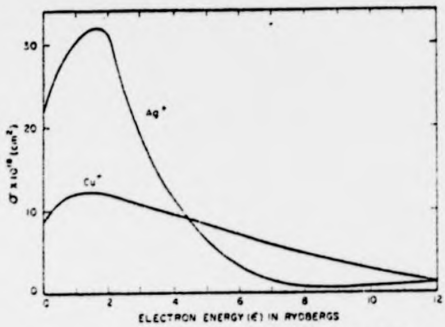

Photoionization cross sections for Ag^+ and Cu^+.

Figure 5.2: Plot of $U_{n\ell}(r)$ and $R_{\ell+1}(r)$ versus r for Ne2p (top panel), Ar3p (middle panel) and Kr4p (lower panel). The d-waves have been ploted for zero energy.
(Photocopied from Cooper (1962)).

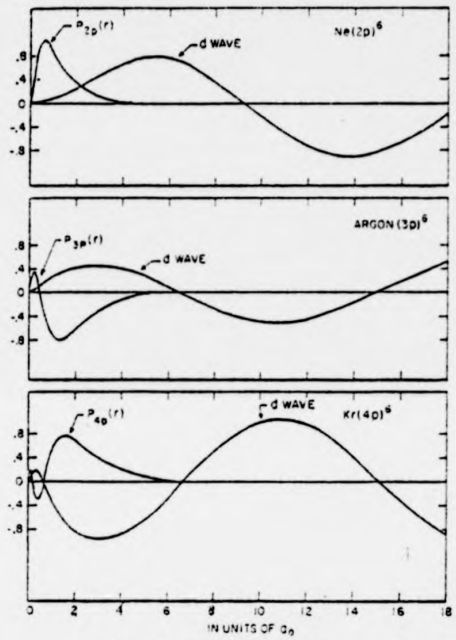

Outer subshell radial wave functions and d waves for $\epsilon=0$ for Ne, Ar, and Kr.

of energy; an example for Cu3d is shown in fig. (5.1). For initial states with nodes ($n \neq \ell+1$), the cross-section decreases to a minimum, (known as the Cooper minimum (Cooper (1962)), and then rises again as the energy increases. An example for Ag4d is shown in Fig. (5.1). The explanation for this may be seen by looking at the photoionization amplitude

$$\sigma_{n\ell,\ell+1} = \int_0^\infty U_{n\ell}(r) R_{\ell+1}(r) r^3 dr \qquad (5.2)$$

where $U_{n\ell}(r)$ is the radial part of the initial state wavefunction and $R_{\ell+1}(r)$ is the radial part of the emitted electron's wavefunction. In fig. (5.2) we show a plot of $R_{\ell+1}(r)$ and $U_{n\ell}(r)$ as a function of the distance from the centre of the atom, for Ar 3p, Ne 2p and Kr 4p. In each case as the energy increases the outgoing d-wave overcomes the centrifugal barrier $\frac{1}{r^2}(\ell+1)\ell$, (equation (2.42)), and so moves towards the origin. For Ne 2p this results in an initial increase of $\sigma_{n\ell,\ell+1}$ with energy as the overlap in $R_{\ell+1}(r)$ and $U_{n\ell}(r)$ increases, and then in a gentle monotonic decrease as the first maximum in $R_{\ell+1}(r)$ passes to the left of the maximum in $U_{n\ell}(r)$. The resulting photoionization cross-section gently increases to a maximum and then monotonically decreases with energy. For Ar 3p, where a node is present in the initial state wavefunction, the photoionization cross-section varies with energy in a different way to that for Ne 2p. $\sigma_{n\ell,\ell+1}$ in this case starts off by being negative. As $\hbar\omega$ increases, the d-wave moves in and $|\sigma_{n\ell,\ell+1}|$ decreases. At a certain energy $\sigma_{n\ell,\ell+1}$ is zero. Beyond this energy, $\sigma_{n\ell,\ell+1}$ becomes positive and gently increases with energy. The resulting photoionization cross-section will decrease to a Cooper minimum and then increase again. The photoionization cross-section for Kr 4p follows a similar behaviour to that for Ar 3p. For some initial states, such as Te 4d, the onset of the Cooper minimum is delayed by the strong centrifugal repulsion on the out-going f-wave. This results in the photoionization

Figure 5.3: The photoionisation cross-section (σ) for the 4d levels of atomic Xe versus photoelectron energy in the vacuum (E).

Full line: experimental data (Ederer 1964).

Dashed line: calculation using Xα potential with α=1.

Dotted line: Hartree-Fock calculation including exchange with 4d states only (Combet Farnoux (1970)).

The peaks have been scaled individually to make the heights equal.

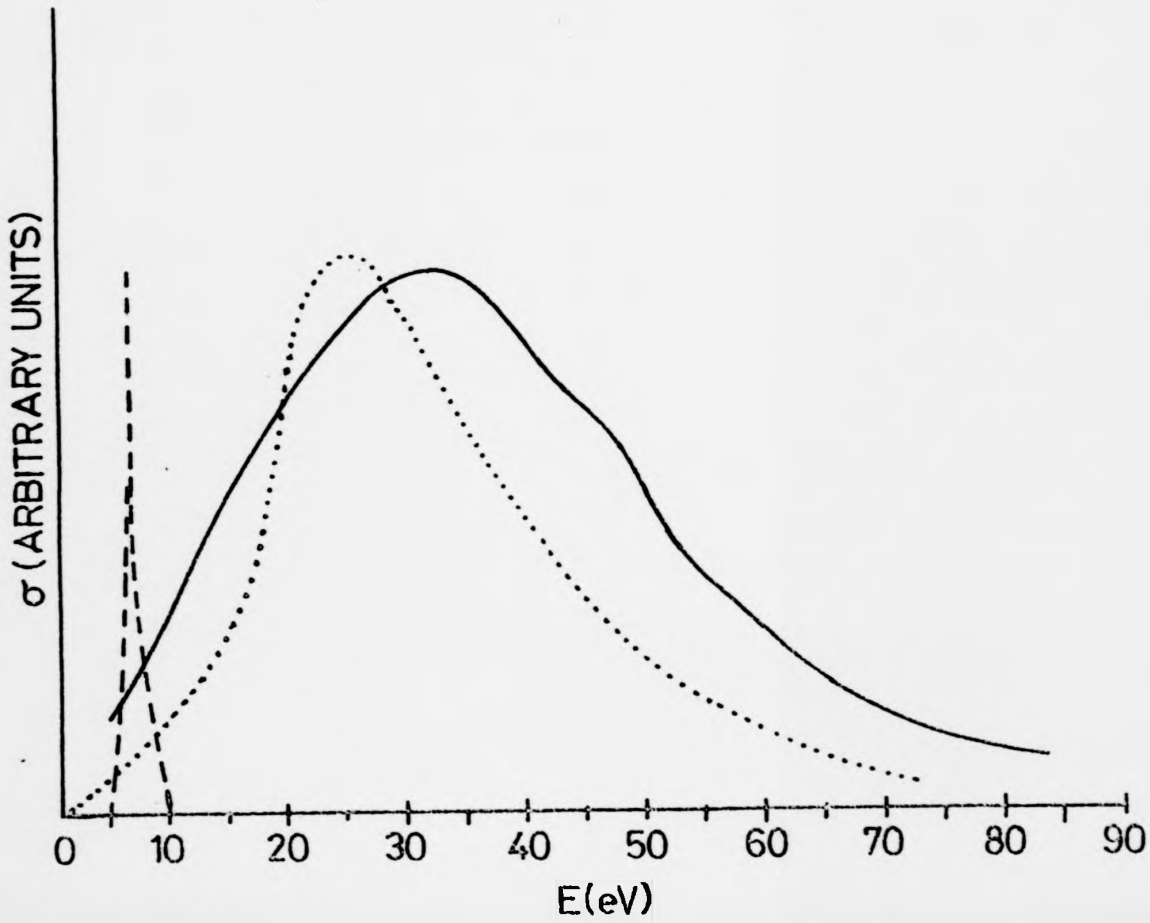
σ (ARBITRARY UNITS)
0
10
20
30
40
50
60
70
80
90
E(eV)

Figure 5.4: Phase shifts for Xe in crystalline form versus electron kinetic energy in the vacuum.

Full curves: Hartree-Fock calculation (Pendry (1974)).

Dashed curves: Xα calculations with α=1.

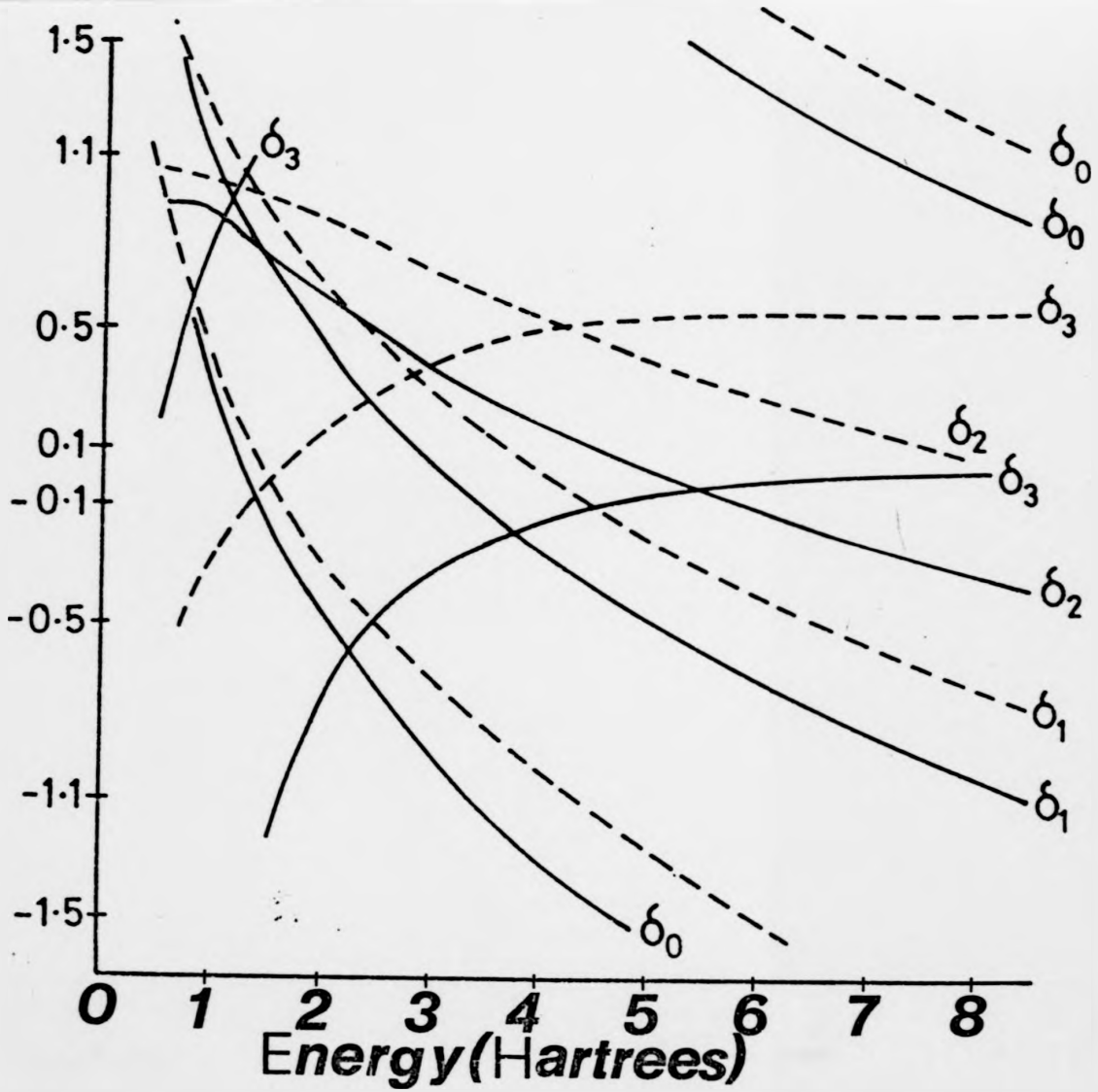
1·5
1·1
0·5
0·1
-0·1
-0·5
-1·1
-1·5
0
1
2
3
4
5
6
7
8
Energy (Hartrees)
δ0
δ1
δ2
δ3

cross-section rising to a sharp peak before going through a Cooper minimum. In the above discussion we have not had cause to discuss the energy dependence of $\sigma_{n\ell,\ell-1}$, because in the energy range of interest, this quantity contributes only in a small way to the photoionization cross-section.

Li and Tong (1979b) have shown that the CIS data taken for emission from initial states with $n\neq\ell+1$ are dominated by the atomic photoionization cross-section. Scattering effects merely show up as small modulations on the experimental curves. Now it is well known that calculations of atomic photoionization cross-sections, which employ the Slater model for the exchange (Slater (1951)), give poor agreement between theory and experiment for such initial states, (see e.g. Manson (1978)). In these calculations, the resonance peak is placed at too low an energy and is far narrower than it should be. This is the potential that Li and Tong (1979) have used in their calculations for Te 4d normal emission from Ni(001) - c(2 x 2)Te. As an illustration of the discrepancies that arise we show in fig. (5.3) a comparison of the experimental data of Ederer (1964) for the Xe 4d photoionization cross-section, with a Hartree-Slater calculation with $\alpha=1$, and a Hartree-Fock calculation where only the exchange interaction of the emitted electron with the remaining 4d electrons is included (Combet Farnoux (1970)). Whilst the Hartree-Fock calculation gives a good description of the experimental data, the Hartree-Slater calculation places the resonance peak at too low an energy with too narrow a width. Clearly the Hartree-Fock calculation is providing a better potential for the Xe atom than the Hartree-Slater calculation. This may also be seen if one compares a Hartree-Fock calculation for the first four phase shifts of Xe (Pendry (1974)) with a Slater $X\alpha$ calculation with $\alpha=1$, (fig. (5.4)). There are discrepancies between the two calculations. In particular the resonance in the $\ell=3$ phase shift is placed at far too low an energy by the $X\alpha$ calculation. The resonance in δ_3 is tied in with

Figure 5.5: Phase shifts for Xe in crystalline form versus electron kinetic energy in the vacuum.

Full curves: Hartree-Fock calculation (Pendry (1974)).

Dashed curves: Xα calculations with α=0.5.

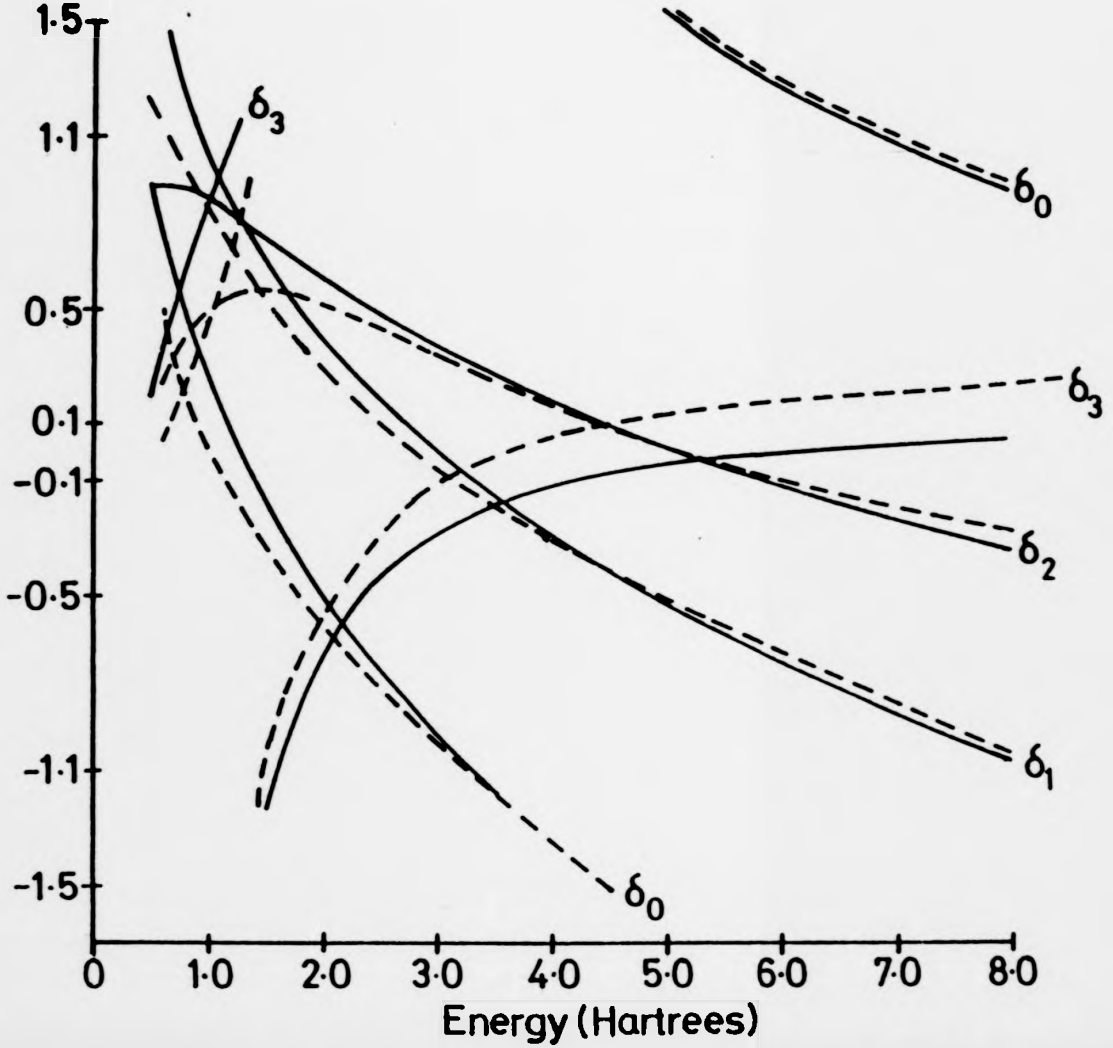
1·5
1·1
0·5
0·1
-0·1
-0·5
-1·1
-1·5
δ3
δ0
δ3
δ2
δ1
δ0
0
1·0
2·0
3·0
4·0
5·0
6·0
7·0
8·0
Energy (Hartrees)

the resonance in the 4d photoionization cross-section. Thus, not only are we performing a poor calculation for the photoionization cross-section but we are also poorly describing the scattering properties of the Xe atom. For photoelectron diffraction experiments that use the azimuthal mode, where emission from 4d levels is studied, data is taken for energies in the region of this resonance in order to maximise the signal. For Xe 4d this region would be $\sim$ 30 eV electron kinetic energy. From fig. (5.4) it may be seen that δ_3 is calculated to be $\sim$ -0.1 from the Xα calculation whilst Hartree-Fock calculates δ_3 to be $\sim$ 1.5. Smaller differences are seen in the other phase shifts. This has serious implications for the calculations for Te 4d emission from Ni(001) - c(2 x 2)Te and I4d emission from Ag(111) - $(\sqrt{3} \times \sqrt{3})R30^{\circ}$I where it is clear that we are using poor potentials for the I and Te atoms. The inadequacy in the Xα calculations for the atomic 4d cross-sections is probably also causing the poor description of McGovern et al's (1979) CIS data for Ni(001) - c(2 x 2)Te. These findings imply that we should be using a Hartree-Fock potential to calculate the phase shifts and photoionization amplitudes. However such calculations need to be iterated to self-consistency and are thus tedious to perform.

Now in the Xα calculations the parameter α multiplying the exchange term can, in principle, be varied between 0 and 1, (Slater and Johnson (1972)). As it is the treatment of exchange that is the main difference between the Hartree-Fock and Hartree-Slater calculations it is of interest to see what the effects are of varying α in the Xα calculations of the photoionization cross-sections and phase shifts for Xe. We have found that by reducing α to 0.5 in the calculation of the exchange potential, the resulting phase shifts for Xe are in much closer agreement with the corresponding Hartree-Fock calculation, (Pendry (1974)); this is shown in fig. (5.5). We now see that in the Xα(α=0.5) calculation the position

Figure 5.7: Photoionisation cross-section versus photon energy for the 4d levels of Te calculated using the Xα potential for a range of α values.

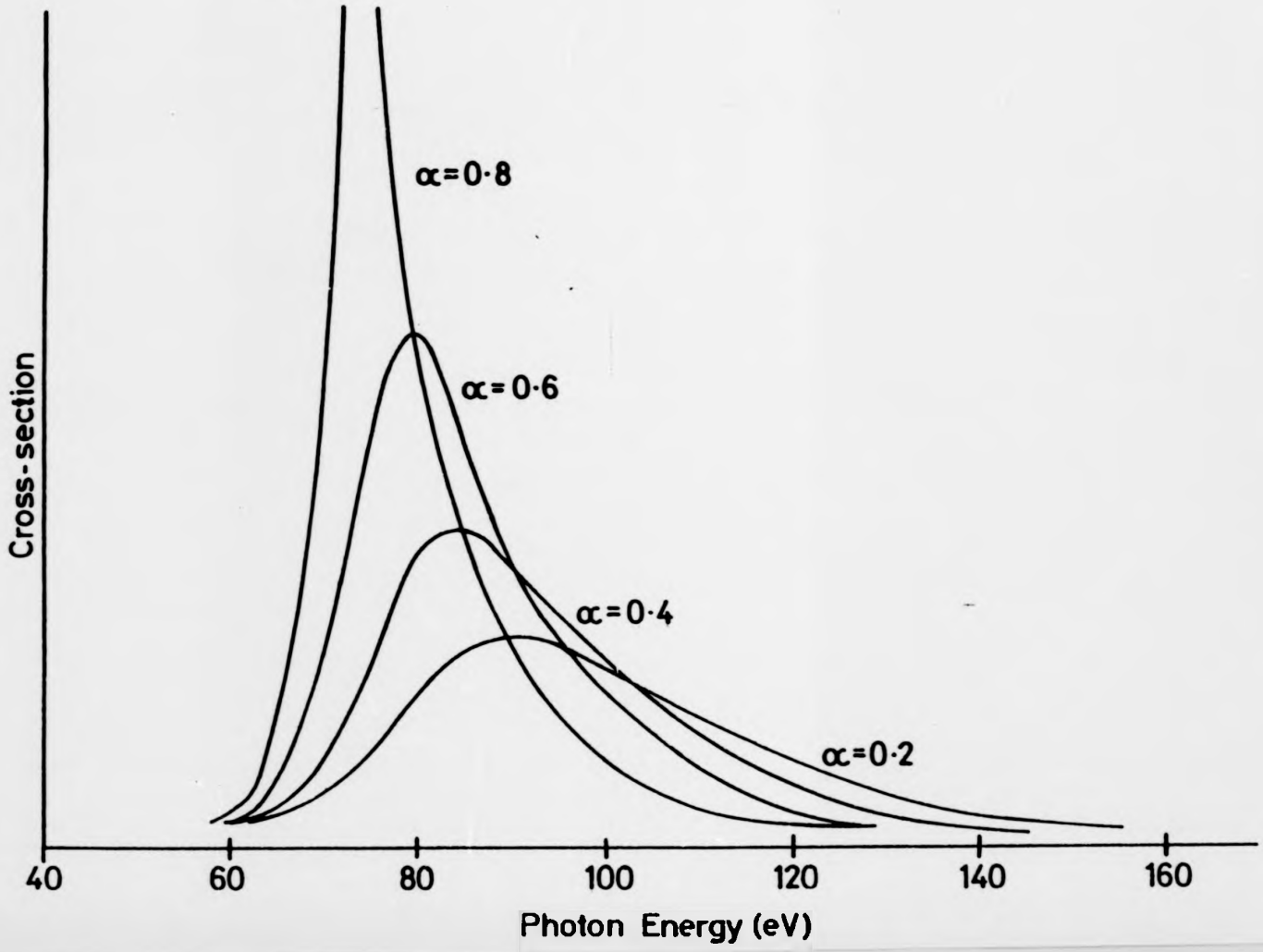
α=0·8
α=0·6
α=0·4
α=0·2
Cross-section
40
60
80
100
120
140
160
Photon Energy (eV)

the resonance in the 4d photoionization cross-section. Thus, not only are we performing a poor calculation for the photoionization cross-section but we are also poorly describing the scattering properties of the Xe atom. For photoelectron diffraction experiments that use the azimuthal mode, where emission from 4d levels is studied, data is taken for energies in the region of this resonance in order to maximise the signal. For Xe 4d this region would be $\sim$ 30 eV electron kinetic energy. From fig. (5.4) it may be seen that δ_3 is calculated to be $\sim$ -0.1 from the Xα calculation whilst Hartree-Fock calculates δ_3 to be $\sim$ 1.5. Smaller differences are seen in the other phase shifts. This has serious implications for the calculations for Te 4d emission from Ni(001) - c(2 x 2)Te and I4d emission from Ag(111) - $(\sqrt{3} \times \sqrt{3})R30^{\circ}$I where it is clear that we are using poor potentials for the I and Te atoms. The inadequacy in the Xα calculations for the atomic 4d cross-sections is probably also causing the poor description of McGovern et al's (1979) CIS data for Ni(001) - c(2 x 2)Te. These findings imply that we should be using a Hartree-Fock potential to calculate the phase shifts and photoionization amplitudes. However such calculations need to be iterated to self-consistency and are thus tedious to perform.

Now in the Xα calculations the parameter α multiplying the exchange term can, in principle, be varied between 0 and 1, (Slater and Johnson (1972)). As it is the treatment of exchange that is the main difference between the Hartree-Fock and Hartree-Slater calculations it is of interest to see what the effects are of varying α in the Xα calculations of the photoionization cross-sections and phase shifts for Xe. We have found that by reducing α to 0.5 in the calculation of the exchange potential, the resulting phase shifts for Xe are in much closer agreement with the corresponding Hartree-Fock calculation, (Pendry (1974)); this is shown in fig. (5.5). We now see that in the Xα(α=0.5) calculation the position

the resonance in the 4d photoionization cross-section. Thus, not only are we performing a poor calculation for the photoionization cross-section but we are also poorly describing the scattering properties of the Xe atom. For photoelectron diffraction experiments that use the azimuthal mode, where emission from 4d levels is studied, data is taken for energies in the region of this resonance in order to maximise the signal. For Xe 4d this region would be $\sim$ 30 eV electron kinetic energy. From fig. (5.4) it may be seen that δ_3 is calculated to be $\sim$ -0.1 from the Xα calculation whilst Hartree-Fock calculates δ_3 to be $\sim$ 1.5. Smaller differences are seen in the other phase shifts. This has serious implications for the calculations for Te 4d emission from Ni(001) - c(2 x 2)Te and I4d emission from Ag(111) - ($\sqrt{3}$ x $\sqrt{3}$)R30°I where it is clear that we are using poor potentials for the I and Te atoms. The inadequacy in the Xα calculations for the atomic 4d cross-sections is probably also causing the poor description of McGovern et al's (1979) CIS data for Ni(001) - c(2 x 2)Te. These findings imply that we should be using a Hartree-Fock potential to calculate the phase shifts and photoionization amplitudes. However such calculations need to be iterated to self-consistency and are thus tedious to perform.

Now in the Xα calculations the parameter α multiplying the exchange term can, in principle, be varied between 0 and 1, (Slater and Johnson (1972)). As it is the treatment of exchange that is the main difference between the Hartree-Fock and Hartree-Slater calculations it is of interest to see what the effects are of varying α in the Xα calculations of the photoionization cross-sections and phase shifts for Xe. We have found that by reducing α to 0.5 in the calculation of the exchange potential, the resulting phase shifts for Xe are in much closer agreement with the corresponding Hartree-Fock calculation, (Pendry (1974)); this is shown in fig. (5.5). We now see that in the Xα(α=0.5) calculation the position

Figure 5.6: Photoionisation cross-section for the 4d levels of atomic Xe (σ) versus electron kinetic energy in the vacuum (E) calculated using the Xα potential for a range of α values.

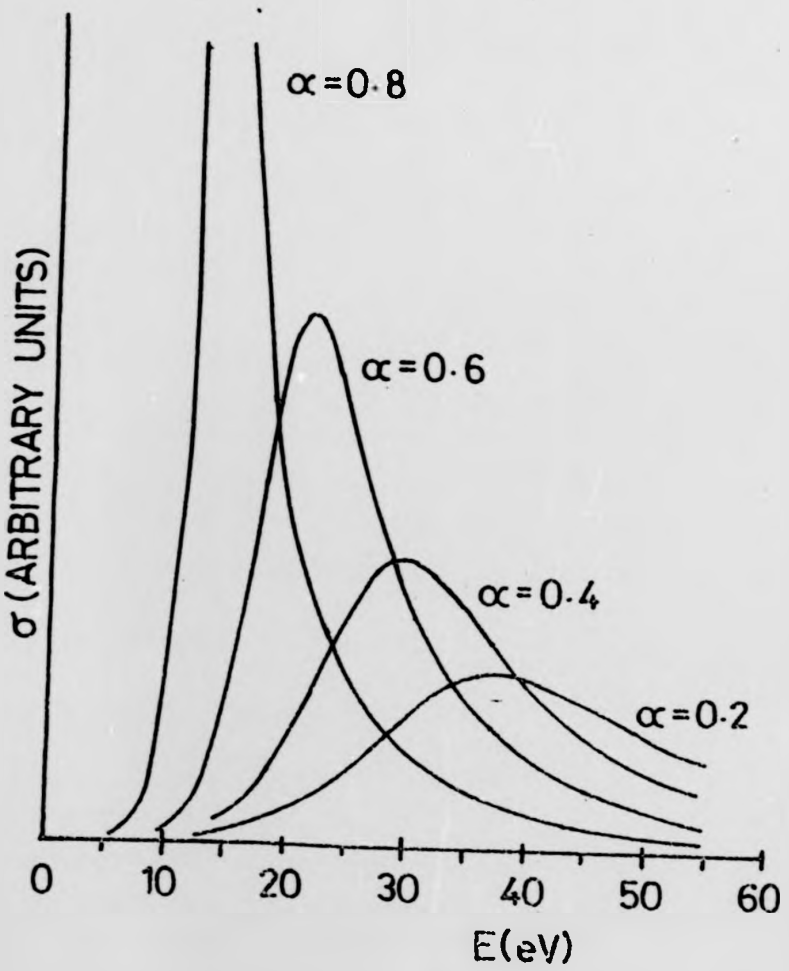

Fig 5.6

Figure 5.7: Photoionisation cross-section versus photon energy for the 4d levels of Te calculated using the Xα potential for a range of α values.

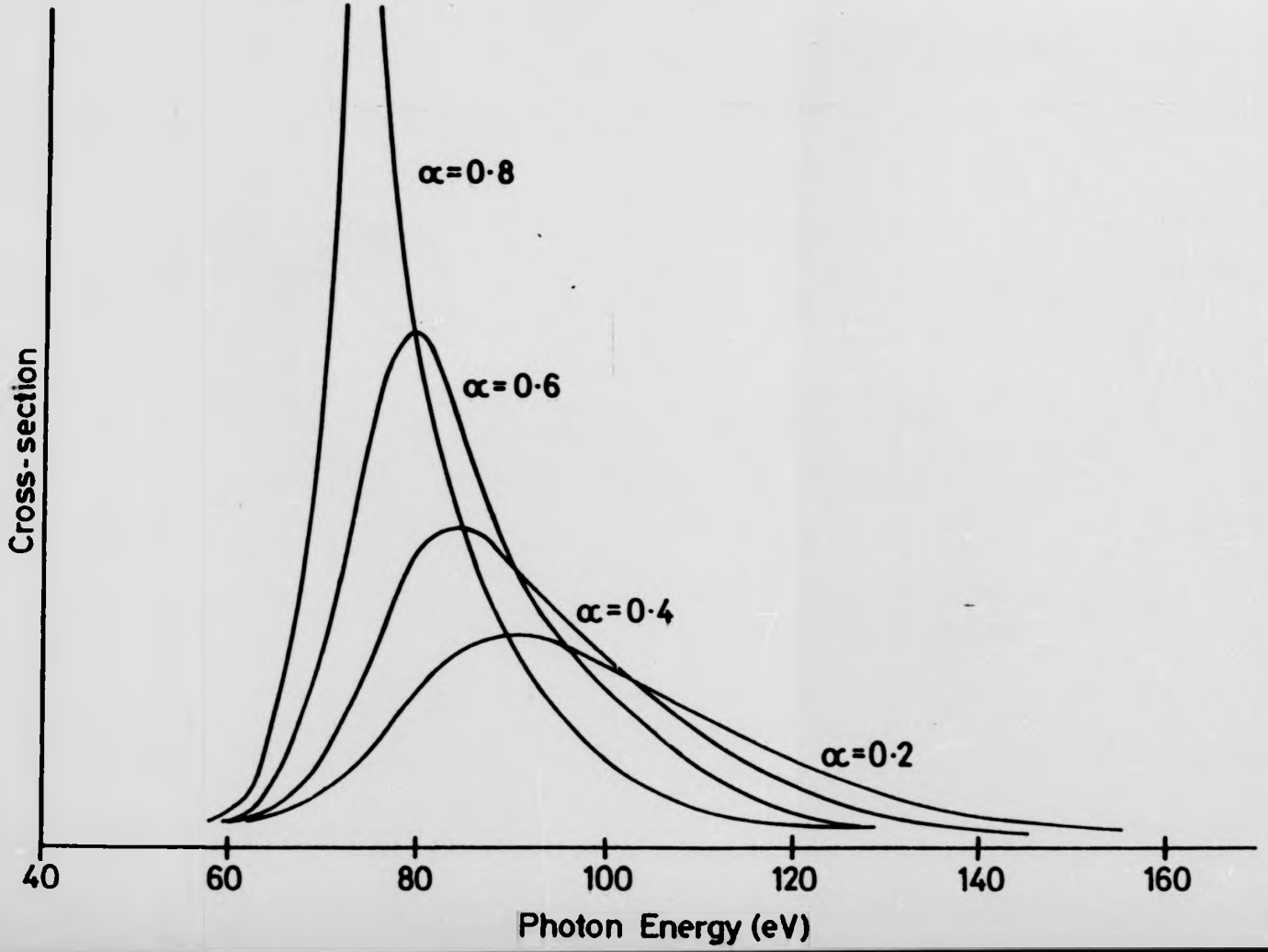
α=0·8
α=0·6
α=0·4
α=0·2
Cross-section
40
60
80
100
120
140
160
Photon Energy (eV)

Fig 5.7

of the δ_3 resonance is now very close to the position predicted by the Hartree-Fock calculation. The effect of varying α in the calculation of the Xe 4d photoionization cross-section is shown in fig. (5.6). The position and width of the resonance is very sensitive to changes in this parameter. The calculation with $\alpha = 0.4$ is in best agreement with the experimental data (Ederer (1964)). Similar atomic cross-section calculations for Te 4d are shown in fig. (5.7). Here, putting $\alpha = 0.2$ gives best agreement with experiment. Thus, in previous Xα calculations of atomic photoionization cross-sections, the exchange contribution to the potential has been over-estimated. The question should now be asked as to why in band-structure calculations is has been found adequate to put α equal to some value between $^2/_3$ and 1 whilst in calculations of atomic photoionization cross-sections we have to reduce α to below $^2/_3$. The answer lies in the fact that the Slater Xα term, (equation (2.53)), is an average below the Fermi level of the Hartree-Fock potential for a free electron gas. Such an average is appropriate in the calculation of ground state properties. In the case of electron scattering off an atom such an average is inappropriate because we are now interested in the exchange interaction between the scattering electron and the electrons bound to the atom. We have already pointed out that this electron has an energy that is typically 5-50 times larger than that of the bound electrons. So it would be more appropriate to use the Dirac potential, equation (2.51a), to calculate the exchange potential. This expression decreases in magnitude as the electron energy increases. As $k_i \to \infty$, the exchange potential V_{ex} tends to zero, and as $k_i \to 0$, $V_{ex} \to \frac{-2}{3}\left\{\frac{3\rho(r)}{8\pi}\right\}^{1/3}$ which is the Kohn-Sham expression (Kohn and Sham (1965)). Thus the reduction of α to below $^2/_3$ in the Xα calculation of the Xe phase shifts and photoionization cross-section is a reflection

of the δ_3 resonance is now very close to the position predicted by the Hartree-Fock calculation. The effect of varying α in the calculation of the Xe 4d photoionization cross-section is shown in fig. (5.6). The position and width of the resonance is very sensitive to changes in this parameter. The calculation with $\alpha = 0.4$ is in best agreement with the experimental data (Ederer (1964)). Similar atomic cross-section calculations for Te 4d are shown in fig. (5.7). Here, putting $\alpha = 0.2$ gives best agreement with experiment. Thus, in previous Xα calculations of atomic photoionization cross-sections, the exchange contribution to the potential has been over-estimated. The question should now be asked as to why in band-structure calculations is has been found adequate to put α equal to some value between $^2/3$ and 1 whilst in calculations of atomic photoionization cross-sections we have to reduce α to below $^2/3$. The answer lies in the fact that the Slater Xα term, (equation (2.53)), is an average below the Fermi level of the Hartree-Fock potential for a free electron gas. Such an average is appropriate in the calculation of ground state properties. In the case of electron scattering off an atom such an average is inappropriate because we are now interested in the exchange interaction between the scattering electron and the electrons bound to the atom. We have already pointed out that this electron has an energy that is typically 5-50 times larger than that of the bound electrons. So it would be more appropriate to use the Dirac potential, equation (2.51a), to calculate the exchange potential. This expression decreases in magnitude as the electron energy increases. As $k_i \to \infty$, the exchange potential V_{ex} tends to zero, and as $k_i \to 0$, $V_{ex} \to \frac{-2}{3}\left[\frac{3\rho(r)}{8\pi}\right]^{1/3}$ which is the Kohn-Sham expression (Kohn and Sham (1965)). Thus the reduction of α to below $^2/3$ in the Xα calculation of the Xe phase shifts and photoionization cross-section is a reflection

Figure 5.8: Photoionisation cross-section (arbitrary units) versus electron kinetic energy in the vacuum (Hartrees) for the 4d levels of atomic Xe calculated using Hara exchange multiplied by an α parameter.

Full curve: $\alpha=1$

Dashed curve: $\alpha=0.5$

XENON PHOTOIONISATION CROSS-SECTION
HARA EXCHANGE

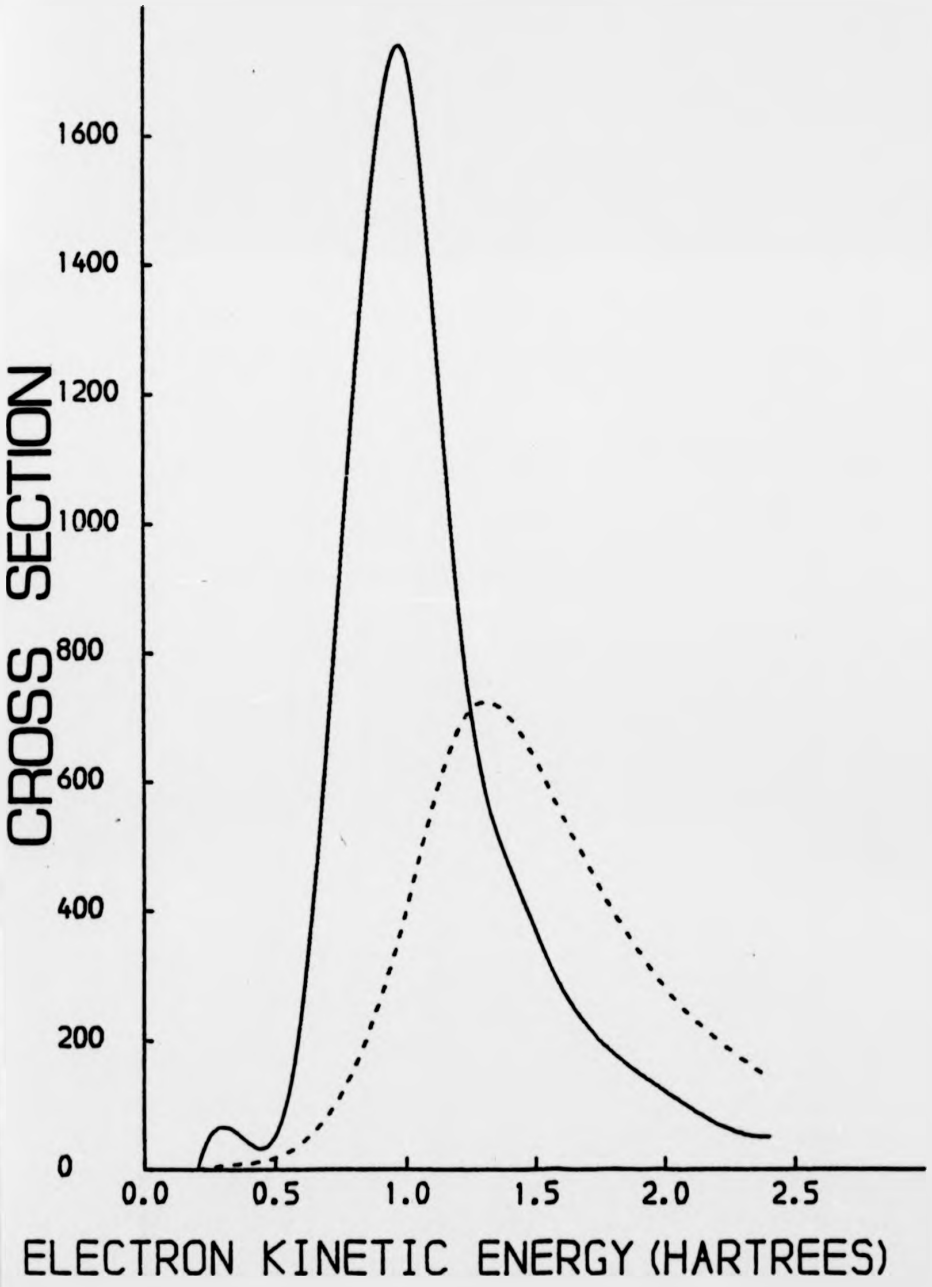

of the fact that the actual exchange potential decreases with increasing energy. It is of interest to recalculate the Xe 4d photoionization cross-section using equation (2.51a) to calculate the exchange potential instead of the Xα term. The derivation of the Dirac expression assumes a common energy zero for both the bound and scattering electrons. Hara (1967) in his work on electron scattering from molecules suggested that k_i be calculated from, (using Hartree atomic units):

$$\frac{k_i^2(r)}{2} = \frac{k_F^2(r)}{2} + \frac{k_\infty^2}{2} + \phi \qquad (5.3)$$

where $k_F(r) = (3\pi^2\rho(r))^{1/3}$ is the local Fermi wavevector, ϕ is the binding energy with respect to the vacuum of the shallowest bound electron, and $\frac{k_\infty^2}{2}$ is the kinetic energy of the scattering electron with respect to the vacuum level. For metals, it is more appropriate to take ϕ as being the workfunction. For atoms, ϕ should be taken as the electron affinity of the atom, (i.e. the energy increase when an electron is added on to the neutral atom). For atomic Xe, the negative ion is unstable, so it is appropriate to put $\phi = 0$ in the calculation of $k_i(r)$. In the same spirit as the Xα approximation, (Slater and Johnson (1972)), we multiply the Dirac potential, equation (2.51a), by an α parameter, ($0 \leq \alpha \leq 1$). The calculation for the Xe 4d photoionization cross-section is shown in fig. (5.8), for α=1 and α=0.5. The calculation using α=1 still places the resonance peak at too low an energy, and with too narrow a width. However this calculation is a considerable improvement over the Xα(α=1) calculation, (fig. 5.6). Optimum agreement with experiment is obtained with α = 0.7. The Dirac potential is preferable to use in calculations of atomic photoionization cross-sections, because it has an energy dependence already built into it. Using the Xα expression, equation (2.53), with a reduced α value may give good agreement with experiment for energies in the vicinity of the resonance, but because the expression is energy independent

Figure 5.9:

(a) Comparison between photoelectron diffraction data for normal emission from the 4d levels of c(2 x 2)Te adsorbed on Ni(001), (McGovern et al (1980), full curve), with photo-absorption data for crystalline Te.

(b) Comparison between a calculation for the normal emission from the 4d levels of c(2 x 2)Te adsorbed on Ni(001), with a calculation of the 4d photoionisation cross-section for atomic Te (Li and Tong (1979)).

(c) Comparison between theoretical and experimental enhancement factors for normal emission from the 4d levels of c(2 x 2)Te adsorbed on Ni(001). The enhancement factor is the intensity of the normal emission from the 4d levels of c(2 x 2)Te adsorbed on Ni(001) divided by the intensity of the 4d emission from crystalline Te.
Photocopied from McGovern et al (1980).

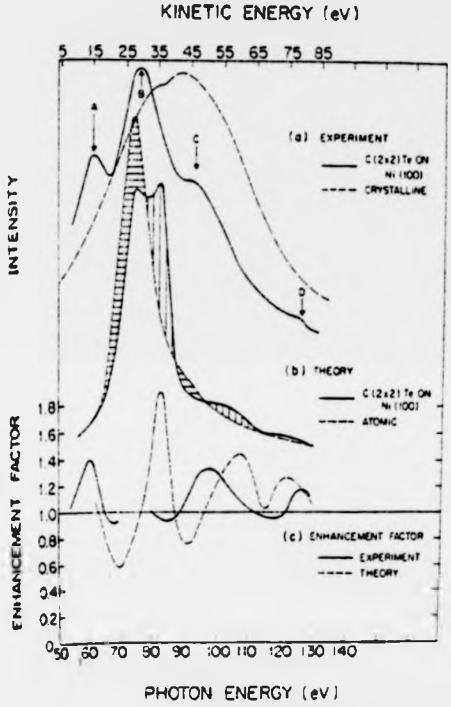

Photoemission cross sections for Te. (a)solid curve,normal emission angle resolved cross section for c(2x2)Te on Ni(100); dashed curve, photoabsorption for crystalline Te[7]: (b) Theoretical normal emission cross sections for an isolated Te atom (dashed) and c(2x2)Te[5]: (c) Enhancement factor for c(2x2)Te,experimental solid and theoretical dashed.

Figure 5.10: Photoelectron diffraction curves for the normal emission from the 4d levels of c(2 x 2)Te adsorbed on Ni(001). Upper full curve: Experimental data (McGovern et al (1980)). Lower full curve: Calculation using ground state Xα potential for Te, (Li and Tong (1979)). Dashed curve: Calculation using Hara potential for Te with α=0.5.

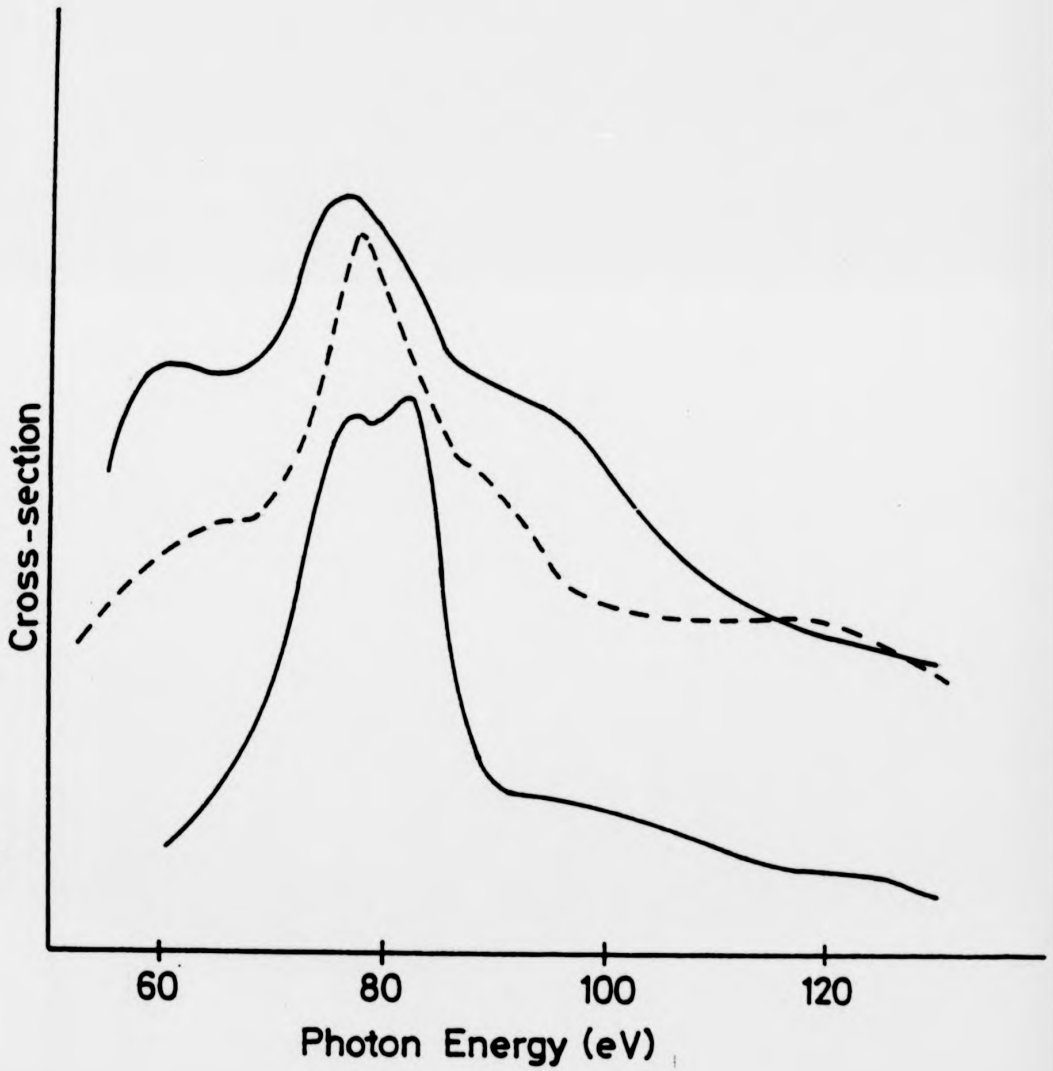
Cross-section
60
80
100
120
Photon Energy (eV)

it will overestimate the exchange potential at higher energies.

In the next section we will use the Dirac expression (2.51a) in the calculation of the exchange potential for Te, to see whether we can fit the data of McGovern et al (1979) for the energy dependence of the normal emission from the 4d levels of c(2 x 2)Te adsorbed on Ni(001).

5.3. Normal Emission from the 4d Levels of c(2 x 2)Te adsorbed on Ni(001)

The experimental data of McGovern et al (1979) along with the calculation of Li and Tong (1979) are shown in fig. (5.9). The agreement between theory and experiment is particularly poor for electron kinetic energies $\leq$ 45 eV.

The input parameters to the calculation are the same as those used in the analysis of the data taken with the azimuthal mode. We also use the same Ni phase shifts as were used before, (Wakoh (1965)). In the calculation of the Te potential, ϕ is put equal to 5 eV which is the workfunction for Ni. In the experiment, the radiation is p-polarised and incidant on the surface at 45° to the surface normal in the direction of the [100] azimuth. The inner potential that we use is taken from Demuth et al's (1975) LEED calculation for Ni(001) where the Ni inner potential is found to be energy dependant.

We find that with $\alpha = 0.5$ in the Dirac calculation of the Te potential we obtain best agreement with experiment, (dotted lines in fig.(5.10)). Not only is the width and position of the main peak well described by the calculation but so also are the positions and relative intensities of the minor peaks. A few discrepancies still remain; for example, the peak at lowest energy is predicted to occur at $\sim$ 5 eV too high in energy and the highest peak occurs at 5 eV too low an energy in the calculation. However, this curve is in much better agreement with experiment than the calculation of Li and Tong which uses Slater exchange. Thus the discrepancy

between theory and experiment found by McGovern et al (1979) is due to the use of a poor Te potential in the original calculation.

It should now be asked why no problem has been encountered in the description of the CIS normal emission data taken for Se 3d emission from Ni(001) - c(2 x 2)Se, (Kevan et al (1978, 1979, 1981), Li and Tong (1979a) and Na 2p emission from Ni(001) - c(2 x 2)Na, (Williams et al (1979), Li and Tong (1979b)). The reason is that for these initial states, $n=\ell+1$, so that the photoionization cross-section is a smoothly varying function of energy. In particular, for Se and Na, no sharp resonances in the cross-sections or the phase shifts occur in the energy range of interest. However, in the case of Te 4d emission from Ni(001) - c(2 x 2)Te, experiments need to be carried out in the vicinity of the resonance in order to maximise the signal. Thus in the calculations for this system, it is essential to correctly position this resonance. This requires a more careful calculation of the atomic potential for Te.

It has been known for some time that the Dirac potential, equation (2.51a) gives better agreement with experiment than the Xα potential in work on electron scattering from molecules, (Hara (1967)). It has also been found necessary to reduce α in the Xα potential to very low values, (≤ 0.1) in order to obtain an adequate potential in the description of electron scattering off atoms, (Walker (1971)).

In LEED, this problem has in most cases not occured; the successful determination of many surface structures have been made using a ground state Xα potential to calculate the scattering properties of the surface atoms. This success is probably due to the fact that for electron energies $\geq$ 100 eV the phase shifts for many atoms change very slowly with energy. Thus for a particular energy, a change in α would not appreciably alter the phase shifts at that energy.

Echinique (1976), and Echinique and Titterington (1977) have found that only minor differences occur in calculated LEED curves when different model

Figure 5.11: Calculations for the azimuthal distribution of photoelectron intensity for emission from the Te4d levels of Ni(001) - c(2 x 2)Te and Ni(001) - p(2 x 2)Te. Input parameters as for the calculations presented in Fig. (4.8) except that now the Hara potential for Te is used with $\alpha = 0.5$.

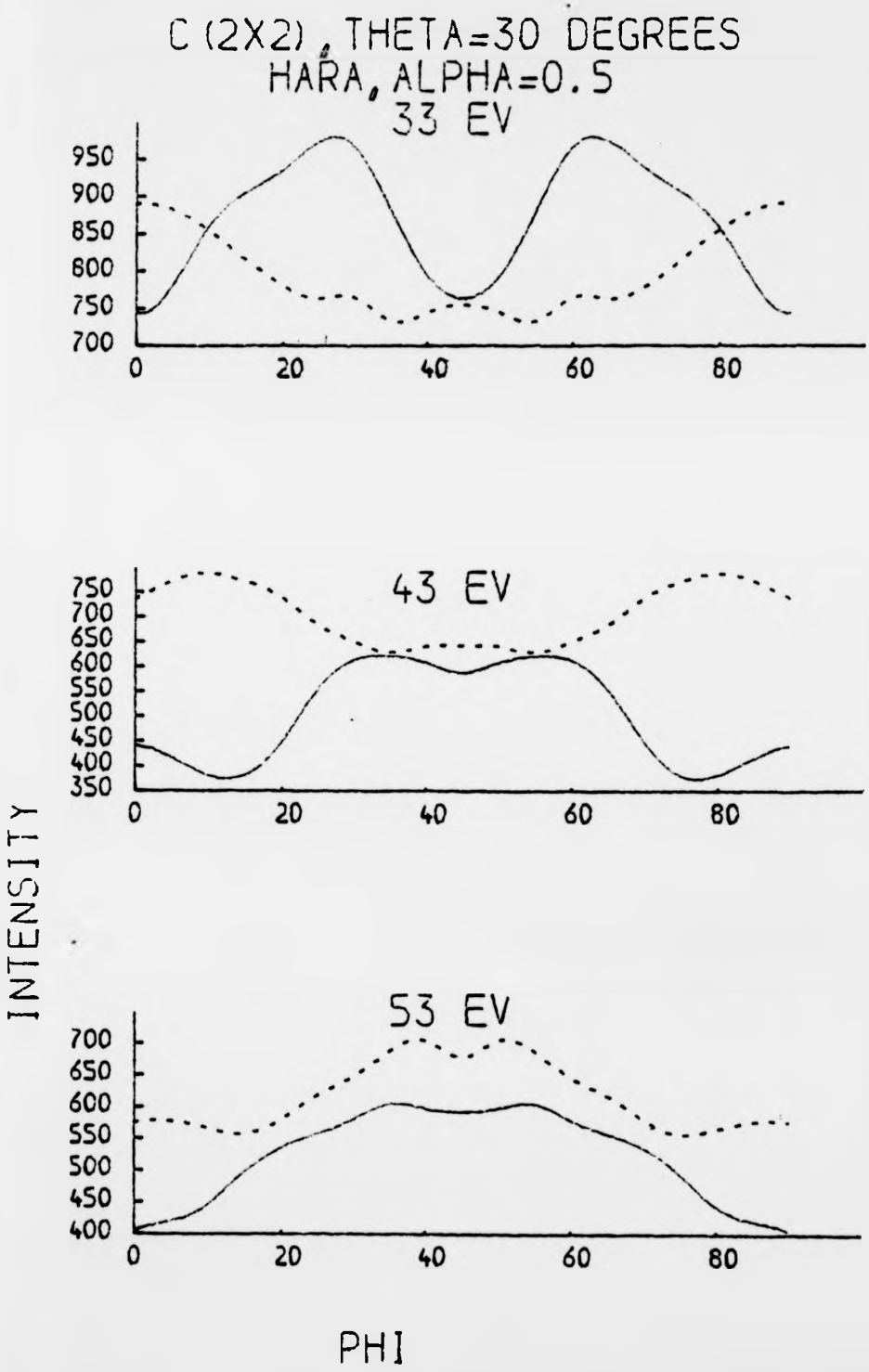
C (2X2), THETA=30 DEGREES
HARA, ALPHA=0.5
33 EV
950
900
850
800
750
700
0
20
40
60
80
43 EV
750
700
650
600
550
500
450
400
350
0
20
40
60
80
53 EV
700
650
600
550
500
450
400
0
20
40
60
80
INTENSITY
PHI

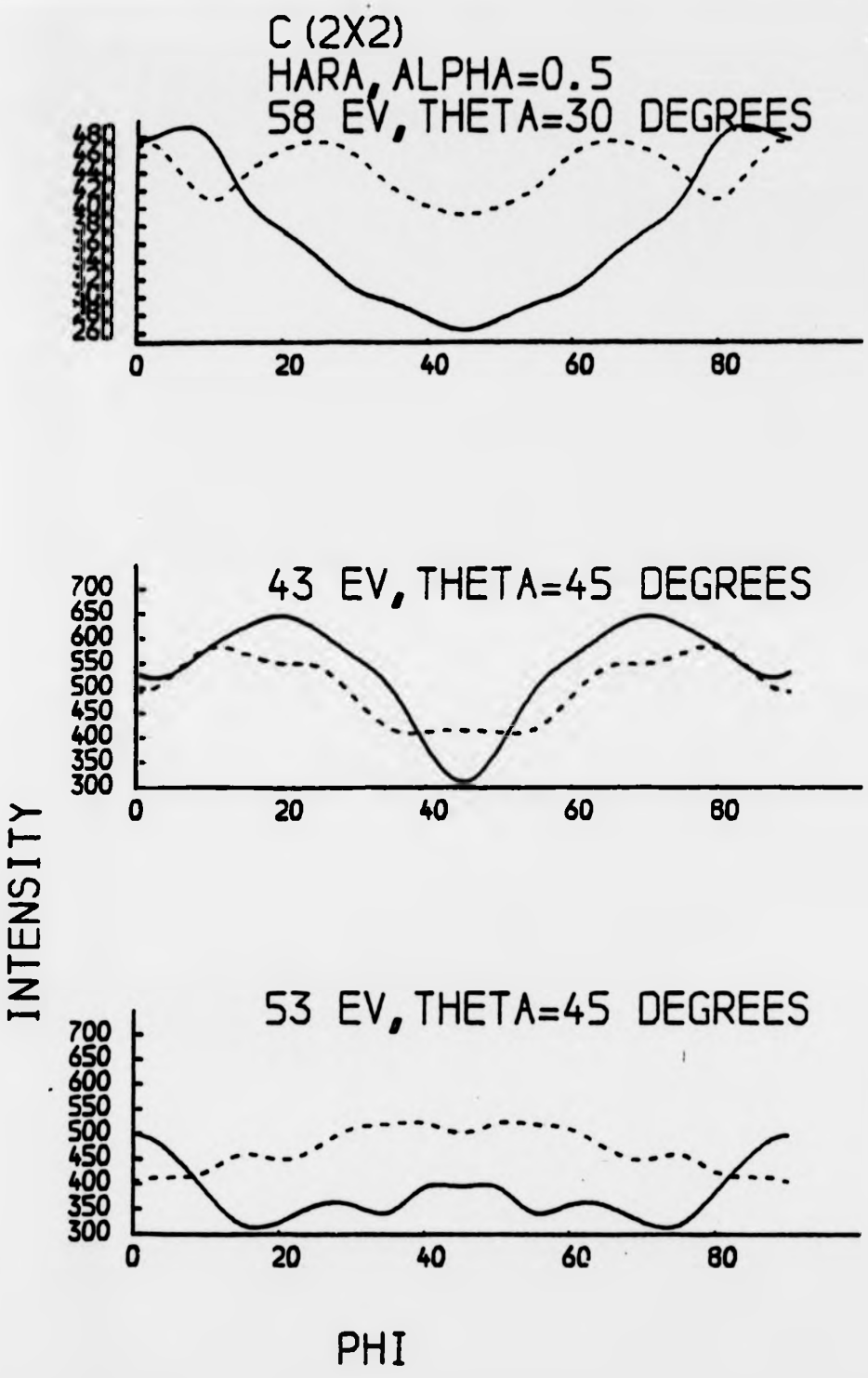
C (2X2)
HARA, ALPHA=0.5
58 EV, THETA=30 DEGREES
0
20
40
60
80
43 EV, THETA=45 DEGREES
700
650
600
550
500
450
400
350
300
53 EV, THETA=45 DEGREES
INTENSITY
PHI

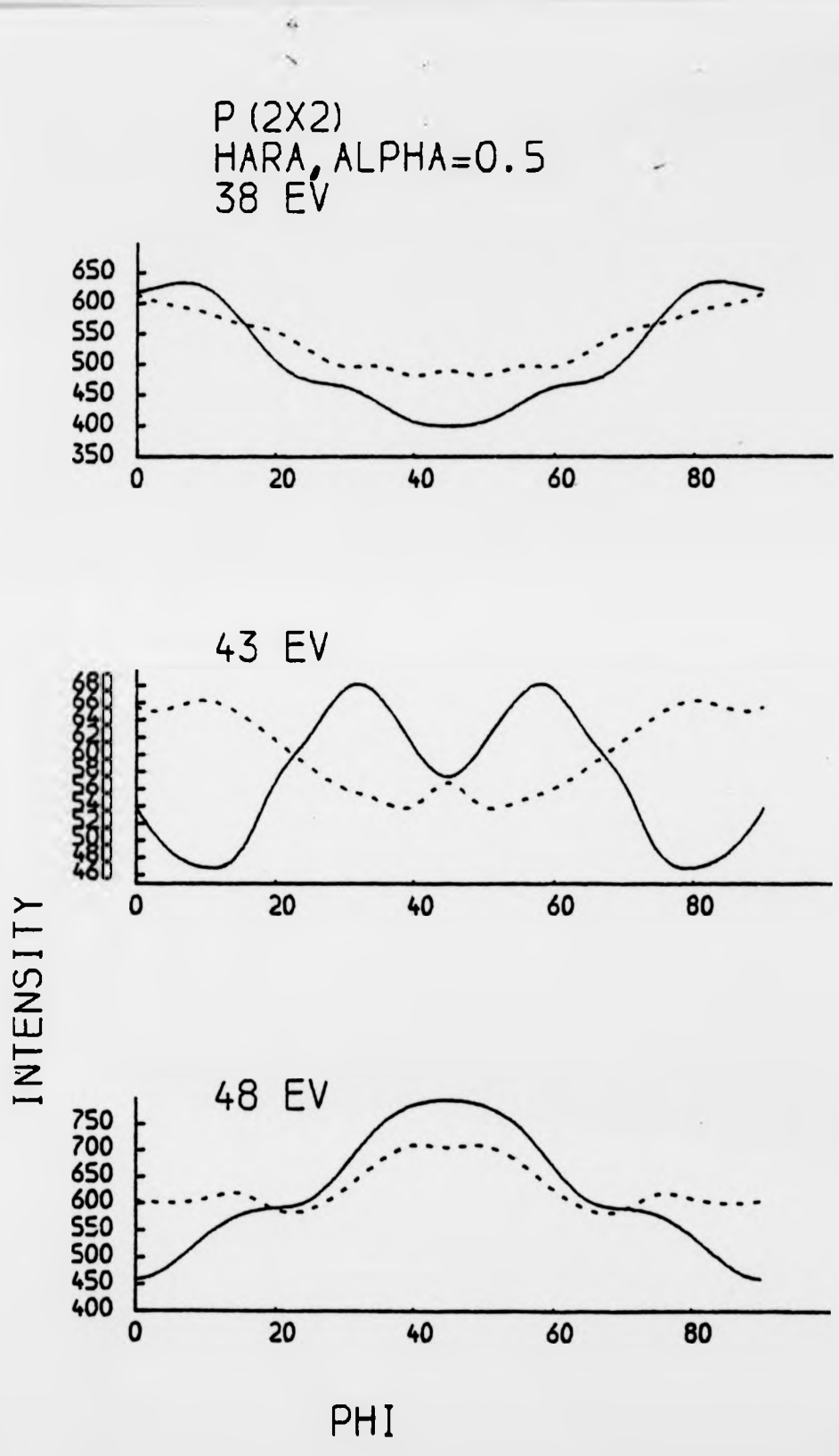
P (2X2)
HARA, ALPHA=0.5
38 EV
650
600
550
500
450
400
350
0
20
40
60
80
43 EV
68
66
64
62
60
58
56
54
52
50
48
46
0
20
40
60
80
48 EV
750
700
650
600
550
500
450
400
0
20
40
60
80
INTENSITY
PHI

potentials are used. However, difficulties have occured in LEED work on NiO(100), (Prutton et al (1979)), where Slater Xα potentials have been used in the calculation of the Ni and O phase shifts. Prutton et al find that optimum agreement with experiment is obtained if $\alpha = 2/3$ is used for energies below 120 eV and $\alpha=0$ above this energy. Meyer et al (1980) have used the Dirac potential in the LEED work on GaAs (110). Small improvements over Xα exchange are found for some of the beams.

Wendin (1981) has also attempted to resolve the discrepancy for McGovern et al's data for normal emission from Ni(001) - c(2 x 2)Te, by using the Random Phase Approximation with Exchange (RPAE) in the calculation of the Te potential. It has been shown (Wendin (1981)) that the RPAE gives a good description of the atomic photoionization cross-section for Te4d. Wendin has shown by modulating the photoionization cross-section data for Te4d by the enhancement factor of Li and Tong (1979b) that fair agreement with the data of McGovern et al may be obtained. A first principle calculation for the CIS curve using this RPAE potential for Te has not yet been made.

5.4. Ni(001) - c(2 x 2)Te and Ni(001) - p(2 x 2)Te: A second Analysis of the Data taken with the Azimuthal Mode.

Having resolved the main discrepancies that have been found for the Ni(001) - c(2 x 2)Te data taken with the CIS mode, we should now return to a further analysis of the data for Ni(001) - c(2 x 2)Te and Ni(001) - p(2 x2)Te taken with the azimuthal mode to see whether, by using the Dirac potential with $\alpha = 0.5$ in the calculation of the Te potential, we can overcome the difficulties that we have encountered in describing the data.

The new calculations for this mode of data collection are shown in fig.(5.11). These calculations were carried out by Drs. D. P. Woodruff and P. D. Johnson. For the c(2 x 2) data we see that with this new

potential for Te, there is better agreement with experiment for electron kinetic energies 43 eV and 53 eV in the vacuum with $\theta = 30^{\circ}$ and kinetic energy 43 eV in the vacuum, with $\theta = 45^{\circ}$. For the p(2 x 2) data better agreement between theory and experiment is found for electron kinetic energies 38 eV and 48 eV in the vacuum. Discrepancies between theory and experiment for some energies, however, still remain. Clearly, further analysis of the data needs to be carried out in order to resolve the remaining discrepancies. The possibility of varying the $d_{\perp}$-spacing by $\pm$ 0.1 Å should be considered. Also, as we mentioned in Chapter 4, the presence of disordered domains of Te atoms on the surface may be causing the difficulties that we are having in matching the data taken with the azimuthal mode, (Becker and Hagstrum (1975)). For Se3d emission from Ni(001) - c(2 x 2)Se, the CIS curves are found to be insensitive to whether or not there is disorder on the surface, (Kevan et al (1979)), and if this holds generally then this would explain why we have had more success in matching the data for Ni(001) - c(2 x 2)Te taken with the CIS mode than for the azimuthal mode.

5.5. The Lee and Beni Potential

Although we have resolved the discrepancy that has been found for the case of Te4d normal emission from Ni(001) - c(2 x 2)Te, there is now an additional parameter that can be varied in the calculation: the α factor multiplying the Dirac exchange term, equation (2.51a). With a $d_{\perp}$-spacing of 1.9 Å and $\alpha = 0.5$ we obtained good agreement with experiment but with other values of $d_{\perp}$ and α it may be possible to obtain just as good an agreement. Thus we really require a potential which has no variable parameters. The fact that we have to reduce α to below 1 in the computation of the Dirac potential, when we perform photoelectron diffraction and atomic photoionization cross-section calculations, implies that the Dirac potential itself is a slight overestimation of the true

exchange potential. This could be due to the neglect of screening effects. Lee and Beni (1977) have recently formulated a method of calculating atomic potentials where screened exchange and correlation effects have been taken into account. In this section we aim to find out whether this potential is an improvement over the Dirac potential in the description of the scattering of electrons off atoms.

5.5.1. Theory

The Lee and Beni model uses the Local Density Approximation (LDA) in the calculation of the exchange and correlation potential, i.e. each small volume element of the electron cloud is assumed to behave like an infinite homogeneous free electron gas with a density equal to the density of the volume element. The exchange potential for a free electron gas in the Hartree-Fock approximation may be written as (Hedin and Lundquist (1969)):

$$V_{ex}(\underset{\sim}{r},\underset{\sim}{r}') = \frac{i}{2\pi}\int e^{i\omega'\delta} v(\underset{\sim}{r}-\underset{\sim}{r}') G_o(\underset{\sim}{r},\underset{\sim}{r}';\omega+\omega')\,d\omega \qquad (5.4)$$

where $v(\underset{\sim}{r}-\underset{\sim}{r}')$ is the unscreened electrostatic potential and $G_o(\underset{\sim}{r},\underset{\sim}{r}';\omega+\omega')$ is the Green function for a homogeneous free electron gas which is given in $\underset{\sim}{k}$-space by:

$$G_o(\underset{\sim}{k},\omega) = [\omega - E(\underset{\sim}{k}) + i\,\mathrm{sgn}(E(\underset{\sim}{k})-\mu)\delta]^{-1} \qquad (5.5)$$

(Hedin and Lundquist (1969)), where δ is a small positive infinitessimal, $E(\underset{\sim}{k})$ is the local electron energy and μ is the chemical potential. Equation (5.4) represents an expansion of the electron self-energy to first order in the unscreened electrostatic interaction $v(\underset{\sim}{r}-\underset{\sim}{r}')$. The Lee and Beni potential involves expanding the self-energy $\Sigma(\underset{\sim}{r},\underset{\sim}{r}',\omega)$ to first order in the dynamically screened Coulomb interaction $w(\underset{\sim}{k},\omega)$ given by:

$$w(\underset{\sim}{k},\omega) = v(\underset{\sim}{k})\varepsilon^{-1}(\underset{\sim}{k},\omega) \tag{5.6}$$

(Hedin and Lundquist (1969)), where $\varepsilon^{-1}(\underset{\sim}{k},\omega)$ is the inverse dielectric function for the free electron gas. $\sum$ is then given by:

$$\sum(\underset{\sim}{k},\omega) = \frac{1}{(2\pi)^4}\int e^{i\omega'\delta} w(\underset{\sim}{k}',\omega') G_o(\underset{\sim}{k}+\underset{\sim}{k}';\omega+\omega')\,d\underset{\sim}{k}'d\omega' \tag{5.7}$$

(Hedin and Lundquist (1969)), Lee and Beni (1977) use the single plasmon pole approximation for ε^{-1}:

$$\varepsilon^{-1}(\underset{\sim}{q},\omega) = 1 + \frac{\omega_p^2(r)}{\omega^2-\omega_1^2(q)} \tag{5.8}$$

where $\omega_p(r) = [4\pi\rho(r)]^{\frac{1}{2}}$ is the local plasmon frequency with $|\underset{\sim}{q}| = 0$ and $\omega_1(\underset{\sim}{q})$ is the local plasmon frequency for a plasmon with wavevector $\underset{\sim}{q}$. The dependence of $\omega_1(\underset{\sim}{q})$ on $|\underset{\sim}{q}|$ is taken to be:

$$\omega_1^2(q) = \omega_p^2 + (16/3)q^2 + q^4 \tag{5.9}$$

In the limit of $q \to 0$, $\omega_1 \to \omega_p$ as it should do and in the limit of large q, $\omega_1 \approx q^2$ which is the free particle limit, (Lindhard (1954)). $\varepsilon(\underset{\sim}{q},\omega)$ is then given by:

$$\varepsilon(\underset{\sim}{q},\omega) = 1 + \frac{3\omega_p^2}{4\left(q^2E_F + \frac{3}{16}(q^4-\omega^2)\right)} \tag{5.10}$$

where E_F is the Fermi energy.

Equation (5.7) is then integrated analytically over ω' to give, (Hedin and Lundquist (1969)):

$$\sum(\underset{\sim}{k},\omega) = -\frac{1}{(2\pi)^3}\int d\underset{\sim}{q}\,\frac{v(\underset{\sim}{q})\,n(\underset{\sim}{k}+\underset{\sim}{q})}{\varepsilon[\underset{\sim}{q},E(|\underset{\sim}{k}+\underset{\sim}{q}|-\omega)]}$$

$$-\int\frac{\omega_p^2}{(2\pi)^3}\,\frac{v(\underset{\sim}{q})\,d\underset{\sim}{q}}{2\omega_1(\underset{\sim}{q})[\omega_1(\underset{\sim}{q})+\omega-E(\underset{\sim}{k}+\underset{\sim}{q})]} \tag{5.11}$$

The first term represents the screened exchange potential and the second

term represents the potential due to the Coulomb hole.

A problem now arises as to the calculation of the local momentum $\underset{\sim}{p}(r)$ of the scattering electron. For a free electron gas, $p(r)$ may be found from (see e.g. Lee and Beni (1977), Sham and Kohn (1966)):

$$\tfrac{1}{2}p^2(r) + \zeta(p,\omega-v(\underset{\sim}{r}_o)) = \omega - v(\underset{\sim}{r}_o) \tag{5.12}$$

where ω is the electron energy (in atomic units) and $\underset{\sim}{r}_o = \tfrac{1}{2}(\underset{\sim}{r}+\underset{\sim}{r}')$. A difficulty now arises in that the Hartree potential $v(\underset{\sim}{r}_o)$ is calculated from self-consistent Hartree-Fock wavefunctions for the atom whilst, to be consistent, it should be calculated from the self-consistent solutions for a free-electron gas. It may happen that $p(r)$ will become less than $k_F(r)$. To overcome this, Lee and Beni (1977) use the fact that if the atom is treated like an inhomogeneous electron gas, μ must be independent of $\underset{\sim}{r}$, and it is then argued that $p(r)$ should be calculated from:

$$\tfrac{1}{2}p^2(r) = \tfrac{1}{2}k^2 + \tfrac{1}{2}k_F^2(r) \tag{5.13}$$

where $\tfrac{1}{2}k^2$ is the kinetic energy of the electron outside the atom. This expression similar to equation (5.3) where we considered the Dirac potential, only now $\phi = 0$. We shall be considering electron scattering off inert gas atoms where it is appropriate to put $\phi = 0$.

Hence, the procedure adopted in the calculation of the atomic potential is to first calculate $\rho(r)$ from Clementi wavefunctions, (Clementi and Roetti (1974)) and to then solve Poisson's equation to obtain the Hartree potential $v(r)$. Then the local electron momentum is calculated from equation (5.13), and $\zeta(p(r), \tfrac{1}{2}p^2(r))$ is then computed by numerical integration of equation (5.11). Then, the total atomic potential V, may be written as:

$$V(\tfrac{1}{2}p^2(r),r) = v(r) + \zeta(p(r), \tfrac{1}{2}p^2(r)) \tag{5.14}$$

Figure 5.12: Calculations for the back-scattering amplitude $|f(\pi)|$, (atomic units), versus electron kinetic energy (Hartrees) for atomic Br, where the Lee and Beni potential is used, (Lee and Beni (1977)).

Full curve: $|f(\pi)|$ calculated by Lee and Beni (1977).

Dashed curve: our calculation.

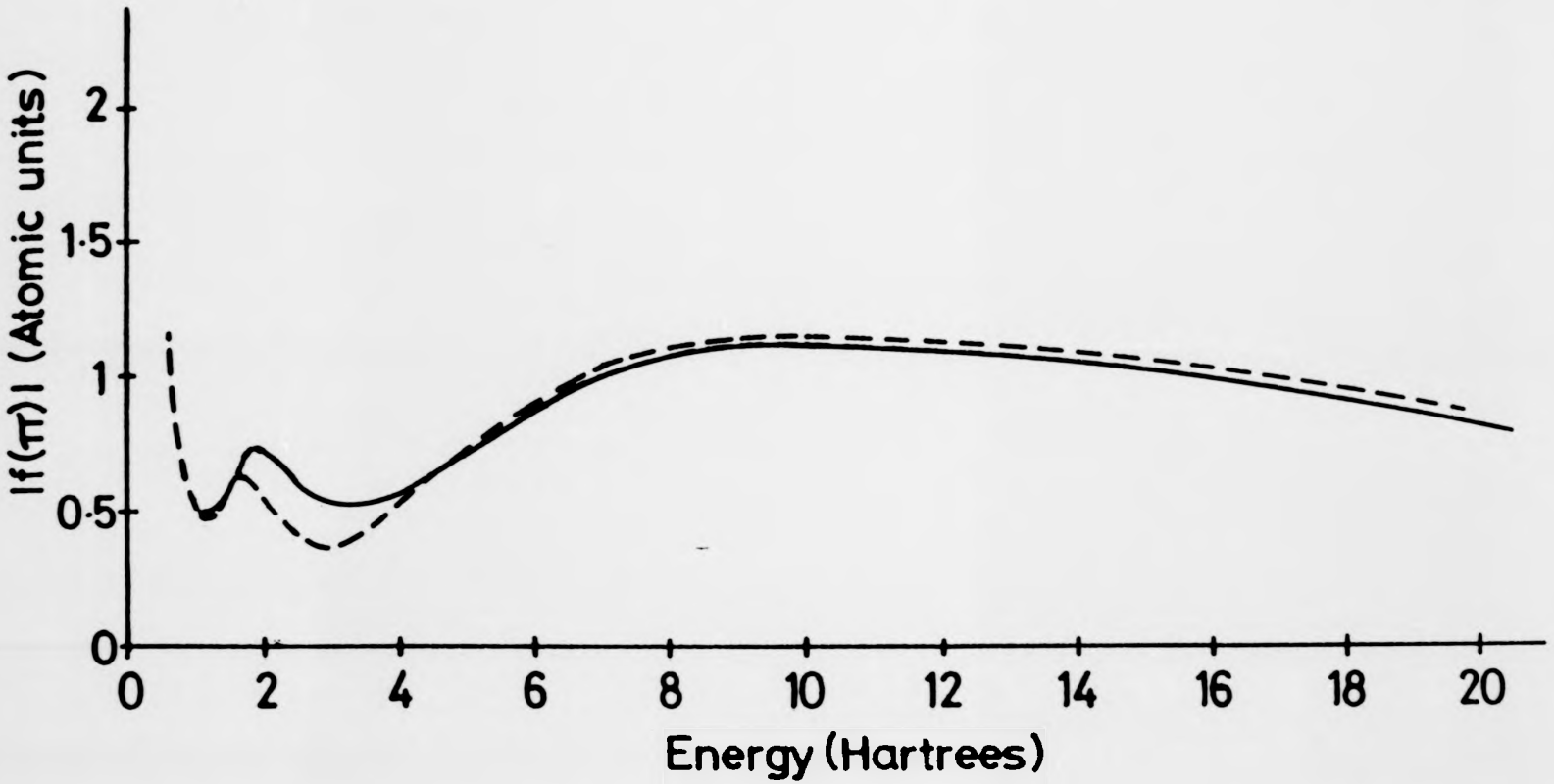
|f(π)| (Atomic units)
2
1·5
1
0·5
0
0
2
4
6
8
10
12
14
16
18
20
Energy (Hartrees)

Then, the procedure outlined in section (2.4) is carried out in order to obtain the atomic phase shifts. It should be mentioned that $\sum(p(r), \frac{1}{2}p^2(r))$ is complex and the imaginary part represents loss of intensity of the elastically scattered electrons due to plasmon excitation. Thus the resulting phase shifts are complex.

5.5.2. Lee and Beni Potentials for Atomic Xe, Kr and Ar.

The MUFPOT programs have been adapted to calculate Lee and Beni potentials by Dr. S. J. Gurman of Leicester University, and we use this modified program in the calculations that we present below. The modified program calculates the electron momentum p(r) from equation (5.12) with $\sum(p, \omega - v(\underset{\sim}{r}_o)) = 0$ with is different to the convention employed by Lee and Beni (1977). We must first test whether this brings about serious discrepancies between our calculations and those of Lee and Beni. We have calculated the backscattering amplitude

$$|f(\pi)| = \left| \frac{1}{2ik} \sum_{\ell} (2\ell+1)(e^{2i\delta_\ell} - 1)(-1)^\ell \right| \qquad (5.15)$$

for atomic Br and in fig. (5.12) we compare our calculations with those of Lee and Beni (1977). The two calculations agree very closely. We have also calculated phase shifts for Cu using our program and there is again excellent agreement with the Lee and Beni calculation.

We now present calculations for the differential and total cross-sections for electron scattering from atomic Xe, Kr and Ar using four models for the atomic potential:

(i) Slater Xα, α = 0.7,

(ii) Slater Xα, α = 0.4

(iii) the full Dirac, (or "Hara" potential (Hara (1967)), and

(iv) the Lee and Beni potential.

Figure 5.13: Calculations and experimental data for the total cross-section (σ) for atomic Ar, (top panel), Kr (middle panel) and Xe (bottom panel), versus electron energy.

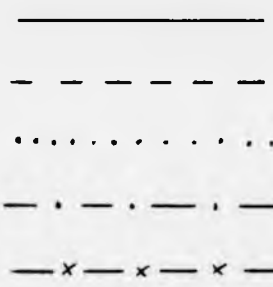

Experiment

Lee and Beni model

Hara Model

Xα ($\alpha = 0.4$)

Xα ($\alpha = 0.7$)

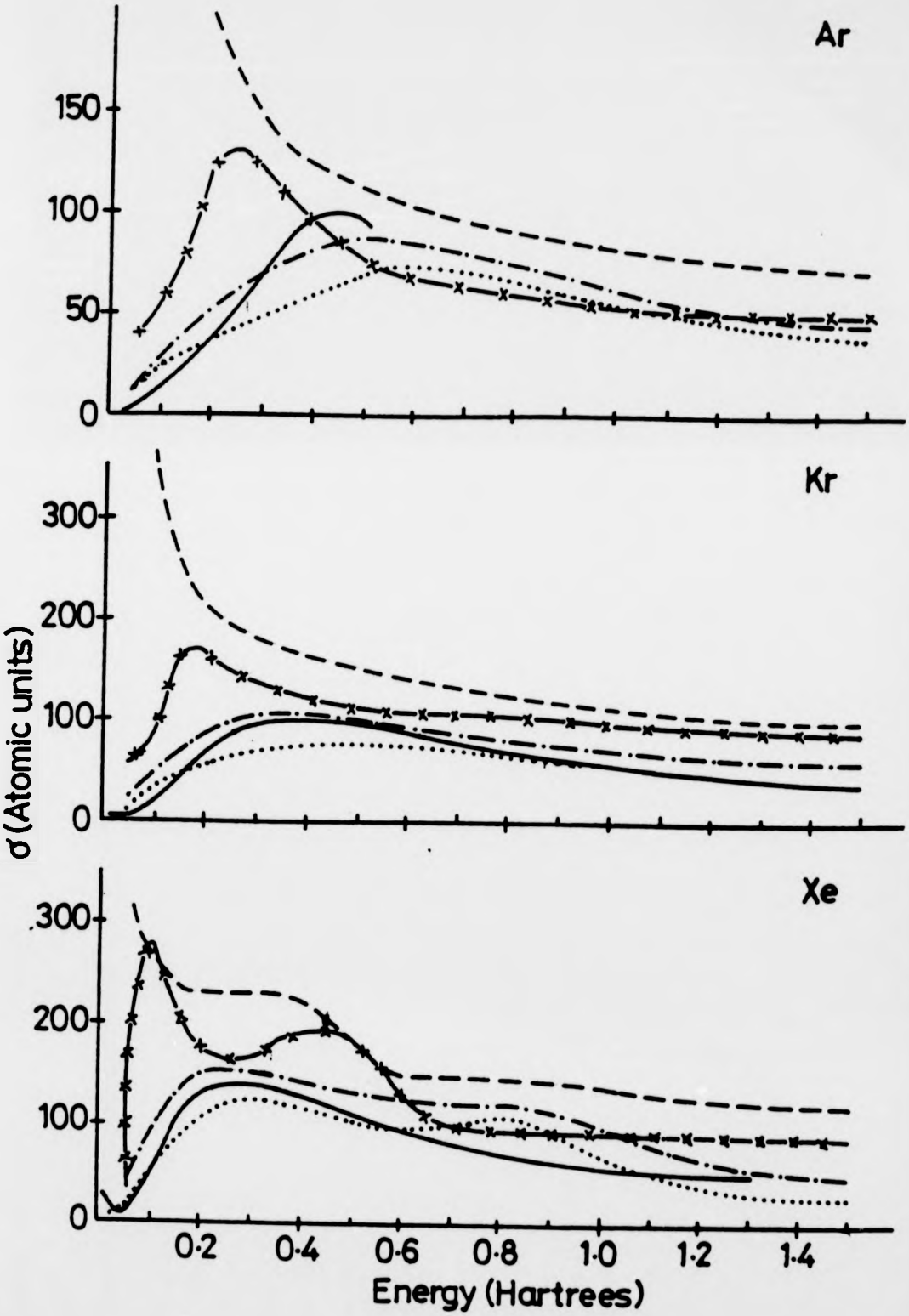
Ar
150
100
50
0
Kr
300
200
100
0
σ (Atomic units)
Xe
300
200
100
0
0·2
0·4
0·6
0·8
1·0
1·2
1·4
Energy (Hartrees)

Figure 5.14: Differential cross-section ($d\sigma/d\Omega$) for elastic scattering from Ar, Kr and Xe at various electron energies, versus scattering angle (θ).

(a) $d\sigma/d\Omega$ vs. θ for Ar at 20 eV.

(b) $d\sigma/d\Omega$ vs. θ for Kr at 20 eV.

(c) $d\sigma/d\Omega$ vs. θ for Kr at 100 eV.

(d) $d\sigma/d\Omega$ vs. θ for Xe at 30 eV.

(a) $d\sigma/d\Omega$ vs. θ for Xe at 60 eV.

(f) $d\sigma/d\Omega$ vs. θ for Xe at 125 eV.

a

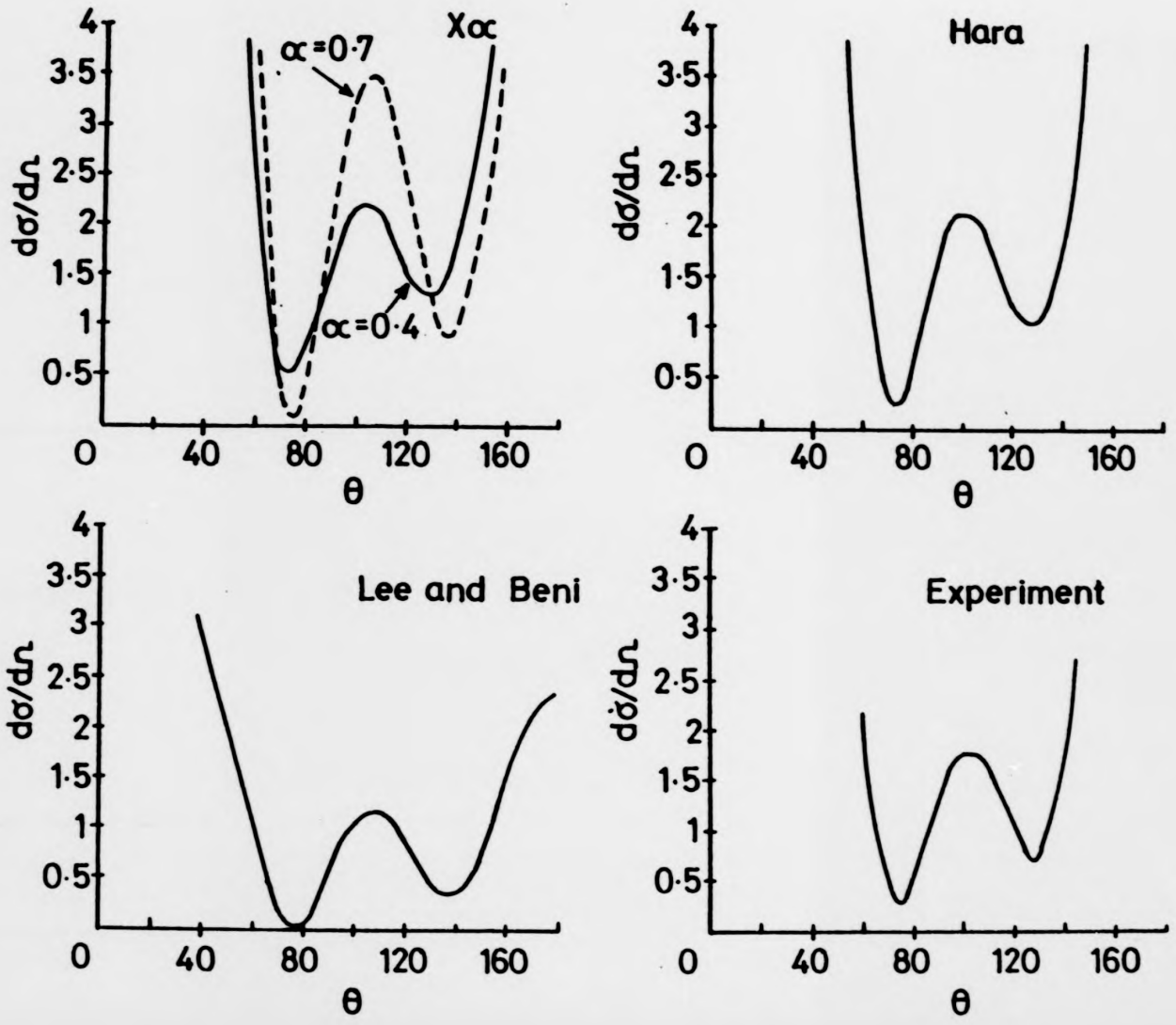
Xα
α=0·7
α=0·4
Hara
Lee and Beni
Experiment
dσ/dΩ
θ
0
40
80
120
160
0·5
1
1·5
2
2·5
3
3·5
4

b

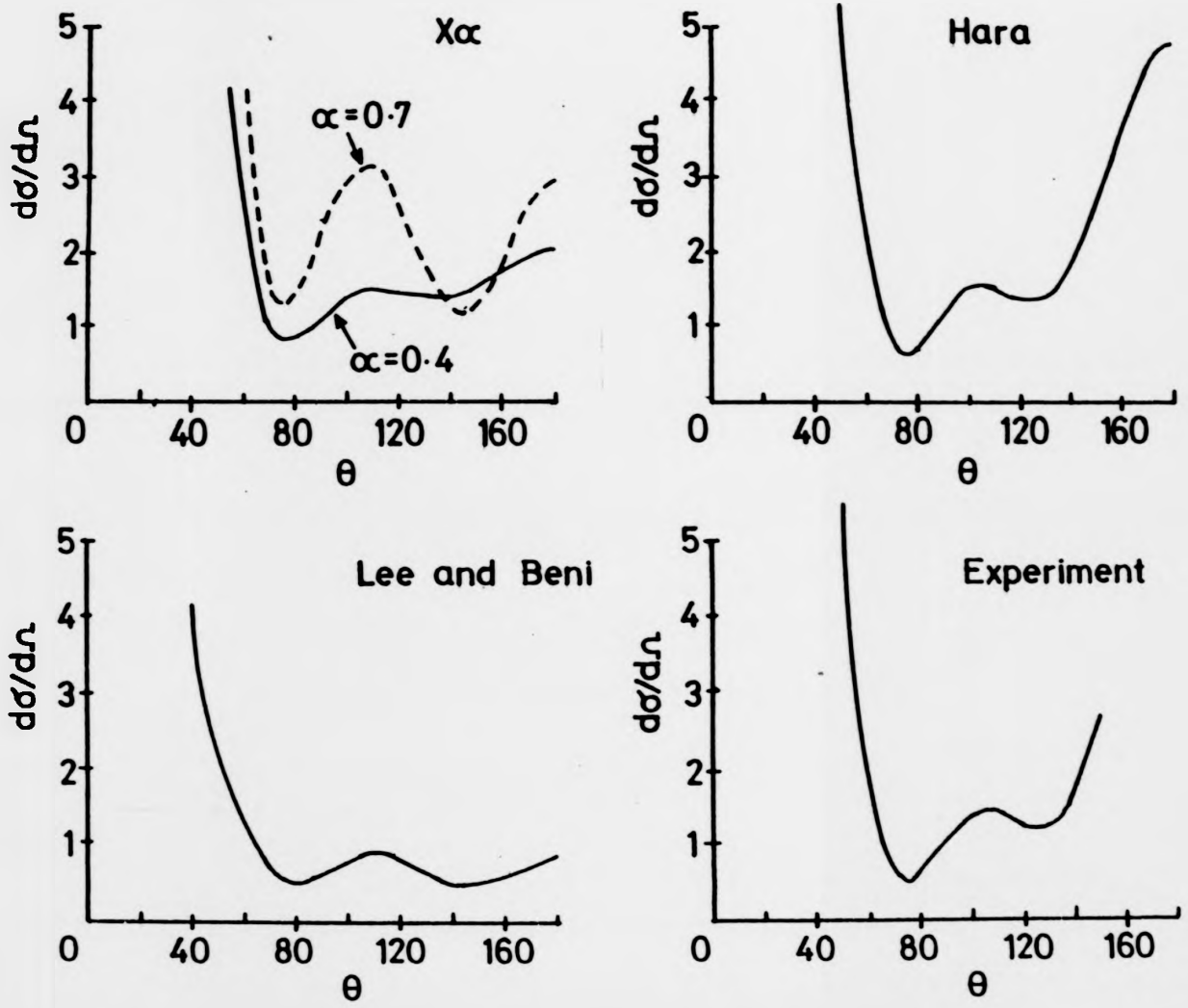
Xα
α=0·7
α=0·4
dσ/dΩ
θ
Hara
Lee and Beni
Experiment
0
40
80
120
160
1
2
3
4
5

c

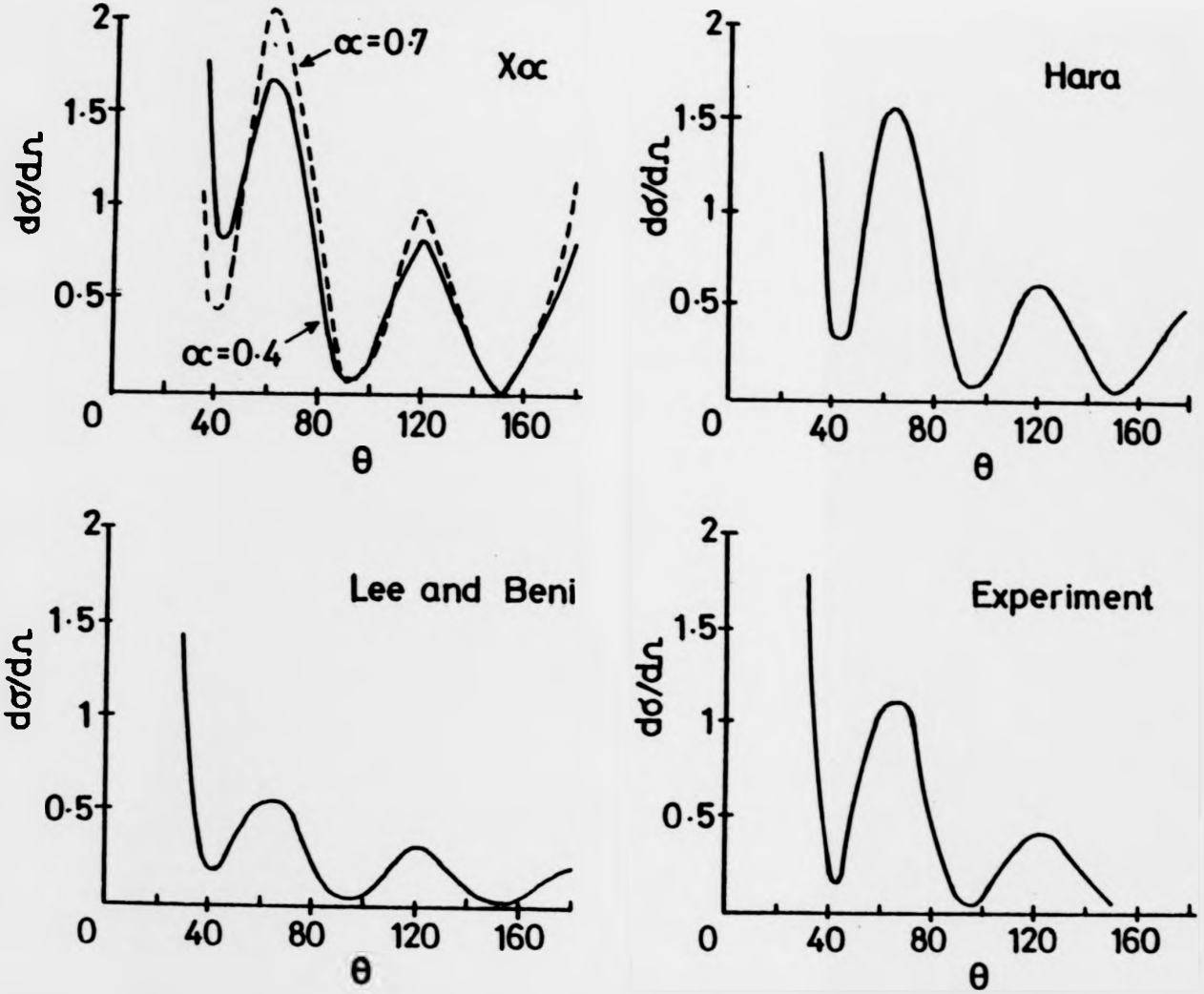
Xα
α=0·7
α=0·4
Hara
Lee and Beni
Experiment
dσ/dΩ
θ
0
40
80
120
160
0·5
1
1·5
2

d

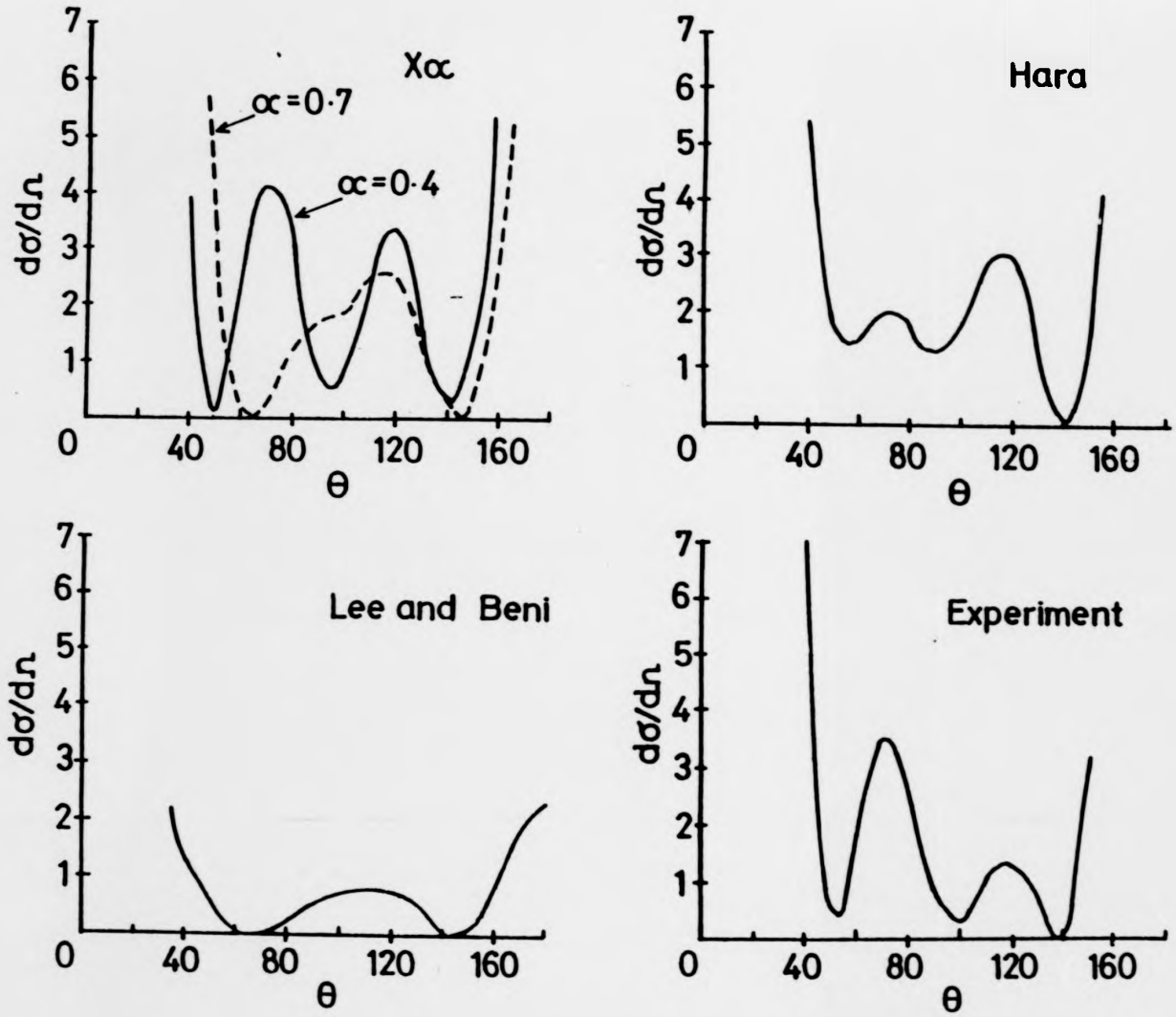
Xα
α=0·7
α=0·4
dσ/dΩ
θ
Hara
Lee and Beni
Experiment
0
40
80
120
160
1
2
3
4
5
6
7

e

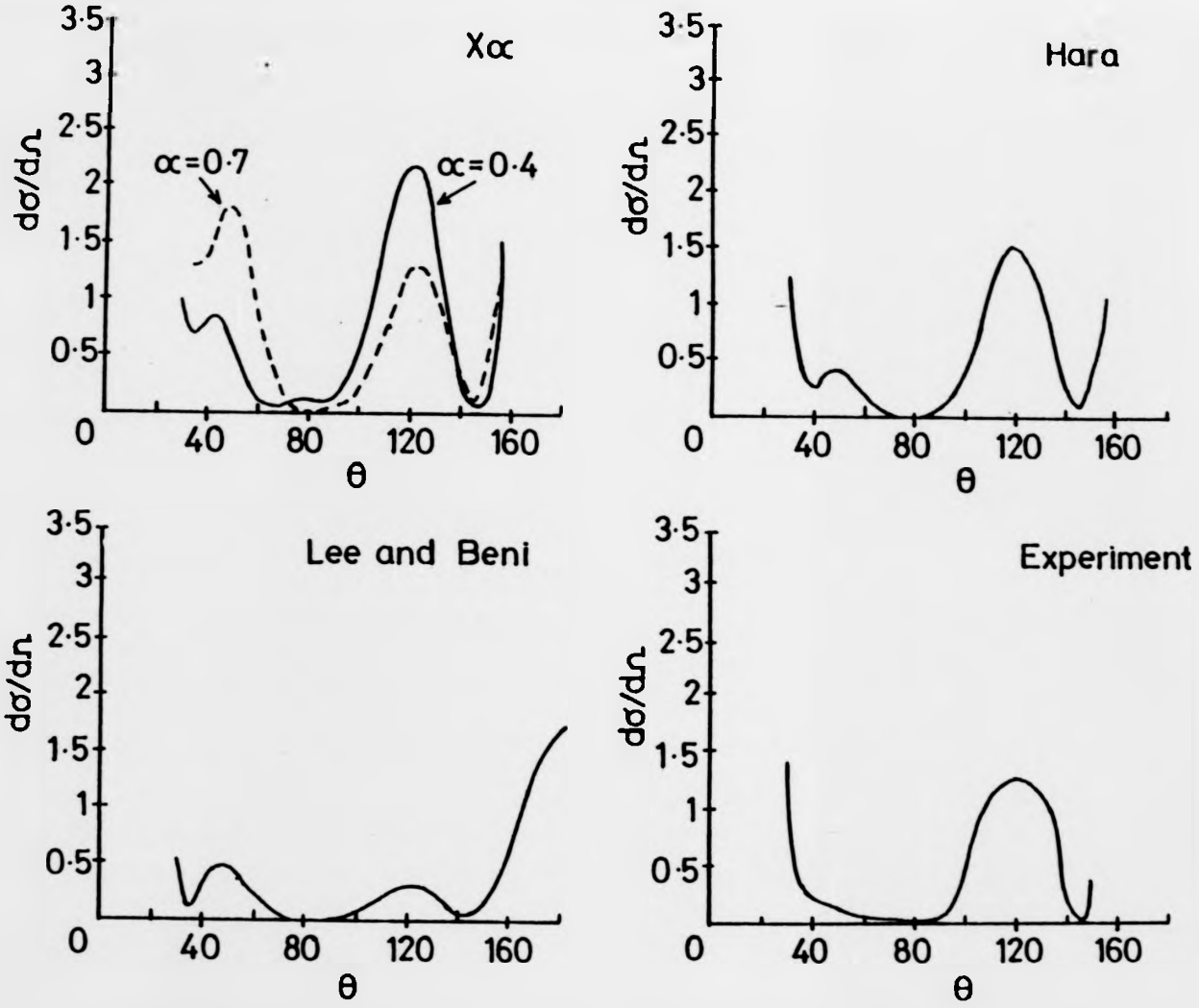
Xα
α=0·7
α=0·4
Hara
Lee and Beni
Experiment
dσ/dΩ
θ
0
0·5
1
1·5
2
2·5
3
3·5
40
80
120
160

f

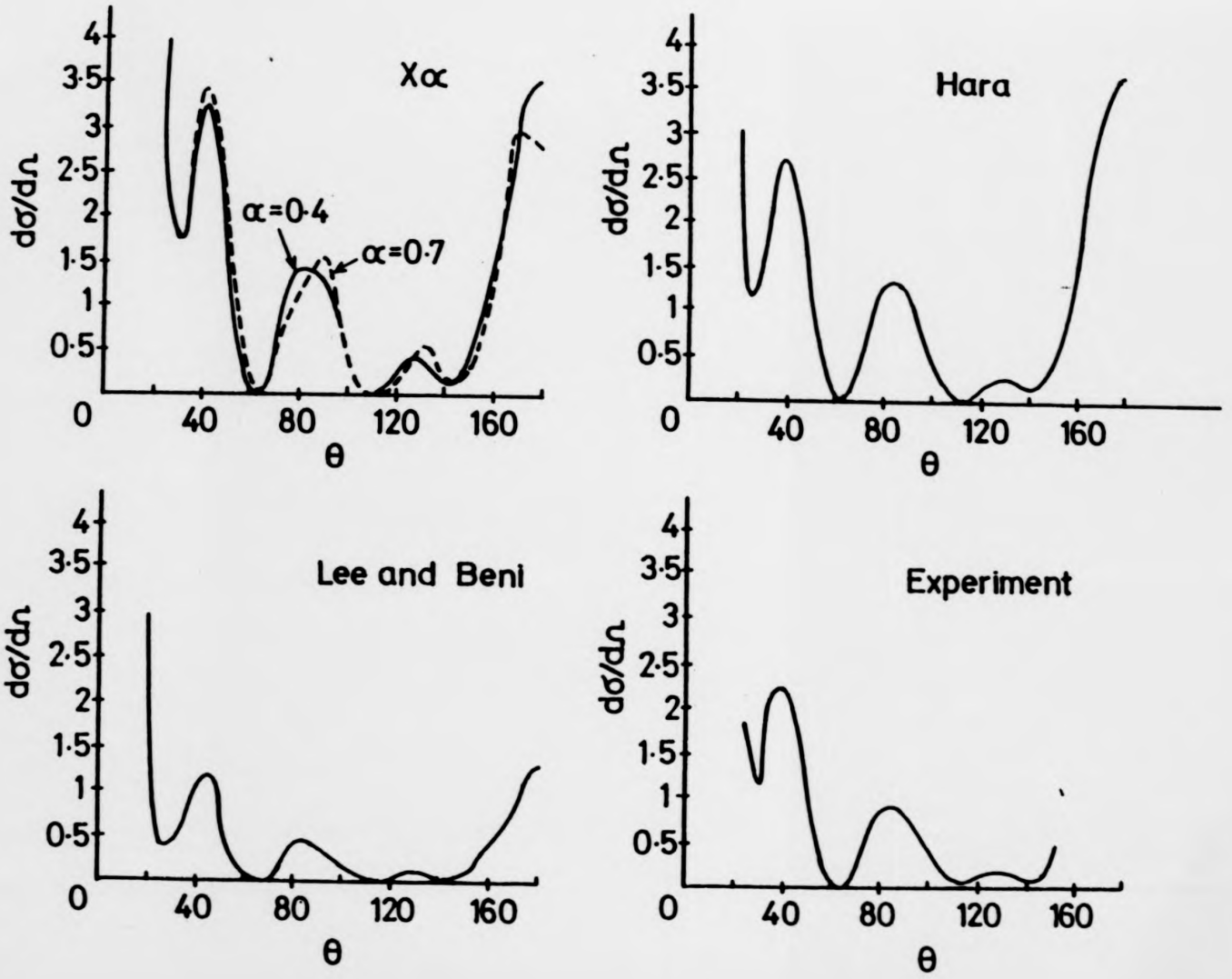
Xα
α=0·4
α=0·7
Hara
Lee and Beni
Experiment
dσ/dΩ
θ
0
40
80
120
160
0·5
1
1·5
2
2·5
3
3·5
4

The calculations and experimental data (Aberth et al (1964), Massey and Burhop (1952)) for the total cross-sections are shown in fig.(5.13). It is clear that for all the atoms, the Lee and Beni and Xα(α = 0.7) potentials poorly describe the experimental data. For Ar and Kr, however, the calculations that employ the Xα(α = 0.4) and Hara potentials are in very good agreement with experiment. For Xe, the Xα(α = 0.4) and Hara calculations are in fairly good agreement with experiment, except that in both calculations, a secondary peak is predicted to occur at 0.8 Hartrees which is not observed experimentally. However, in the experimental data, this secondary peak may be masked by inelastic effects which are not included in the Xα and Hara potentials.

The calculations and experimental data (Williams and Willis (1975), Williams and Crowe (1975)) for the differential cross-sections for these atoms are shown in fig.(5.15). At low energies, (20 eV for Ar, 20 eV for Kr and 30 eV and 60 eV for Xe), the calculations that use the Xα(α = 0.4) and Hara potentials are in excellent agreement with experiment. Small discrepancies occur in the Hara calculations for Xe at 30 eV and 60 eV, but these discrepancies disappear if we look at the data of Mehr (1967). The use of the Lee and Beni and Xα(α = 0.7) potentials leads to poor agreement with experiment at these energies. At higher energies, however, (100 eV for Kr and 125 eV for Xe), all four potentials give a good description of the experimental data; clearly, at these energies the model that is adopted for the exchange is not critical in calculating the scattering properties of atoms. It should be mentioned that for EXAFS, the overall phases of the unscattered and scattered electrons are important in determining bondlengths and so, even at the high energies that are used in these experiments, the choice of model potential can be critical.

It is clear from our calculations that the Xα(α = 0.7) and Lee and Beni potentials are inadequate in the description of electron scattering

for energies ≤ 60 eV. That the Xα(α = 0.7) potential is inadequate for a proper description of electron scattering comes as no surprise to us; we have already seen that the use of this potential leads to poor agreement between theory and experiment for Te4d emission from Ni(001) - c(2 x 2)Te. What is surprising is that the Lee and Beni potential is also inadequate in the description of low energy electron scattering. This model is supposed to be an improvement over the Hara potential. In fact, Lee and Beni (1977) have shown that this potential gives good agreement with experiment for EXAFS work on Br_2, $GeCl_4$ and Ge. The problem probably lies in the inadequacy of the LDA to model the electron density over the whole region of the atom. Hedin and Lundquist (1969) have pointed out that whilst the density of the valence electrons is smoothly varying with position, the density of the core electrons varies very rapidly due to the dominance of the nuclear potential. Hedin and Lundquist suggest that the LDA should only be applied to the valence electrons. We should now ask why the Hara and Xα (with a reduced α) potentials, which are also calculated within the LDA, work so well. It is difficult to say why; it may be that a cancellation of errors is occuring. Thus, to improve on the Hara model, one would probably have to dispense with the LDA, at least for the core electrons. The success of the Lee and Beni potential in the description of some EXAFS data shows that this potential does not fail in all cases, (Lee and Beni (1977)).

5.6. Discussion

We have shown that the discrepancy that has been found in the description of the experimental data for Te4d normal emission from Ni(001) - c(2 x 2)Te, (McGovern et al (1979)) is due to the inadequacy of the Slater Xα potential to properly model the exchange interaction between the emitted and bound electrons for the Te atom in the energy

range of interest. The use of the energy dependant Hartree-Fock potential for a free-electron gas premultiplied by an α parameter resolves this discrepancy. This potential for Te has then been used to reanalyse the data taken with the azimuthal mode for Te4d emission from Ni(001) - c(2 x 2)Te. Improved agreement with experiment has been obtained for some energies but some discrepancies between theory and experiment still remain. It is suggested that the presence of disordered domains of Te, or of different ordered domains may be causing the discrepancies that still remain. We have then proceeded to use the Lee and Beni potential which takes into account screened exchange and correlation effects to calculate the total and differential cross-sections for electron scattering off inert gas atoms, and we have compared our results with calculations that use the Xα(α = 0.7), Xα(α = 0.4) and Hara potentials. The total cross-sections are best described by the Xα(α = 0.4) and Hara potentials, whilst the Xα(α = 0.7) and Lee and Beni potentials give poor agreement with experiment. As regards the description of the differential cross-section data, it is clear that for electron kinetic energies ≤ 60 eV the calculations that use the Xα(α = 0.4) and Hara potentials are in good agreement with experiment whilst the Lee and Beni and Xα(α = 0.7) calculations fail to adequately describe the data in this energy region. At higher energies (≥ 100 eV) the choice of model potential is not so critical, and all four potentials do a good job in describing the data. We suggest that the Lee and Beni potential works badly due to a breakdown of the LDA, and the success of using the Hara and Xα(α = 0.4) potentials may well be due to a cancellation of errors.

We must now discuss the implications of our findings on the potential usefulness of photoelectron diffraction as a structural technique for atomic adsorbate systems. In LEED, by using the energy independent Xα

model for the exchange, considerable success has been achieved in the solution of many structures. The reason for the success of using this simple model for the exchange lies in the fact that in the energy range of interest for LEED experiments, the phase shifts of many atoms vary smoothly with energy; in particular no sharp resonances occur. For photoelectron diffraction, to maximise the signal, experiments usually need to be carried out for electron energies $\leq$ 100 eV, and in the energy range of interest, the photoionization amplitudes and phase shifts for many atoms vary more rapidly with energy and so they are more sensitive to the model potential that is being used. Whilst for some cases (e.g. Se 3d normal emission from Ni(001) - c(2 x 2)Se), one can get away with using the $X\alpha$ potential for the Se, for Te4d normal emission from Ni(001) - c(2 x 2)Te it is essential to use a more sophisticated model for the exchange interaction. The need to sometimes use a more sophisticated potential in the calculations places core-state photoelectron diffraction as a disadvantage as compared with LEED when considering it as a surface structural technique. The inadequacy of using Slater exchange at low energies may also be of relevance to the new technique of X-ray absorption Near Edge Structure (XANES), (Durham and Pendry (1981)). The sensitivity of XANES calculations to different model potentials should be investigated.

It should also be pointed out that the for the case of Ni(001) - c(2 x 2)Te, the only clue that the Te potential was at fault in the original calculation came from an analysis of the CIS curve for normal emission which is sensitive to atomic effects. This stresses the importance in any future photoelectron diffraction study to carry out experiments using both the CIS and azimuthal modes. The analysis of the CIS curve will provide a test of the potential that is being used, and having optimised the potential, one can then proceed to analyse the data taken with the azimuthal mode and, hopefully, make a determination of the structure.

REFERENCES FOR CHAPTER 5

Aberth, W., Sunshine, G. and Bederson, B., Proceedings of the Third Int. Conf. on the Physics of Electronic and Atomic Collisions, edited by M. R. C. McDowell (Amsterdam, North Holland 1964).

Becker, G. E. and Hagstrum, H. D., J. Vac. Sci. Technol, 12, 234 (1975).

Clementi, E. and Roetti, C., Atomic Data and Nuclear Data Tables, 14, 177 (1974).

Combet Fornoux, F., J. Phys. (Paris) 31, C4-203 (1970).

Cooper, J. W., Phys. Rev. 128, 682 (1962).

Demuth, J. E., Marcus, P. M., and Jepsen, D. W., Phys. Rev. B11, 1460 (1975).

Durham, P. J. and Pendry, J. B., Solid State Comm. 38, 159 (1981).

Echinique, P. M., J. Phys. C9, 3193 (1976).

Echinique, P. M. and Titterington, D. J., J. Phys. C10, 625 (1977).

Edarer, D. L., Phys. Rev. Lett, 13, 760 (1964).

Hara, S., J. Phys. Soc. Japan, 22, 710 (1967).

Hedin, L. and Lundqvist, S., Solid State Phys. 23, 2 (1969).

Kevan, S. D., Rosenblatt, D. H., Denley, D., Lu, B-C, and Shirley, D. A., Phys. Rev. Lett. 41, 1565 (1978).

Kevan, S. D., Rosenblatt, D. H., Denley, D., Lu, B-C and Shirley, D. A., Phys. Rev. B20, 4133 (1979).

Kevan, S. D., Tobin, J. G., Rosenblatt, D. H., Davis, R. F. and Shirley, D. A., Phys. Rev. B23, 493 (1981).

Kohn, W. and Sham, L. J., Phys. Rev. 140, A1133 (1965).

Lee, P. A. and Beni, G., Phys. Rev. B15, 2862 (1977).

Li, C. H. and Tong, S. Y., Phys. Rev. B19, 1769 (1979a).

Li, C. H. and Tong, S. Y., Phys. Rev. Lett. 42, 901 (1979b).

Lindhard, J., Kgl, Danske Videnskab Selskab., Mat. Fys. Medd. 28, No. 8, (1954).

Manson, S. T., in Photoemission in Solids, Eds. M. Cardona and L. Ley, (Springer-Verlag, Berlin, 1978).

McGovern, I. T., Eberhardt, W. and Plummer, E. W., Solid State Comm. 32, 963 (1979).

Massey, H. S. W. and Burhop, E. H. S., Electronic and Ionic Impact Phenomena, (Oxford, Clarendon Press, 1952).

Mehr, J., Z. Phys. 198, 345 (1967).

Meyer, R. J., Duke, C. B. and Paton, A., Surface Sci., 97, 512 (1980).

Pendry, J. B., Low Energy Electron Diffraction, (Academic Press, London, 1974).

Prutton, M., Walker, J. A., Walton-Cook, M. R. and Felton, R. C., Surface Sci, 89, 95 (1979).

Sham, L. J. and Kohn, W., Phys. Rev. 145, 561 (1966).

Slater, J. C., Phys. Rev. 81, 385 (1951).

Slater, J. C. and Johnson, K. H., Phys. Rev. B5, 844 (1972).

Wakoh, S., J. Phys. Soc. Japan, 20, 1984 (1965).

Walker, D. W., Adv. in Phys., 20, 257 (1971).

Wendin, G., Solid State Comm. 38, 197 (1981).

Williams, G. P., Carrin, F., McGovern, I.T. and Lapeyre, G. J., Solid State Comm. 31, 15 (1979).

Williams, J. F. and Willis, B. A., J. Phys. B8, 1670 (1975).

Williams, J. F. and Crowe, A., J. Phys. B8, 2233 (1975).

CHAPTER 6

ANGLE-RESOLVED PHOTOEMISSION FROM ADSORBED MOLECULES

6.1. Introduction

So far we have looked at core-state emission from adsorbed atoms where the emphasis has been on isolating multiple scattering effects in the diffraction pattern and eliminating contributions from the initial state symmetry. In theory, this should optimise the sensitivity of the diffraction patterns to structure. However, it has been known for some time that by isolating these initial state effects for emission from the valence levels of adsorbed molecules it should be possible to obtain valuable information as regards the orientation of the molecule on the surface.

The first significant photoemission study of a molecular adsorbate system was Cashion and Eastman's work on O and CO adsorbed on polycrystalline Ni (Cashion and Eastman (1971)). In the gas phase three molecular orbitals are detected when HeI($\hbar\omega$ = 21.2 eV) radiation is used. These have been identified as the 5σ, 1π and 4σ molecular orbitals. On adsorption onto Ni, only two peaks are observed at 7.5 eV and 10.7 eV below the Fermi level. Cashion and Eastman identified the 7.5 eV peak as coming from the 5σ level which is involved in the bonding to the substrate whilst the peak at 10.7 eV was identified as arising from the non-bonding 1π level. This original assignment of the molecular orbitals for adsorbed CO is now known to be erroneous and later angle-resolved and angle-integrated work has identified the 7.5 eV peak as arising from a combination of the 1π level and the 5σ level which has been shifted down in energy through bonding to the substrate. The 11 eV peak has been assigned to the non-bonding 4σ orbital. Since 1971, a considerable amount

Figure 6.1: Photoemission spectra of CO adsorbed on various transition metal surfaces compared with the spectra for $Ir_4(CO)_{12}$ and for gas phase CO. Note the similarity of the spectra. (Photocopied from Gustafsson and Plummer (1978)).

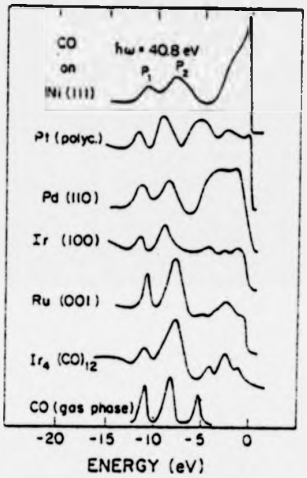

Photoemission spectra of CO adsorbed on transition metals. The two peaks below 8 eV are induced by CO adsorption. The structure above 8 eV, which changes from metal to metal, is due to emission mainly from the metal d-orbitals. For comparison, we show also the photoelectron spectrum of $Ir_4(CO)_{12}$ and gas phase CO[29]. (The bottom two spectra have been shifted in an arbitrary way to facilitate comparison)

of work has been carried out into investigating the electronic structure of CO adsorbed on various transition metal surfaces, (e.g. Horn et al (1978a) and references contained therein, Gustafsson and Plummer (1978)). It has been observed that the EDC's of adsorbed CO vary slightly between different substrates. Hence it is very difficult to detect trends in the bonding of CO to various transition metal surfaces. In fig.(6.1) spectra are shown for CO adsorbed on various metal surfaces. Also shown is the spectrum for the gas phase. From angle-integrated work, the only clue to the orientation of CO has come from the fact that the 5σ level is involved in the bonding to the substrate. This rules out any possibility of CO lying flat on the surface, for then one would expect the 1π orbital to be perturbed. Molecular orbital calculations for free CO, (Blyholder (1974)) have shown that the 5σ electrons are mainly concentrated around the C atom. This suggests that in the adsorbed state the C atom is nearest to the substrate. This sort of argument, however, is only qualitative.

The potential use of angle-resolved photoemission in studies on the orientation of adsorbed molecules may be seen by the study of the matrix element $M = \langle \epsilon \ell' m' | \underset{\sim}{A}.\underset{\sim}{p} | n \ell m \rangle$ in equation (2.10), neglecting for the moment multiple scattering. If one varies $\underset{\sim}{A}.\underset{\sim}{p}$ in M either by keeping the angle of incidence constant and varying the detector angle or vice-versa, then the resultant angle-resolved intensity so obtained is characteristic of the symmetry of the initial state orbital with respect to the substrate, (see e.g. Davenport (1976)). Hence if one looks at the angle-resolved intensity from a molecular orbital that is little perturbed by the substrate, so that the wavefunction of the initial state is well approximated by the corresponding wavefunction for the free molecule, then is should be possible to determine the orientation of the molecule with respect to the substrate. This has successfully been done for the cases of CO on

Figure 6.2: Normal emission from the 4σ level for CO adsorbed on Ni(001). Curve (1) is the SW-Xα calculation for vertical CO with C nearest the substrate, (2) is the calculation for vertical CO with the O atom nearest to the substrate and (3) is the calculation for CO lying in the substrate plane. The open circles are the experimental data.
(Photocopied from Allyn et al (1977)).

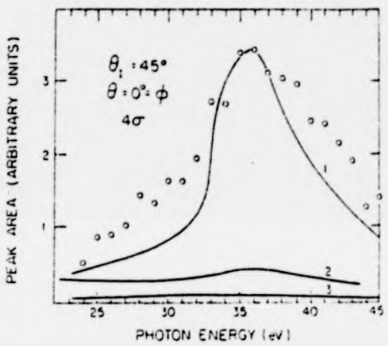

4σ peak area for normal exit, $\theta_I = 45°$, versus photon energy. Solid curves are calculations for (1) CO axis normal to the surface, carbon end down, (2) CO axis normal to surface, oxygen end down, and (3) CO axis in surface plane. Experimental data normalized to theory at $\hbar\omega = 36$ eV.

Ni(001), (Allyn et al (1977), Smith et al (1976, 1977), Lapeyre et al (1976)), CO on Ni(111), (Allyn et al (1977a)), CO on Cu(110), (Kanski et al (1978)), CO on Ir(100), (Seabury and Rhodin (1980)), CO on Cu(100), (Allyn et al (1977b)), CO on Pt(111), (Shirley et al (1980)), N_2 on W(110), (Umbach et al (1980)), C_2H_2 and C_2H_4 on Ni(001) (Horn et al (1978a)), C_5H_5N on Cu(110), (Bandy et al (1979), Nyberg (1980)), C_6H_6 on Pd(100), Ni(111), and Pd(111) (Lloyd et al (1977), Nyberg and Richardson (1979)). For CO on Ni(001) photoelectron diffraction experiments have also been performed using the CIS mode to study the energy dependence of the normal emission from the 4σ level, (Allyn et al (1977a)). The resulting curve, (fig. 6.2) shows a resonance at photon energy $\hbar\omega$ = 35 eV which results in anomalous emission in the direction of the molecular axis. This has been attributed as arising from the emitted electron being trapped between the C and O atoms by virtue of the fact that the electron wavelength is equal to twice the CO bondlength, (Dill and Dehmer (1974), Dehmer and Dill (1975)). This resonance can only be excited if $\underline{A}$ has a component parallel to the C = O bond, (Davenport (1976)).

Extensive calculations have been performed in the analysis of the angle-resolved photoemission data from adsorbed CO, (Davenport (1976)). The approach that has been adopted in these calculations is to assume that the substrate acts only to orient the molecule on the surface. The effects of the substrate on the initial and final states have been ignored as also has scattering between molecules. The molecular potential is constructed using the Scattered-Wave Xα method (SWXα), (Slater and Johnson (1972)) and this potential is used in the calculation of both the initial and final states. This model has worked surprisingly well in the analysis of the experimental data. In particular, when analysing the CIS data for normal emission from the 4σ level, these calculations correctly predict the position and width of the resonance peak only by assuming that the CO adsorbs perpendicular to the Ni(001) surface with the C atom being

nearest to the substrate, (Davenport (1976)). This finding is in agreement with the LEED analysis for this system, (Andersson and Pendry (1979), Passier et al (1979)). Li and Tong (1978) have extended this analysis of the CIS data by also including the effects of molecule-molecule and molecule-substrate scattering in their calculation. The position of the resonance peak is found to be unaffected by including scattering off the substrate, but the width of the peak is best described by putting the CO molecules at the one-fold sites on the Ni(001) surfaces. Davenport (1978) has also considered the effects of the substrate on the variation of the intensity with polar angle by performing calculations for the hypotehetical NiCO molecule. The emission from the 1π and 5σ orbitals have been found to be significantly influenced by the presence of the Ni atom. Substrate effects have also been considered in the analysis of the data taken for the case of N_2 adsorbed on W(110), (Umbach et al (1980)). The calculations have been carried out for a $(Ni)_9N_2$ cluster representing N_2 adsorbed on Ni(001). The validity of this procedure is questionable because W and Ni have different scattering properties and will have different effects on the N_2 molecular orbitals. However the calculations for this system have convincingly shown that, in certain cases, the substrate atoms can significantly influence the angle-resolved intensity.

The analysis of the data for C_2H_2, C_2H_4, C_6H_6 and C_5H_5N adsorbed on transition metal surfaces has been qualitative in nature, and is based on selection rules for emission from a molecular orbital of a particular symmetry. Multiple scattering effects have not been included at all in these analyses.

The aim of this chapter is to investigate further the approximation of neglecting multiple scattering in the calculation of the angle-resolved intensity from oriented molecules. In section (6.2) we will outline the calculational procedure that we adopt in calculating the angle-resolved photoemission intensity from valence states. Then, in section (6.3) we

present calculations for emission from the valence orbitals of CO, where final state scattering is neglected, and we will compare our calculations with those of Davenport (1976) where intramolecular scattering is included. We will then put CO onto a Ni surface and include multiple scattering in order to assess the effects of multiple scattering for this system. Subsequently we will present calculations for the angle resolved intensity from oriented ethylene (C_2H_4) and acetylene (C_2H_2), where final state scattering is neglected but the effects of the atomic potentials on the emitted electron are included. We will be able to assess the validity of the neglect of final state scattering for oriented C_2H_2 and C_2H_4 by comparing with data taken by Horn et al (1978a) for C_2H_2 on Ni(001) and with data (Johnson (1980)) for C_2H_2 adsorbed on Ni(111). In section (6.4) we will summarize and discuss the results of the previous sections.

6.2. Theory

We concentrate on the analysis of angle-resolved photoemission data from molecular orbitals that are known to be only weakly perturbed by the substrate. We require to know the initial state as a linear combination of atomic orbitals (LCAO), (Coulson (1965)):

$$\psi_i = \sum_k \sum_\ell C_{k\ell}\phi_{k\ell} \qquad (6.1)$$

where $\phi_{k\ell}$ is the ℓ^{th} atomic orbital centred on atom k, and $C_{k\ell}$ is a coefficient giving the contribution from the electrons in atomic orbital $\phi_{k\ell}$ to the molecular orbital ψ_i. The calculation of the $\{C_{k\ell}\}$ proceeds by standard methods, (see e.g. Pople (1970)), and suffice it to say that the molecular orbitals for many small molecules are tabulated in the chemical literature.

We use equation (2.10) to calculate the wavefunction $\psi_{k\ell}$ of the electron emitted from each atomic orbital $\phi_{k\ell}$ in the expansion in equation (6.1), neglecting scattering in the final state. The contributions from

all the atomic orbitals are then coherently combined according to equation (6.1) to obtain the wavefunction ψ' of the emitted electron:

$$\psi' = \sum_k \sum_\ell C_{k\ell}\psi_{k\ell} \tag{6.2}$$

The intensity I may then be written as:

$$I = |\psi'|^2 \tag{6.3}$$

As we are considering the electron travelling straight to the detector, we will find it convenient to approximate $h_\ell^+(K|\underset{\sim}{r}-\underset{\sim}{e}|)$ in equation (2.10) for large $|\underset{\sim}{r}|$ by using the relation, (see e.g. Messiah (1961)):

$$\lim_{|\underset{\sim}{r}|\to\infty} h_\ell^+(K|\underset{\sim}{r}-\underset{\sim}{e}|) = \frac{i^{-\ell} e^{-i\underset{\sim}{K}.\underset{\sim}{e}}}{\underset{\sim}{K}.\underset{\sim}{r}} \tag{6.4}$$

By calculating the intensity in this way it should be noted that although we are neglecting the effects of scattering off the neighbouring ion cores, we are considering the influence on the outgoing electron of the potential of the atom from which the electron originated. Thus we are not using the plane wave final state which is known not to work in certain situations, (see e.g. Gadzuk (1975)). We are including, through the $\exp(-i\underset{\sim}{k}.\underset{\sim}{e})$ term, interference effects between electrons emitted from different atomic centres. We shall, for the sake of simplicity, neglect the effect of refraction of the outgoing electron by the surface barrier. However, as most of the data that we will analyse are taken from experiments that use low energy radiation, we will need to consider the effects of superposition of the incident and reflected electromagnetic waves at the surface. If r_s and r_p are respectively the reflectivities of the substrate for s- and p- polarised light and if $\hat{\underset{\sim}{z}}$ is the direction of the outward surface normal, then it may be shown (Scheffler et al (1977)) that by combining the incident and reflected waves, $\underset{\sim}{A}$ for p-polarised light may be written as:

$$\begin{pmatrix} Ax \\ Ay \\ Az \end{pmatrix} = \begin{pmatrix} (1-r_p)\cos\theta' \cos\phi' \\ (1-r_p)\cos\theta' \sin\phi' \\ (1+r_p)\sin\theta' \end{pmatrix} \qquad (6.5)$$

and for s-polarised light, $\underset{\sim}{A}$ is given by:

$$\begin{pmatrix} Ax \\ Ay \\ Az \end{pmatrix} = \begin{pmatrix} (1+r_s)\cos\phi' \\ (1+r_s)\sin\phi' \\ 0 \end{pmatrix} \qquad (6.6)$$

Here, ϕ' and θ' are respectively the azimuthal and polar angles of the $\underset{\sim}{A}$-vector. Refraction of the electromagnetic wave is particularly important for experiments where the angle of incidence is varied and the detector is kept fixed (see e.g. Weeks and Plummer (1977)). We use the expressions derived by Whitaker (1978) for r_s and r_p:

$$r_p = \frac{([\varepsilon_1^2 + \varepsilon_2^2]\cos^2\theta' - S^{\frac{1}{2}}) + i\sqrt{2}(\cos\theta)U_-(S^{\frac{1}{2}} - \sin^2\theta)}{(\varepsilon_1^2 + \varepsilon_2^2)\cos^2\theta + S^{\frac{1}{2}} + \sqrt{2}(\cos\theta)U_+(S^{\frac{1}{2}} + \sin^2\theta)}$$

$$r_s = \frac{\cos^2\theta - S^{\frac{1}{2}} - \sqrt{2}iU_-(\cos\theta)}{\cos^2\theta + S^{\frac{1}{2}} + \sqrt{2}U_+(\cos\theta)} \qquad (6.7)$$

where θ is the angle of incidence of the radiation with respect to the surface normal,

$$S = (\varepsilon_1 - \sin^2\theta)^2 + \varepsilon_2^2$$

and

$$U_\pm = [S^{\frac{1}{2}} \pm (\varepsilon_1 - \sin^2\theta)]^{\frac{1}{2}} \quad .$$

For unpolarised light it may be shown that the intensity I for emission may be written as:

$$I = I_p + I_s \qquad (6.8)$$

(Weeks and Plummer (1977), Jacobi et al (1977), Scheffler et al (1977)), where I_p is the intensity for emission for p-polarised radiation only and I_s is the intensity for emission by s-polarised radiation only.

6.3. Comparison Between Theory and Experiment for Various Molecular Adsorbate Systems.

6.3.1. CO adsorbed on Ni

The adsorption of CO on transition metal surfaces has been extensively studied by various surface techniques including angle-resolved photoemission. It is now clear that on {100} and {111} surfaces CO stands upright with the C atom being nearest to the substrate whilst on {110} surfaces it is thought that CO may be tilted with respect to the normal direction with the C atom being nearest to the substrate.

6.3.1.1. Calculations for Oriented CO

We first use the method that is outlined in section (6.2) to calculate the angle-resolved intensity from the 5σ, 1π and 4σ levels of oriented CO. By comparing with Davenport's multiple scattering calculation we can then assess the importance of scattering within the molecule.

In our calculations we take the CO wavefunctions from a semiempirical calculation due to Blyholder (1974). A problem arises as to the calculation of the CO potential. As we mentioned earlier, we cannot simulate a molecular cluster with the MUFPOT program. We use the model suggested by Andersson and Pendry (1978) where the C and O atoms are put onto an NaCl lattice, and we put $\alpha = 0.75$, (the Schwartz value, (Schwartz (1972)), in the calculation of the exchange potential. For each molecular orbital two calculations of the angle-resolved intensity are carried out: (i) for $\underline{A}$ parallel to the molecular axis and (ii) for $\underline{A}$ perpendicular to the molecular

Figure 6.3: The angle-resolved photoemission intensity (arbitrary units) as a function of detector angle (ψ) for emission from molecular orbitals of oriented CO. (a) to flare calculations that neglect multiple scattering. The photon energy is 40.8 eV.

(a) 5σ level, $\underline{A}$ parallel to molecular axis.

(b) 1π level, $\underline{A}$ parallel to molecular axis.

(c) 4σ level, $\underline{A}$ parallel to molecular axis.

(d) 5σ level, $\underline{A}$ perpendicular to molecular axis.

(e) 1π level, $\underline{A}$ perpendicular to molecular axis.

(f) 4σ level, $\underline{A}$ perpendicular to molecular axis.

(g) Davenport's calculations incorporating multiple scattering within the molecule, (Davenport (1976), (photocopied from Liebsch (1978)).

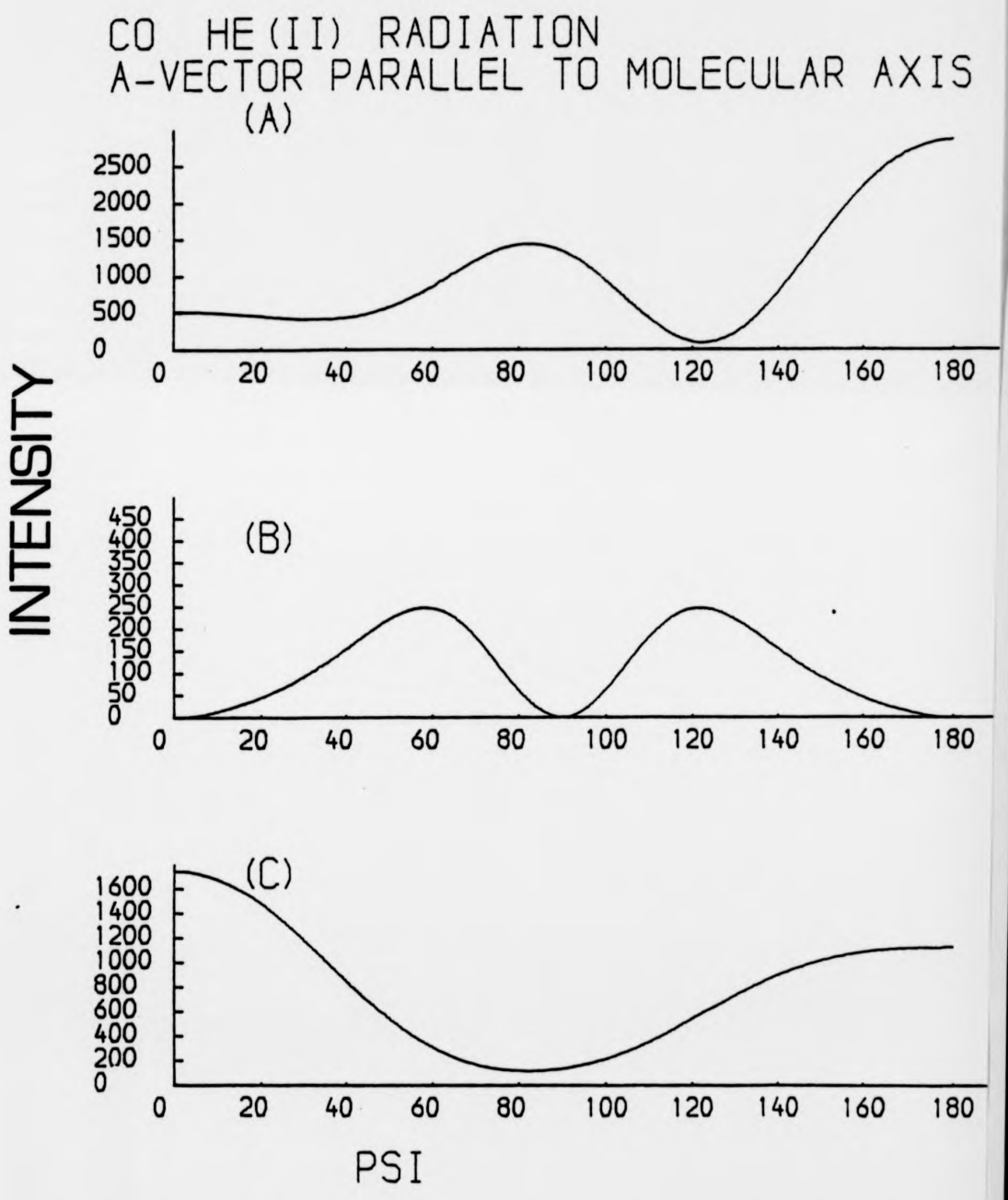
CO HE(II) RADIATION
A-VECTOR PARALLEL TO MOLECULAR AXIS
(A)
2500
2000
1500
1000
500
0
(B)
450
400
350
300
250
200
150
100
50
0
(C)
1600
1400
1200
1000
800
600
400
200
0
0 20 40 60 80 100 120 140 160 180
INTENSITY
PSI

CO HE(II) RADIATION
A-VECTOR PERPENDICULAR TO MOLECULAR AXIS

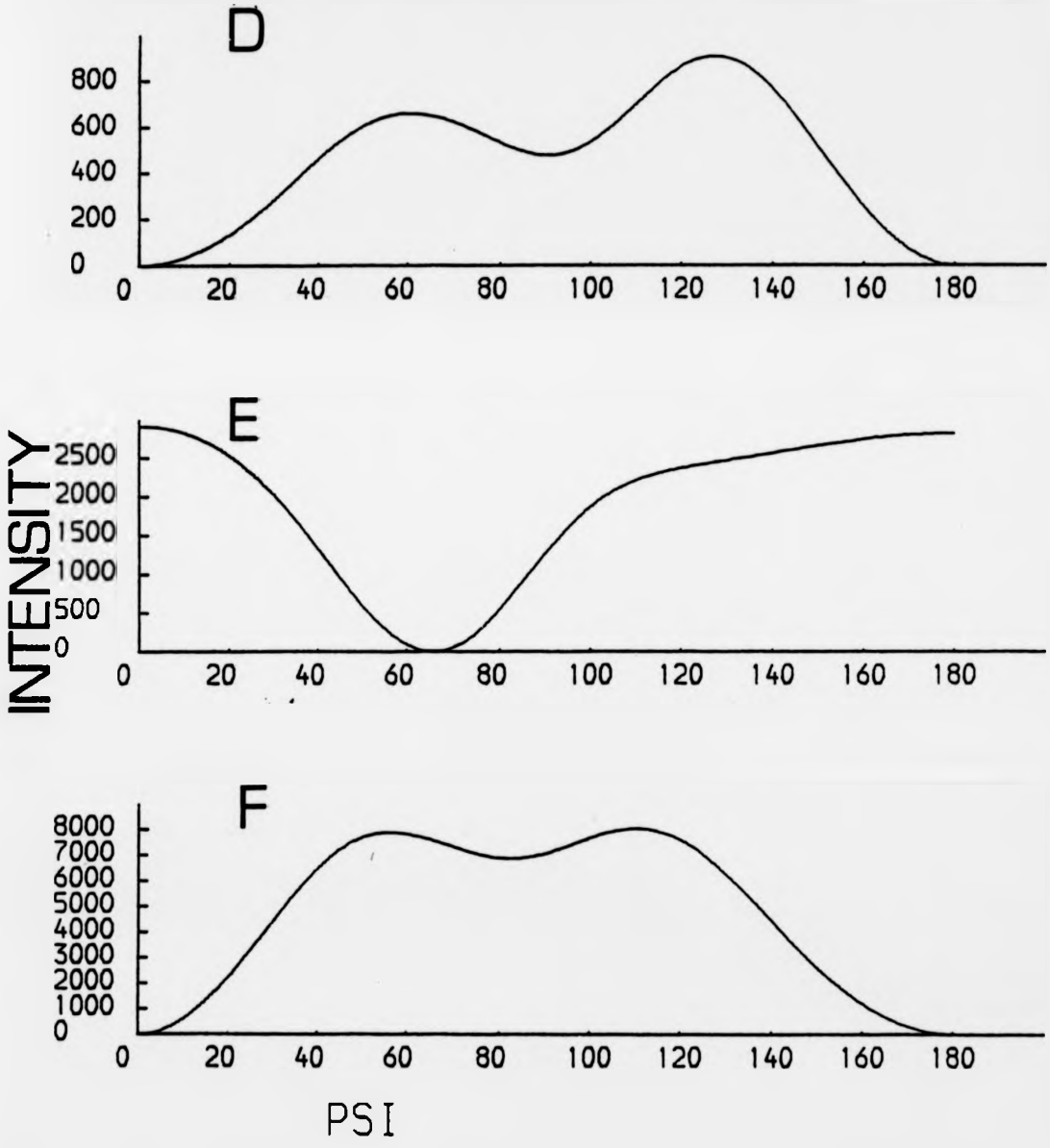

(G)

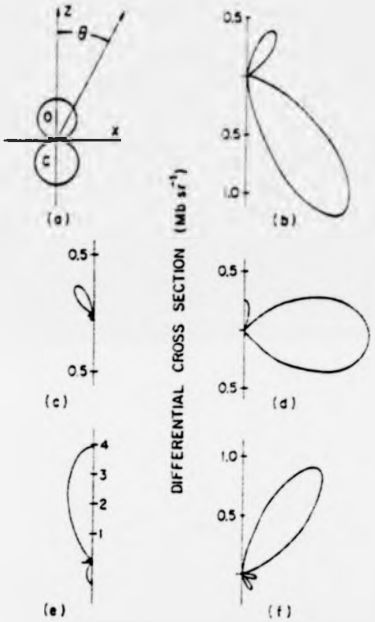

Angular distribution of photoemitted electrons from an oriented CO molecule at $\omega = 41$ eV. (a) Molecular orientation. (b)–(f) Polar plots of differential cross section in Mb sr^{-1} for the (b) 5σ level with $\vec{A}$ along X axis, (c) 1π level with $\vec{A}$ along Z, (d) 1π level with $\vec{A}$ along X, (e) 4σ level with $\vec{A}$ along Z, and (f) 4σ level with $\vec{A}$ along X. For clarity only half of each distribution is shown but they are all symmetrical about the Z axis. Note the different scales.

Figure 6.4: The angle-resolved photoemission intensity (arbitrary units) as a function of detector angle (ψ) for emission from the 4σ level of oriented CO for $h\omega$ = 40 eV and 60 eV. The $\underline{A}$-vector is at 45^{o} to the surface normal.

(a) Calculations that neglect scattering.

Full curve: $\hbar\omega$ = 60 eV

Dashed curve: $\hbar\omega$ = 40 eV

(b) Full curves: Scattered Wave Xα calculations

Open circles: Experimental data for CO on Ni(111)

(Photocopied from Gustafsson (1980)).

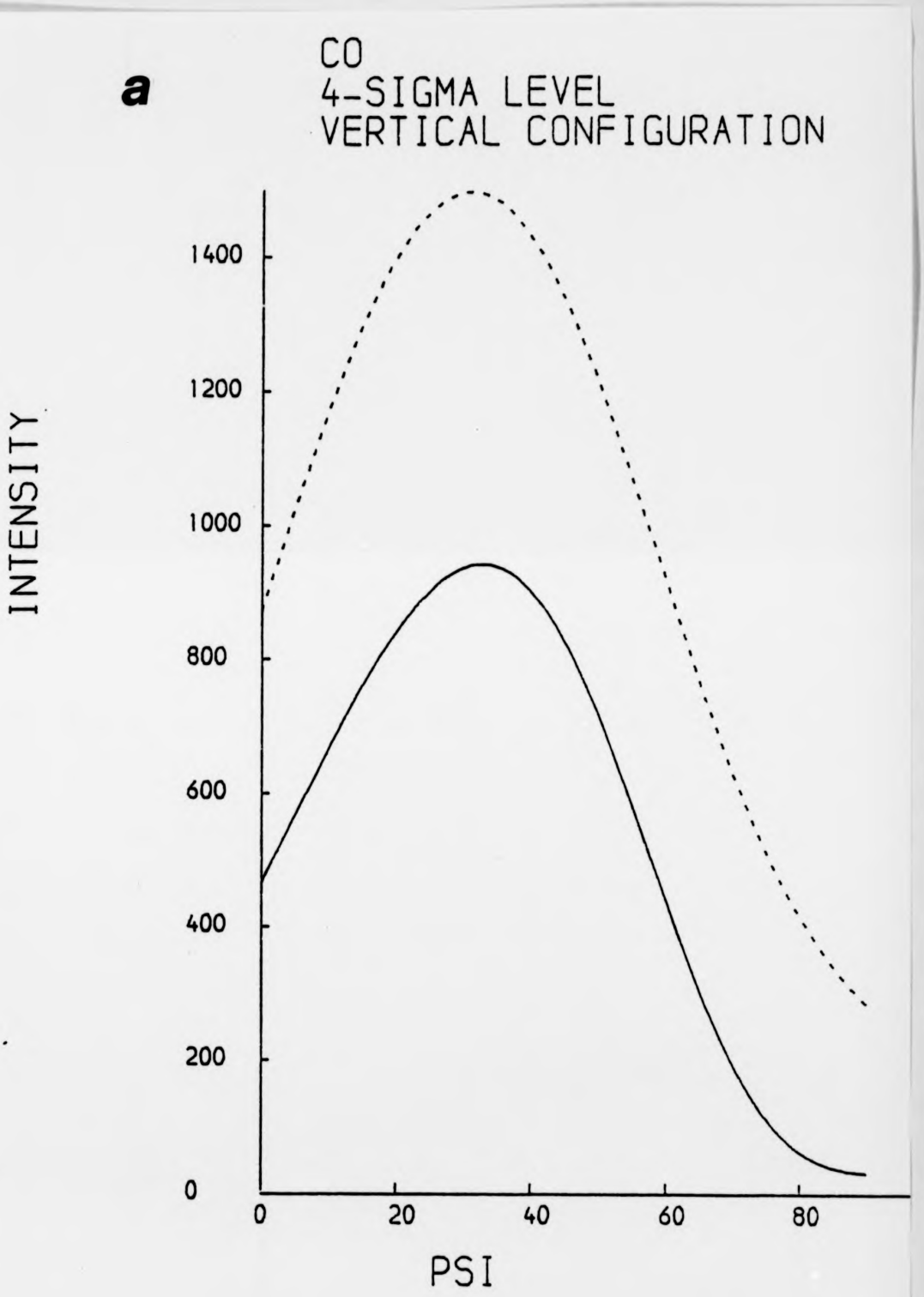
a
CO
4-SIGMA LEVEL
VERTICAL CONFIGURATION
INTENSITY
1400
1200
1000
800
600
400
200
0
0
20
40
60
80
PSI

b

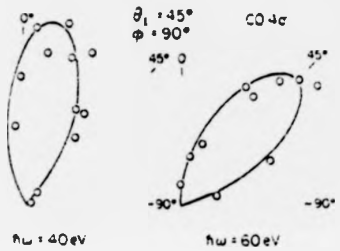

Measured intensity from the 4σ orbital of CO chemisorbed on Ni(111) as a function of polar angle at $\hbar\omega = 40$ and $\hbar\omega = 60$ eV. The angle of incidence of the light is 45° and the electrons are detected in the plane of incidence ($\phi = 90°$), in the quadrant containing the A vector. The full drawn curve is the calculated result (only the main emission lobe is shown). The data points have been normalized so as to best fit the calculated curve.

axis. In our calculations the CO molecule is assumed to be standing straight up on the surface with the C atom being nearest to the substrate. The photon energy is set equal to that for HeII radiation, ($\hbar\omega$ = 40.8 eV). In our plots of the angle-resolved intensity, the zero of the polar angle, (θ), is taken as the outward surface normal. A comparison between our calculation and those of Davenport is shown in fig. (6.3). For the 4σ level the calculation for $\underline{A}$ perpendicular to the molecular axis is slightly different from Davenport's calculation, although the overall shape is similar. A similar discrepancy is seen for the 5σ level with the same orientation of the $\underline{A}$-vector. For the 1π level, with $\underline{A}$ perpendicular to the molecular axis, whilst our calculations places a large peak at $\theta = 180^{\circ}$, no such peak occurs in Davenport's calculation. The discrepancies that occur could be due to the neglect of intramolecular scattering in our calculations. Another possibility is that we should be using a more realistic potential in the calculation of the factors $\{\delta_{\ell}\}$ and $\sigma_{n\ell,\ell\pm1}$ occuring in equation (2.10) for the unscattered emitted electron. In fig. (6.4) we present calculations for emission from the 4σ level of adsorbed CO for photon energies $\hbar\omega$ = 40 eV and 60 eV. The radiation is unpolarised and incident at 45° to the surface normal with the detector and light source in the same plane but on opposite sides of the surface normal. In our calculations the CO molecule is assumed to stand straight up with the C atom underneath the O atom. We compare our calculation with data taken for CO adsorbed on Ni(111), (Gustafsson (1980)), and with SW-Xα calculations, (Davenport (1976), Gustafsson (1980)). For $\hbar\omega$ = 40 eV there is excellent agreement between the SW-Xα calculation (Davenport (1976)) and experiment. Our calculation neglecting scattering in the final state places the peak at $\theta = 30^{\circ}$ which is 15° higher than it should be. For $\hbar\omega$ = 60 eV there is again excellent agreement between the SW-Xα calculation and experiment.

Figure 6.5: The angle-resolved photoemission intensity from the 4σ level of CO adsorbed on Ni(001) as a function of detector angle θ_p for photon energy $h\omega$ = 28 eV

Circles: Experimental Data

Full curves: Scattered Wave Xα calculations

In the figure θ_A is the orientation of the A-vector with respect to the outward surface normal.

(Photocopied from Smith et al. (1976)).

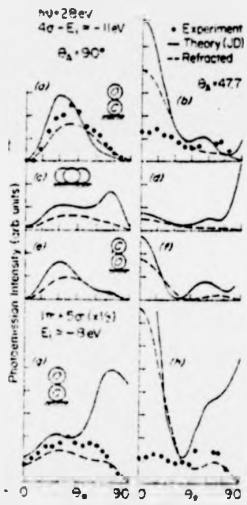

Calculated photoemission polar intensities for three orientations of a CO molecule for *s*- and *p*-polarized radiation (solid curves). The dashed curves show the possible effects of refraction at the surface, and the filled circles indicate the measured emission peak heights. Panels (g) and (h) are reduced by a factor of 2, relative to the other panels.

Figure 6.6: Calculations that neglect scattering for the data presented in fig. (6.5):

(a) $\theta_A = 90°$

(b) $\theta_A = 47.7°$

CO
4-SIGMA LEVEL
VERTICAL CONFIGURATION

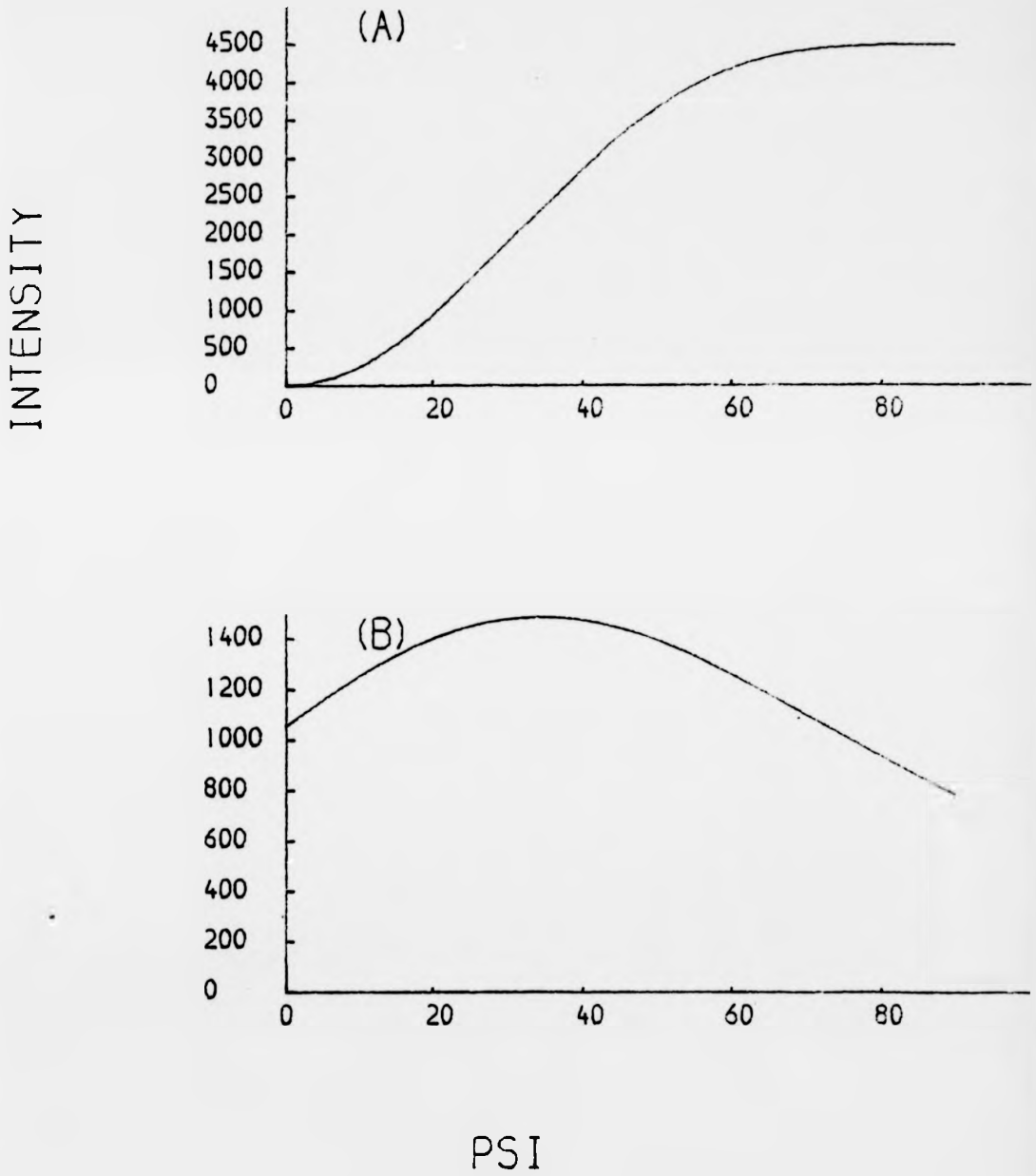

In our calculation for this energy the peak is at $\theta = 35^{\circ}$ which is 10° too low. We have found that in our calculations the position of the peak is fairly insensitive to the potential that is used in the calculation of the phase shifts and photoionization amplitudes. We thus conclude that it is the neglect of multiple scattering that is causing our disagreement with experiment.

We finally look at the data taken by Smith et al (1976) for the emission from the 4σ level of CO adsorbed on Ni(001) for photon energy $\hbar\omega = 28$ eV, (fig. (6.5)). Two orientations of the $\underline{A}$-vector are used: (i) in the plane of the surface and (ii) at 45° to the surface normal. In both cases the $\underline{A}$-vector and detector are coplanar with the detector and light source being on opposite sides of the surface normal. The experimental data have been compared with SW-Xα calculations (Davenport (1976)). For experimental configuration (i), by using the LEED structure, (Passier et al (1979), Andersson and Pendry (1979)), good agreement between theory and experiment has been obtained between theory and experiment for both the 4σ and "$1\pi + 5\sigma$" levels. For experimental geometry (ii), however, for both levels the SW-Xα calculations predict too large an intensity for normal emission. The reason for this is that the data is taken for photon energies in the vicinity of the 4σ resonance. For experimental geometry (ii) there is a component of the $\underline{A}$-vector in the direction of the molecular axis, and so there will be additional intensity in the normal direction, (Dill and Dehmer (1974), Dehmer and Dill (1975)). The SW-Xα calculation overestimates this additional intensity and this could be due to the inadequacy of the molecular potential that is being used in the description of final state scattering in the vicinity of the resonance. Another possible cause for this disagreement is that one should be considering the effects of backscattering off the substrate in the calculation of the angle-resolved intensity. Our calculations for this data, where scattering is neglected are shown in fig. (6.6), where the CO molecule is assumed to

stand vertically on the surface with the C atom being nearest to the substrate. For experimental geometry (ii) there is good agreement between our calculations and experiment, but the agreement with the SW-Xα calculation (fig. (6.5) is poor. For experimental geometry (i) the agreement between our calculation and the experimental data is poor. We conclude that near a resonance it is important to put in multiple scattering into these calculations.

6.3.1.2. Calculations for CO adsorbed on Ni(001) and Ni(111)

Most of the calculations of the angle-resolved photoemission intensity from adsorbed CO have not investigated the effects of backscattering off the substrate. However, we have seen that the SW-Xα calculations, which consider just scattering within the molecule, can sometimes give a poor description of the experimental data. It is therefore of interest to extend these calculations to consider scattering off the substrate, to see whether it is the neglect of this effect that is causing the problems that have been encountered. In this subsection we will perform such calculations for the case of c(2 x 2)CO adsorbed on Ni(001) and p(2 x 2)CO adsorbed on Ni(111) and we will compare the results of our calculation with SW-Xα calculations,((Davenport (1976), Gustafsson (1980)), and the experimental data for these systems, (Allyn et al (1977), Williams et al (1976)).

It has been mentioned in section (6.3.1.1) that it is difficult to simulate a molecular potential with the MUFPOT programs. In the calculations that neglect scattering in the final state we model the CO potential by putting the C and O atoms onto a NaCl lattice. It is important to ascertain whether this potential is adequate in the description of scattering in the final state. As a test, we use this potential in the calculation of the energy dependence of the normal emission intensity from the 4σ level of c(2 x 2)CO adsorbed on Ni(001). We compare our

Figure 6.7: Energy dependence of the intensity for normal emission from the 4σ level of c(2 x 2)CO adsorbed on Ni(001).

(a) Solid curve: Calculation of Li and Tong (1979) which assumes that the CO molecule bonds at the one fold sites with the C atom nearest to the substrated.

Broken curve: Calculation for CO bonded at the four-fold sites, V_o = 11.2 eV.

Dashed-dotted line: Calculations for CO bonded at the four-fold sites, V_o = 0 eV.

Open circles: experimental data (Allyn et al (1976)).

(b) Photoelectron diffraction calculation for the data presented in (a) where atomic charge densities have been used in the construction of the CO potential.

Full curve: α = 0.75

Dashed curve: α = 0.50

Part (a) of this figure is photocopied from Li and Tong (1979).

a

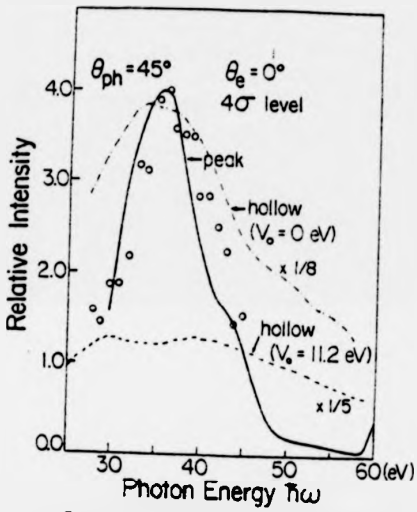

Comparison of photon resonance curves for $c(2 \times 2)$ CO-Ni(001). Solid line, peak-bonded CO; broken line, fourfold-bonded CO, $V_0 = 11.2$ eV; dash-dotted line, fourfold-bonded CO, $V_0 = 0$ eV; open circles, experiment.

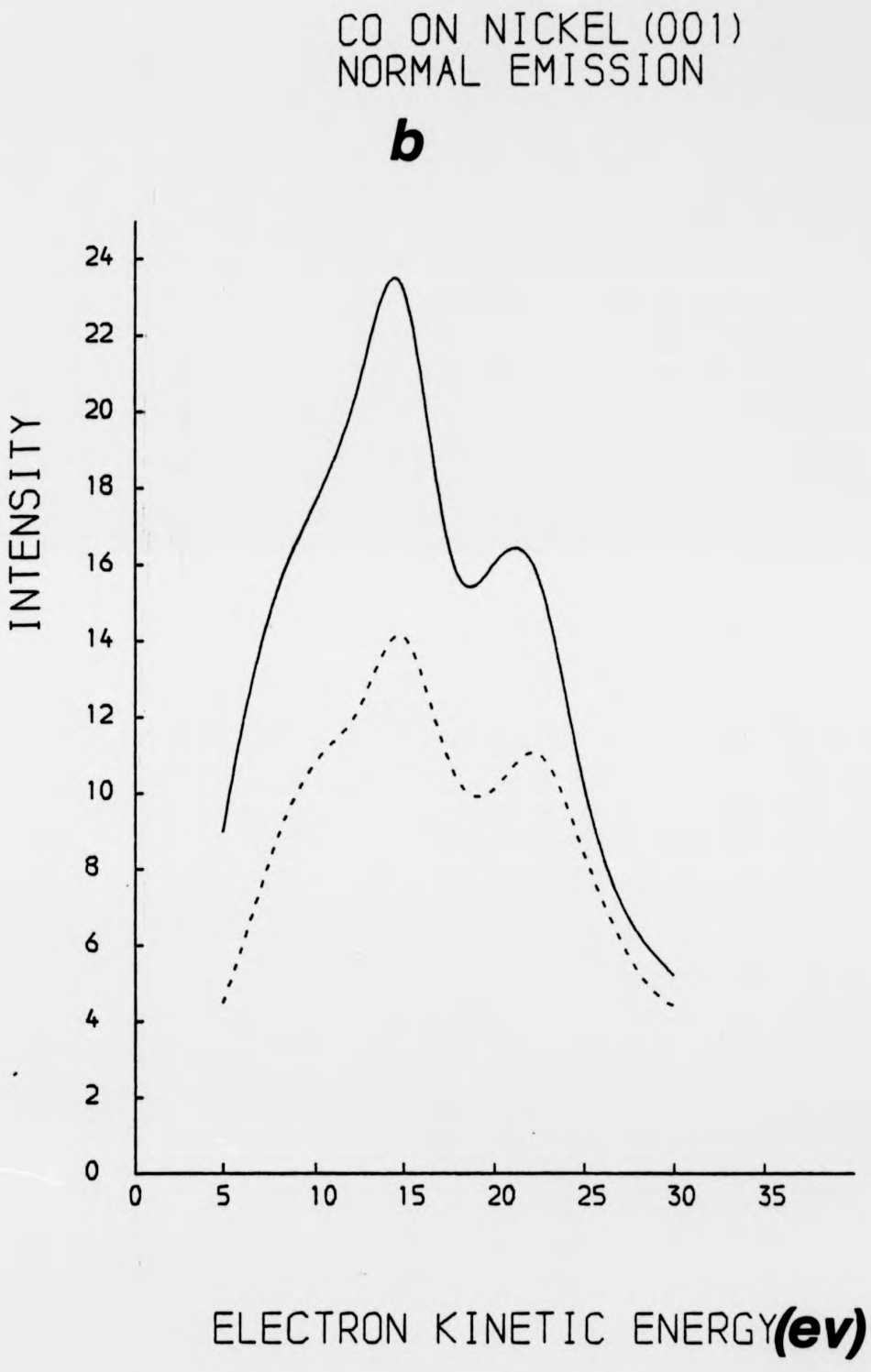
CO ON NICKEL (001)
NORMAL EMISSION
b
INTENSITY
0
2
4
6
8
10
12
14
16
18
20
22
24
0
5
10
15
20
25
30
35
ELECTRON KINETIC ENERGY (ev)

CO ON NICKEL (001)
NORMAL EMISSION

b

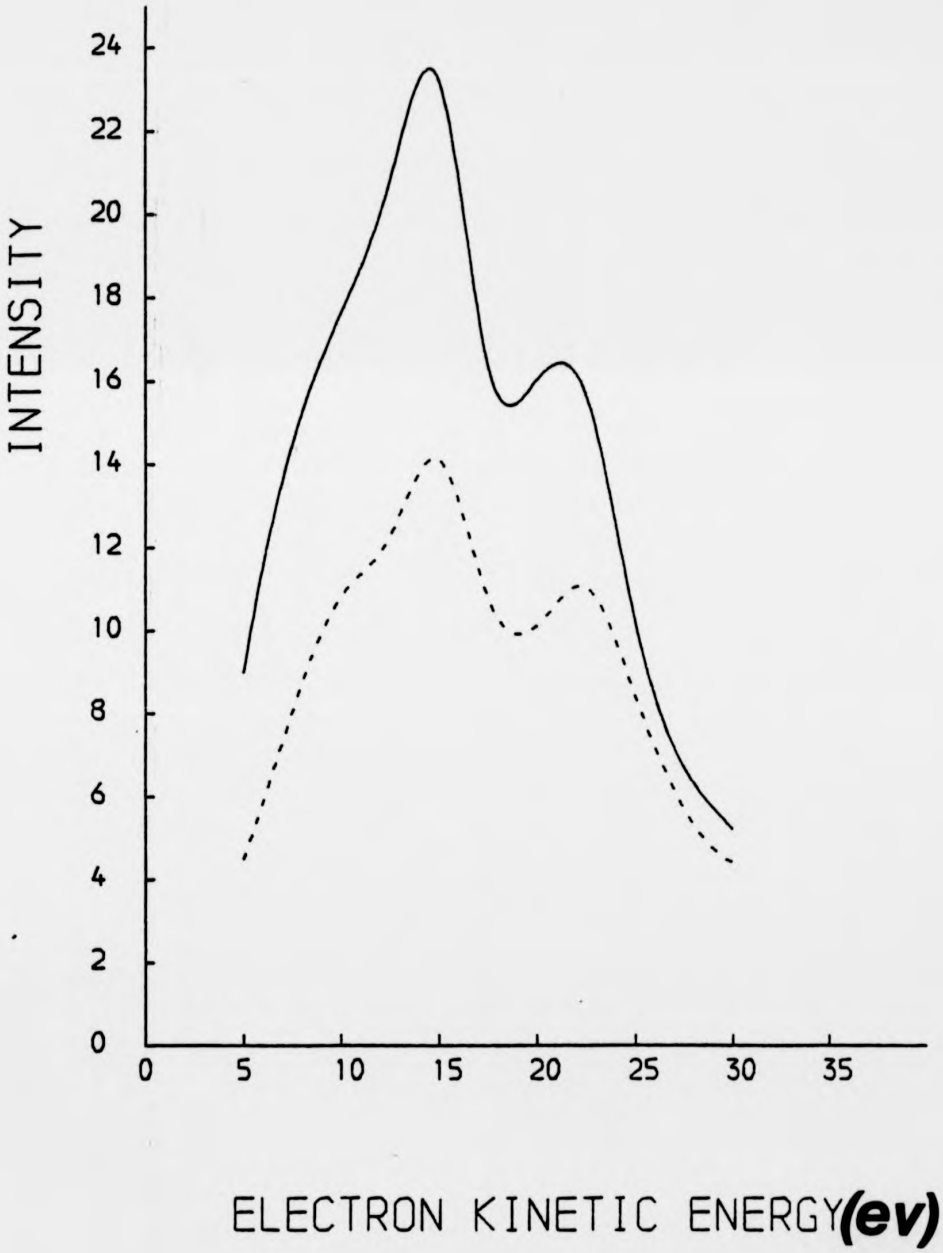

calculations with the calculations of Li and Tong (1978), who use a SW-Xα potential for the CO, and with the experimental data of Allyn et al (1977). We use the following models for the CO potential in our calculation: (i) C and O on a NaCl lattice, α = 0.75 and (ii) as (i) but with α = 0.50. The nearest neighbour distance in the calculation of the potential is set equal to 1.15 Å, which is the bond-length of adsorbed CO, (Passier et al. (1979), Andersson and Pendry (1979)). The Ni phase shifts are taken from the Wakoh potential, (Wakoh (1965)). The surface is modelled by a slab consisting of a layer of CO molecules plus two layers of Ni atoms. The addition of more layers of Ni is found to have a negligible effect on the diffraction pattern. The mean free path of the electron is taken to be 8Å, (Demuth et al (1975)), and the scattering electron is described by four partial waves. The binding energy of the 4σ level is taken to be 17 eV below the vacuum level, (Smith et al (1976)). The inner potential is initially set to be 0 eV; by aligning the positions of the calculated and experimentally found resonance peaks it should be possible to obtain an estimate of the actual inner potential. The structure for this system is taken from the LEED calculations, with the Ni-C and C-O distances being respectively set at 1.82 Å and 1.15 Å, (Passier et al (1979), Andersson and Pendry (1979), Tong et al (1980)). We initially used reverse scattering perturbation theory to sum the multiple scattering series, but divergences were found to occur for electron energies ≤ 30 eV. Therefore the matrix inversion method, outlined in section (2.3), is used to evaluate this series.

The results of our calculations along with the calculations of Li and Tong (1978) and the experimental data, (Allyn et al (1977)) are shown in fig. (6.7). Both our calculations are in qualitative agreement with experiment. The calculations do not appear to be sensitive to α. The calculation

Figure 6.8: Calculations for the variation of the intensity with polar angle (ψ) of photoelectrons emitted from the 4σ level of p(2 x 2)CO adsorbed on Ni(111).

Full curve: $h\omega$ = 60 eV

Dashed curve: $h\omega$ = 40 eV.

CO ON NICKEL (111)

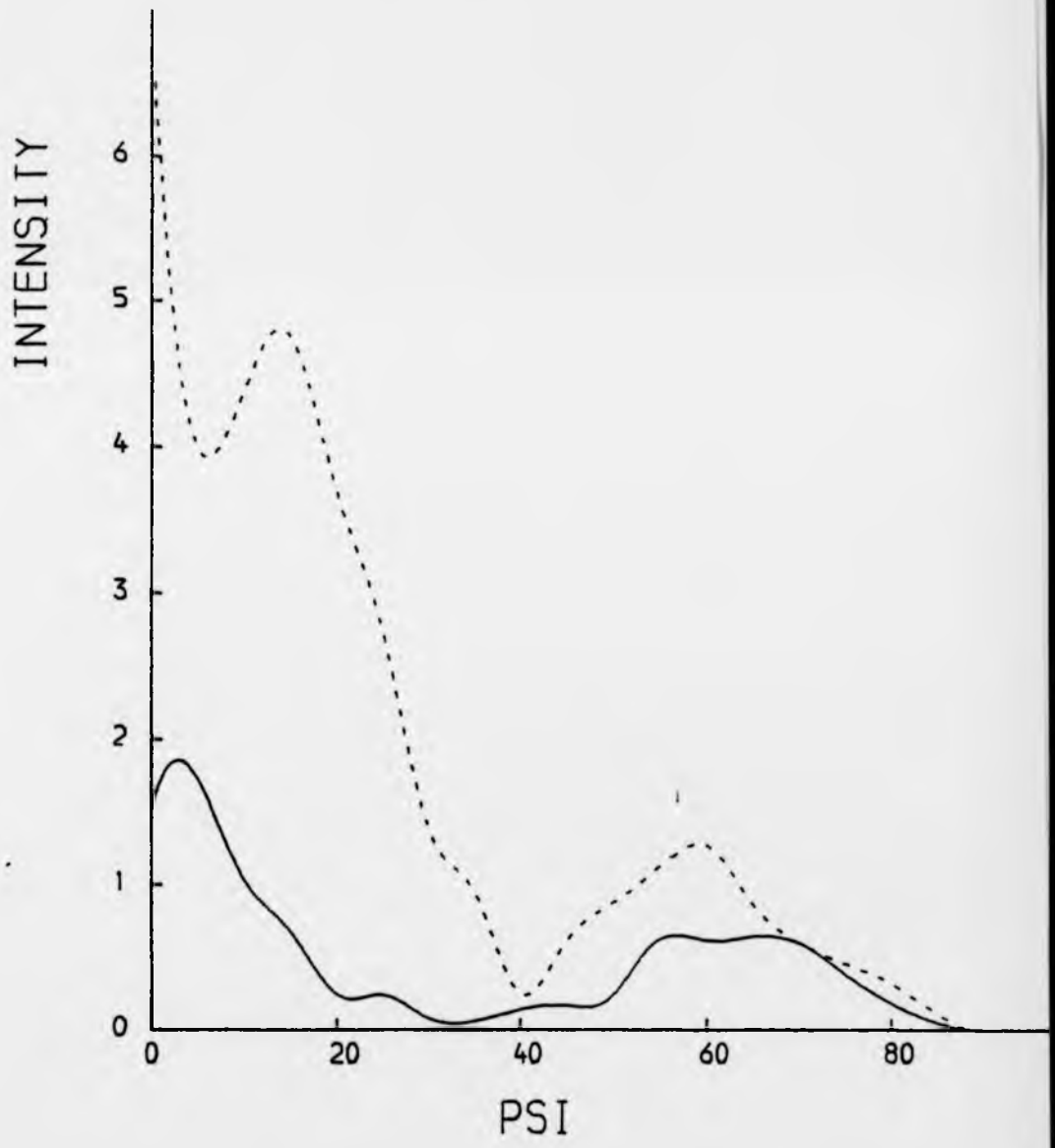

that uses the $\alpha = 0.75$ phase shifts is in slightly better agreement with experiment in that it shows a gentle feature at $\sim$ 40 eV photon energy, in agreement with experiment whilst the calculation that uses the $\alpha = 0.5$ phase shifts shows a much sharper feature at this energy. In both calculations, however, the calculated resonance peak is far broader than the experimental peak. Thus, there are still inadequacies in the potential for CO that we are using. The fact that Li and Tong (1978) and Davenport (1976) obtain better fits to the peak width implies that the SW-Xα method is providing a better potential for the CO, than the method that we are using. We shall, in subsequent calculations, use model (i) for the CO potential.

We first turn to the analysis of the data taken for CO adsorbed on Ni(111), (Williams et al (1976)) which we have already analysed neglecting scattering in the final state. Calculations are performed for one layer of CO molecules and two layers of Ni atoms, and the CO are put at the one-fold sites on the Ni(111) surface, in a p(2 x 2) configuration. The other input parameters that we use are the same as those used in the CIS calculation. The azimuth of the outgoing electron is taken to be in the [011] direction. The results of our calculations are shown in fig.(6.8). For $h\omega = 40$ eV the peak in the data at $\theta = 15^{\circ}$ is reproduced in the calculation, but another peak in the intensity is predicted to occur at normal exit angle which is not observed experimentally. The corresponding SW-Xα calculation, (Davenport (1976)), shown in fig. (6.4), does not show a peak at $\theta = 0^{\circ}$ and is in better agreement with experiment. For $h\omega = 60$ eV, however, the agreement with both the SW-Xα calculation and experiment is very poor. Whilst our calculation predicts a peak to occur at $\theta = 5^{\circ}$, both the SW-Xα calculation (Gustafsson (1980)) and the experimental data, (both shown in fig. (6.4)), exhibit a peak at $\theta = 45^{\circ}$. This again indicates the superiority of the SW-Xα potential for use in these calculations.

Figure 6.9: Calculations for the variation of the intensity with polar angle (ψ) of photoelectrons emitted from the 4σ level of c(2 x 2)CO adsorbed on Ni(001) for photon energy 28 eV.

Top panel: $\underline{A}$-vector at 45^{o} to the surface normal

Full curve: [100] azimuth

Dashed curve: [110] azimuth

Lower panel: $\underline{A}$-vector in the surface plane.

Full curve: [100] azimuth

Dashed curve: [110] azimuth.

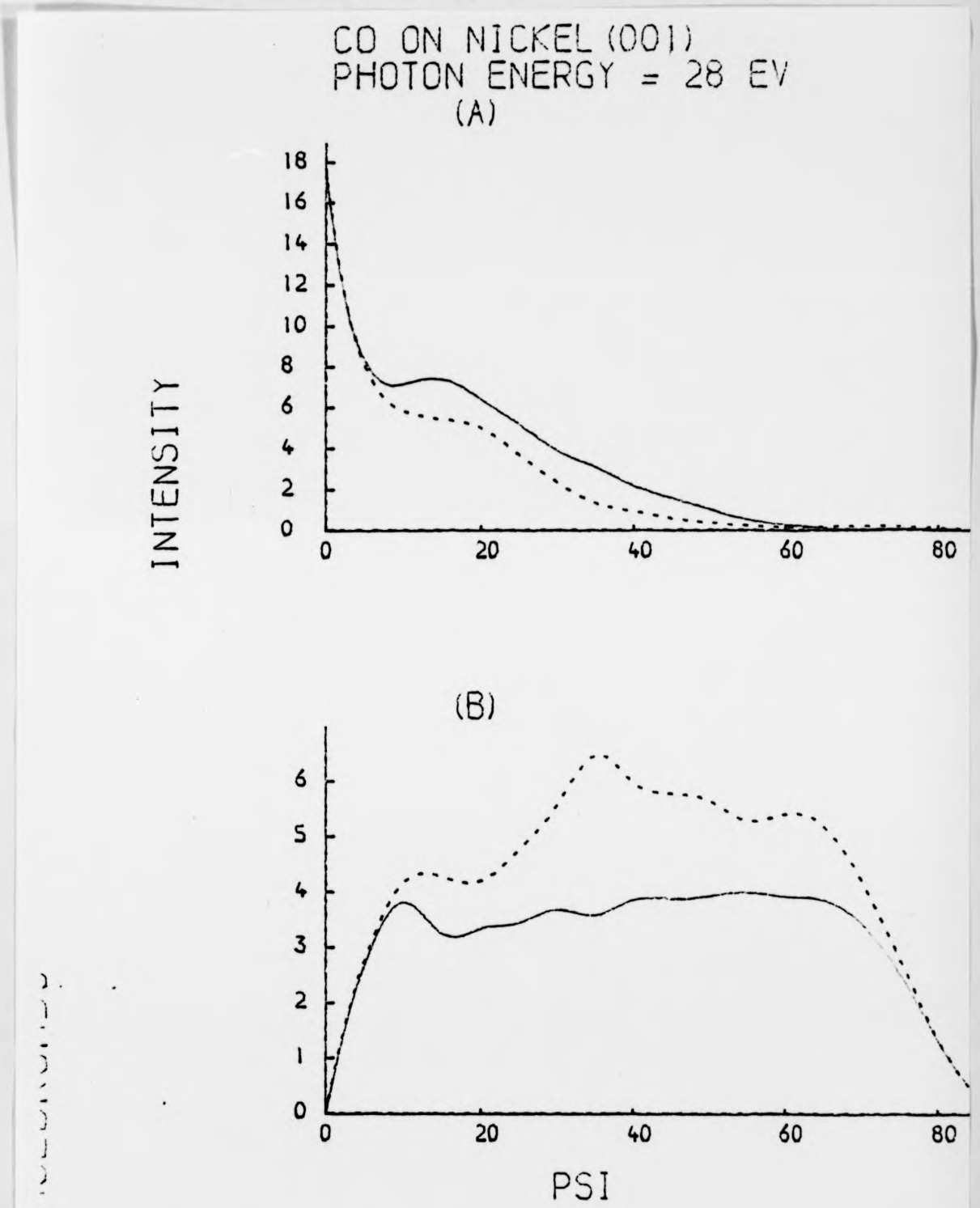
CO ON NICKEL (001)
PHOTON ENERGY = 28 EV
(A)
INTENSITY
18
16
14
12
10
8
6
4
2
0
0
20
40
60
80
(B)
6
5
4
3
2
1
0
0
20
40
60
80
PSI

CO ON NICKEL (001)
PHOTON ENERGY = 28 EV

(A)

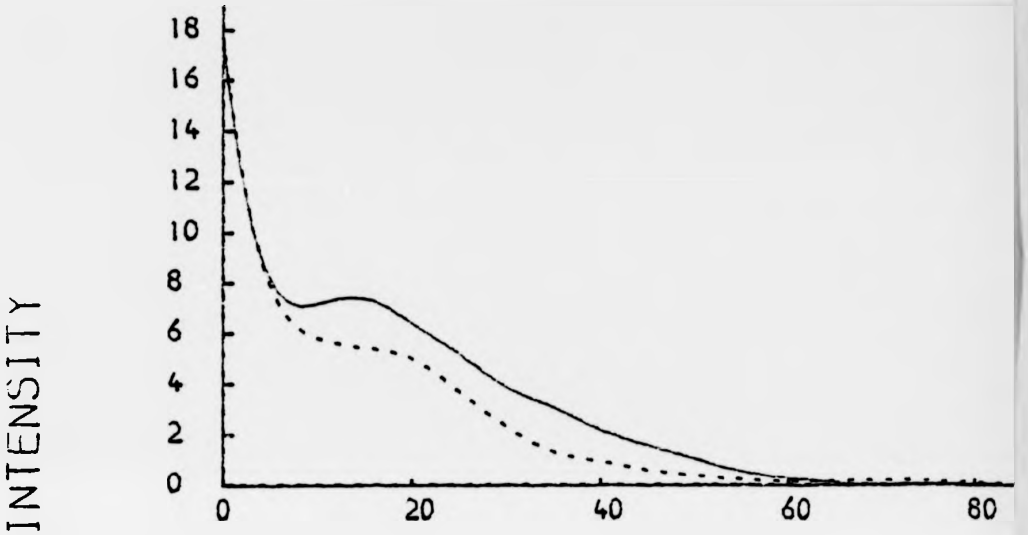

(B)

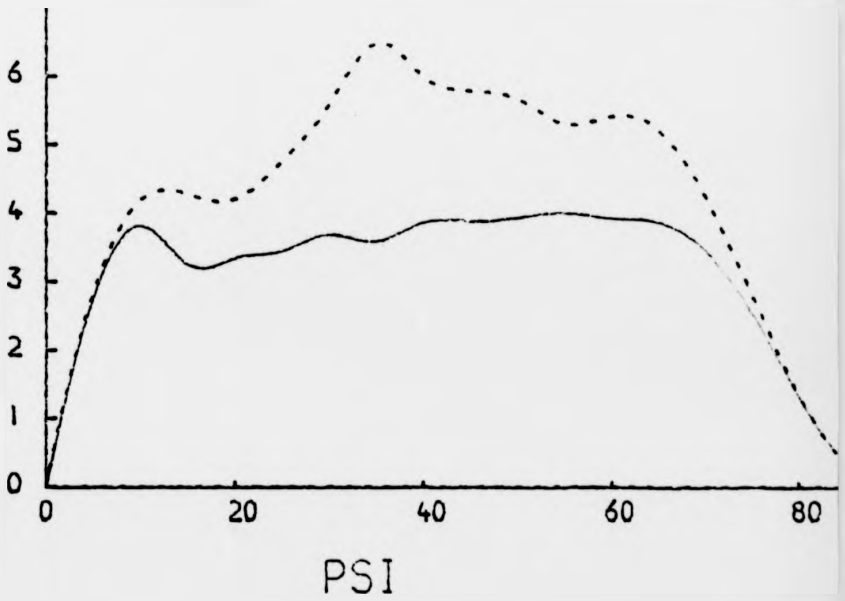

We now turn to the analysis of the data of Smith et al (1976) for CO 4σ emission from Ni(001) - c(2 x 2)CO. The calculations are performed for one layer of CO molecules and two layers of Ni. Smith et al have found that the measured angle-resolved intensity is independent of the azimuthal plane in which the electrons are detected. To test this, we perform calculations for electrons collected in the [100] and [110] azimuths. Our results are shown in fig.(6.9). For $\underset{\sim}{A}$ in the plane of the crystal surface there is good agreement between theory and experiment for the electrons detected in the [110] azimuth, but for the [100] azimuth the agreement is poor. Our calculations also suggest that the angle-resolved intensity does depend on the azimuth in which the electrons are detected. For $\underset{\sim}{A}$ at 45° to the surface normal, the agreement between theory and experiment is very poor; we predict there to be a large peak in the intensity at $\theta = 0^{\circ}$ which is not observed experimentally. The SW-Xα calculation for this particular experimental configuration also predicts this anomalous intensity at normal emission. Our calculations also show that the angle-resolved intensity for this particular experimental configuration is not sensitive to the azimuth in which the electrons are detected. Now with $\underset{\sim}{A}$ at 45° to the surface normal, the 4σ resonance is being excited because there is a component of $\underset{\sim}{A}$ parallel to the molecular axis. With $\underset{\sim}{A}$ in the plane of the crystal surface, this resonance is not being excited. So it is clear that as long as the resonance is not being excited, we can obtain a good fit to the data by using a potential for CO that is calculated by superposing atomic charge densities.

In conclusion we have seen that in some cases the neglect of final state scattering is a good approximation when analysing the angle-resolved photoemission data from adsorbed molecules. However, we have seen that in the vicinity of a resonance it is essential to put multiple scattering effects into the calculation. We have also found that the formalism that MUFPOT uses to model the C and O potentials, (i.e. superposing atomic

charge densities), is inadequate in describing the scattering in the region of the resonance, and better results are obtained by using the more sophisticated SW-Xα potential, (e.g. Davenport (1976), Li and Tong (1978)), which takes into account the bonding between the C and O atoms.

6.3.2. C_2H_2 on Ni(001) and Ni(111)

One of the practical goals of surface science is the understanding of catalytical processes at surfaces. Hence, eventually one would like to have a good understanding of the structural and electronic properties of adsorbed hydrocarbons. In this respect, LEED work has so far concentrated on the adsorption of C_2H_2 on Ni(001), (Casalone et al (1981), C_2H_2 on Pt(111), (Kesmodel et al (1976, 1977, 1978), Lo et al (1977)), and C_2H_4 on Pt(111), (Kesmodel et al (1978)).

Angle resolved photoemission experiments have been performed on the surface systems Ni(001) - c(2 x 2)C_2H_2 and Ni(001) - c(2 x 2)C_2H_4, (Horn et al (1978a)). In these experiments the intensity of electrons emitted normal to the surface is measured as a function of the angle of incidence of the unpolarised HeI radiation. The analysis of the experimental data is based on an analysis of the symmetry properties of the matrix element $M = \langle f|\underline{A}.\underline{p}|i\rangle$. The LEED patterns indicate that at low temperatures both molecules adopt a c(2 x 2) configuration on the Ni(001) surface. Horn et al in their analysis of the experimental data, assume that for both of these adsorbate systems, the molecules are lying flat on the surface with parallel C-C axes. It may then be shown that if the initial state is of A_1 symmetry, then the intensity $I(A_1)$ may be written as:

$$I(A_1) \sim |1 + r_p|^2 \sin^2\alpha \qquad (6.9)$$

where r_p is the p-polarised reflectivity of the substrate and α is the

Figure 6.10: Electron distribution curves for Ni(001) - c(2 x 2)C_2H_2 as a function of angle of photon incidence. (Photocopied from Horn et al (1978)).

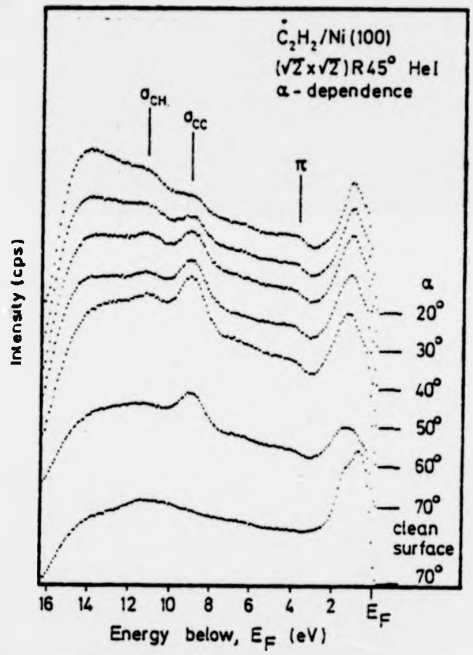

EDC's for the $(\sqrt{2} \times \sqrt{2})R45°$-$C_2H_2$ structure on Ni 100) at 90 K as function of angle of photon incidence. Bottom curve: clean nickel(100) surface at $\alpha = 70°$ and $\theta = 0°$, He I, [110] azimuth.

Figure 6.11: Electron distribution curves for Ni(001) - c(2 x 2)C_2H_4 as a function of angle of photon incidence. (Photocopied from Horn et al (1978)).

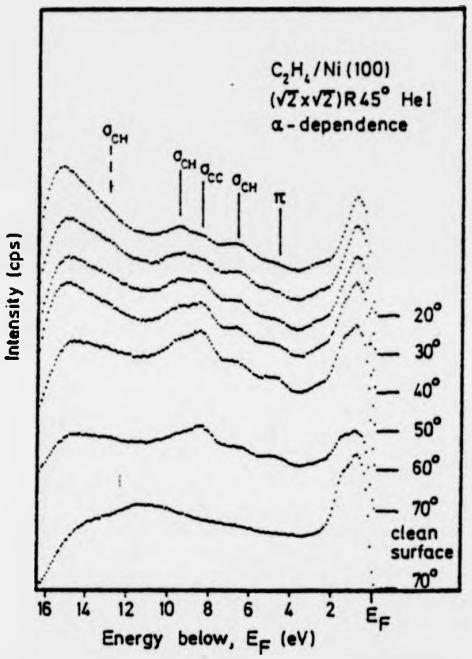

for the $(\sqrt{2} \times \sqrt{2})R45°$-$C_8H_4$ structure on Ni(100) at 80 K as a function of angle of photon incidence. Bottom curve: clean nickel(100) surface at $\alpha = 70°$ and $\theta = 0°$, He I, [110] azimuth.

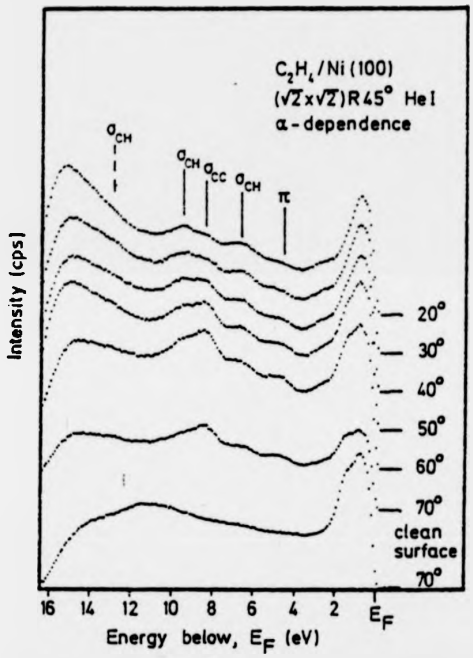

for the $(\sqrt{2} \times \sqrt{2})R45°$-$C_2H_4$ structure on Ni(100) at 80 K as a function of angle of photon incidence. Bottom curve: clean nickel(100) surface at $\alpha = 70°$ and $\theta = 0°$. He I, [110] azimuth.

Figure 6.12: Calculations for the data presented in fig. (6.10) for Ni(001) - c(2 x 2)C_2H_2. Alpha is the angle of photon incidence.

Full curves: C_2H_2 lying flat in surface plane

Dashed curves: C_2H_2 standing up on surface

(a) 1π level

(b) 3σ level

(c) 2σ level

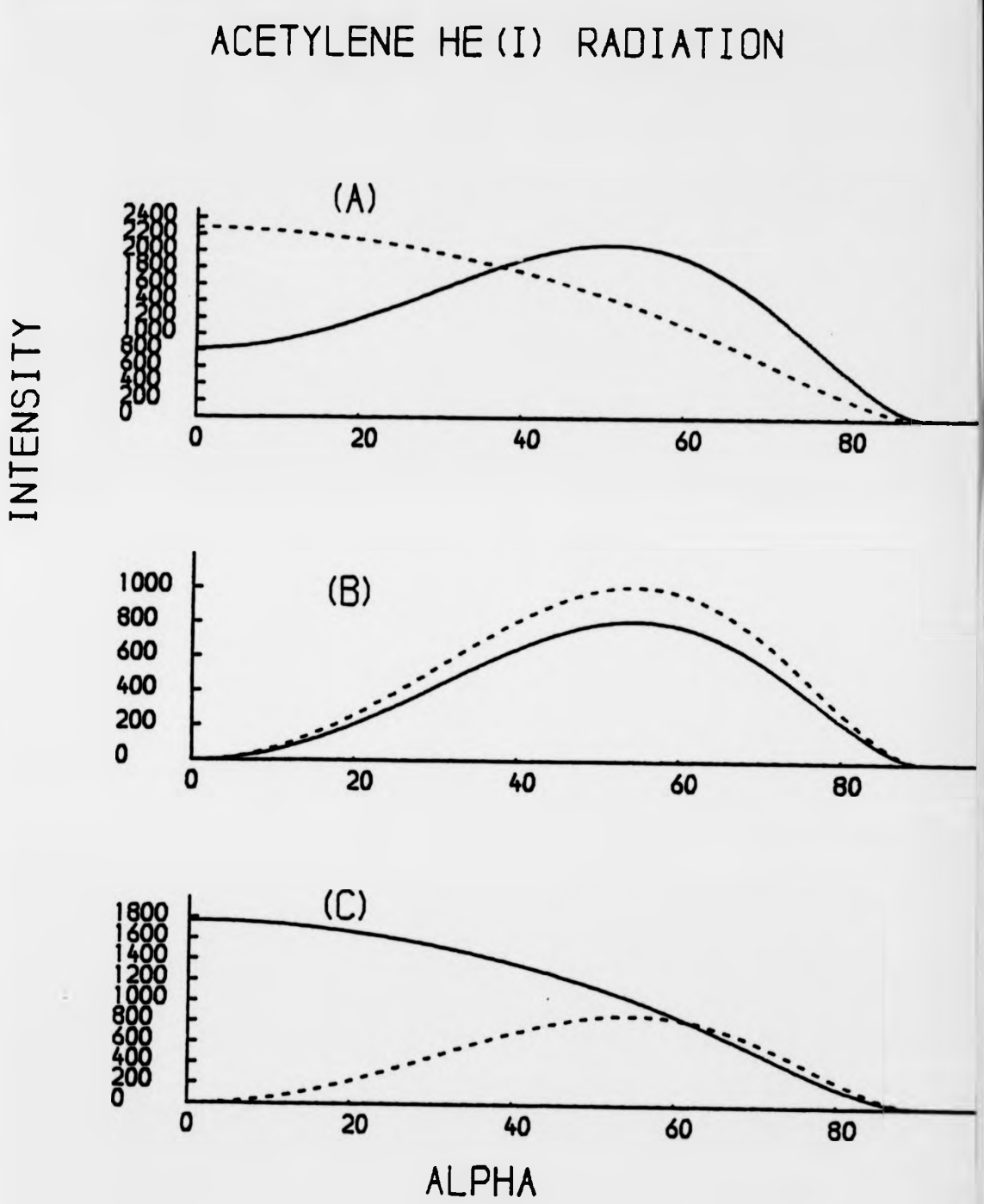
ACETYLENE HE(I) RADIATION
INTENSITY
(A)
2400
2200
2000
1800
1600
1400
1200
1000
800
600
400
200
0
0
20
40
60
80
(B)
1000
800
600
400
200
0
0
20
40
60
80
(C)
1800
1600
1400
1200
1000
800
600
400
200
0
0
20
40
60
80
ALPHA

angle of incidence of the radiation. For initial states of B_1 and B_2 symmetry, then the intensity $I(B_1,B_2)$ may be written as:

$$I(B_1,B_2) \sim |1 - r_p|^2 \cos^2\alpha + |1 + r_s|^2 \qquad (6.10)$$

where r_s is the s-polarised reflectivity of the substrate. In particular, for $|i>$ having A_1 symmetry, no emission is expected at normal exit angle which is not the case if $|i>$ is of B_1 or B_2 symmetry.

The experimental data for both surface systems are shown in fig. (6.10) and (6.11), in the form of EDC's taken at different values of α. We first concentrate on the analysis of the acetylene data. By comparison with the gas phase spectra of acetylene, the peaks at 3.9 eV, 9.0 eV and 11.3 eV below the Fermi level have been respectively correlated with the $1\pi_u$, $3\sigma_g$ and $2\sigma_u$ orbitals of the free molecule.

In our calculations we neglect the effects of multiple scattering. The potentials for the C and H atoms are computed using the formalism described in section (2.4) with each type of atom being put ont a simple cubic lattice with a lattice parameter of twice the covalent radius. For both atoms, α is set equal to 0.75. The co-ordinates of the C and H atoms and the wavefunctions of the initial state orbitals are taken from a SCF Hartree-Fock LCAO calculation, (Palke and Lipscomb (1966)). The overall shapes of the curves are found to be quite insensitive to the azimuth of the incident radiation and so we arbitrarily set $\phi = 0^\circ$. In fig. (6.12) we present calculations for C_2H_2 lying flat on the surface and for C_2H_2 standing perpendicular to the surface. Our analysis favours the lying down geometry which may be clearly seen by comparing the α dependence of the emission from the $2\sigma_u$ level for the two different geometries.

We not turn to the analysis of data taken for C_2H_2 adsorbed on Ni(111) where the angle of incidence is kept constant and the detector angle is varied, (Johnson (1980)). In this set of experiments the radiation, which comes from a HeI source is unpolarised and incident on the surface at 50°

Figure 6.13: Variation of the intensity with detector angle for C_2H_2 adsorbed on Ni(111), angle of incidence = 50°, $h\omega$ = 21.2 eV.

(a) Experimental Data

Full line: $2\sigma_u$ level

Dashed line: $3\sigma_g$ level

(b) Calculation for the $2\sigma_u$ level assuming a standing-up geometry for the C_2H_2 molecule.

(c) Calculations for the $2\sigma_u$ level for the lying-down geometry for the C_2H_2 molecule.

Upper full curve: Detector plane parallel to the $[11\bar{2}]$ azimuth.

Dashed curve: $[01\bar{1}]$ azimuth

Lower full curve: $[\sqrt{3}+3, \sqrt{3}-3, -2\sqrt{3}]$ azimuth

(d) Calculation for the $3\sigma_g$ level assuming a standing up geometry for the molecule.

(e) Calculation for the $3\sigma_g$ level for the lying-down geometry.

$[11\bar{2}]$ azimuth

$[01\bar{1}]$ azimuth

$[\sqrt{3}+3, \sqrt{3}-3, -2\sqrt{3}]$ azimuth

$[1\bar{1}0]$ azimuth

a

ACETYLENE HE(I)
EXPERIMENTAL DATA
ANGLE OF INCIDENCE = 50 DEGREES

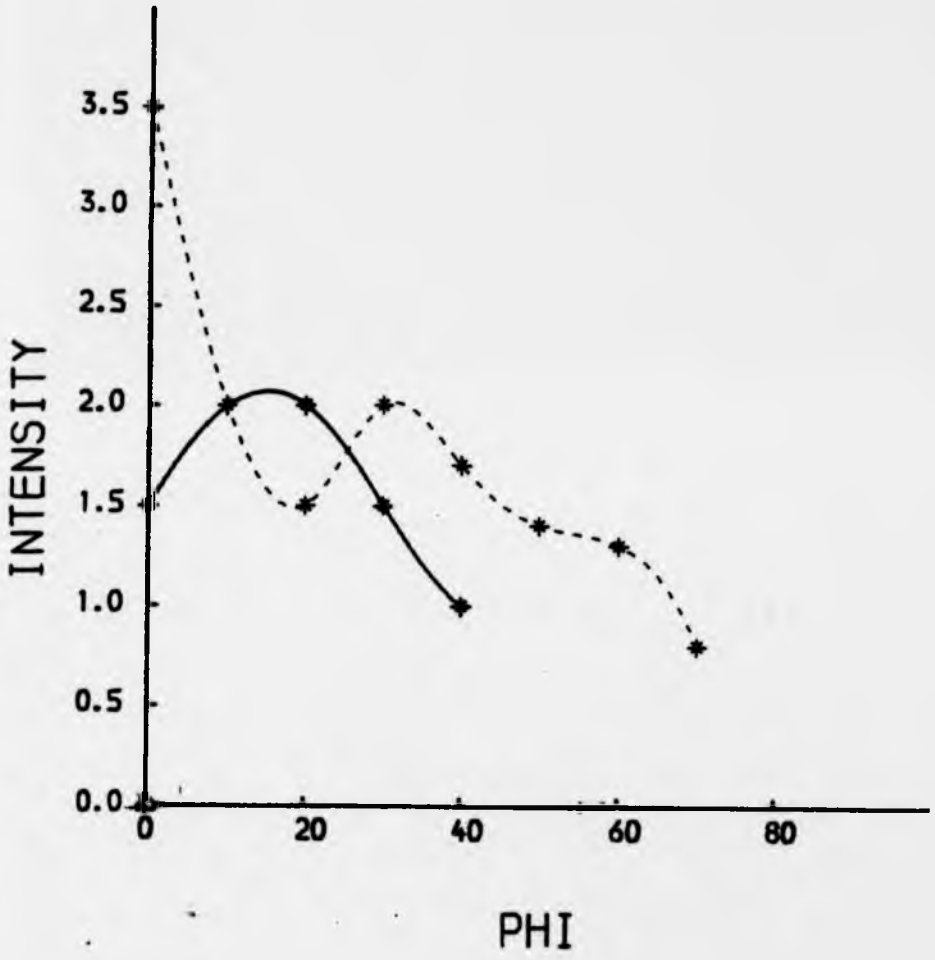

b

ACETYLENE
2-SIGMA LEVEL
VERTICAL CONFIGURATION

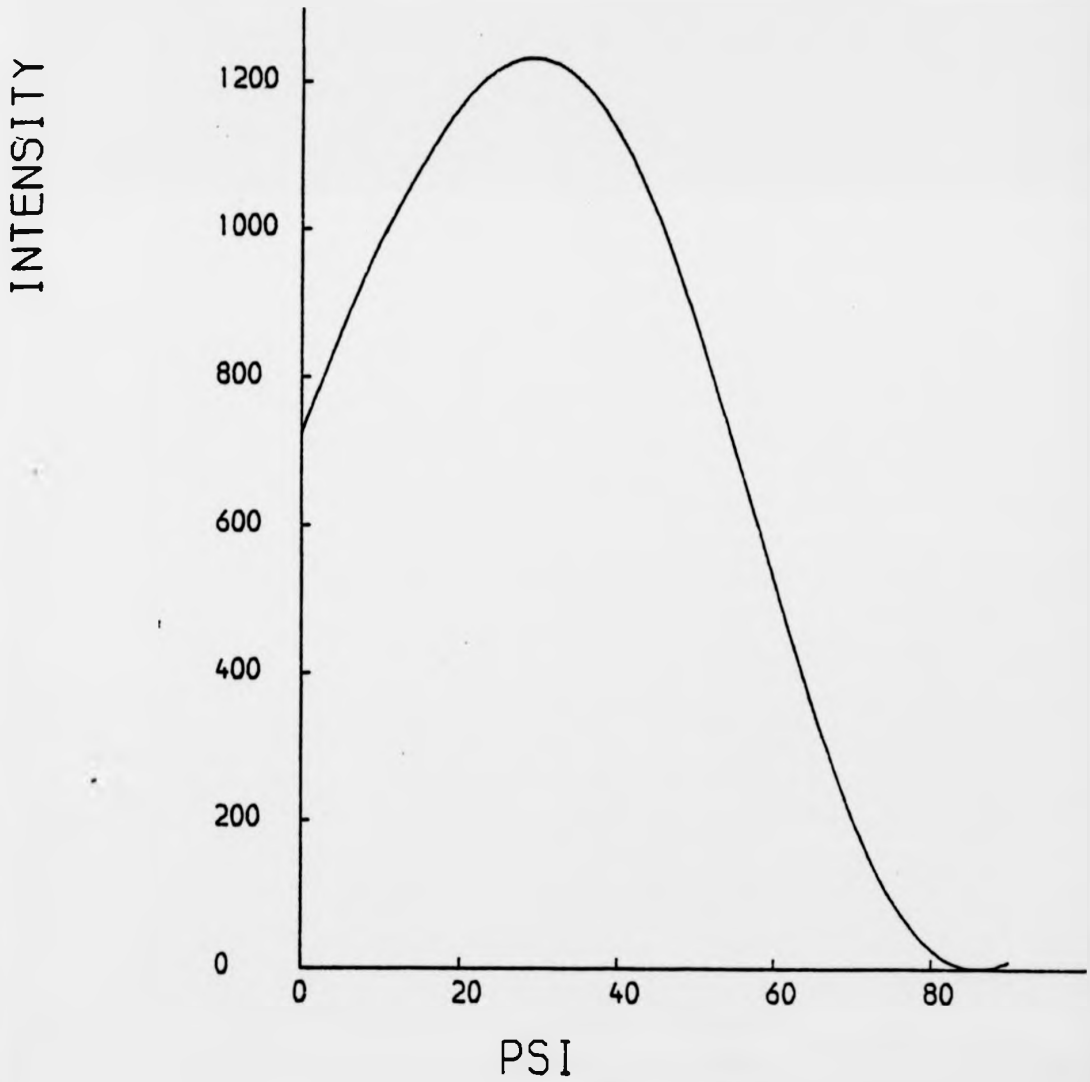

c

ACETYLENE
2-SIGMA LEVEL
HORIZONTAL CONFIGURATION

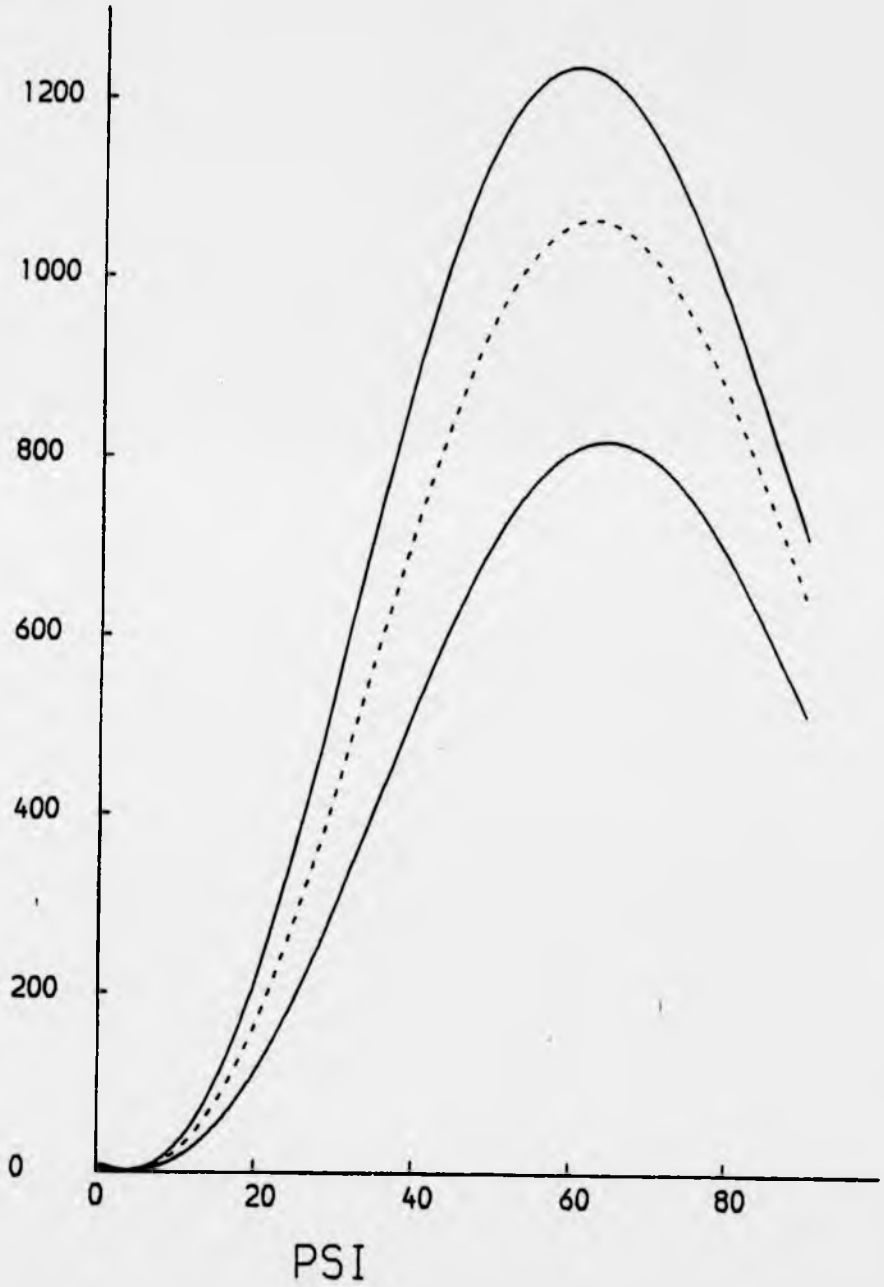

d

ACETYLENE
3-SIGMA LEVEL
VERTICAL CONFIGURATION

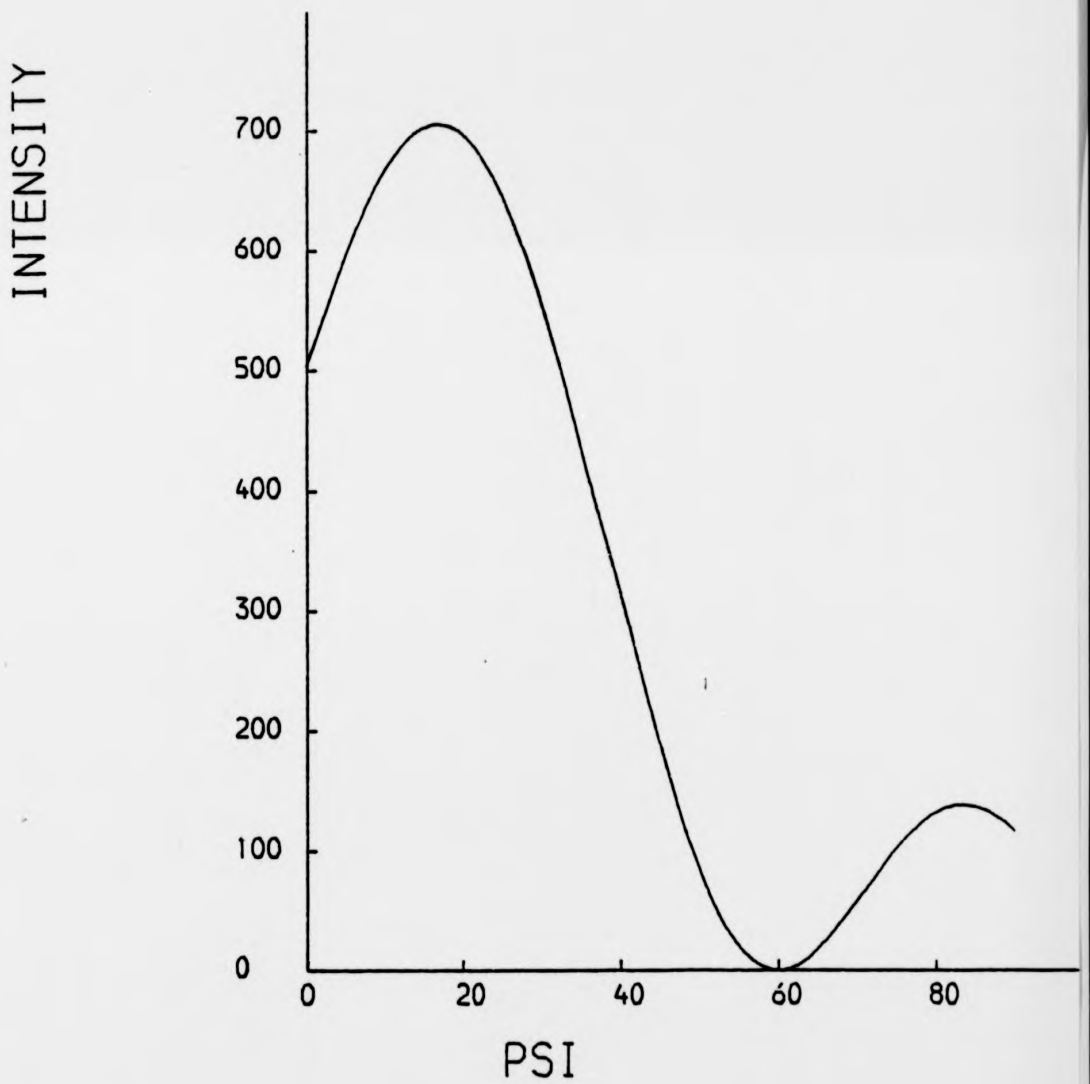

e

ACETYLENE
3-SIGMA LEVEL
HORIZONTAL CONFIGURATION

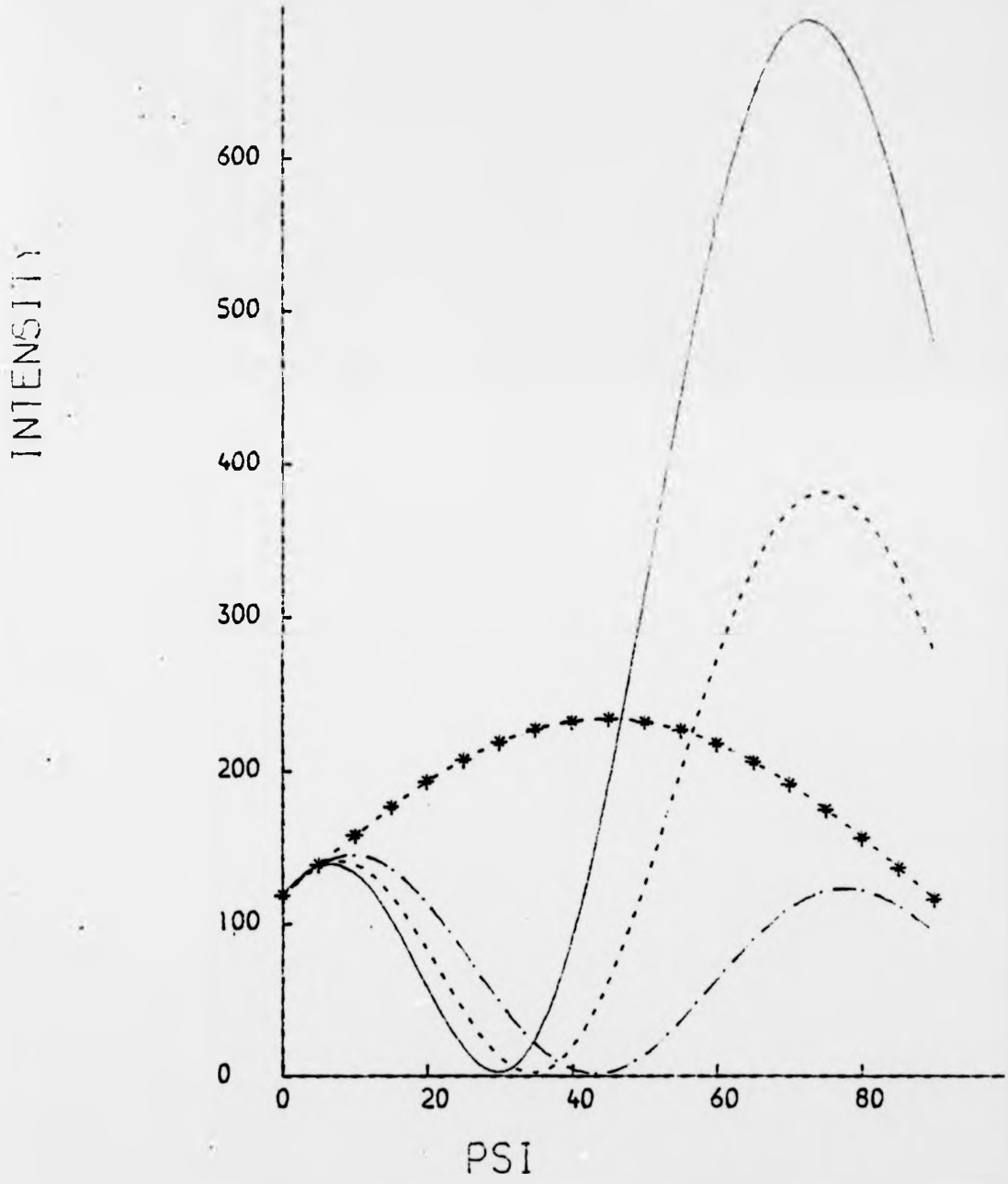

to the surface normal. The HeI source and detector are coplanar and on opposite sides of the surface normal. The data for the 1π level is found not to exhibit off-normal emission. The analyser is positioned along the $[\bar{1}\bar{1}2]$ azimuth on the Ni(111) surface. We again perform calculations for C_2H_2 standing upright and also for the lying-down geometry. For the lying-down geometry, calculations are separately performed for C_2H_2 lying parallel to the $[11\bar{2}]$, $[01\bar{1}]$ and $[1\bar{1}0]$ azimuths. The comparison between theory and experiment for the $2\sigma_u$ and $3\sigma_g$ orbitals are shown in fig. (6.13). For the $2\sigma_u$ orbital, best agreement is obtained for C_2H_2 standing perpendicular to the Ni(111) surface. Even so there is still a 15° discrepancy between the theoretical and experimental peak positions. For the emission from the $3\sigma_g$ level, none of the calculations is in good agreement with experiment. Whilst in the experiment there is a peak at normal exit angle, none of the calculations produce such a peak. There are various possibilities as to why we are obtaining a poor fit to the data: (i) we should be including the crystal inner potential into the calculation, (ii) the effect of multiple scattering should be taken into account and (iii) in the vertical configuration, the possibility of acetylene existing as ethylidene, (Kesmodel et al (1978)) may result in wavefunctions for the molecular orbitals that are significantly different to that for C_2H_2. The inclusion of an inner potential is not going to produce the peak at normal exit angle for the $3\sigma_g$ level. Possibility (ii) is more difficult to explore because of the difficulty in obtaining an adequate potential for C_2H_2 with the MUFFPOT programs. The third possibility requires a molecular orbital calculation for the $\rightarrow C\text{-}CH_3$ complex.

6.3.3. C_2H_4 on Ni(001)

We now turn to an analysis of the data of Horn et al (1978) for the normal emission from the orbitals of C_2H_4 adsorbed on Ni(001). As for C_2H_2, the intensity is measured as a function of the angle of incidence

Figure 6.14: Calculations for the data presented in fig. (6.11).

———— lying-down geometry

– – – – – – standing-up geometry

(a) $1b_{2u}$ level

(b) $1b_{1u}$ level

(c) $3a_g$ level

(d) $1b_{1g}$ level

α is the angle of photon incidence

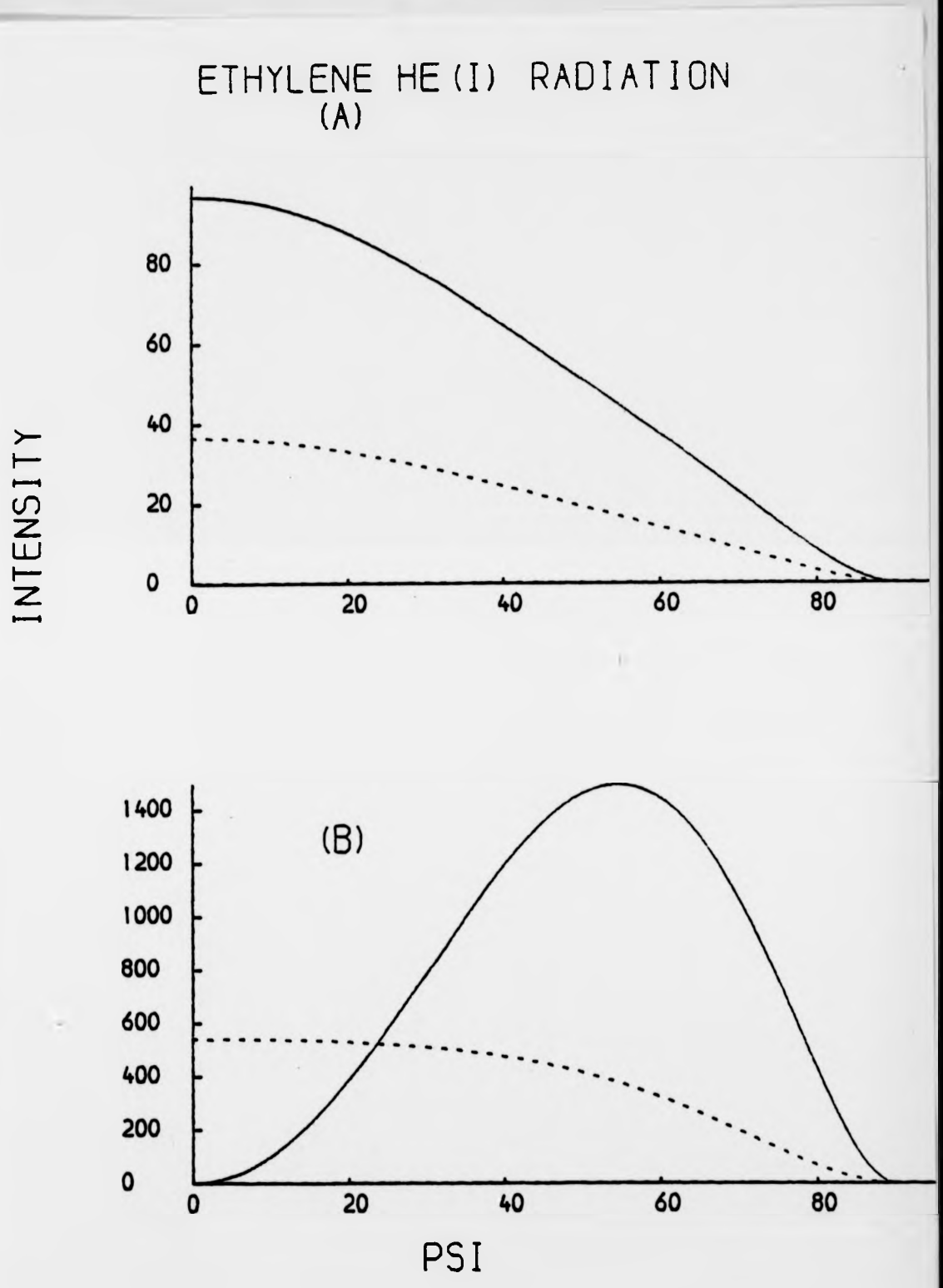
ETHYLENE HE(I) RADIATION
(A)
INTENSITY
80
60
40
20
0
0
20
40
60
80
(B)
1400
1200
1000
800
600
400
200
0
0
20
40
60
80
PSI

ETHYLENE HE(I) RADIATION

(C)

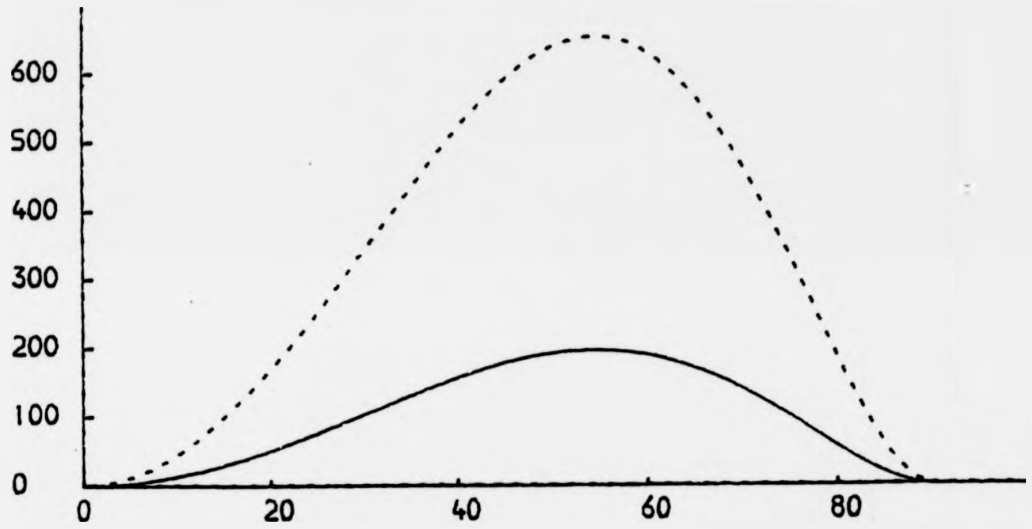

(D)

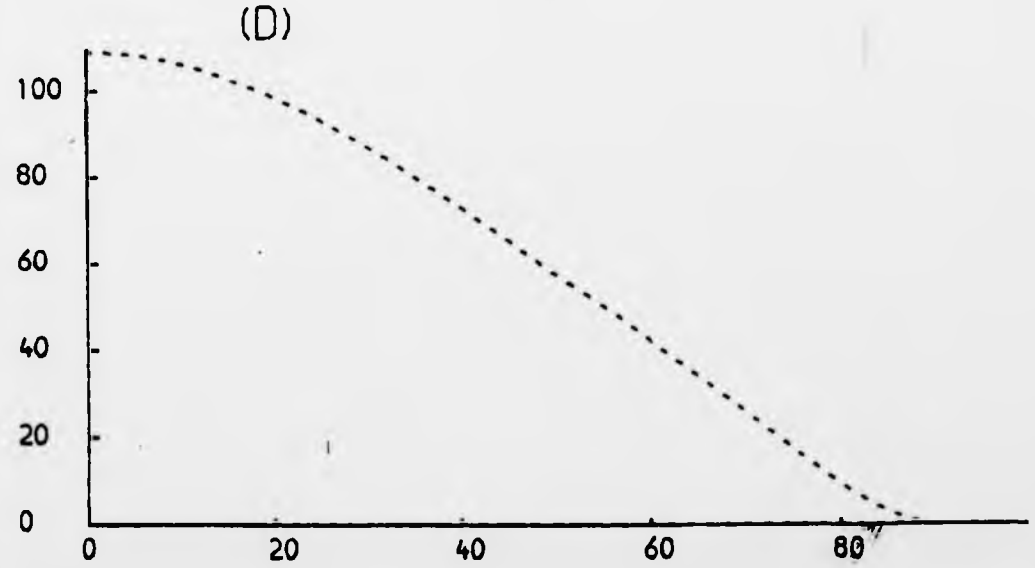

α. The LEED patterns for this system show that the C_2H_4 molecules adopt a c(2 x 2) configuration on the Ni(001) surface. The data that Horn et al obtain for this system is shown in fig.(6.11). The peaks at 4.7 eV, 6.6 eV, 8.3 eV and 9.3 eV below E_F have been respectively correlated with the $1b_{1u}$, $1b_{1g}$, $3a_g$, and $1b_{2u}$ levels of the free molecule. Horn et al, using an analysis based on equations (6.9) and (6.10) have found that with the exception of the emission from the $1b_{1g}$ level, the dependence of the peak intensities on α can be best explained by assuming that C_2H_4 lies flat on the Ni(001) surface with parallel C = C axes. In theory for this particular molecular configuration there should be no emission from the $1b_{1g}$ level at normal exit angle. The fact that such emission is detected contradicts the postulated structure for the C_2H_4 molecules. Horn et al suggest that this discrepancy could be due to twisting of the C_2H_4 molecule about the C = C axis, resulting in molecular orbitals that have a different symmetry to those of the untwisted molecule. Felter and Weinberger (1981) from electronic structure calculations have suggested that C_2H_4 may be twisted when adsorbed on Ni(111).

In our calculations, the potentials that we use, for the C and H atoms are the same as those used in the analysis of Horn et al's data for Ni(001) - c(2 x 2)C_2H_2. The wavefunction of the molecular orbitals and the co-ordinates of the C and H atoms are taken from a Hartree-Fock Self Consistent Field LCAO calculation, (Palke and Lipscombe (1966)), for the free molecule. The azimuth is arbitrarily set to be along the $\phi = 0^\circ$ direction: altering the azimuthal angle does not significantly effect the calculated curve. We perform calculations for C_2H_4 lying down falt on the surface and also for C_2H_4 standing perpendicular to the surface plane. The results of our calculations are shown in fig.(6.14). For the lying-down configuration we obtain the same discrepancy that is found by Horn et al for the emission from the $1b_{1g}$ level. However, the

Figure 6.15: Calculation for the variation of intensity with detector angle (ψ) for oriented C_2H_4, $h\omega$ = 21.2 eV, angle of incidence = 50°.

Full lines: lying-down geometry

Dashed lines: standing-up geometry

(a) $1b_{2u}$ level

(b) $1b_{1u}$ level

(c) $1b_{1g}$ level

(d) $3a_g$ level.

Figure 6.15: Calculation for the variation of intensity with detector angle (ψ) for oriented C_2H_4, $h\omega$ = 21.2 eV, angle of incidence = 50°.

Full lines: lying-down geometry

Dashed lines: standing-up geometry

(a) $1b_{2u}$ level

(b) $1b_{1u}$ level

(c) $1b_{1g}$ level

(d) $3a_g$ level.

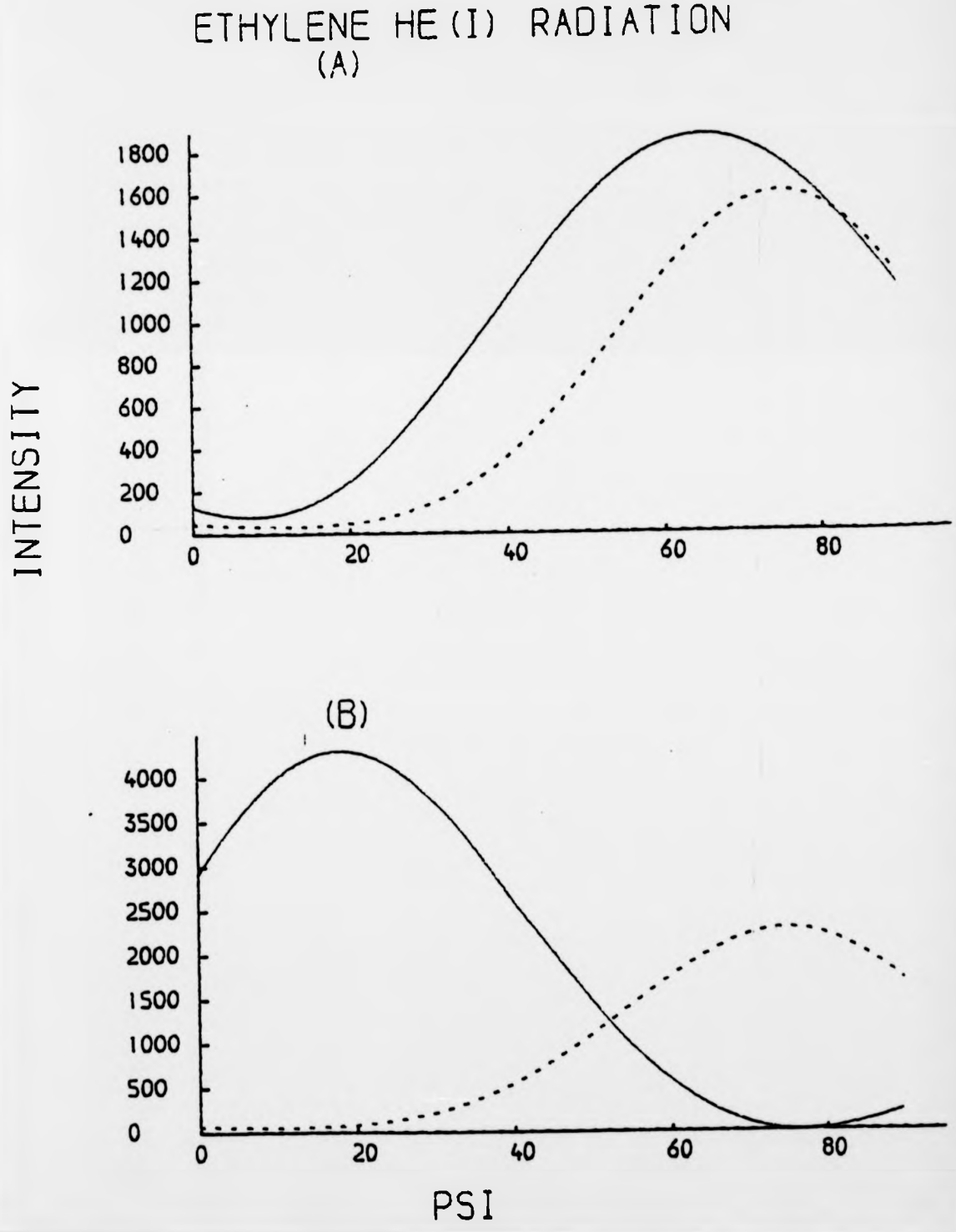
ETHYLENE HE(I) RADIATION
(A)
INTENSITY
1800
1600
1400
1200
1000
800
600
400
200
0
0
20
40
60
80
(B)
4000
3500
3000
2500
2000
1500
1000
500
0
0
20
40
60
80
PSI

ETHYLENE HE(I) RADIATION

(C)

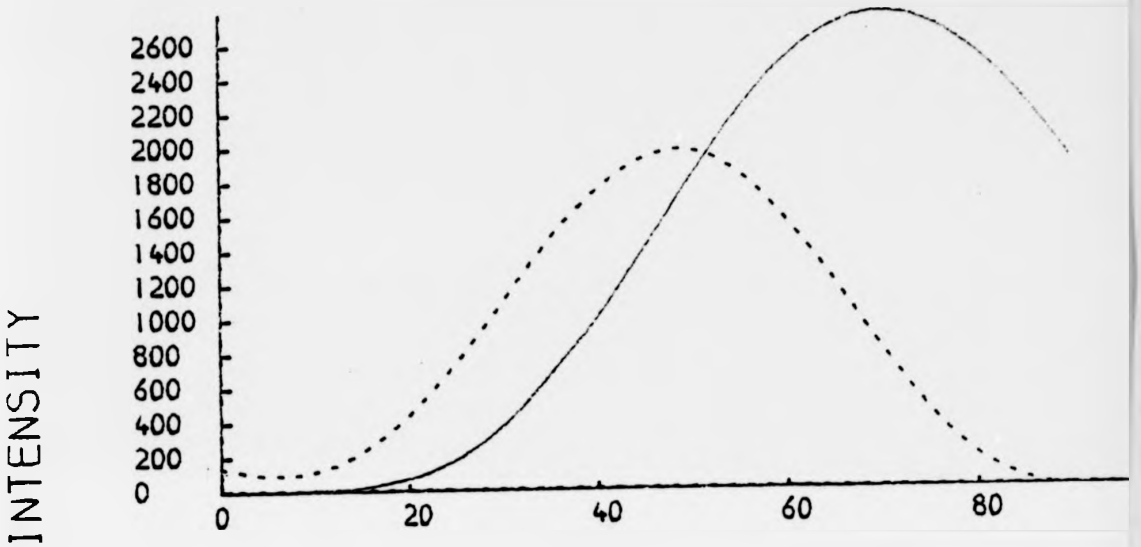

(D)

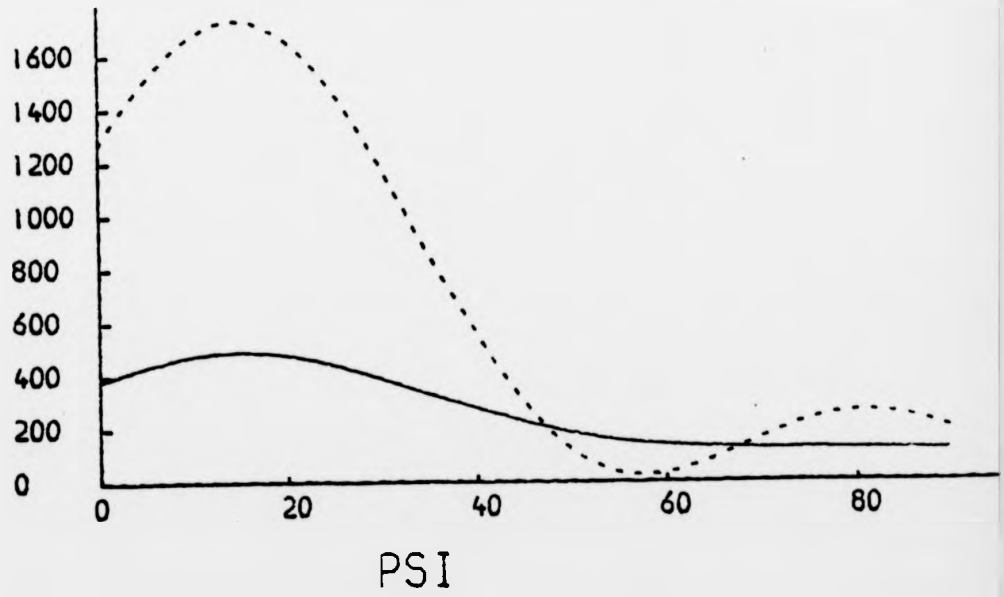

calculations for C_2H_4 standing vertically on the surface give good agreement between theory and experiment for the emission from the $1b_{1g}$ level; the agreement is now poor for the emission from the $1b_{1u}$ (π) level. Thus there is no reason to prefer either model for the orientation of the molecule on the surface. Experiments on adsorbed C_2H_4 where the angle of incidence is kept constant and the detector angle is varied have not yet been performed. We present, in fig. (6.15) calculations for the emission from the $1b_{2u}$, $3a_g$, $1b_{1g}$, and $1b_{1u}(\pi)$ levels where the detector angle is varied and the angle of incident is kept fixed at 45° to the surface normal. The photon energy is set equal to 21.2 eV (i.e. the energy of HeI radiation), and the detector and light source are in the same plane but on opposite sides of the surface normal. The calculations for the $3a_g$ and $1b_{2u}$ levels are insensitive to whether the ethylene is standing straight up or lying flat on the surface. For the $1b_{1g}$ and $1b_{1u}(\pi)$ levels however, there is considerable sensitivity of the angle-resolved intensity to the orientation of the molecule. If multiple scattering is unimportant, then by studying the detector angle dependence of the emission from these levels it should be possible to distinguish between these two geometries.

6.4. Summary

For the case of CO 4σ emission from Ni(001) - c(2 x 2)CO and Ni(111) - p(2 x 2)CO we have found that it is usually necessary to incorporate multiple scattering effects into the calculation of the detector angle dependence of the intensity. It is particularly important to include such effects when one is close to a resonance. It is clear from a comparison of our calculations and those of Davenport (1976), that the Mattheis prescription of superposing atomic charge densities is inadequate in the description of the emission and scattering properties

of the CO molecule.

For the case of emission from c(2 x 2)C_2H_2 adsorbed on Ni(001) the calculations that neglect scattering in the final state are adequate in describing the normal emission data taken with variable angle of incidence, (Horn et al (1978)). However, for the data taken for this system where the detector angle is being varied, (Johnson (1980)), these calculations are in poor agreement with the experimental data. This disagreement may be arising from the neglect of multiple scattering in the final state. Another possibility is the formation of ethylidene (Kesmodel et al (1978)) on the Ni(111) surface, and the wavefunctions for the molecular orbitals of this complex may differ significantly from those of acetylene.

For the case of c(2 x 2)C_2H_4 adsorbed on Ni(001) we find that the normal emission data taken with variable angle of incidence can be equally well described whether we consider the ethylene molecule to stand straight up or lie down flat on the surface. We have shown with model calculations that neglect multiple scattering that by studying the dependence of the angle-resolved intensity on the detector angle for emission from the $1b_{1u}(\pi)$ and $1b_{1g}$ levels, it should be then possible to distinguish between the two possible orientations of the ethylene molecule.

Thus there will be occasions when multiple scattering has to be included when calculating the angle-resolved photoemission intensity from the valence states of adsorbed molecules. In the construction of the molecular potential that describes the emission and scattering properties of the molecule, it is essential to model realistically the distribution of electronic charge between the constituent atoms of the molecule. It is thus preferable to use the SW-Xα method for this purpose, rather than using the Mattheis prescription of superposing atomic charge densities.

REFERENCES FOR CHAPTER 6

Allyn, C. L., Gustafsson, T. and Plummer, E. W., Chem. Phys. Lett. 47, 127 (1977a).

Allyn, C. L., Gustafsson, T. and Plummer, E. W., Solid State Comm. 24, 531 (1977b).

Allyn, C. L., Gustafsson, T. and Plummer, E. W., Solid State Comm. 28, 85 (1978).

Andersson, S. and Pendry, J. B., Surf. Sci. 71, 75 (1978).

Andersson, S. and Pendry, J. B., Phys. Rev. Lett., 43, 363 (1979).

Bandy, B. J., Lloyd, D. R. and Richardson, N. V., Surf. Sci. 89, 344 (1979).

Blyholder, G., J. Vac. Sci. Tech. 11, 865 (1974).

Casalone, G., Cattania, M. G. and Moretta, M. S., Surf. Sci. 103, L121 (1981).

Cashion, J. K. and Eastman, D. E., Phys. Rev. Lett. 27, 1520 (1971).

Coulson, C. A., Valence, (Oxford University Press, Second Edition, 1965).

Davenport, J. W., Phys. Rev. Lett. 36, 945 (1976).

Davenport, J. W., J. Vac. Sci. Tech. 15, 433 (1978).

Dehmer, J. L. and Dill, D., Phys. Rev. Lett. 35, 213 (1975).

Dill, D. and Dehmer, J. L., J. Chem. Phys. 61, 692 (1974).

Felter, T. C. and Weinberger, W. H., Surf. Sci. 103, 265 (1978).

Gadzuk, J. W., Phys. Rev. B12, 5608 (1975).

Gustafsson, J. and Plummer, E. W. in Photoemission and the Electronic Properties of Surfaces, (Wiley, New York, 1978).

Gustafsson, J., Surf. Sci. 94, 593 (1980).

Horn, K., Bradshaw, A. M. and Jacobi, K., Surf. Sci. 72, 719 (1978a).

Horn, K., Bradshaw, A. M. and Jacobi, K., J. Vac. Sci. Tech. 15, 575 (1978b).

Jacobi, K., Scheffler, M., Kambe, K. and Forstmann, F., Solid State Comm. 22, 17 (1977).

Johnson, P. D., (1980), private communication.

Kanski, J., Ilver, L. and Nilsson, P. O., Solid State Comm. 26, 339 (1978).

Kesmodel, L. L., Dubois, L. H. and Somerjai, G. A., Chem. Phys. Lett. 56, 267 (1978).

Lapeyre, G. P., Andersson, J. and Smith, R. J., Phys. Rev. Lett, 37, 108 (1976).

Li, C. H. and Tong, S. Y., Phys. Rev. Lett. 40, 46 (1978).

Lloyd, D. R., Quinn, C. M. and Richardson, N. V., Solid State Comm. 23, 141 (1977).

Messiah, A. Quantum Mechanics, Vol. I (North Holland, Amsterdam, 1961).

Nyberg, G. L., Surf. Sci. 95, L273 (1980).

Nyberg, G. L. and Richardson, N. V., Surf. Sci. 85, 335 (1979).

Palke, W. E. and Lipscombe, W. N., J. Am. Chem. Soc. 88, 2384 (1966).

Passier, M., Ignatiev, A., Jona, F., Jepsen, D. W. and Marcus, P. M., Phys. Rev. Lett. 43, 360 (1979).

Pople, J. A. and Beveridge, D. L., Approximate Molecular Orbital Theory, (McGraw Hill, New York, 1970).

Scheffler, M., Kambe, K. and Forstmann, F., Solid State Comm. 23, 789 (1977).

Schwartz, K., Phys. Rev. B5, 2466 (1972).

Shirley, D. A., Stöhr, J., Wehner, P., Williams, R. S., and Apai, G., Surf. Sci. 97, 377 (1980).

Slater, J. C. and Johnson, K. H., Phys. Rev. B5, 844 (1972).

Smith, R. J., Anderson, J. and Lapeyre, G. J., Phys. Rev. Lett. 37, 1081 (1976).

Umbach, E., Schuhl, A. and Menzel, D., Solid State Comm. 36, 93 (1980).

Weeks, S. P. and Plummer, E. W., Solid State Comm. 21, 695 (1977).

Whitaker, M. A. B., J. Phys. C11, L151 (1978).

Williams, P. M., Butcher, P., Woods, S. and Jacobi, K., Phys. Rev. B14, 3215 (1976).

CHAPTER 7

CONCLUSIONS

We have found that for some photon energies, core-state photoelectron diffraction using the azimuthal mode has the potential to determine surface structure to a considerable accuracy. For other energies there is little sensitivity of the diffraction patterns to changes in structure, but by using a synchrotron this difficulty may be overcome. Sensitivity to non-structural parameters also occurs in certain cases and so one has to know these parameters to a considerable accuracy in order to make a determination of the structure.

We have then proceeded to analyse photoelectron diffraction data for Te4d emission from p(2 x 2)Te and c(2 x 2)Te adsorbed on Ni(001) and also for I4d emission from $(\sqrt{3} \times \sqrt{3})R30^{\circ}$I on Ag(111). For Ag(111) - $(\sqrt{3} \times \sqrt{3})R30^{\circ}$I quite good agreement has been obtained between theory and experiment by using the structure determined by LEED and SEXAFS. Whilst there is considerable sensitivity of the diffraction patterns to changes in the bonding site, the sensitivity to $d_{\perp}$ is not so great. For Ni(001) - c(2 x 2)Te and Ni(001) - p(2 x 2)Te by transferring all the structural and non-structural parameters from the LEED calculation, poor agreement with experiment is obtained. This discrepancy is not resolved by varying the structure.

We have then looked at data taken with the CIS mode for the normal emission from the 4d levels of c(2 x 2)Te adsorbed on Ni(001) where the disagreement between theory and experiment has led to the suggestion that the theoretical formalism that is being used is deficient (McGovern et al (1979)). We have shown that the discrepancy has arisen because the Te potential had been calculated using the energy independent Slater exchange potential which is inappropriate to use when describing the scattering of electrons by atoms. The discrepancy is resolved by replacing the Slater

exchange term in the calculation of the Te potential by the Hartree-Fock exchange potential for a free electron gas premultiplied by an α parameter, (known also as "Hara" or "Dirac" exchange). By using this new potential for Te in the analysis of the data for Ni(001) - p(2 x 2)Te and Ni(001) - c(2 x 2)Te taken with the azimuthal model improved agreement between theory and experiment is obtained for some of the data. Disagreement with experiment still remains for some energies and we have suggested that such disagreement may be due to disorder of the Te atoms on the Ni(001) surface.

We have then investigated whether the Lee and Beni potential, which takes into account screened exchange and correlation effects, is an improvement over the Hara potential in the description of electron scattering off atoms. To do this we have calculated electron-atom total and differential scattering cross-section for Ar, Kr and Xe using four different model potentials: (i) Xα(α = 0.7), (ii) Xα(α = 0.4), (iii) Hara and (iv) Lee and Beni. These calculations have been compared with the experimental data. In the calculations of the total cross-sections only the Hara and Xα(α = 0.4) potentials give good agreement with experiment, as is also the case for the differential cross-sections at low energies ($\lesssim$ 60 eV). We suggest that the Lee and Beni potential works badly because of a breakdown of the Local Density Approximation (LDA) in the calculation of atomic potentials. It is also suggested that the Hara and Xα(α = 0.4) potentials work well within the LDA only because of a fortuitous cancellation of errors.

Then, angle-resolved photoemission from adsorbed molecules is looked at with a view to ascertain the effects of multiple scattering on the angle-resolved intensity. We have found that by modelling the CO potential using the Mattheis prescription (i.e. superposing atomic charge densities), poor agreement is obtained between theory and experiment for adsorbed CO

when we put scattering into the calculation. Calculations that use more realistic potentials (Davenport (1976)) but which neglect substrate scattering are in better agreement with experiment that our calculations and so we conclude that, particularly near to a resonance, it is important to incorporate bonding effects when constructing the molecular potential. We have then calculated the angle-resolved intensity for adsorbed acetylene and ethylene where scattering in the final state has been neglected. For the acetylene data taken with variable angle of incidence good agreement with experiment has been obtained by assuming a lying-down geometry in agreement with the findings of Horn et al (1978). The analysis of the data taken with variable detector angle is inconclusive: poor agreement with experiment is obtained whether one assumes a lying-down or standing-up geometry for the acetylene. We suggest that one possible reason for this disagreement is the neglect of scattering in the final state. The analysis of the data for Ni(001) - c(2 x 2)C_2H_4 taken with variable angle of incidence is inconclusive as regards the orientation of the molecule on the surface.

Further investigation clearly needs to be carried out into the construction of atomic potentials for use in photoelectron diffraction calculations. Whilst it is clear from our findings in Chapter 5 that the Hara potential is a good model to use in photoelectron diffraction work, it is still important to investigate whether, by dispensing with the LDA in the calculation of the atomic potential one can obtain better agreement with experiment when analysing photoelectron diffraction data. The inadequacy of Slater exchange in the description of electron-atom scattering at low energies is also of relevance to XANES where electron energies $\leq$ 60 eV are commonly used. It is essential that a thorough investigation be made into the sensitivity of XANES calculations to

different model potentials. The same point also applies to LEED whenever electron energies ≤ 100 eV are used.

Thus if core-state photoelectron diffraction is going to be seriously considered as a surface structural technique, then it is essential to use an energy dependent potential in the analysis of the data. The Hara potential appears to be adequate for this purpose, but more calculations for other adsorbate systems need to be carried out in order to properly test the usefulness of this potential. The main advantage of photoelectron diffraction is that it can be used on surfaces where there is no long-range order, (Farrell et al (1980)); this has been seen in the analysis of the photoelectron diffraction data for Ag(111) - (1 x 1)I, (Kang et al (1980)). However, we have seen that in some cases $d_\perp$ is not going to be determined to any greater accuracy than LEED. In any future work on core-state photoelectron diffraction it is essential to take data using both the CIS and azimuthal modes. The analysis of the CIS data would provide a valuable check on the model that is being used for the atomic potentials. It should also be possible to estimate the inner potential from a comparison between the calculated and experimentally found peak positions. Having optimised the input parameters in this way one can then turn to an analysis of the data taken with the azimuthal mode, and hopefully then determine the structure.

As regards the work on oriented molecules it is clear that one should be using the SWXα method to model the molecular potential. This has already been done in calculations for adsorbed CO (Davenport (1976), Li and Tong (1978)) and N_2 (Umbach et al (1980)). It would be of interest to calculate the potential for C_2H_2 using this method, and this potential should then be used in the analysis of angle-resolved photoemission data taken for C_2H_2 adsorbed on Ni(111) where the detector angle is varied. It would be of interest to see whether the inclusion of multiple scattering into the calculation leads to better agreement between theory and experiment than

those calculations that leave out this effect.

Thus, the approach of determining the orientation of adsorbed molecules by using arguments based on the symmetry of the initial state will breakdown whenever multiple scattering effects are important, and so it is preferable to use calculations that incorporate full multiple scattering in the analysis of the data.

REFERENCES FOR CHAPTER 7

Davenport, J. W., Phys. Rev. Lett., 36, 945 (1976).

Horn, K., Bradshaw, A. M. and Jacobi, K., J. Vac. Sci. Tech. 15, 575 (1978).

Li. C. H. and Tong, S. Y., Phys. Rev. Lett, 40, 46 (1978).

McGovern, I. T., Eberhardt, W. and Plummer. E. W., Solid State Comm. 32, 963 (1979).

Umbach, E., Schuhl, A. and Menzel, D., Solid State Comm. 36, 93 (1980).

Appendix 1 - Evaluation of $\langle \varepsilon \ell' m' | \underset{\sim}{\varepsilon}.\underset{\sim}{p} | n\ell m \rangle$

Let $M = \langle \varepsilon \ell' m' | \underset{\sim}{\varepsilon}.\underset{\sim}{p} | n\ell m \rangle$. Without loss of generality let $\underset{\sim}{p}$ be directed along the z-direction of a cartesian co-ordinate system, so that $\underset{\sim}{\varepsilon}.\underset{\sim}{p} = p_z$, (remembering that $\underset{\sim}{\varepsilon}$ is a unit vector). Thus:

$$M = \langle \varepsilon \ell' m' | p_z | n\ell m \rangle$$

$$= \langle n\ell m | p_z | \varepsilon \ell' m' \rangle^*$$

$$= i\hbar \langle n\ell m | \frac{\partial}{\partial z} | \varepsilon \ell' m' \rangle \qquad \text{(A.1.1)}$$

Converting to spherical polars we may write:

$$\frac{\partial}{\partial z} = u \frac{\partial}{\partial r} + \frac{(1-u^2)}{r} \frac{\partial}{\partial u} \text{ , where } u = \cos\theta \text{ .} \qquad \text{(A.1.2)}$$

$$\text{Let } |n\ell m\rangle = U_{n\ell}(r)\ Y_{\ell m}(\theta,\phi) \qquad \text{(A.1.3)}$$

$$\text{and} \qquad |\varepsilon \ell' m'\rangle = R_{\ell'}(r)\ Y_{\ell' m'}(\theta,\phi) \qquad \text{(A.1.4)}$$

Now the matrix element M is independent of quantum number m, (see Landau and Lifschitz (1959)). Thus, without loss of generality, we may put $m = m' = 0$.

From equations (A.1.1) to (A.1.4) we may write for M:

$$M = \frac{i\hbar(2\ell+1)^{\frac{1}{2}}(2\ell'+1)^{\frac{1}{2}}}{4\pi} \int_{\Omega} U_{n\ell}(r) P_{\ell}(\cos\theta) \left[u \frac{\partial}{\partial r} + \frac{(1-u^2)}{r} \frac{\partial}{\partial u} \right]$$

$$\times R_{\ell'}(r)\ P_{\ell'}(\cos\theta) d\Omega \qquad \text{(A.1.5)}$$

where the relation

$$Y_{\ell}^{0}(\theta,\phi) = \left(\frac{2\ell+1}{4\pi}\right)^{\frac{1}{2}} P_{\ell}(\cos\theta) \qquad \text{(A.1.6)}$$

has been used.

By using orthogonality and recurrence relations for the Legendre polynomials, it may be shown that:

$$M = \frac{i\hbar(\ell+1)}{(2\ell+1)^{\frac{1}{2}}(2\ell+3)^{\frac{1}{2}}}\left[\int_0^\infty \{U_{n\ell}(r) + ((\ell+2)U_{n\ell}(r)\frac{1}{r}R_{\ell'}(r))\}r^2dr\right] \quad \text{for } \ell' = \ell+1 \tag{A.1.7}$$

and

$$M = \frac{i\hbar\ell}{(2\ell-1)^{\frac{1}{2}}(2\ell+1)^{\frac{1}{2}}}\left[\int_0^\infty \{U_{n\ell}(r) - (\ell-1)U_{n\ell}(r)\frac{1}{r}R_{\ell'}(r))\}r^2dr\right] \quad \text{for } \ell' = \ell-1 \tag{A.1.8}$$

Now

$$\left\{U_{n\ell}(r)\left[\frac{\partial}{\partial r}(R_{\ell'}(r))\right]\begin{Bmatrix}+(\ell+2)\\-(\ell-1)\end{Bmatrix}U_{n\ell}(r)\frac{1}{r}R_{\ell'}(r)\right\}r^2$$

$$= U_{n\ell}(r)r\{\frac{\partial}{\partial r} \pm \frac{(2\ell+1\pm1)}{2r}\}R_{\ell'}(r)r \tag{A.1.9}$$

and so

$$M \propto \int_0^\infty rU_{n\ell}(r)\{\frac{d}{dr} \pm \frac{(2\ell+1\pm1)}{2r}\}rR_{\ell'}(r)dr \quad \text{for } \ell' = \ell\pm1 \tag{A.1.10}$$

REFERENCE FOR APPENDIX 1

Landau, D. and Lifschitz, E. M., Quantum Mechanics - Non Relativistic Theory, (Pergamon, London, 1959).

APPENDIX 2: Expansion of $h_{\ell}^{+}(K|\underline{r}-\underline{e}|)\, Y_{\ell m}(\underline{r}-\underline{e})$ in plane waves

We will show that:

$$h_{\ell}^{+}(K|\underline{r}-\underline{e}|)Y_{\ell m}(\underline{r}-\underline{e}) = \frac{-i^{1}}{2K\pi^{2}} \int d^{3}\underline{k}\, \frac{\exp[i\underline{k}.(\underline{r}-\underline{e})]Y_{\ell m}(\underline{k})j_{\ell}(kn)}{(K^{2}-k^{2})j_{\ell}(kn)} \qquad (A.2.1.)$$

Firstly consider the integral

$$I = \left(\frac{1}{2\pi}\right)^{3} \int d^{3}\underline{k}\, \frac{\exp[i\underline{k}.(\underline{r}+\underline{R}-\underline{x})]}{(K^{2}-k^{2})} \qquad (A.2.2.)$$

where $\underline{R}$ is the separation of two ion cores, $\underline{r}$ is a position vector centred on one of the ion cores and $\underline{x}$ is centred on the other such that $|\underline{r}|, |\underline{x}| < R_{MT}$ the muffin-tin radius.

Expanding the factors $\exp[i\underline{k}.(\underline{r}+\underline{R})]$ and $\exp(-i\underline{k}.\underline{x})$ in eqn. (A.2.2.) in real spherical harmonics, and integrating over the angular $\underline{k}$ components gives:

$$I = \left(\frac{2}{\pi}\right) \sum_{\ell,m} Y_{\ell m}(\underline{r}+\underline{R})Y_{\ell m}(\underline{x}) \int_{0}^{\infty} \frac{k^{2}j_{\ell}(k|\underline{r}+\underline{R}|)j_{\ell}(kx)\,dk}{(K^{2}-k^{2})} \qquad (A.2.3.)$$

The integrand is an even function of k, so:

$$I = \frac{1}{\pi} \sum_{\ell,m} Y_{\ell m}(\underline{r}+\underline{R})Y_{\ell m}(\underline{x})J \qquad (A.2.4.)$$

where

$$J = \int_{-\infty}^{\infty} \frac{k^{2}j_{\ell}(k|\underline{r}+\underline{R}|)j_{\ell}(kx)\,dk}{(K^{2}-k^{2})} \qquad (A.2.5.)$$

Expanding $j_{\ell}(k|\underline{r}+R|)$ in terms of the Hankel functions $h_{\ell}^{+}(k|\underline{r}+\underline{R}|)$ and $h_{\ell}^{-}(k|\underline{r}+\underline{R}|)$, (as defined in Messiah (1964)), J may then be separated out as

$$J = J_{1} - J_{2}$$

where

$$J_1 = \int_{-\infty}^{\infty} \frac{ik^2 j_\ell(kx) h_\ell^-(k|\underline{r}+\underline{R}|)\,dk}{2(K^2-k^2)} \qquad \text{(A.2.6.)}$$

and

$$J_2 = \int_{-\infty}^{\infty} \frac{ik^2 j_\ell(kx) h_\ell^+(k|\underline{r}+\underline{R}|)\,dk}{2(K^2-k^2)} \qquad \text{(A.2.7.)}$$

K is complex, and we see that the integrands in J_1 and J_2 have simple poles at $k=\pm K$ in the complex k-plane. Integrating over k it may be shown that

$$I = -K \sum_{\ell,m} j_\ell(Kx) Y_{\ell m}(\underline{x}) h_\ell^+(K|\underline{r}+\underline{R}|) Y_{\ell m}(\underline{r}+\underline{R}) \qquad \text{(A.2.8.)}$$

Now if we only expand the factor $\exp(-i\underline{k}.\underline{x})$ in the integrand in equation (A.2.2), we obtain:

$$I = \sum_{\ell,m} \frac{i^{-\ell}}{2\pi^2} \int d^3\underline{k}\, \frac{\exp[i\underline{k}.(\underline{r}+\underline{R})]}{(K^2-k^2)}\, j_\ell(kx) Y_{\ell m}(\underline{x}) Y_{\ell m}(\underline{k}) \qquad \text{(A.2.9.)}$$

A comparison of equations (A.2.8.) and (A.2.9.) yields the required result:

$$h_\ell^+(K|\underline{r}+\underline{R}|) Y_{\ell m}(\underline{r}+\underline{R}) = \frac{-i^{-\ell}}{2K\pi^2} \int d^3\underline{k}\, \frac{\exp[i\underline{k}.(\underline{r}+\underline{R})] j_\ell(kx) Y_{\ell m}(\underline{k})}{(K^2-k^2)\quad j_\ell(Kx)} \qquad \text{(A.2.10.)}$$

REFERENCE FOR APPENDIX 2

Messiah, A., Quantum Mechanics, Vol. I (North Holland, Amsterdam, 1961).

D42862'82

END